

Investigation of the role of putative chaperones in retinal degeneration.

Tatiana Novoselova, MBBS, MD

A thesis submitted for the degree of Doctor of Philosophy

Division of Molecular and Cellular neuroscience

Institute of Ophthalmology

University College London

Bath Street, London

EC1V 9EL

2009

Declaration

I declare that this thesis submitted for the degree of Doctor of Philosophy is composed by myself, and the work herein is my own, or that the author involved is clearly stated.

Tatiana Novoselova

Abstract

Retinitis pigmentosa (RP) is characterized by impaired night vision and constriction of visual fields, which with disease progression leads to blindness. RP can develop as an independent disorder or as a part of a syndrome caused by cilia dysfunction, such as Bardet-Biedl syndrome (BBS). Mutations in several potential chaperones, similar to cytosolic chaperonin (CCT) subunits, have been shown to cause BBS, such as BBS6, 10 and 12. Furthermore, mice homozygous for a *prefoldin 5 (pfdn5)* amino acid substitution have been reported to have retinal degeneration. Prefoldin 5 (PFDN5) is a subunit of the prefoldin chaperone complex, which assists in folding of tubulin, and is thus potentially important for microtubule function in the retina.

Another putative chaperone, RP2, which has homology to another chaperone of the tubulin folding pathway, cofactor C, causes X-linked RP. This protein is ubiquitous as are its currently described interacting partners. The reason why *RP2* mutations cause a retina restricted phenotype is not understood yet. A study into potential mechanisms by which *RP2* could be involved in retina pathways is presented in this thesis. For this purpose *RP2* was tested for retina specific interactions using two approaches – yeast two-hybrid and proteomic screening. During yeast two-hybrid screening of *RP2* with a retina cDNA library, rod arrestin was identified as a potential interacting partner, binding to the N-terminus of *RP2*. Using a proteomic approach of affinity pull down of retinal proteins, a retina specific protein, transducin- β subunit, was identified. These two novel interacting partners can possibly improve our understanding why *RP2* mutations lead to a retina restricted phenotype. Several other putative interacting partners with ubiquitous expression were also identified by yeast two-hybrid screening.

For the genetic screening of *PFDN5*, two panels of patients were selected, BBS of unknown aetiology and severe and early onset retinal degeneration. No disease associated sequence changes were detected in the coding sequence or exon/intron boundaries of these patient groups, suggesting that the mutations in such a gene could cause another type of ciliopathy or phenotype such as embryonic lethality.

Acknowledgments

I would like to express my gratitude to Professor Mike Cheetham, my principal supervisor, who made it possible for me to work with his vibrant research group on such an interesting and challenging project as RP2. I'd like to say huge thanks for those three years of hard work he and Dr Alison Hardcastle have done supervising me. Actually, I never had a chance to say these two people how talented they are, extremely intelligent and gifted. They both made my PhD an interesting and enjoyable experience and I would do it all over again!

I owe huge thanks to everyone in MCN group who are a great team, very supportive and a lot of fun socially. However, I would like to say special thanks to my colleague and husband Sergey Novoselov for everything (a long list would follow here). I would like to thank two other special for me people, Nele Schwarz and Jane Evans, who work on RP2 project. They have been great and working with them was a pleasure. I'd like to say huge thanks to one more RP2 person, Paul Chapple, who has always been very helpful and ready to answer all my questions. Thanks a lot to all the people in the Institute of Ophthalmology. Huge thanks to Beverley Scott for ensuring my sequencing was smooth and to Peter Munro for help with using the confocal microscope.

I would like to thank our collaborators: Dr Phillip Beales, who provided DNA samples for *PFDN5* screening, Dr Robin Wait for mass spectrometry analysis and Dr Seva Gurevich was providing plasmids. I look forward to our possible future collaborations.

Thanks to Dorothy Hodgkin Postgraduate Award for funding my PhD, it was an honour for me to be awarded by this prestigious award.

Sincere thanks to my parents for their great support and encouragement even from a very long distance. I shall no longer be a student and I hope it is a sign of relief for you both. Thanks to my brother for being so supportive for my parents when I'm away from home. Finally, I would like to thank my little boy Igor, who lights my life up and for whom any words of gratitude would never be enough.

Dedication

I dedicate this thesis to my father.

Table of contents

Title page	1
Declaration	2
Abstract	3
Acknowledgments	4
Dedication	5
Table of contents	6
List of figures	13
List of tables	16
List of abbreviations	17

Chapter I. Introduction

1.1. The eye	20
1.2. The retina	20
1.2.1. The retinal pigment epithelium	22
1.2.2. The neural retina	22
1.2.2.1. Rod and cone photoreceptors	24
1.2.2.2. Outer segment morphogenesis	25
1.2.2.3. The connecting cilium	25
1.2.3. Visual phototransduction	27
1.2.3.1. G protein coupled receptor signalling	27
1.2.3.2. G proteins	30
1.2.3.3. Phototransduction cascade	34
1.2.3.4. Transducin	37
1.2.3.5. Arrestin	39
1.2.3.6. Light dependent translocation of phototransduction cascade components	41
1.2.3.6.1. Diffusion hypothesis	42
1.2.3.6.2. Active transport hypothesis	44
1.2.3.6.3. Calcium-myristoyl switch mechanism	45

1.3. Inherited retinal dystrophies	45
1.3.1. Retinitis pigmentosa	46
1.3.1.1. X-linked retinitis pigmentosa	48
1.3.1.1.1. Retinitis pigmentosa GTPase regulator	48
1.3.2. Syndromic forms of retinitis pigmentosa	49
1.3.2.1. Ciliopathies	50
1.3.2.2. Bardet–Biedl syndrome	50
1.3.3. Oguchi disease	52
1.3.4. Cone-rod dystrophy	53
1.3.4.1. Unc 119	54
1.3.5. Leber congenital amaurosis	54
1.4. Molecular chaperones	55
1.4.1. Heat shock proteins	56
1.4.1.1. Heat shock proteins 70 kDa	56
1.4.2. Cytosolic chaperonin	59
1.4.3. Prefoldin	60
1.4.4. Tubulin folding cofactors and tubulin folding pathway	60
1.5. RP2	63
1.5.1. <i>RP2</i> gene	63
1.5.2. RP2 protein	63
1.5.2.1. Cofactor C homology domain	66
1.5.2.2. Nucleoside diphosphate kinase homology domain	66
1.5.3. Localisation of RP2 protein	70
1.5.4. RP2 function	72
1.5.4.1. Interaction of RP2 with Arl3	72
1.6. ADP-ribosylation factors (ARF)-like GTPases	73
1.6.1. Arl3	74
1.6.2. Arl2	75
1.6.3. Interacting partners of Arl2 and Arl3	75

1.7. Potential mechanisms of XLRP caused by RP2 76

1.8. Aims of this study 77

Chapter II. Materials and Methods

2.1. Basic molecular biology techniques 78

2.1.1. Polymerase chain reaction 78

2.1.2. TA cloning 80

2.1.3. *E.coli* transformation 80

2.1.4. Plasmid purification and DNA quantification 81

2.1.5. Restriction enzyme digestion 81

2.1.6. Alkaline phosphatase vector treatment 81

2.1.7. Analysis of PCR products and restriction digests 82

2.1.8. Vectors and constructs 82

2.1.9. Short interfering RNA 84

2.2. CytoTrap® yeast-two hybrid 85

2.2.1. CDC25 yeast strain long term storage and resuscitation 85

2.2.2. Yeast transformation 85

2.2.3. Library screening 86

2.2.4. Total yeast DNA isolation 86

2.2.5. pMyr plasmids isolation 87

2.2.6. Protein-protein interaction verification by yeast two-hybrid 87

2.3. Cell based techniques 88

2.3.1. Cell culture maintenance and storage 88

2.3.2. Transfection procedure 88

2.3.3. Transfection with short interfering RNA (siRNA) 89

2.3.4. Immunocytochemistry 90

2.3.5. Microscopy 91

2.3.6. Subcellular fractionation 91

2.3.7. Detergent resistant membrane fraction isolation 92

2.3.8. Retinal lysate preparation 93

2.4. Protein based techniques	94
2.4.1. Protein concentration determination	94
2.4.2. Sample preparation and SDS-polyacrylamide gel electrophoresis (SDS-PAGE)	94
2.4.3. Staining of protein gels using Coomassie Blue	95
2.4.4. Silver stain of protein gels	95
2.4.5. Western blotting	96
2.4.6. Production of recombinant proteins	98
2.4.7. Preparation of recombinant proteins	98
2.4.8. Purification of GST-fused recombinant protein	98
2.4.9. GST pull-down	99
2.4.10. Mass spectrometry	99
2.4.11. Co-immunoprecipitation from mammalian cell or retinal lysates	100
2.5. Automated DNA sequencing	101
2.5.1. Genomic sequencing	101
2.5.2. Plasmid sequencing	102
2.6. Bioinformatics and software	103

Chapter III. Novel putative interacting partners of RP2 identified by yeast two-hybrid screening

3.1. Introduction	104
3.2. CytoTrap® system characterisation	110
3.3. Screening of the bovine retinal cDNA library with the full length human RP2	112
3.3.1. Nucleolin	115
3.3.1.1. Characterisation of NCL interaction with RP2 in CytoTrap®	115
3.3.2. Drebrin-like protein	119
3.3.2.1. RP2 domain mapping of the interaction with clone 20	119

3.3.3. Unc119.....	121
3.4. Screening of the N-terminus of RP2 using CytoTrap®	124
3.4.1. Rod arrestin.....	125
3.4.1.1. Characterisation of RP2-rod arrestin interaction by CytoTrap®.....	128
3.4.1.2. Expression of rod arrestin fragment in SK-N-SH cells.....	128
3.4.1.3. Specific binding of rod arrestin to RP2	131
3.4.1.4. Arrestins and endogenous Arl3	134
3.4.1.5. Co-Immunoprecipitation of rod arrestin with RP2 mutants	135
3.4.1.6. RP2 is a putative calcium binding protein.....	135
3.4.1.7. Subcellular localisation of rod arrestin and RP2.....	138
3.4.2. Other novel interacting partners identified in CytoTrap® screening of the N-terminal fragment of RP2.....	141
3.4.2.1. Chaperones as putative interacting partners of RP2	141
3.4.2.1.1. Hsc70.....	141
3.4.2.1.2. Cytosolic chaperonin subunit 6A (CCT6A).....	143
3.4.2.2. 26S proteasome non-ATPase subunit 4 (PSMD4).....	145
3.5. Discussion.....	148
3.5.1. Screening a retinal cDNA library with RP2.....	148
3.5.2. Nucleolin.....	148
3.5.3. Drebrin-like protein	150
3.5.4. Unc119.....	151
3.5.5. Rod arrestin.....	151
3.5.6. Other potential interacting partners identified by yeast two hybrid.....	159
Chapter IV. Transducin-β subunit as a putative interacting partner of RP2	
4.1. Introduction	162
4.2. Results.....	166
4.2.1. Expression and purification of recombinant GST-Arl3 and GST-RP2 in <i>E.coli</i>	166

4.2.2. GST pull-down optimisation.....	168
4.2.3. Identification of transducin- β subunit as a potential RP2 interacting partner.....	171
4.2.4. Confirmation of transducin- β interaction with RP2 in retinal lysate	176
4.2.5. Interaction of transducin- β with RP2 in immunoprecipitation assay	176
4.2.6. The effect of RP2 mutations on the interaction with transducin- β	178
4.2.7. The subcellular localisation of transducin- β and RP2 overlap	180
4.2.8. Subcellular localisation of other G β proteins and RP2	182
4.2.9. L253R mutation in the C-terminus of RP2 affects transducin- β co-localisation with RP2.....	184
4.2.10. Subcellular fractionation assay of transducin- β localisation upon co-transfection with RP2.....	187
4.2.11. Detergent resistant membrane isolation from cells co-transfected with transducin- β and RP2.....	190
4.2.12. Arl3 siRNA does not alter the overlap in subcellular co-localisation of transducin- β and RP2.....	192
4.2.13. Arl3 is able to alter co-localisation of RP2 with transducin- β	194
4.3. Discussion.....	196

Chapter V. Prefoldin 5 as a candidate gene for retinal degeneration

5.1. Introduction.....	203
5.1.1. The human <i>PFDN5</i> gene.....	203
5.1.2. PFDN5 protein.....	203
5.1.3. PFDN5 as a part of a chaperone complex.....	205
5.1.4. PFDN5 as a candidate gene for retinal degeneration.....	205
5.2. Results	211
5.2.1. Screening of patients with non-syndromic and syndromic forms of retina degeneration	211
5.2.2. PFDN5 protein purification.....	213

5.2.3. GST pull-down with mammalian cell lysates.....	215
5.2.4. PFDN5 in CytoTrap®.....	219
5.3. Discussion.....	221
Chapter VI. Discussion and future work.....	224
References.....	231
Appendix.....	264
CD ROM.....	attached

List of figures

Figure 1.1. Structure of the human eye.....	21
Figure 1.2. A fundus image of a human retina	21
Figure 1.3. Structure of the retina.....	23
Figure 1.4. Diagrammatic representation of a rod and cone cell.....	23
Figure 1.5. The rod connecting cilium structure	26
Figure 1.6. G protein signalling pathway	29
Figure 1.7. Phylogenetic tree of G protein subunits.....	33
Figure 1.8. Phototransduction cascade in rods	36
Figure 1.9. Structure of the transducin complex and its subunits.....	38
Figure 1.10. Rod arrestin structure and oligomerisation.....	38
Figure 1.11. A model of phosducin function in transducin translocation	43
Figure 1.12. Conditions that induce the heat shock response.....	57
Figure 1.13. The Hsp70 protein-folding cycle.....	57
Figure 1.14. Model of the tubulin heterodimer assembly.....	62
Figure 1.15. Position of pathogenic missense and nonsense mutations in the <i>RP2</i> gene and <i>RP2</i> protein domain organisation.....	64
Figure 1.16. Sequence conservation between the N-terminus of <i>RP2</i> and the C- terminal domain of cofactor C.....	67
Figure 1.17. Structure of the human <i>RP2</i> protein.....	68
Figure 1.18. Comparison of the C-terminus of <i>RP2</i> with NDPK.....	69
Figure 1.19. Localisation of <i>RP2</i> protein	71
Figure 3.1. Schematic of yeast two-hybrid hSOS recruitment system (CytoTrap®)	106
Figure 3.2. Schematic of fragments and mutants of <i>RP2</i> used in CytoTrap®.....	109
Figure 3.3. Interaction of hSos- <i>RP2</i> constructs with positive and negative controls.....	111
Figure 3.4. Summary of CytoTrap® screening performed in this study.....	114
Figure 3.5. Interaction of clone 30 with <i>RP2</i> in CytoTrap®.....	116

Figure 3.6. Characterisation of clone 30	117
Figure 3.7. Clone 20 characterisation and its interaction with RP2.....	120
Figure 3.8. Characterisation of clone 58	122
Figure 3.9. Subcellular localisation of Unc119	123
Figure 3.10. Interaction of clone 46 with RP2 in CytoTrap®.....	126
Figure 3.11. Comparison of clone 46 to bovine rod arrestin.....	127
Figure 3.12. Subcellular localisation of myc-rod arrestin fragment and RP2-GFP	130
Figure 3.13. The alignment of bovine rod arrestin to bovine β -arrestin-2 protein sequences.....	132
Figure 3.14. Co-immunoprecipitation of rod arrestin-FLAG with RP2-GFP.....	133
Figure 3.15. Co-IP of rod arrestin-FLAG with wild type RP2-GFP and RP2 mutants.....	136
Figure 3.16. RP2 is a putative calcium binding protein	137
Figure 3.17. Subcellular localisation of bovine rod arrestin in SK-N-SH cells.....	139
Figure 3.18. Subcellular localisation of bovine rod arrestin and human RP2 in SK-N-SH cells.....	140
Figure 3.19. Characterisation of clone 44.....	142
Figure 3.20 Characterisation of clone 55	144
Figure 3.21. Characterisation of clone 43 and its interaction with RP2.....	146
Figure 3.22. Alignment of yeast Cin4 protein sequence to human Arl3.....	152
Figure 3.23. Potential calcium binding sites in the RP2 protein	157
Figure 4.1. Expression and solubility of GST-Arl3 and GST-RP2.....	167
Figure 4.2. GST pull-down with GST-Arl3 and GST-RP2	170
Figure 4.3. Pull-down assay of GST-RP2 and GST-Arl3 mutants with porcine retinal lysate	172
Figure 4.4. Transducin- β subunit identification	175
Figure 4.5. Interaction of transducin- β with RP2.....	177
Figure 4.6. Interaction of RP2 mutants with transducin- β	179
Figure 4.7. Subcellular localisation of transducin- β and RP2	181

Figure 4.8. Subcellular localisation of transducin- β , G β 3, G β 5L, G β 5 and RP2-GFP in SK-N-SH cells.....	183
Figure 4.9. Effect of RP2 mutations on transducin- β intracellular staining.....	185
Figure 4.10. Effect of RP2 mutants on transducin- β localisation.....	186
Figure 4.11. Changes in the subcellular localisation of transducin- β upon co-transfection with RP2.....	189
Figure 4.12. Detergent resistant membrane fractionation of ARPE19 cells.....	191
Figure 4.13. GST-Arl3 pull down with retina lysate and the effect of Arl3 siRNA on RP2 co-localisation with transducin- β	193
Figure 4.14. Subcellular localisation of transducin- β and RP2 upon co-transfection with Arl3.....	195
Figure 4.15. Alignment of transducin- β protein to other G β proteins.....	197
Figure 4.16. G protein coupled receptor dependent and alternative NDK dependent G protein activation.....	200
Figure 5.1. Organisation of human PFDN 5 isoforms.....	204
Figure 5.2. Proposed model of the PFDN complex structure.....	204
Figure 5.3. Schematic of the wnt signaling pathway in a ciliated cell.....	208
Figure 5.4. Primer design for <i>PFDN5</i> screening and examples of PCR products amplified from patient DNA samples.....	212
Figure 5.5. Sequence changes found in the <i>PFDN5</i> gene in patients with retinal degeneration.....	214
Figure 5.6. PFDN5 protein purification.....	216
Figure 5.7. Binding of β -tubulin by GST-PFDN5 in an affinity pull-down assay.....	218
Figure 5.8. PFDN5 in the CytoTrap® system.....	220
Figure 6.1. A schematic of potential pathways where RP2 may function.....	230

List of tables

Table 1.1. Classes of GPCRs.....	28
Table 1.2. G protein α subunits classification and main pathways	31
Table 1.3. Human G protein $\beta\gamma$ subunits and their properties.....	32
Table 1.4. Examples of genes and pathways implicated in retinal degeneration	47
Table 1.5. Genetic heterogeneity of Bardet-Biedl syndrome.....	51
Table 1.6. Reported pathogenic mutations in <i>RP2</i>	65
Table 2.1. Sequences of primers used in this study for cloning	79
Table 2.2. Sequences of primers used for <i>PFDN5</i> amplification	79
Table 2.3. Vectors used in this study and their characteristics.....	83
Table 2.4. Plasmids made in this study.....	83
Table 2.5. Provided plasmids used in this study.....	84
Table 2.6. siRNA sequences used in this study	84
Table 2.7. Transfection of mammalian cells with DNA	89
Table 2.8. Primary antibodies used for immunocytochemistry	91
Table 2.9. Buffers and conditions used for cell and retinal lysis.....	94
Table 2.10. Primary antibodies used for Western blotting and immunoprecipitation	97
Table 2.11. HRP conjugated secondary antibody used for Western blotting	97
Table 2.12. Primers used for sequencing of pMyr clones.....	102
Table 4.1. The proteins and peptides identified in ESI-MS/MS analysis of GST- RP2 pull-down with the retinal lysate.....	174
Table 5.1. Summary of PFDN5 CytoTrap® results.....	220

List of abbreviations

ADP	Adenosine diphosphate
Arf	ADP-ribosylation factor
Arl	ADP-ribosylation factor-like
ATCC	American tissue culture collection
ATP	Adenosine triphosphate
BART1	Binder of Arl2
BBS	Bardet-Biedl syndrome
BLAST	Basic local alignment research tool
BSA	Bovine serum albumin
CAP	Cyclase associated protein
CC	Connecting cilium/cilia
CCT	Cytosolic chaperonin
cDNA	Complementary DNA
cGMP	Cyclic guanosine monophosphate
CIAP	Calf intestinal alkaline phosphatase
CRD	Cone-rod dystrophy
DAPI	4'6-Diamidino-2-phenylindole
DBNL	Drebrin-like protein
dH ₂ O	Distilled water
DMEM	Dulbecco's modified Eagle's medium
DNA	Deoxyribonucleic acid
DRM	Detergent resistant membranes
ECL	Enhanced chemiluminescence
EDTA	Ethylenediamine tetraacetic acid
EGTA	Ethyleneglycol tetraacetic acid
FBS	Fetal bovine serum
<i>g</i>	Acceleration due to gravity
g	gramm
GAP	GTPase activating protein
GAPDH	Glyceraldehyde 3-phosphate dehydrogenase
GCL	Ganglion cell layer

GDP	Guanosine diphosphate
GEF	Guanine nucleotide exchange factor
GFP	Green fluorescent protein
GPCR	G protein coupled receptor
GST	Glutathione S-transferase
GTP	Guanosine triphosphate
HBSS	Hanks balanced salt solution
HRP	Horse radish peroxidase
Hsp	Heat shock protein
IFT	Intraflagellar transport
IPTG	Isopropyl- β -D-thiogalactopyranoside
INL	Inner nuclear layer
IPL	Inner plexiform layer
IS	Inner segment
kb	Kilobase
Kd	Dissociation constant
kDa	Kilo Dalton
LCA	Leber congenital amaurosis
MAP	Microtubule associated protein
mg	milligramm
MS	Mass spectrometry
MTOC	Microtubule organising center
NCBI	National centre for biotechnology information
NCL	Nucleolin
NDPK	Nucleoside diphosphate kinase
NP40	Nonidet P40
OLM	Outer limiting membrane
OMIM	Online Mendelian inheritance in man
ONL	Outer nuclear layer
OPL	Outer plexiform layer
OS	Outer segment
PBS	Phosphate buffered saline
PCR	Polymerase chain reaction
PDB	Protein databank

PDE	Phosphodiesterase
PIC	Protease inhibitors cocktail
PFAM	Protein families database
PFND	Prefoldin
PSMD4	26S proteasome non-ATPase subunit 4
RAN	Ras-related nuclear protein
RGS	Regulator of G protein signalling
RP	Retinitis pigmentosa
RPE	Retinal pigment epithelium
RPGR	Retinitis pigmentosa GTPase regulator
SAG	S-antigen
SDS	Sodium dodecyl sulphate
SDS-PAGE	SDS polyacrylamide gel electrophoresis
SNP	Single nucleotide polymorphism
SRS	Sos recruitment system
TAE	Tris acetate buffer
TCA	Trichloroacetic acid
TM	Transmembrane
TNPO3	Transportin 3
v/v	volume/volume
w/v	weight/volume
XLRP	X-linked retinitis pigmentosa

Chapter I. Introduction

1.1. The eye

The human eye is the organ of vision. It consists of three main layers (figure 1.1). The first layer is a fibrous coat and includes the cornea and sclera. The second layer is called the uvea and is composed of the choroid, ciliary body, lens and iris. The choroid is the layer of blood vessels from *arteria ophthalmica* that supplies the eye. The ciliary body is the circumferential tissue inside the eye composed of the ciliary muscle and ciliary processes. This structure is attached to the lens, regulates lens shape and therefore is partially responsible for light focus on the retina. When the ciliary muscle relaxes, it flattens the lens, generally improving the focus for farther objects and vice versa. The third layer of the eye is known as the retina and lines the back of the eye (figure 1.1).

The eye has three chambers of fluid: anterior chamber (between cornea and iris), posterior chamber (between iris, zonule fibers and lens) and the vitreous chamber (between the lens and the retina). The first two chambers are filled with aqueous humour whereas the vitreous chamber is filled with a more viscous fluid, the vitreous humour.

1.2. The retina

The retina is composed of neural retina, interphotoreceptor matrix and retinal pigment epithelium (RPE) cells layer (figure 1.1). The adult human retina is approximately 42 mm diameter, 0.5 mm thick (Pipe and Rapley, 1984). The optic nerve disc near the centre of the retina is a circular to oval white area measuring about 2 mm across. Here the optic nerve forms the output of the neural retina to the brain. This area does not contain any photoreceptors and is known as the “blind spot”. From its centre radiate the major blood vessels. Approximately two optic disc diameters to the left of the optic nerve disc, can be seen a blood vessel-free spot, the fovea, which is at the centre of the area known as the macula (figure 1.2). The retina is a highly organized structure of neural retina cells and RPE cells and is composed of a large number of cell types, each with a different function (Pipe and Rapley, 1984).

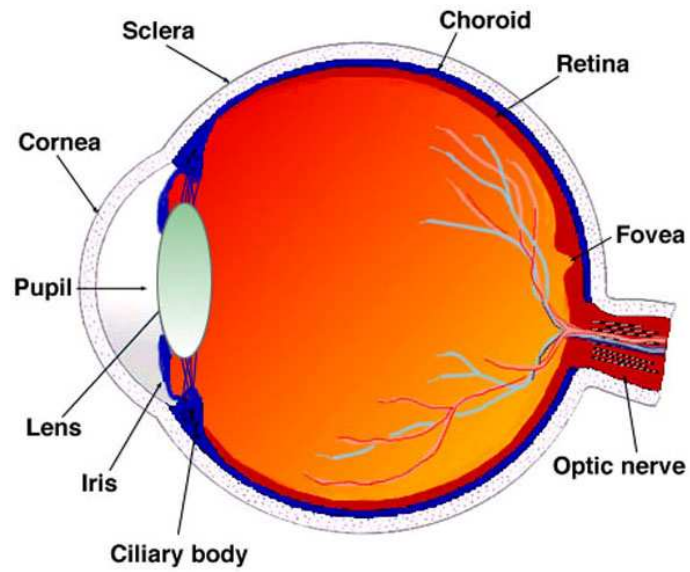


Figure 1.1. Structure of the human eye

A cross-sectional view of the human eye (from www.webvision.med.utah.edu)

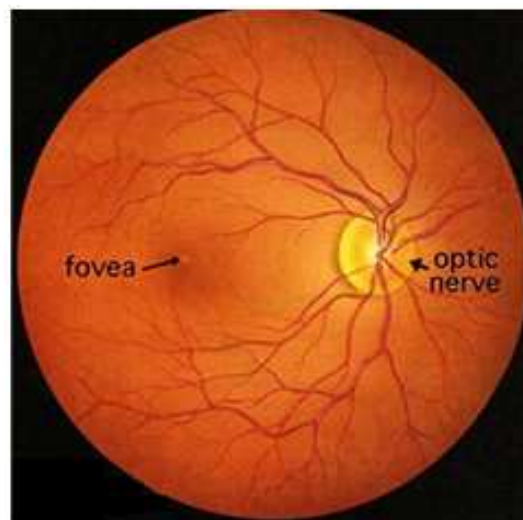


Figure 1.2. A fundus image of a human retina

An ophthalmoscopic image of a human retina showing the fovea, optic nerve and blood vessels (from www.webvision.med.utah.edu).

1.2.1. The retinal pigment epithelium

A monolayer of epithelial cells separates the neural retina from choroid known as the retinal pigment epithelium (RPE) (figure 1.3a). This layer has several functions. The RPE nourishes neural retina cells, supplying small molecules, such as amino acids, from the blood vessels of the choroid. The RPE also serves as a barrier between blood vessels and neural retina. Third, RPE cells recycle 11-*cis* retinal and thus, take part in visual cycle. RPE cells play an important role in the phagocytosis of outer segments (OS) discs. Shed discs undergo phagocytosis which occurs through the apical processes of RPE cells that surround the photoreceptor OS (Andersen *et al.*, 1978). Each RPE cell contacts approximately 45 OS and the estimated turnover of outer segments discs is 10 % daily (Bosch *et al.*, 1993). The RPE also absorbs scattered light as it is rich in melanosomes (LaVail and Gorrin, 1987).

1.2.2. The neural retina

The neural retina is arranged into histologically distinct layers. The outer nuclear layer (ONL) contains the cell bodies of the rod and cone photoreceptors (figure 1.3) The distribution of rods and cones is not even throughout the retina. The central retina is cone-dominated and the periphery is a rod rich region. Within the macula, cone photoreceptors are highly concentrated. This region includes a 200 µm fovea pit, where only cones are present (Pipe and Raley, 1984).

The first layer of synapses is the outer plexiform layer (OPL). This layer contains axons of photoreceptor cells and dendrites of the cells from the inner nuclear layer (INL). The INL is composed of bipolar, horizontal and amacrine cells, which are adjacent to the inner plexiform layer (IPL). This is the second layer of synapses in the retina. The IPL has axons of the cells of INL, dendrites of the ganglion cells and a second population of amacrine cells which form the ganglion cell layer (GCL) (figure 1.3). The GCL contains the ganglion cell nuclei and axons of these cells that form the optic nerve conducting the signal to the visual cortex of the brain (Pipe and Raley, 1984).

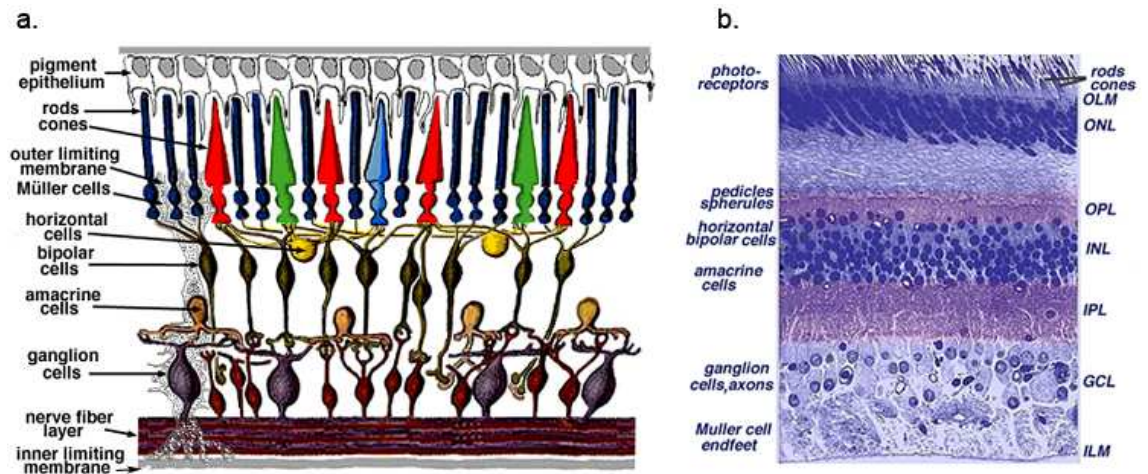


Figure 1.3. Structure of the retina

a. A schematic of the human retina showing the organisation of various cell types in the retina. **b.** Light micrograph of the vertical section through central human retina. OLM, outer limiting membrane; ONL, outer nuclear layer; OPL, outer plexiform layer; INL, inner nuclear layer; IPL, inner plexiform layer; GCL, ganglion cell layer; ILM, inner limiting membrane (from www.webvision.med.utah.edu).

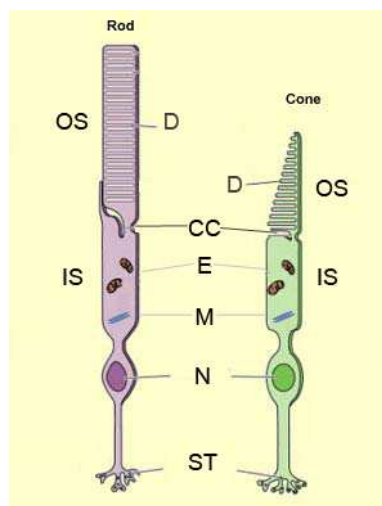


Figure 1.4. Diagrammatic representation of a rod and cone cell

OS, outer segment; IS, inner segment, D, discs; CC, connecting cilium; E, ellipsoid; M, myoid; N, nuclear region; ST, synaptic terminal (from Djamgoz and Kolb, 1993).

The retina has glial cells called Muller cells. Their adherent junctions together with the photoreceptor cell inner segments form the outer limiting membrane (OLM) of the retina. The inner limiting membrane (ILM) of the retina is likewise composed of laterally contacting Muller cells and the components of the basement membrane. The ILM is the inner surface of the retina bordering the vitreous humour and thereby forms a diffusion barrier between neural retina and vitreous humour (Pipe and Raley, 1984).

Light travels through the optical systems of the eye and retinal structures before striking the photoreceptor outer segments which transform photon energy into membrane depolarisation and the visual process begins.

1.2.2.1. Rod and cone photoreceptors

The human retina has two basic types of photoreceptors, rods and cones (figures 1.3 and 1.4). Rods are highly sensitive photoreceptors and contain the visual pigment – rod opsin. This type of photoreceptor is used for vision under dark-dim light conditions. Cones contain cone opsins as their visual pigments and these have different wavelength sensitivity, forming the basis of trichromatic colour perception. The number of rod cells is approximately twenty times higher than cones (Curcio *et al.*, 1990).

Cones are conical-shaped structures that have their cell bodies situated in a single row right below the outer limiting membrane (OLM) and their inner and outer segments protrude into the sub-retinal space towards the pigment epithelium. Rods are slim rod-shaped structures with their inner and outer segments that fill the area between the larger cones in the sub-retinal space and stretch to the pigment epithelium cells (figure 1.4).

Both rods and cones have a similar structure consisting of outer (OS) and inner segment (IS) connected by the connecting cilium (CC), cell body and synaptic terminal. The outer segments of rods are a stack of numerous membranous discs, surrounded by a plasma membrane. They have no connection between each other or the plasma membrane, apart from the most basal ones. In contrast, in cones all the discs are continuous with one another and the plasma membrane (figure 1.4) (Anderson *et al.*, 1978).

1.2.2.2. Outer segment morphogenesis

The outer segments of rods and cones are continually renewed through the process of morphogenesis and shedding. They are produced by invaginations of the plasma membrane near the connecting cilium and then internalised. At the same time old discs are displaced up the outer segment and are pinched off at the tips and engulfed by the apical processes of the pigment epithelium. These discarded discs become phagosomes in RPE (section 1.2.1) (Steinberg *et al.*, 1977).

There is a burst of disc shedding in the morning in rods (LaVail, 1980) and in the evening in cones (Young, 1978), judged by increased numbers of phagosomes in the pigment epithelium shortly thereafter. Outer segment proteins are produced in the inner segment, which is divided into ellipsoid and myoid region. The myoid mainly contains organelles necessary for protein synthesis and is suggested to be a docking region, whereas the ellipsoid region has high density of mitochondria (figure 1.4) (Carter-Dawson and LaVail, 1979).

1.2.2.3. The connecting cilium

The connecting cilium (CC) is a specialised non-motile cilium which connects the OS with the IS of photoreceptors. It contains nine pairs of microtubules in 9+0 arrangement, and compared to a motile cilium it lacks the central microtubule doublet and dynein arms (Rohlich, 1975). The cilium arises from a modified centriole known as the basal body, which acts as a microtubule organising centre for the photoreceptor (Troutt and Burnside, 1988). From the basal body the axoneme extends further up into the outer segment and the cytoskeletal structure extends down into the cell body forming a rootlet (figure 1.5) (Yang *et al.*, 2002).

The connecting cilium is essential for the transport of proteins produced in the inner segment to the outer segment (Miyaguchi and Hashimoto, 1992). This type of transport is known as intraflagellar transport (IFT) and is mediated by motor proteins such as kinesin II for anterograde traffic (Cole *et al.*, 1998) and dynein 1B for retrograde (Pazour *et al.*, 1998).

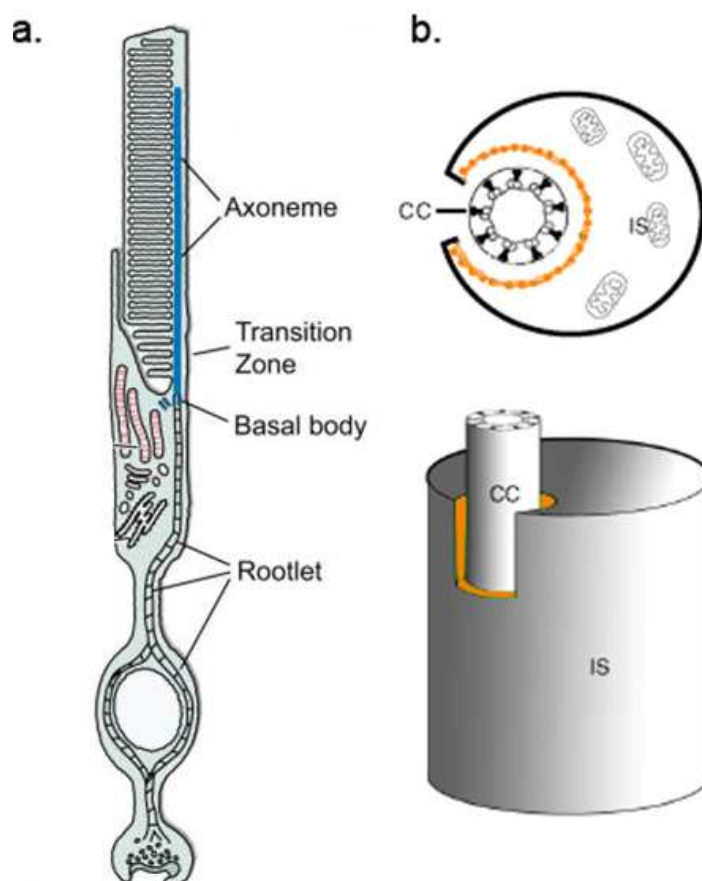


Figure 1.5. The rod connecting cilium structure

a. A longitudinal profile of a photoreceptor with the connecting cilium structure shown as indicated (from Liu *et al.*, 2007a). **b.** A cross-sectional view through the connecting cilium (CC) and a 3D rendition of the photoreceptor inner segment in relation to the connecting cilium are shown. The periciliary ridge region is indicated in orange (modified from Liu *et al.*, 2007b).

A large number of mutations in genes encoding proteins involved in IFT have been reported to date. The phenotype in such disorders usually affects the retina, for example Bardet-Biedl syndrome (described in section 1.3.2.2) (Bergsma and Brown 1975, Nishimura *et al.*, 2004). Furthermore, other retinal disease proteins have been localized to the connecting cilium structure e.g. RPGR (discussed in section 1.3.1.1.1) (Hong *et al.*, 2000), RP1 (Ostrowski *et al.*, 2002) (figure 1.5a).

The connecting cilium is surrounded by a region known as the periciliary ridge (Watanabe *et al.*, 1999). This is a region of the photoreceptor plasma membrane at the apical inner segment that encircles the connecting cilia (figure 1.5b). The connecting cilia of photoreceptors sit in a recess formed by the invagination of apical inner segment plasma membrane. The narrow band of periciliary matrix materials separates the plasma membranes of the inner segment and of the connecting cilium. Some retinal disease proteins are localised to this region, for example Usherin (Liu *et al.*, 2007b).

1.2.3. Visual phototransduction

Human visual phototransduction occurs in the photoreceptors and is a process that converts the light energy into an electric signal. It is based on guanine nucleotide binding protein (G protein) coupled receptor (GPCR) signalling.

1.2.3.1. G protein coupled receptor signalling

A variety of processes in cells is regulated by extracellular signals (neurotransmitters, neuromodulators, hormones etc.) that are transmitted into the cell via different pathways. The most common pathway is a three step G protein signalling cascade (figure 1.6). The first step is the activation of a GPCR. Proteins of the superfamily of GPCR have similar structure and are known to have seven transmembrane (TM) domains linked by intracellular and extracellular loops (Trumpp-Kallmeyer *et al.*, 1992, Feng *et al.*, 1999). Extracellular loops together and/or TM domains are known to be responsible for ligand binding, and intracellular loops bind to guanine nucleotide binding proteins (G proteins) (reviewed in Wess, 1997). GPCRs are conventionally divided into six classes A-F (table 1.1).

Class of GPCR	Distinctive feature	Receptors examples
Class A (rhodopsin-like)	Agonist binds within the cavity in the heptahelical domain and/or extracellular loops between the helices	Rhodopsin; α and β adrenoreceptors; muscarinic cholinergic; dopamine; odorant;
Class B	Large extracellular N-terminal ligand binding site	Secretin receptor family: Corticotrophin-releasing factor receptor; parathyroid hormone receptor;
Class C	Function only as dimers	Pheromone receptors: Homodimeric metabotropic glutamate receptor; homodimeric metabotropic calcium sensing receptor; heterodimeric GABA _B ; sweet and umami taste receptors;
Class D	Low sequence similarity to other GPCRs	Fungal pheromone mating factor receptors: STE2, STE3
Class E	Low sequence similarity to other GPCRs	Cyclic AMP receptors in amoeba
Class F	transmission and interpretation of cell polarity information; cell density sensing	Frizzled, Smoothened

Table 1.1. Classes of GPCRs

Modified from Breitwieser, 2004; Chen and Struhl, 1996; Vinson *et al.*, 1999

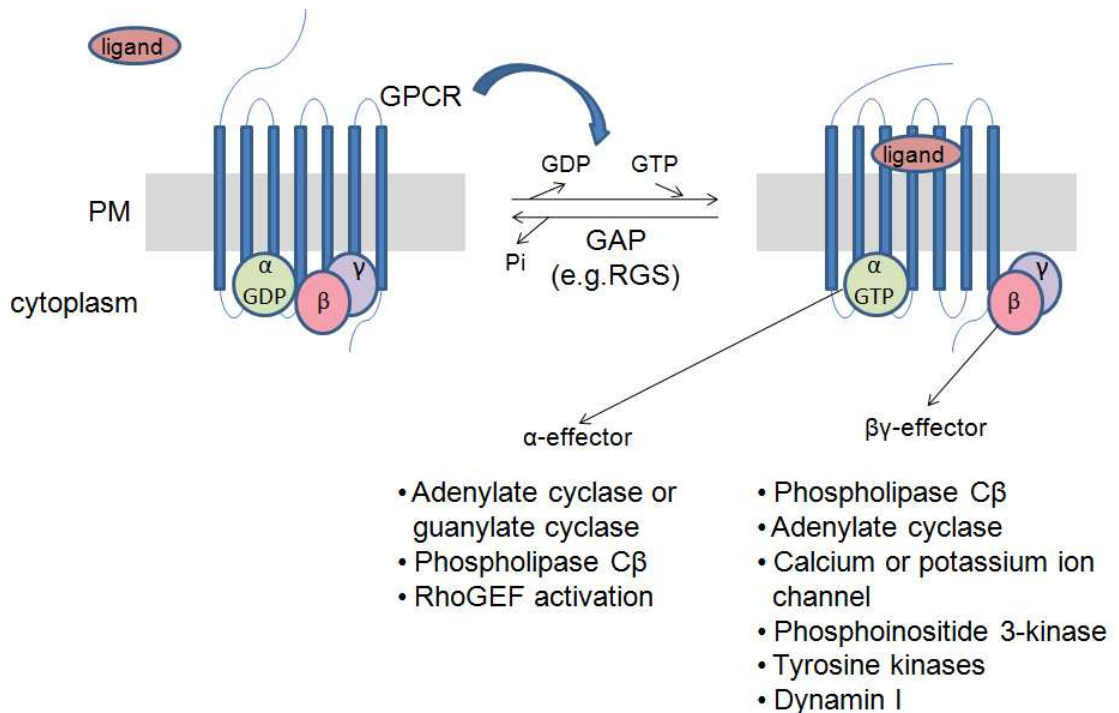


Figure 1.6. G protein signalling pathway

A schematic of the GDP/GTP cycle governing activation of heterotrimeric GPCR signaling pathways. In the absence of ligand, the $G\alpha$ subunit is GDP bound and closely associated with the $G\beta\gamma$ heterodimer. This $G\alpha$ -GDP/ $G\beta\gamma$ heterotrimer interacts with the cytosolic loops of a seven transmembrane domain GPCR. $G\beta\gamma$ facilitates the coupling of $G\alpha$ to receptor and also acts as a guanine nucleotide dissociation inhibitor (GDI) for $G\alpha$ -GDP, slowing the spontaneous exchange of GDP for GTP. Ligand-bound GPCR acts as a guanine nucleotide exchange factor (GEF) by inducing a conformational change in the $G\alpha$ subunit, allowing it to exchange GTP for GDP. $G\beta\gamma$ dissociates from $G\alpha$ -GTP, and both $G\alpha$ -GTP and $G\beta\gamma$ are competent to signal to their respective effectors. The cycle returns to the basal state when $G\alpha$ hydrolyzes the gamma-phosphate moiety of GTP, a reaction that is augmented by a GTPase-accelerating protein (GAP) such as RGS (modified from McCudden *et al.*, 2005).

Ligand binding causes conformational changes in a GPCR that promotes its interaction with distinct classes of G protein heterotrimers consisting of α -, β -, and γ -subunits. Thus, an activated GPCR acts as a guanine nucleotide exchange factor (GEF) for a G protein α subunit.

This process triggers the second step of G protein signalling cascade - the exchange of GDP for GTP on the α -subunit and this leads to the dissociation of the G protein from the receptor (figure 1.6). The important feature of this cascade step is the signal amplification since one activated molecule of GPCR is able to cause dissociation of upto 120 G protein heterotrimers per one activated GPCR molecule per s^{-1} (reviewed in Arshavsky *et al.*, 2002).

Released G protein α subunit and G protein $\beta\gamma$ heterodimer are able to interact with second messengers, such as distinct effector enzymes and channels. This interaction leads to a cellular response, which is the third step of G protein signalling cascade (figure 1.6) (reviewed in Neer and Clapham, 1988).

The G protein activation becomes terminated by enzymes called GTPase activating proteins (GAP) which hydrolyse GTP to GDP on the G protein α activated subunit. The most extensively studied GAPs are phospholipase C and regulators of G protein signalling (RGS) (Ross and Willkie, 2000).

1.2.3.2. G proteins

As mentioned above, G proteins are composed of three subunits, $\alpha\beta\gamma$, with the GTP binding domain located on the α subunit. There are four families of heterotrimeric G proteins classified by sequence homology of the α subunit (figure 1.7). There are currently 15 $G\alpha$ genes in the human genome (NCBI and UCSC databases) (table 1.2). G protein α subunits are N-terminally modified by the covalent attachment of the fatty acids myristate and/or palmitate (Nurnberg *et al.*, 1995).

There are five G protein β and ten G protein γ human subunit genes known to date (table 1.3), resulting in a large number of potential combinations of $G\beta\gamma$ dimers and effector pathways. All G protein γ subunits are C-terminally prenylated post-translationally: $G\gamma_t$, $G\gamma_8$ and $G\gamma_{11}$ with a 15-carbon farnesyl moiety, and the rest with a 20-carbon geranylgeranyl (Nurnberg *et al.*, 1995).

Gα class	Gα	Gene symbol and locus	Tissue distribution	Other protein names
Gs; stimulates the production of cAMP (or cGNP) from ATP (or GTP)	Gα _s	<i>GNAS1</i> 20q13.3	ubiquitous	secretogranin VI; GN regulatory protein; adenylate cyclase-stimulating G α protein; G protein α stimulating activity polypeptide1
	Gα _{olf}	<i>GNAL</i> 18p11.22- p11.21	olfactory neuro-epithelium	GN binding protein, α -subunit, olfactory type; GN binding protein (G protein), α activating activity polypeptide, olfactory type;
Gi; inhibit the production of cAMP (or cGMP) from ATP (or GTP)	Gα _{i1}	<i>GNAI1</i> 7q21	brain, spinal cord	Gi1 protein α subunit; GN binding protein (G protein), α inhibiting activity polypeptide 1;
	Gα _{i2}	<i>GNAI2</i> 3p21	blood cells, lung, muscle, placenta	GN binding protein (G protein), α inhibiting activity polypeptide 2; GTP-binding regulatory protein Gi α -2 chain;
	Gα _{i3}	<i>GNAI3</i> 1p13	blood cells	GN binding protein (G protein), α inhibiting activity polypeptide 3;
	Gα _o	<i>GNAO1</i> 16q13	brain	GN binding protein, α activating polypeptide O, A; CRA-a isoform
	Gα _{t1}	<i>GNAT1</i> 3p21	retinal rod cells	transducin α -1 chain; transducin, rod-specific; GN binding protein, α transducing activity polypeptide 1;
	Gα _{t2}	<i>GNAT2</i> 1p13.1	retinal cone cells	transducin α -2 chain; cone-type transducin α subunit; transducin, cone-specific, α polypeptide; GNB protein G(t), α -2 subunit; GN binding protein, α transducing activity polypeptide 2;
	Gα _z	<i>GNAZ</i> 22q11.22	predominately brain	GN binding (G protein), α z polypeptide;
Gq stimulates phospholipase C β	Gα _q	<i>GNAQ</i> 9q21	ubiquitous	GN binding protein (G protein), q polypeptide
	Gα ₁₁	<i>GNA11</i>	prostate, thyroid, heart, uterus, placenta, lung	GN binding protein (G protein), α 11
	Gα ₁₄	<i>GNA14</i> 9q21	spinal cord, thyroid, liver kidney, heart	GN binding 14 protein 14
	Gα ₁₅	<i>GNA15</i> 19p13.3	tissues of hematopoietic lineage	
G12 targets Rho family GTPase signaling	Gα ₁₂	<i>GNA12</i> 7p22.2	Ubiquitous	GN binding protein (G protein), α 12
	Gα ₁₃	<i>GNA13</i> 17q24.3	Ubiquitous	GN binding protein (G protein), α 13

Table 1.2. G protein α subunits classification and main pathways; guanine nucleotide (GN) Modified from Downes and Gautam, 1999.

G protein subunit	Gene symbol	Locus	Expression	Alternative names
Gβ1	<i>GNB1</i>	1p36.33	ubiquitous	transducin β; guanine nucleotide-binding protein G(I)/G(S)/G(T) β subunit 1; transducin β chain 1;
Gβ2	<i>GNB2</i>	7q22	predominantly blood cells	transducin β chain 2
Gβ3	<i>GNB3</i>	12p13.31	predominantly liver, brain	transducin β chain 3; hypertension associated protein β
Gβ4	<i>GNB4</i>	3q26.32	predominantly lung, placenta	transducin beta chain 4; G protein β-4 subunit;
Gβ5	<i>GNB5</i>	15q31.2	brain	GB5; transducin β chain 5; G protein, β subunit 5;
Gβ5L			retina	G protein, β subunit 5L
Gγ1	<i>GNGT1</i>	7q21.3	rod cells	GNG1
Gγc	<i>GNGT2</i>	17q21	cone cells, olfactory neuroepithelium, brain	GNG9; GNGT8; G- GAMMA-8; G-GAMMA-C; GNGT2
Gγ2	<i>GNG2</i>	14q21.1	brain	G protein γ subunit 2
Gγ3	<i>GNG3</i>	11p11	brain, testis	NBP gamma-3; G protein γ subunit 3
Gγ4	<i>GNG4</i>	1q42.3	brain, kidney, pancreas, skeletal muscle;	G protein γ subunit 4
Gγ5	<i>GNG5</i>	1p22	blood cells, lung, placenta, liver, heart	G protein γ subunit 5
Gγ7	<i>GNG7</i>	19p13.3	striatum, other tissues	G protein γ subunit 7
Gγ10	<i>GNG10</i>	9q31.3	ubiquitous	G protein γ subunit 10
Gγ11	<i>GNG11</i>	7q21	abundantly expressed in all tissues tested except for brain	GNGT11; G protein γ subunit 11
Gγ12	<i>GNG12</i>	1p31.3	kidney, placenta, lung, endocrine system, uterus, heart.	FLJ31352; G protein γ subunit 12

Table 1.3. Human G protein βγ subunits and their properties Modified from Downes and Gautam, 1999.

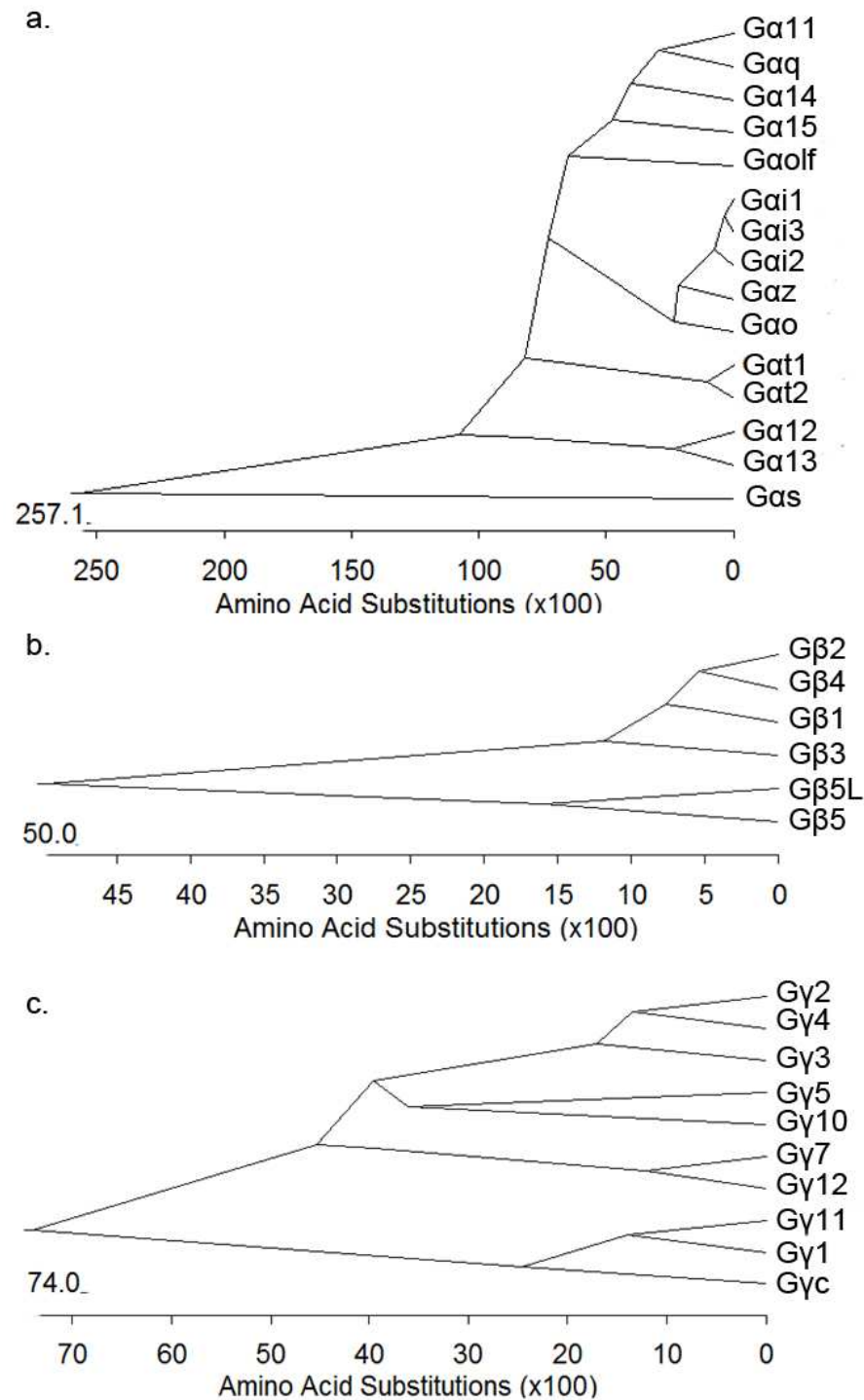


Figure 1.7. Phylogenetic tree of G protein subunits

Relationships among human G protein α subunits (**a**), β subunits (**b**) and γ subunits (**c**). The alignment was performed with ClustalW. Subunits are grouped by amino acid identity.

This lipid modification of the G γ polypeptide is believed to be important for the membrane localisation of the G $\beta\gamma$ dimer. G β subunits have not been shown to undergo such modifications, however it was demonstrated that some of them (G β t) could be targeted to the plasma membrane independently of the G γ subunit by an unknown mechanism (Chisari *et al.*, 2007).

Most G $\beta\gamma$ combinations can form functional heterodimers (Jones *et al.*, 2004) however, there are exceptions e.g. G β 2 can pair with G γ 2 but not G γ t (Schmidt *et al.*, 1992). Evidence supporting the role of specific G $\beta\gamma$ combinations in receptor coupling and effector activation is sparse but growing (Jones *et al.*, 2004). Most *in vitro* assays show little difference in receptor coupling profile or effector activation (reviewed by McCudden *et al.*, 2005).

However, there are some *in vivo* examples of the importance of specific G $\beta\gamma$ pairs for specific signaling pathways. Inhibition of low-voltage-activated T-type calcium channels is mediated selectively by G β 2 γ 2 (Wolfe *et al.*, 2003). G β 3 γ 3 was shown to be important for coupling the somatostatin receptor to voltage-sensitive L-type calcium channels, while G β 4 γ 4 was found to be required for coupling the muscarinic receptor to the same channels (Kleuss *et al.*, 1993).

G $\beta\gamma$ t, also called transducin $\beta\gamma$, interacts more robustly with rhodopsin and phosducin than other G $\beta\gamma$ combinations (Muller *et al.*, 1996). The Gat1 subunit, that is alternatively termed as transducin α , binding to the G $\beta\gamma$ t (transducin $\beta\gamma$) heterodimer forms a transducin complex (Gat-GDP-G $\beta\gamma$ t) which takes part in the phototransduction cascade.

1.2.3.3. Phototransduction cascade

Photoreceptors detect light through activation of a special type of GPCR proteins. In rod cells the GPCR is rod opsin (R), in cones by cone opsins. Like all GPCRs they have a typical seven TM domain structure with intracellular and extracellular loops (Palczewski *et al.*, 2000). However, unlike other GPCRs, they are covalently bound to their ligand 11-*cis* retinal via a Schiff base (Koutalos and Ebrey, 1986). 11-*cis* retinal is an antagonist for opsin, but it becomes an agonist when it undergoes photoisomerisation into *all-trans* retinal.

The phototransduction cascade will be described for the most studied opsin, rhodopsin (R) (figure 1.8).

11-*cis* retinal isomerisation triggers a rhodopsin conformational change and thus, starts the second step of the G protein signalling cascade. Activated R molecules (R*) interact with the GDP-bound form of a retina specific G protein, transducin $\alpha\beta\gamma$ trimers (Vuong *et al.*, 1984). The R* activates transducin by triggering of rapid exchange of GDP for GTP on the transducin α with rapid dissociation from the R*. At the same time active transducin α -GTP dissociates from transducin $\beta\gamma$ (Bruckert *et al.*, 1992) (figure 1.8).

During the third step of the phototransduction cascade transducin α -GTP stimulates the activity of its effector enzyme, the cGMP phosphodiesterase (PDE), also known as PDE6 (Gillespie and Beavo, 1989). The PDE is a heterotetramer consisting of two nearly identical catalytic subunits ($\alpha\beta$ in rods, $\alpha\alpha$ in cones) and two identical regulatory γ subunits (PDE γ) (Hamilton *et al.*, 1993). PDE γ serve as inhibitors of PDE activity and are responsible for maintaining basal activity at a low level.

Activation of the PDE heterotetramer results in removing the inhibitory constraint that PDE γ had imposed on the catalytic site of the PDE α or β subunits (Arshavsky and Bownds, 1992). This process causes a reduction in the cytoplasmic concentration of cGMP, which is the second messenger of the third step of phototransduction. This reduction in concentration causes closure of the cation selective cGMP-gated channels located in the plasma membrane (figure 1.8)

Closure of these channels reduces the steady inward current that is normally carried by Na^+ and Ca^{2+} ions in the dark. This results in membrane hyperpolarisation and decreased release of the synaptic transmitter glutamate in rods and glycine in cones at the synaptic terminal (Molday and Molday, 1998). The drop in the neurotransmitter concentration is detected by bipolar cells which generate a signal that is further processed in the retina and transmitted to the visual cortex (Vaney *et al.*, 1998).

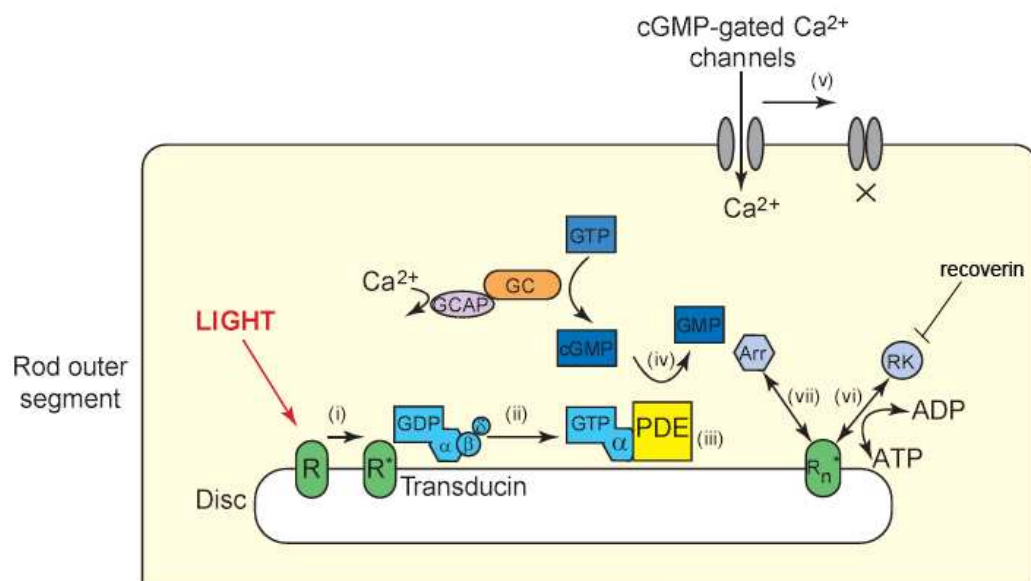


Figure 1.8. Phototransduction cascade in rods

Rhodopsin (R) is activated by light (R^*) (i) and causes transducin heterotrimer complex dissociation ($GDP\alpha\beta\gamma$) with the release of GTP-bound transducin α ($GTP\alpha$) (ii), which in turn activates the PDE complex (iii), resulting in the hydrolysis of cGMP to 5'-GMP (iv). The decrease in cGMP levels closes the cGMP-gated Ca^{2+} channels (v) in the plasma membrane of photoreceptors leading to a decrease in Ca^{2+} influx and the consequent hyperpolarisation of the cell. The desensitisation of rhodopsin ($R^* \rightarrow R_n^*$) is mediated by the phosphorylation of rhodopsin kinase (RK) (vi) with subsequent binding with arrestin (Arr) (vii) (adapted from Mendes *et al.*, 2005).

The recovery of phototransduction starts when the drop in intracellular calcium concentration activates rhodopsin kinase that phosphorylates R*. Further rhodopsin inactivation is completed by arrestin binding to the phosphorylated receptor.

Transducin inactivation is catalysed by specific GAPs, RGS4 and RGS9, returning the G protein to a GDP-bound state (Nekrasova *et al.*, 1997). Remarkably, RGS9 acts as a GAP in a complex with another retina specific G protein, G β 5 long isoform (G β 5L), and R9AP (Makino *et al.*, 1999). This process allows PDE α and/or β subunits to bind to γ inhibitory subunits (figure 1.8).

Moreover, the low calcium concentration activates retinal guanylate cyclase (RetGC) by its activating protein (GCAP) and thereby restores the concentration of cGMP. The cGMP-gated ion channels open and the photoreceptor returns to a depolarised state (figure 1.8). The intracellular concentration of calcium increases and promotes inhibition of rhodopsin kinase by recoverin.

1.2.3.4. Transducin

As described above, the G protein taking part in the phototransduction cascade is transducin. The synthesis of transducin subunits begins in the IS of the photoreceptors and are then transported to the OS in the dark (IS→OS) (described in section 1.2.3.5).

Structurally the transducin α subunit is composed of two domains: a nucleotide binding domain with high structural homology to the Ras-superfamily of GTPases, and an all- α -helical domain that, in combination with the Ras-like domain, helps to form a deep pocket for binding guanine nucleotide (figure 1.9a) (reviewed in Sprang, 1997). Transducin α contains three flexible regions designated switch-I, -II and -III that change conformation in response to GTP binding and hydrolysis (Lambright *et al.*, 1996). The GTP-bound conformation of transducin α results in decreased affinity for transducin $\beta\gamma$.

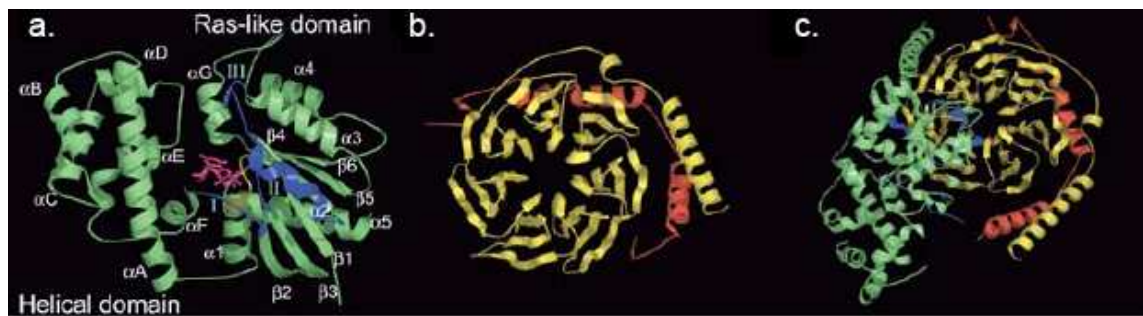


Figure 1.9. Structure of the transducin complex and its subunits

a. Ribbon diagram of the transducin α subunit (green) with the switch region highlighted in blue and a bound nucleotide is shown in pink (protein databank (PDB) 1TAD). **b.** Ribbon diagram of transducin $\beta\gamma$ heterodimer where the transducin β subunit is yellow and the transducin γ is red (PDB 1TBG). **c.** Ribbon diagram of transducin $\alpha\beta\gamma$ heterotrimer (subunits are colour coded as α – green, β – yellow, γ – red) (PDB 1GOT) (modified from Sondek *et al.*, 1996).

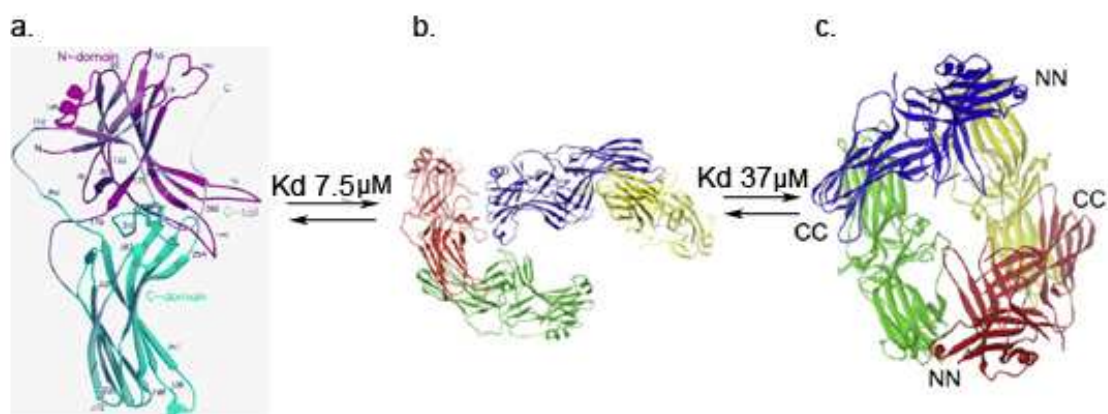


Figure 1.10. Rod arrestin structure and oligomerisation

a. Ribbon diagram of rod arrestin monomer with the N-domain shown in pink and C-domain in green (PDB 1CF1). **b.** One of the rod arrestin dimer states is shown with each arrestin monomer colour coded. **c.** Model of a representative structure from the rod arrestin largest cluster, which was identified as the best structural model. K_d are as indicated for dissociation of monomer/dimer and dimer/tetramer (Modified from Hirsch *et al.*, 1999 and Hanson *et al.*, 2008a).

Transducin $\beta\gamma$ is a functional heterodimer that forms a stable structural unit. The transducin β subunit contains seven WD-40 repeats, a tryptophan-aspartic acid sequence that repeats about every 40 amino acids and form antiparallel β strands (Neer *et al.*, 1994). Crystal structures of the transducin $\beta\gamma$ dimer and transducin trimer revealed that the seven WD-40 repeats of the transducin β subunit folds into a seven-bladed β -propeller or torus-like structure, while the N-terminus forms an α -helix (figure 1.9b) (Wall *et al.*, 2005; Sondek *et al.*, 1996). Transducin γ folds into two α -helices. The N-terminal helix forms a coiled-coil with the α -helix of transducin β , while the C-terminal helix makes extensive contacts with the base of the transducin γ -torus. Unlike the conformationally flexible transducin α subunit, the transducin $\beta\gamma$ dimer does not change conformation when it dissociates from the G protein heterotrimer (figure 1.9c) (Sondek *et al.*, 1996).

After synthesis, transducin undergoes lipid modifications. Rod transducin α is fatty acetylated at the extreme N-terminus Gly residue by lauroyl, myristoyl and tetradecaenoyls moieties (Neubert *et al.*, 1992) whereas cone transducin α is only myristoylated (Rosenzweig *et al.*, 2007). Transducin γ subunit is known to be prenylated and this modification is suggested to serve as a membrane anchor for transducin $\beta\gamma$ (Lai *et al.*, 1990; Saini *et al.*, 2007; Chisari *et al.*, 2007).

1.2.3.5. Arrestin

Arrestins are a family of proteins which shut down the G protein signalling pathway (described in 1.2.2.2). There are four types of arrestin in mammals reported by date: arrestin1 (called visual or rod arrestin, S-antigen or 48 kDa protein), arrestin2 (also known as β -arrestin or β -arrestin-1), arrestin3 (β -arrestin-2) and arrestin4 (cone arrestin or X-arrestin) (Gurevich and Gurevich 2006). Structurally and functionally the family can be divided into two subfamilies: visual or sensory (arrestin1 and arrestin4) and non-visual (arrestin2 and arrestin3) (Gurevich and Gurevich 2006).

In vertebrates, arrestins are encoded by large genes containing 14-17 exons, some of which are only 10 nucleotides long (Yamaki *et al.*, 1990). The multi-exon structure of vertebrate arrestins gives rise to splice variants of rod arrestin

and both non-visual subtypes (Sterne-Marr *et al.*, 1993). The protein products usually consist of two domains and a variable carboxyl-terminal tail.

Rod arrestin (p48) also has a short splice variant (p44) that lacks most of the carboxyl-terminal tail and has functional characteristics distinct from the longer variant, such as binding to unphosphorylated activated rhodopsin (Palczewski *et al.*, 1994). Other non-visual arrestins have been shown to have long and short forms which differ by 8 or 11 residues in the proximal carboxyl-terminal tail (Gurevich *et al.*, 1995). The functional significance of this is unclear.

Rod arrestin is the only arrestin from this family of proteins that invariably crystallises as a tetramer (Wacker *et al.*, 1987; Granzin *et al.*, 1998). Each monomer is composed of two domains: an N domain (residue 8–180) and a C domain (residue 188–362) (figure 1.10a). Each rod arrestin domain is constructed from a seven-stranded β sandwich and isolated N and C domains are functional (Gurevich *et al.*, 1993).

The N domain has a single α helix, while the C domain contains two short helices in a long loop that provides some of the interface between the two domains. The very carboxyl terminus of the protein or “C tail” (residues 372–404) is connected by a flexible linker (residues 362–371) to the C domain. The C “tail” contains a short stretch that forms a parallel β sheet interaction with the lateral strand of the N domain. In addition, the C tail makes other interactions with various parts of both the N and C domains (Hirsch *et al.*, 1999). Recently the crystal structure of the rod arrestin tetramer was solved (Hanson *et al.*, 2008). It demonstrated different conformational states of arrestin monomer/dimer/tetramer and described the final “diamond” crystal of arrestin tetramer (figure 1.10).

Rod arrestin is a soluble, predominantly cytoplasmic protein. Binding to phosphorylated active rhodopsin and termination of the phototransduction cascade was the first arrestin function described (Kuhn and Wilden, 1987). Phosphorylation of rhodopsin is the key to the interaction with arrestin: a single attached phosphate does not facilitate arrestin binding, two are necessary to induce high affinity interaction, and three phosphates fully activate arrestin (Vishnevetsky *et al.*, 2007).

Interestingly, rod arrestin binds to microtubules and rod arrestin domains have been demonstrated to have higher affinity to microtubules than full-length rod arrestin (Hanson *et al.*, 2006). The role of such binding to cytoskeleton elements is not clear, however it has been suggested to be a storage form of arrestin (Hanson *et al.*, 2008). The p44 isoform, lacking the C “tail” is known to have higher affinity for microtubules than the full-length protein (p48). Enhanced microtubule binding of p44 is suggested to underlie preferential localisation of p44 to detergent-resistant membrane microdomains, where it is anchored via membrane-associated microtubules in a rhodopsin-independent fashion (Nair *et al.*, 2002; Nair *et al.*, 2004).

1.2.3.6. Light dependent translocation of phototransduction cascade components

In order to prevent rod photoreceptor cells from over activating signal transduction under intense light, adaptation is necessary. Light driven translocations of signalling molecules have been suggested to contribute to photoreceptor cell adaptation in vertebrates and invertebrates (reviewed in Slepak and Hurley, 2008).

In vertebrate rod photoreceptor cells, recoverin (Strissel *et al.*, 2005), arrestin and transducin undergo light dependent translocation into and out of the OS (Broekhuysse *et al.*, 1985; Brann and Cohen, 1987). This phenomenon was first noted about two decades ago and has developed into an active field in photoreceptor cell biology. The adjustment of the protein composition in the outer segment may optimise the sensitivity and efficiency of the photoresponse (Strissel *et al.*, 2004).

It is known that 80-90 % of transducin in the dark state concentrates in the OS (Sokolov *et al.*, 2002). Within minutes of sufficient light illumination, 80 % of transducin moves from the outer segment to the inner segment of rod photoreceptor cells (OS→IS). In contrast, the return of transducin subunits to the outer segment in the dark takes much longer (Sokolov *et al.*, 2002). This process is more typical for rod rather than for cone transducin which was demonstrated to translocate only in response to very high intensity light (Chen *et al.*, 2007). Reciprocal to transducin movement, arrestin translocated during

dark adaptation into the inner segment and during light adaptation into the outer segment (IS→OS).

While the functional role of light dependent translocation is starting to be decrypted (Calvert *et al.*, 2006), the molecular and cellular mechanisms governing these adaptive movements through the cytoplasm is still elusive (Slepek and Hurley, 2008). There are reports of conflicting mechanisms. Two principle distinct mechanisms are possible by which signalling proteins could change their cellular compartment: by diffusion or by active transport mediated by molecular motors along with actin filaments or microtubules.

1.2.3.6.1. Diffusion hypothesis

Recent studies have suggested molecular diffusion as the major force for driving the intersegmental exchange of arrestin and transducin. Diffuse translocation of arrestin from IS→OS upon light illumination could be explained by its high affinity for activated phosphorylated rhodopsin (Strissel *et al.*, 2006). However, studies in mice deficient in rhodopsin phosphorylation and transducin activation demonstrated unaffected arrestin translocation upon light illumination (Mendez *et al.*, 2003).

For transducin the diffusion could be driven by membrane affinity to the disc membranes, which is very high in OS. Therefore, to translocate upon light exposure from OS→IS, transducin should lower its affinity for membrane binding. This process is suggested to be mediated by phosducin (figure 1.11) (Gaudet *et al.*, 1996).

Phosducin is abundant in the IS and has been shown to reduce affinity of transducin $\beta\gamma$ to the membrane by burying the C-terminal farnesyl group of transducin γ in a cleft of transducin β , preventing membrane localisation (Gaudet *et al.*, 1996; Loew *et al.*, 1998). Moreover, phosducin has been demonstrated to prevent re-association of transducin α with $\beta\gamma$ and thus, to facilitate transducin translocation (Sokolov *et al.*, 2004).

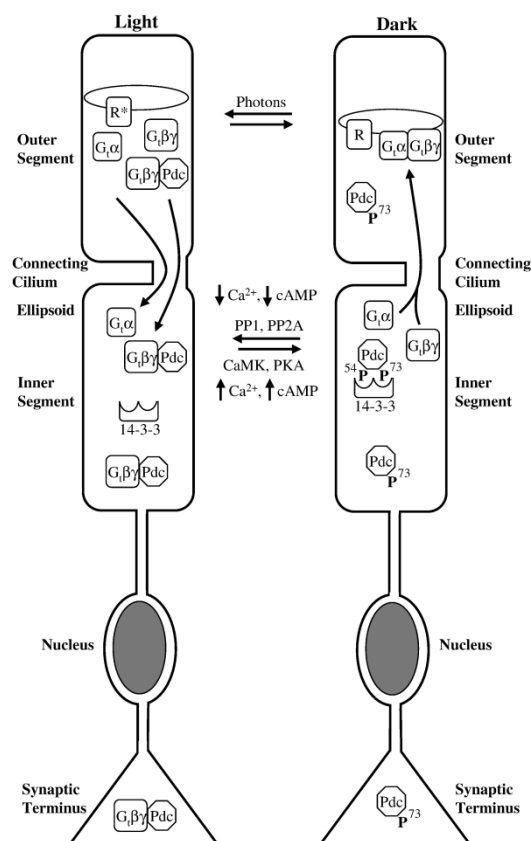


Figure 1.11. A model of phosducin function in transducin translocation

Upon light exposure, Ca²⁺ and cAMP concentrations in rod photoreceptors fall, resulting in dephosphorylation of phosducin by PP2A and PP1. Phosducin binds transducin βγ and maintains it in a soluble form, assisting its diffusion throughout the rod cell. Upon return to the dark, Ca²⁺ and cAMP concentrations rise, and phosducin is phosphorylated. Upon phosphorylation, 14-3-3 protein binds to phosducin and transducin βγ is released from complex with phosducin. Transducin βγ then reassociates with transducin α and either binds membranes in the ellipsoid region that are trafficking to the outer segment, or diffuses to the outer segment before binding to disc membranes there. R - rhodopsin; Gt α, β or γ – transducin subunits as indicated; Pdc - phosducin; P – phosphate (adapted from Willardson and Howlett, 2007).

1.2.3.6.2. Active transport hypothesis

Several studies support the hypothesis of an active molecular motor mediated mode of transducin transport during dark adaptation (IS→OS). It has been shown that transducin and arrestin translocation may be an energy-dependent process (Nair *et al.*, 2005; Reidel *et al.*, 2008; Marszalek *et al.*, 2000), suggesting it is motor-mediated. It was also demonstrated that siRNA of GAPDH in photoreceptors slowed transducin translocation during dark adaptation (Chen *et al.*, 2008). GAPDH is present in OS at high concentration and the energy required for ATP and GTP synthesis is likely to be derived from glycolysis in OS (Hsu and Molday, 1990). Therefore, the effect of GAPDH knock-down on transducin translocation could be due to an energy-dependent mechanism.

Using cytoskeleton disrupting drugs, it was proposed that the transport is dependent on microtubules and/or actin (Peterson *et al.*, 2005). The loss of the KIF3A subunit of kinesin-II caused impaired transport of arrestin (Marszalek *et al.*, 2000), suggesting it is mediated by IFT. Rod arrestin has been shown to be localised to the connecting cilium in dark adapted rods suggesting a role of this structure in dark adaptation (McGinnis *et al.*, 2002).

Active transport of transducin through the cilium has also been proposed. In dark adaptation (IS→OS), transducin-carrying vesicles or protein complexes may fuse at the periciliary ridge plasma membrane (described in section 1.2.2.3). The membrane surface in this region could then be utilised by IFT complexes to move transducin to the OS (reviewed in Roepman and Wolfrum, 2007). Diffusion of transducin through the inner lumen of the cilium is proposed to be controlled by Ca²⁺ binding proteins, centrins. They bind to transducin βγ in a Ca²⁺ dependent manner (Giessl *et al.*, 2006).

Recent reports on testing cytoskeleton disrupting drugs in *ex vivo* retina co-cultivated with RPE demonstrated that the translocation of both arrestin and transducin was disrupted only in dark adaptation and not in light adaptation. However, the drug which was used to destabilize microtubules (thiabendazole) surprisingly was not found to affect cilia (Reidel *et al.*, 2008), suggesting a possible role of other unknown non-cilia mediated mechanisms.

Interestingly, along with transducin, the RGS9--Gβ5L complex was found to translocate to the detergent-resistant membrane (DRM) microdomains upon light illumination (Nair *et al.*, 2002). It was demonstrated that the transducin α - RGS9 - Gβ5L complex had the highest affinity to detergent resistant membrane microdomains in the transition state of the GTPase. Phosphorylation of RGS9 was found to occur exclusively in such microdomains. Many other proteins of the phototransduction cascade were also found in DRM's. Rhodopsin and PDE were identified in DRM and non-DRM portions of the photoreceptor membrane whereas guanylate cyclase was present exclusively in the raft. Distribution of these proteins did not change in the light or dark (Nair *et al.*, 2002).

1.2.3.6.3. Calcium-myristoyl switch mechanism

Another protein that translocates from the OS to the IS upon light exposure in the retina is recoverin (Strissel *et al.*, 2005). Recoverin is a component of the phototransduction cascade and is responsible for the inhibition of rhodopsin kinase (figure 1.8) (Tanaka *et al.*, 1995). Recoverin has been shown to translocate via a calcium-myristoyl switch mechanism (Ames *et al.*, 1997). High levels of intracellular Ca^{2+} in the dark induce conformational changes leading to extrusion of the N-terminal myristoyl group on recoverin, enabling it to interact with the lipid bilayer membrane of OS discs (Tanaka *et al.*, 1995). When the calcium level drops upon phototransduction cascade activation, it causes the reverse effect and recoverin translocates to the IS.

1.3. Inherited retinal dystrophies

Inherited retinal dystrophies are both clinically and genetically heterogeneous disorders which affect 1 in 2000 people worldwide (Rivolta *et al.*, 2002). There are currently 192 loci with 144 disease causing genes identified (RetNet, <http://www.sph.uth.tmc.edu/Retnet/>, November 2008). Autosomal dominant, autosomal recessive, X-linked, digenic, mitochondrial and complex patterns of inheritance have been reported (Daiger *et al.*, 2007). Retinal dystrophies can also be classified by their clinical symptoms such as age of onset, severity and pattern of visual loss.

Genes in which mutations have been shown to result in retinal dysfunction or degeneration can be characterised by their expression profile. Some of them are expressed exclusively in the eye and are the components of the phototransduction cascade or visual cycle. Another group of proteins with ubiquitous expression patterns have been shown to cause retinal dysfunction alone or as a part of a syndromic disorder. A summary of some of the genes and the affected pathways implicated in retinal diseases is shown in table 1.4.

1.3.1. Retinitis pigmentosa

Retinitis pigmentosa (RP; OMIM #268000) is a subtype of retinal dystrophy featuring retinal pigment deposits and the loss of photoreceptors. The prevalence of RP is approximately 1/4000 people (Hamel, 2003). Non-syndromic forms of retinitis pigmentosa comprise approximately 65 % of all RP cases (Daiger *et al.*, 2007). There are currently 41 loci for non-syndromic RP with 32 causative genes identified (RetNet, November 2008). RP can be inherited as an autosomal dominant (approximately 20 %), an autosomal recessive (approximately 25 %) or X-linked condition (approximately 10-15 %). The remaining 40–55 % cases of RP are still to be classified (Wang *et al.*, 2005a).

Night blindness is the earliest symptom of RP which appears before morphological signs. Later as the disease progresses, morphological signs in the fundus occur. The fundus of patients with RP shows pigmentary deposits resembling bone spicules predominantly in peripheral retina where the rod cells are concentrated, attenuation of retinal blood vessels and waxy pallor of the optic disc. Clinically, patients suffer from visual field constriction with tunnel vision. As disease progresses, cone photoreceptors also degenerate resulting in blindness (Bird, 1975).

The first linkage study of RP revealed an XLRP locus, later identified as *RP2* (Bhattacharya *et al.*, 1984; Schwann *et al.*, 1998). The first RP causing gene identified was *RHO*, encoding rhodopsin (Driya *et al.*, 1990).

Pathway/ Function	Gene	Expression profile	Disease	First identified by
Visual cycle	<i>LRAT</i>	retina	arRP/arLCA	Thompson <i>et al.</i> , 2001
	<i>ABCA4</i>	retina	arRP/arCRD ar Stargardt	Creemers <i>et al.</i> , 1998
	<i>RPE65</i>	RPE	arRP/arLCA	Gu <i>et al.</i> , 1997
Photo Transduction	<i>PDE6A</i>	retina	arRP	Dryja <i>et al.</i> , 1999
	<i>PDE6B</i>	retina	arRP	Bayes <i>et al.</i> , 1995
	<i>RHO</i>	retina	adRP/arRP/ adCSNB	Dryja <i>et al.</i> , 1990
	<i>SAG</i>	retina	arRP/Oguchi	Yoshii <i>et al.</i> , 1998
photoreceptor structure	<i>RDS</i>	retina	adRP	Kajiwara <i>et al.</i> , 1994
retinal polarity	<i>CRB1</i>	retina, brain	arRP/arLCA	den Hollander <i>et al.</i> , 1999
extracellular matrix	<i>USH2A</i>	broad but not ubiquitous	ar Usher/arRP	Rivolta <i>et al.</i> , 2000
Transcription	<i>NRL</i>	retina	adRP/arRP	Bessant <i>et al.</i> , 1999
	<i>TULP1</i>	retina, brain	arRP/arLCA	Banerjee <i>et al.</i> , 1998
	<i>CRX</i>	retina, pineal gland	arLCA/adCRD	Freund <i>et al.</i> , 1997
cilia function	<i>RPGRIP</i>	retina, testis	arCRD/arLCA	Dryja <i>et al.</i> , 2001
	<i>RP1</i>	retina	adRP/arRP	Bowne <i>et al.</i> , 1999
	<i>BBS1-12</i>	ubiquitous	BBS	see table 1.5
mRNA splicing	<i>PRPF31</i>	ubiquitous	adRP	Vithana <i>et al.</i> , 2001
	<i>PRPF8</i>	ubiquitous	adRP	McKie <i>et al.</i> , 2001
	<i>PRPF3</i>	ubiquitous	adRP	Chakarova <i>et al.</i> , 2002
	<i>PAP1</i>	ubiquitous	adRP	Maita <i>et al.</i> , 2005
unknown function	<i>RP2</i>	ubiquitous	XLRP	Schwann <i>et al.</i> , 1998
	<i>RPGR</i>	ubiquitous	XLRP	Meindl <i>et al.</i> , 1995

Table 1.4. Examples of genes and pathways implicated in retinal degeneration

arRP – autosomal recessive retinitis pigmentosa; adRP - autosomal dominant retinitis pigmentosa; arLCA - autosomal recessive Leber congenital amaurosis; BBS – Bardet-Biedl syndrome (detailed table of mutations 1.3), XLRP- X-linked retinitis pigmentosa.

1.3.1.1. X-linked retinitis pigmentosa

X-linked retinitis pigmentosa (XLRP) is the most severe form of RP with early onset and fast disease progression leading to blindness by 40 years of age (Bird, 1975). There are six RP loci on the X-chromosome and for four of them the causative gene is not known. However, causative genes were found for two loci. The *retinitis pigmentosa 2* gene (*RP2*) (Schwann *et al.*, 1998) will be described in section 1.5. The other identified XLRP gene is the *retinitis pigmentosa GTPase regulator* (*RPGR*, *RP3*) (Meindl *et al.*, 1995; Roepman *et al.*, 1996).

1.3.1.1.1. Retinitis pigmentosa GTPase regulator

The retinitis pigmentosa GTPase regulator (*RPGR*, *RP3*) protein is encoded by the *RPGR* gene spanning approximately 60 kb on the X-chromosome (locus Xp11.4). Originally, *RPGR* was described to have 19 exons and *RPGR* protein was found to be ubiquitously expressed (Meindl *et al.*, 1995). However, later studies revealed the presence of an alternative exon, ORF15, where most of the disease causing mutations are located (Vervoort *et al.*, 2000). The isoform produced by alternative splicing to contain ORF15 was demonstrated to be expressed preferentially in the retina and testis, suggesting a possible retina specific role (Vervoort *et al.*, 2000). This isoform was shown to be able to fully substitute for *RPGR in vivo* (Hong *et al.*, 2003).

The *RPGR* protein contains three 'regulator of chromosome condensation' domains (RCC1) in its N-terminus (protein families database (PFAM) [00415](#)) within one large α -tubulin suppressor domain (ATS1) (PFAM [COG5184](#)). RCC1 is a guanine nucleotide exchange factor (GEF) for a small GTP-binding protein RAN. Some of the XLRP causing mutations, which are not located in ORF15, were found in this domain, suggesting its importance for disease pathogenesis (Meindl *et al.*, 1995).

The region of *RPGR* homologous to RCC1 was investigated for interacting partners using a yeast-two hybrid approach. It was revealed that *RPGR* bound to a retina and testis specific protein named retinitis pigmentosa GTPase regulator interacting protein 1 (*RPGRIP1*) (Roepman *et al.*, 2000; Boylan *et al.*,

2000). Later, mutations in the gene encoding this protein were found to cause Leber congenital amaurosis (LCA) and cone-rod dystrophy (CRD) (Driya *et al.*, 2001; Gerber *et al.*, 2001; Hameed *et al.*, 2003).

RPGR and RPGRIP1 have been shown to localise to the photoreceptor connecting cilia (described in section 1.2.3.2) (Hong *et al.*, 2003; Hong *et al.*, 2005; Shu *et al.*, 2005). Studies in mice demonstrated that knock-down of *Rpgrip1* disrupted cilia localization of RPGR (Pawlyck *et al.*, 2005), suggesting that RPGRIP1 tethers RPGR to this structure highlighting the importance of the interaction with this retina specific protein. RPGR was also shown to bind nucleophosmin 1 (NPM), a nuclear chaperone involved in chromosome duplication (Shu *et al.*, 2005).

Recently, a homologue of RPGRIP1 was identified RPGRIP1-like (RPGRIP1L) (Arts *et al.*, 2007). It was shown to localise to the cilia although it demonstrated a ubiquitous expression level. Mutations in the gene encoding this protein were found to cause Joubert syndrome, a ciliopathy with developmental defects and mainly affecting the kidneys (described in 1.3.2) (Delous *et al.*, 2007).

Mutations in RPGR were also demonstrated to cause a syndromic form of retinitis pigmentosa with impaired hearing and sinorespiratory infections (Zito *et al.*, 2003). Interestingly, mutations in RPGR also cause cone cell death resulting in cone-rod dystrophy (Demicri *et al.*, 2002; Yang *et al.*, 2002).

Thus, the mechanism by which mutations in RPGR result in RP remains to be discovered but the data suggest is that RPGR has a role in an important retina specific cilia mediated pathway.

1.3.2. Syndromic forms of retinitis pigmentosa

Syndromic RP comprises approximately 35 % of all RP cases and can be found as a part of hereditary syndrome such as Bardet-Biedl syndrome (OMIM [209900](#)), Fahr disease (OMIM [213600](#)), Usher's syndrome (OMIM [276900](#)), Refsum's disease (OMIM [266500](#)), Senior-Loken syndrome (OMIM [266900](#)), Alstrom syndrome (OMIM [203800](#)), Sjogren-Larsson syndrome (OMIM [270200](#)), mitochondrial encephalomyopathy (OMIM [256000](#)), Kearns-Sayre

syndrome (OMIM 530000), medullary cystic renal disease (OMIM 174000), Mirhosseini-Holmes-Walton syndrome (OMIM 268050), and tapetochoroidal dystrophy (OMIM 303100). This group of disorders is very heterogeneous and implicates a variety of molecular/cellular pathways.

1.3.2.1. Ciliopathies

It is now recognised that certain forms of syndromic RP can be classified as ciliopathies. Primary cilia are found not only in photoreceptors but in a number of organs, such as the liver and pancreas, as well as numerous cell types, including endothelial cells, the myocardium, cortical and hypothalamic neurons (list of cells and tissues containing cilia <http://members.global2000.net/bowser/cilialist.html>). Consistent with the broad and varied tissue and cellular distribution, dysfunction of cilia and the basal body has been implicated in numerous human diseases. Diseases in which the motile and/or sensory cilia are affected, such as Bardet-Biedl syndrome (BBS), Usher's, Alstrom (ALMS), Senior-Loken syndromes and medullary cystic renal disease, include retinitis pigmentosa as part of their phenotype.

1.3.2.2. Bardet–Biedl syndrome

Bardet–Biedl syndrome (OMIM 209900) is an autosomal recessive inherited disorder and one of the most studied ciliopathies. It is characterised by renal abnormalities, central obesity, postaxial polydactyly, mental retardation, hypogonadism, anosmia and RP. Other features, not always present, include hepatic fibrosis, diabetes mellitus, endocrinological disturbances, short stature, developmental delay, and speech deficits (Beales *et al.*, 1999).

There are twelve disease causing genes identified to date, BBS1-12 (summarised in table 1.5). Protein products of genes causing BBS6, BBS10 and BBS12 belong to a novel branch of the type II chaperonin superfamily, but they are considered unlikely to assemble in a complex, similar to cytosolic chaperonin (CCT) (described in section 1.5.2) (Stoetzel *et al.*, 2007).

Causing Gene	Locus	Protein feature	Reference
<i>BBS1</i>	11q13	unknown function	Leppert <i>et al.</i> , 1994
<i>BBS2</i>	16q21	unknown function	Kwitek-Black <i>et al.</i> , 1993
<i>BBS3 (Arl6)</i>	3p13-p12	small GTPase	Sheffield <i>et al.</i> , 1994; Ghadami <i>et al.</i> , 2000
<i>BBS4</i>	15q22.3-q23	adaptor for p150 subunit of dynein complex cilia localisation	Carmi <i>et al.</i> , 1995 Kim <i>et al.</i> , 2004
<i>BBS5</i>	2q31	unknown	Young <i>et al.</i> , 1999
<i>BBS6</i>	20p12	chaperonin-like	Slavotinek <i>et al.</i> , 2000
<i>BBS7 (BBS2-like)</i>	4q26-q27	homologue of BBS1 and BBS2	Badano <i>et al.</i> , 2003
<i>BBS8 (TTC8)</i>	14q32.11	contains 8 TPR domains, involved in centriolar replication during ciliogenesis	Ansley <i>et al.</i> , 2003 Kubo <i>et al.</i> , 1999
<i>BBS9 (PTHB1)</i>	7p14	PTH-responsive	Nishimura <i>et al.</i> , 2005
<i>BBS10 (C12ORF58)</i>	12q 21.2	chaperonin-like	Stoetzel <i>et al.</i> 2006
<i>BBS11 (TRIM32)</i>	9q31-q34.1	putative E3 ligase	Chiang <i>et al.</i> , 2006 Kudryashova <i>et al.</i> , 2005
<i>BBS12 (C4ORF24)</i>	4q27	chaperonin-like	Stoetzel <i>et al.</i> 2007

Table 1.5. Genetic heterogeneity of Bardet-Biedl syndrome

TPR – tetratricopeptide repeat, PTH – parathyroid hormone.

BBS6, 10 and 12 are thought to perform cilia-related functions with special importance for the photoreceptor connecting cilia. BBS6 was also shown to be a centrosomal component required for cytokinesis (Kim *et al.*, 2005). Apart from homology to CCT, BBS10 also has an ATP binding site suggesting that it is a bona fide chaperonin (Stoetzel *et al.*, 2006). Recently, another putative chaperone, BBS12, causing Bardet-Biedl syndrome was identified. BBS12 is highly similar to group II chaperonins except the ATP-binding region is not conserved, similar to the BBS6 protein (Stoetzel *et al.*, 2007). Suppression of each BBS6, 10 or 12 in zebrafish yielded gastrulation-movement defects characteristic of other BBS morphants, whereas simultaneous suppression of all three chaperonin-like BBS proteins resulted in severely affected embryos, possibly hinting at partial functional redundancy between these proteins (Stoetzel *et al.*, 2007). Thus, some of the proteins causing BBS have high homology to group II chaperonins, demonstrating the conservation with the cytosolic chaperonin domain architecture. Meanwhile, they have specific insertions, probably giving these proteins another chaperone function that is critical for ciliated cells.

1.3.3. Oguchi disease

Mutations in the *SAG* gene, encoding rod arrestin, cause an autosomal recessive form of RP (Yoshii *et al.*, 1998) and a special type of a rare autosomal recessive congenital stationary night blindness, Oguchi disease (OMIM [258100](#)). The condition is associated with golden fundus discolouration and abnormally slow dark adaptation. After 2 or 3 hours in total darkness, the normal colour of the fundus returns (Usui *et al.*, 2004).

Fuchs and colleagues (1995) first reported that a homozygous frame shift mutation (1147delA) in the *SAG* gene was detected in 5 out of 6 unrelated Japanese patients with Oguchi's disease. The condition is more frequent in Japanese than other nationalities, however it was also found in an Indian family with a stop codon mutation at codon 193 in *SAG* (Maw *et al.*, 1998). However, it was shown later that a more frequent cause of this disease is mutations in rhodopsin kinase gene *GRK1* (Yamamoto *et al.*, 1997).

The reason why the same mutation in the SAG gene leads to Oguchi disease in one patient and to retinitis pigmentosa in another patient is not identified. There was a case reported that one male patient had the typical Oguchi phenotype in both his eyes, however, his brother had a typical Oguchi phenotype in one eye and retinitis pigmentosa in the other eye (Yoshii *et al.*, 1998). Therefore, the mechanism of retinal degeneration caused by mutations in arrestin is to be elucidated.

1.3.4. Cone-rod dystrophy

Cone-rod dystrophies (CRD) (prevalence 1/40,000) belong to a group of central retinal disorders with pigmentary deposits predominantly localized to the macular region (Hamel, 2007). Symptomatically, CRD is different to RP. The first symptom of CRD is usually decreased visual acuity (age of onset ranging from first decade to the sixties), hypersensitivity to bright lights, and poor color vision. Color vision testing usually reveals many errors on both red-green and blue-yellow plates (reviewed in Hamel, 2007). Therefore, patients see better at dusk and have progressive difficulty with daytime vision. Visual acuity usually deteriorates gradually, but it can deteriorate rapidly. Later, in more severe cases, it drops to “counting fingers” vision. Usually with disease progression patients suffer from a loss in peripheral vision and night blindness as a result of rod cell death.

CRDs are most frequently non syndromic, but they have been reportedly associated with several syndromes such as Bardet Biedl syndrome and Spinocerebellar Ataxia Type 7 (Beales, 1999; Aleman *et al.*, 2002). Non syndromic CRDs are genetically heterogeneous. There are currently 8 known causative genes for CRD identified and 14 loci mapped (RetNet, November 2008). The most studied causative genes involved in the pathogenesis of CRDs is *ABCA4*, which causes Stargardt disease and also 30 to 60 % of autosomal recessive CRDs (Cremers *et al.*, 1998, Hamel, 2007). Other genes are cone-rod homeobox-containing gene *CRX* and retinal guanylate cyclase (*GUCY2D*), responsible for many reported cases of autosomal dominant CRDs (Freund *et al.*, 1997; Gregory-Evans *et al.*, 2000). RPGR is known to cause an undetermined percentage of X-linked CRDs (described in 1.3.2.1.1).

1.3.4.1. Unc 119

Higashide and colleagues (1996) identified a retina-specific cDNA (*HRG4*, human retinal gene-4) that is now known as *UNC119*. Sequence comparison between species revealed that the human gene had 57 % homology with *Caenorhabditis elegans* Unc-119 (Higashide *et al.*, 1998). The *UNC119* gene was mapped to chromosome 17q11.2 and was shown to consist of five exons (Higashide *et al.*, 1999). The 240-amino-acid encoded protein (NP [005139](#)) has a two-domain structure consisting N-terminal region (amino acids 1-78) predicted to interact with other proteins (Higashide *et al.*, 1998) and PDE δ subunit homology domain (amino acids 79-198) (PFAM [05351](#)), which is highly conserved between species.

Unc119 protein was localised to the synaptic termini of rod and cone photoreceptors (Higashide *et al.*, 1998) and to the basal body of the connecting cilium (Li *et al.*, 2004). Unc119 was found to bind at least two small GTPases ADP-ribosylation factors 2 and 3 (Arl2 and Arl3, described in 1.7) (Kobayashi *et al.*, 2003; Linari *et al.*, 1999). Interestingly, both GTPases bind to PDE δ , which is homologous to Unc119 (Linari *et al.*, 1999).

An *UNC119* heterozygous mutation creating a stop codon was associated with late onset cone-rod dystrophy in one family (Kobayashi *et al.*, 2000). This *Unc119* mutation was reproduced in a knock-in mouse model and the transgenic animals exhibited retinal degeneration (Kobayashi *et al.*, 2000; Ishiba *et al.*, 2007).

1.3.5. Leber congenital amaurosis

Leber congenital amaurosis (LCA) (OMIM [204000](#)) is a rare autosomal recessive severe retinal dystrophy with an incidence of approximately 1/80,000 (Sohocki *et al.*, 2000). The disease is genetically and clinically heterogeneous with 9 known loci of which 7 have the causative genes identified (RetNet, reviewed in Kaplan, 2008). These disease genes causing LCA are diverse and include ones of the visual cycle and phototransduction such as *RPE65* (Morimura *et al.*, 1998) and *retinal guanylate cyclase* (Perrault *et al.*, 2004).

Recently, another LCA causing gene was identified, *LCA5* (den Hollander *et al.*, 2007). The protein product of this gene, lebercilin, is ubiquitous and is localised to cilia, and the reason why mutations in this gene do not cause syndromic form of retina degeneration is not yet known (den Hollander *et al.*, 2007).

Another LCA causing gene is *AIPL1*. The AIPL1 protein is expressed only in the pineal gland and retinal photoreceptors (van der Spuy *et al.*, 2002). AIPL1 is named based on its similarity (49 % amino acid identity) with the aryl hydrocarbon receptor (AhR)-interacting protein (AIP) (Kuzhandaivelu *et al.*, 1996; Carver and Bradfield, 1997). These proteins share the common co-chaperone tetratricopeptide repeat (TPR) motif that mediates protein-protein interactions, suggesting that AIPL1 may be a member of the family of TPR co-chaperones.

This suggestion was supported by a recent study showing that AIPL1 interacted with the molecular chaperones Hsp90 and Hsp70 (described in section 1.4.1). Mutations within the TPR domain of AIPL1 or removal of the chaperone TPR acceptor site abolished the interactions. Importantly, LCA-causing mutations in AIPL1 also compromised these interactions, suggesting that the essential function of AIPL1 in photoreceptors may involve the interaction with Hsp90 and Hsp70 (Hidalgo-de-Quintana *et al.*, 2008). The client proteins of AIPL1 remain to be defined but studies in mouse models suggest that cGMP PDE subunits are possible retina specific candidates (Liu *et al.*, 2004).

1.4. Molecular chaperones

Molecular chaperones are a class of proteins that assist the non-covalent folding and assembly of other macromolecular structures without being part of the finished product (Ellis & van der Vies 1991). One major function of molecular chaperones is to prevent both newly synthesised polypeptide chains and assembled proteins from aggregating into nonfunctional structures. The primary amino acid sequence of a polypeptide contains sufficient information to direct its folding to the native state (Anfinsen, 1973). However, under cellular conditions, which feature high macromolecular solute concentrations, misfolding can occur. Misfolding usually results in exposure of hydrophobic surfaces that

should have become buried in the interior of a protein in its native state. Molecular chaperones bind such exposed surfaces through their own hydrophobic binding sites, thus preventing misfolding and aggregation and ultimately releasing bound proteins to allow them to proceed with further steps of biogenesis (reviewed in Ellis, 2007).

1.4.1. Heat shock proteins

A study by Tissieres and colleagues (1974) demonstrated a rapid and selective increase in the expression of a group of proteins, following heat exposure of *Drosophila melanogaster* larvae. These proteins were termed heat-shock proteins (Hsps) and were annotated by molecular weight; Hsp100, Hsp90, Hsp70, Hsp60, Hsp40, and small heat-shock protein (sHsp) families (Chang et al. 2007a; Tang et al. 2007). Many subsequent studies revealed that a large number of other cell stresses could lead to very similar changes in gene expression (figure 1.12) (reviewed in Georgopoulos and Welch, 1993).

Genes encoding chaperone proteins are of three regulatory classes: i) constitutively expressed and regulated during growth and development, ii) constitutive and inducibly regulated, and iii) strictly inducible. The expression of some chaperones is essential for normal growth and development and to survive stress (reviewed in Morimoto, 2008). One of the best characterised stress proteins is the Hsp70 family.

1.4.1.1. Heat shock proteins 70 kDa.

The 70 kDa heat shock proteins (Hsp70s, HSPA) are a family of ubiquitously expressed heat shock proteins found in most living organisms. Prokaryotes express three Hsp70 proteins: DnaK, HscA (Hsc66), and HscC (Hsc62). Eukaryotic organisms express several slightly different Hsp70 proteins and they share a common domain structure. The family of Hsp70 proteins in humans is currently described to have 12 members (Kampinga *et al.*, 2008).

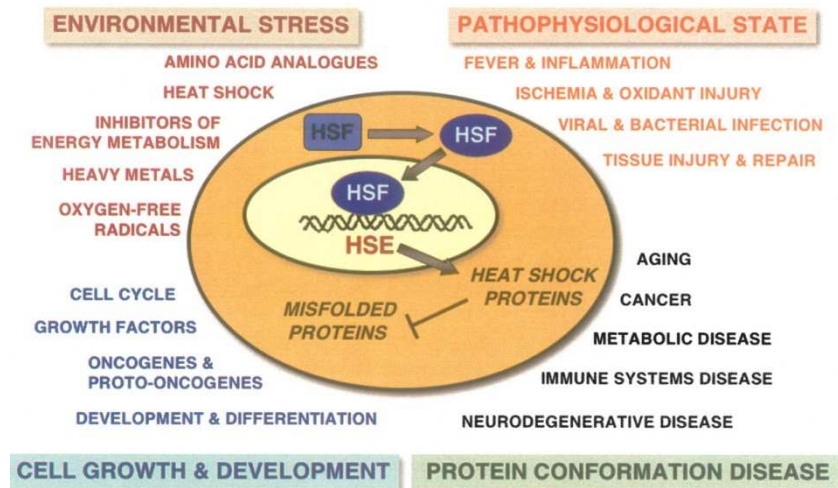


Figure 1.12. Conditions that induce the heat shock response

Heat shock gene expression is activated by heat shock factors (HSF) and binding to heat shock effectors (HSE) results in the elevated expression of heat shock proteins (from Morimoto, 2008).

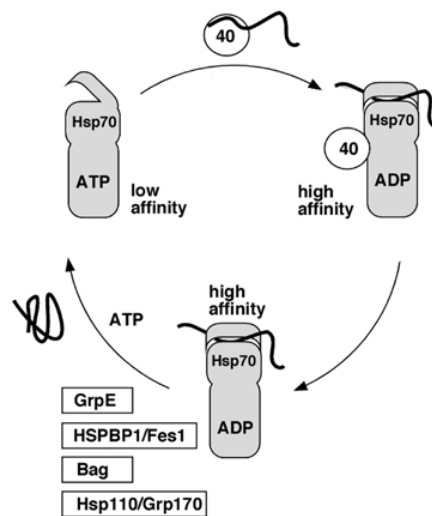


Figure 1.13. The Hsp70 protein-folding cycle

Hsp70 is shown in gray, with the substrate-binding domain on top. The hinged lid is shown open or closed to indicate low- and high-affinity substrate-binding states. Substrate protein is depicted as an extended line in the "unfolded" state, and a compact shape in the "folded," or native state. Hsp70 ATPase activating proteins (40) are depicted as circles, nucleotide exchange factor proteins are shown as rectangles (from Morano, 2007).

All Hsp70 molecules share a conserved architecture consisting of an N-terminal 44 kDa adenine nucleotide-binding domain (NBD, ATPase domain) and a 27 kDa carboxy-terminal substrate/peptide-binding domain (SBD, or PBD). This region can be further divided by an 18 kDa domain, “lid”, whose conformation dictates substrate-binding affinity (Morshauser *et al.*, 1999). The interdomain linker connecting the NBD and SBD is highly conserved and plays an important role in the allosteric switch mechanism controlling Hsp70 chaperone function (Vogel *et al.*, 2006). Hsp70s are known to exist in two stable conformations, regulated by ATP binding to the NBD. Cycling between these two states is controlled by nucleotide binding, hydrolysis and release results in substrate folding (figure 1.13).

A number of co-chaperones have been described that modulate Hsp70 ATPase activity. The best studied among these are Hsp40 proteins, containing a J-domain. J-domain proteins bind to EEVD motif at the C-terminus of Hsp70 (Freeman *et al.*, 1995). This interaction stimulates Hsp70 ATPase activity, thus accelerating substrate-folding reactions (Cheetham *et al.*, 1994; Minami *et al.*, 1996). Hsp40 proteins also bind substrates and in at least some folding scenarios are responsible for initial presentation of the unfolded protein to Hsp70 (reviewed in Morano, 2007). Another group of co-chaperones of Hsp70 function as nucleotide exchange factors (NEFs), stimulating the release of bound ADP for ATP to release a client protein and to initiate a new folding cycle (figure 1.13).

Hsp70s have also been found to have non-folding roles. It has been reported that together with the co-chaperone, CHIP, Hsp70 promotes protein degradation by 26S proteasome (Elliot *et al.*, 2007). Hsp70 proteins have also been shown to be a crucial component in chaperone-mediated autophagy (Dice *et al.*, 1990). Hsp70 is known to inhibit caspase activation and thus, protect from apoptotic cell death (Zhou *et al.*, 2001).

Hsp70 can also be excreted by some cells upon heat shock and could be internalised by other cells protecting them from cell death (Guzhova *et al.*, 2001; Novoselova *et al.*, 2005). Extracellular Hsp70 can act as cytokine binding to Toll-like receptors (TLR)-2 and -4 on antigen presenting cells (Arnold-Schild *et*

al., 1999; Asea *et al.*, 2002). Numerous publications support the theory that Hsp70 is a chaperokine acting as an initiator of immune response (reviewed in Asea, 2008).

1.4.2. **Cytosolic chaperonin**

The chaperonins, a sub-group of molecular chaperones found in virtually all organisms, comprise a family of ATPases of approximately 60 kDa that assemble into twin rings, stacked back-to-back, with a large central cavity where unfolded polypeptides may bind and undergo productive folding (Ranson *et al.*, 1998). Based on their evolutionary origin, chaperonins can be grouped into two distinct classes. Type I chaperonins, found in the bacterial cytosol and in endosymbiont-derived organelles of eukaryotes, form heptameric rings and are represented by bacterial GroEL, mitochondrial hsp60, and chloroplast cpn60. Type II chaperonins, present in the eukaryotic cytoplasm and in archaea, include the archaeal thermosome and the eukaryotic cytosolic chaperonin (CCT, chaperonin containing TCP-1) (Frydman *et al.*, 1992).

CCT is composed of two rings of eight different subunits. Each subunit consists of three domains: an equatorial domain containing a nucleotide binding site; an intermediate connector domain; an apical domain responsible for binding to the target protein and closure of the chaperonin cavity. CCT adopts at least two conformations, an ADP or nucleotide free conformation and an ATP-bound state when its cavity is closed (Gao *et al.*, 1992; Llorca *et al.*, 1998).

In mammalian cells, the main function of CCT is folding of cytoskeletal components such as actin and α -, β - tubulins. Unlike most other chaperones, which recognise substrates only by exposed hydrophobic residues, CCT is able to bind the substrate via discrete binding determinants, which explains the high substrate specificity of CCT-mediated folding (Llorca *et al.*, 1999; Ritvo-Vonsovici and Willinson, 2000). CCT does not function in isolation but works in conjunction with another molecular chaperone named prefoldin (PFDN; GimC) (Vainberg *et al.*, 1998) and the tubulin folding cofactors (see section 1.4.4).

1.4.3. Prefoldin

Prefoldin (PFDN) is a heterohexameric protein that exists in archaeobacterial and eukaryotic organisms (Stirling *et al.*, 2006a). In the case of archaeal PFDN, the chaperone contains two different proteins (i.e. two α -subunits and four β -subunits). However, in eukaryotes, PFDN exists as a more complex oligomer assembled from six different proteins, two of which are α -like and four of which are β -like (Leroux *et al.*, 1999).

The complex is arranged into an “octopus”-like structure where α -like subunits (PFDN3 and PFDN5) are located in the centre, while the four β -like subunits (PFDN1, PFDN2, PFDN4 and PFDN6) are at the periphery (Martin-Benito *et al.*, 2002). The coiled-coils of PFDN subunits form “tentacles” of the complex, which capture the substrate, non-native α -, β -, γ - tubulins, actin, or Cdc20 (Leroux *et al.*, 1999). The non-native substrate is bound by PFDN without using chemical energy (e.g. ATP) and transported to CCT which transforms the substrate into a native state by rounds of ATP-dependent folding (Siegert *et al.*, 2000).

Recently, an antagonist to PFDN complex was identified. It is a novel co-chaperone of the CCT complex phosducin-like protein 3 (PhLP3). It binds CCT and significantly diminishes the chaperonin ATPase activity, and accordingly, excess PhLP3 perturbs actin or tubulin folding *in vitro* (Stirling *et al.*, 2006b).

1.4.4. Tubulin folding cofactors and tubulin folding pathway

Tubulin, a major component of microtubules, is a heterodimer of α - and β -tubulin. The initial steps of tubulin folding are assisted by CCT and PFDN as described above. After folding by CCT, tubulin subunits require the action of cofactors to form the tubulin heterodimer. In mammals five such cofactors have been identified which are involved in the folding and association of tubulin *in vitro* (Tian *et al.*, 1995; Lewis *et al.*, 1997, Bartolini *et al.*, 2005). The specific role of each cofactor in tubulin folding is yet not fully understood, but the following model has been proposed (figure 1.14) (Bhamidipati *et al.*, 2000).

Nascent chains of tubulin polypeptides are captured by the PF1D1 complex and then guided to CCT for ATP-dependent folding. Cofactor A (CoA) then binds to β -tubulin and cofactor B (CoB) to α -tubulin monomers. These cofactors are suggested to be a reservoir for excess β - and α -tubulin. These complexes transfer the tubulin subunits to cofactors E and D (CoE and CoD) (figure 1.14). At this point cofactor C (CoC) binds to the CoE, CoD and β -tubulin complex.

Hydrolysis of GTP to GDP acts as a switch mechanism for the release of the native tubulin heterodimer that can polymerise into microtubules once GDP has been exchanged for GTP (figure 1.14). Cofactor D (CoD), cofactor E (CoE) and cofactor C (CoC) are also able to disrupt tubulin dimers and thus depolymerise microtubules (Bhamidipati *et al.*, 2000).

The tubulin folding pathway is proposed to be regulated by ADP-ribosylation factors (Arf)-like proteins such as Arl2 (figure 1.14). Arl2 was shown to regulate the binding of CoD to tubulin and microtubule destabilisation induced by overexpression of CoD in mammalian cells could be rescued by co-expression of Arl2 (Bhamidipati *et al.*, 2000).

Another protein which is proposed to be involved in tubulin folding pathway regulation is gigaxonin. Mutations in the gene encoding this protein were shown to cause giant axonal neuropathy (Bomont *et al.*, 2000). One of the features of disease is reduced levels of microtubules (Bomont *et al.*, 2003). Gigaxonin was shown to interact with CoB and to target it for proteasomal degradation (figure 1.14) (Wang *et al.*, 2005b).

Tubulin folding cofactors are described to have homologues. For instance, a homologue of cofactor E, cofactor E-like protein, is known to depolymerise microtubules by committing tubulin to proteasomal degradation (Bartolinini *et al.*, 2005). Cofactor C is suggested to have several homologues (Stephan *et al.*, 2007) and one of them is retinitis pigmentosa 2 (RP2) protein (Bartolini *et al.*, 2002).

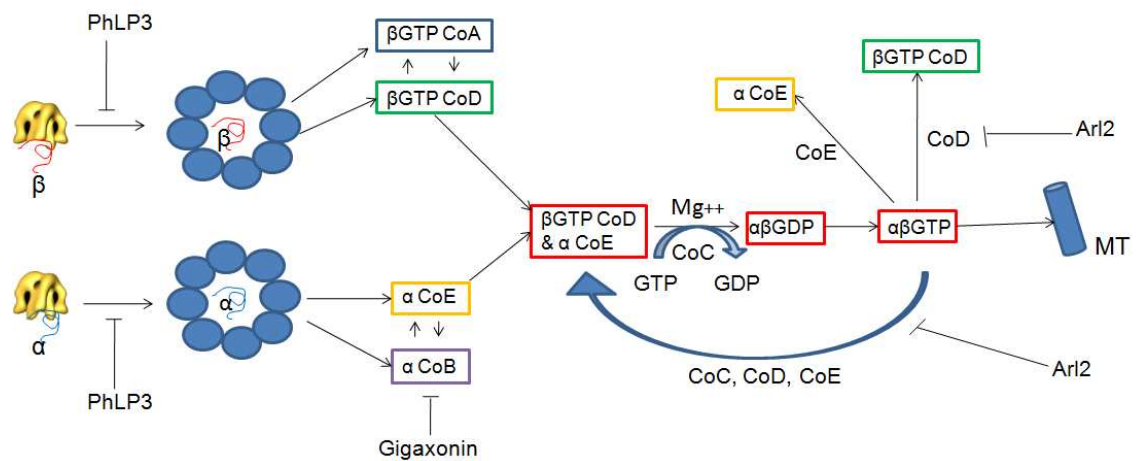


Figure 1.14. Model of the tubulin heterodimer assembly

Schematic showing the proposed mechanism by which nascent chains of α and β tubulin are folded and incorporated to form microtubules. The nascent chains of tubulin polypeptides are shown as blue and red lines. PFDN complex is shown as yellow octopus-like shape. PFDN delivers tubulin peptides to CCT for further ATP-dependent folding. This step is regulated by phosphducin-like protein 3 (PhLP3). CCT is depicted as a ring of eight subunits (blue circles). After folding by CCT, tubulin folding cofactors (shown as blue, green, yellow or purple colour-coded boxes as indicated) assist in formation of tubulin heterodimers from tubulin monomers. Red boxes indicate tubulin heterodimers. The involvement of Arl2 and gigaxonin in the regulation of cofactor activity is also shown. Modified from Bhamidipati *et al.*, 2000; Vainberg *et al.*, 1998; Wang *et al.*, 2005b; Stirling *et al.*, 2006b.

1.5. RP2

RP2 mutations cause X-linked retinitis pigmentosa (XLRP) and are responsible for between 7-20 % cases of XLRP (section 1.3.1.1, Hardcastle *et al.*, 1999; Sharon *et al.*, 2003; Vorster *et al.*, 2004). Mutations in *RP2* have also been shown to cause macular and peripapillar atrophy, thus expanding the clinical phenotype to the central retina (Dandekar *et al.*, 2004).

1.5.1. *RP2* gene

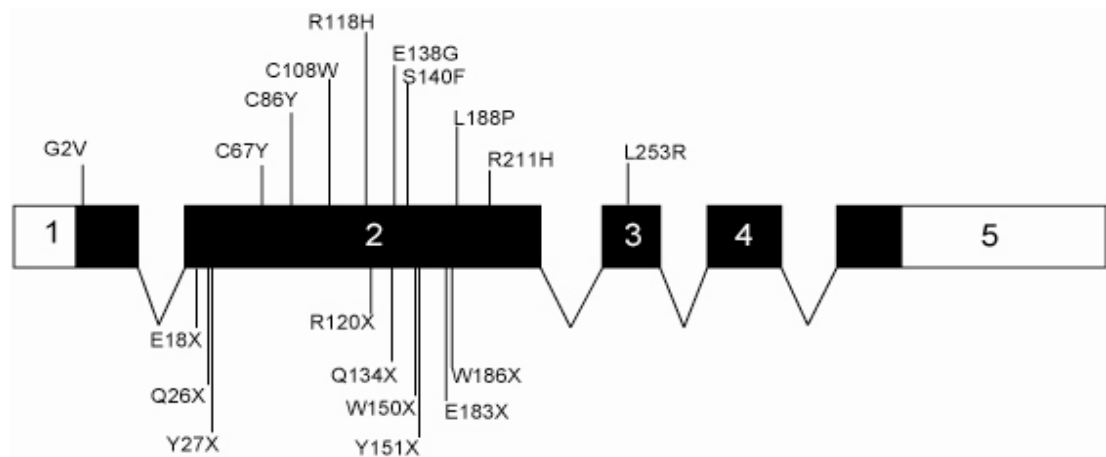
RP2 maps to Xp11.4 and is composed of 5 exons (figure 1.15a). There are 53 disease mutations reported to date (table 1.6). The majority of these mutations (67 %) are predicted to result in a truncated protein. Missense mutations account for 22 % while the remaining 11 % of mutations are located in splice-sites, or are caused by large deletions and insertions.

Most of the missense mutations cluster in exon 2, encoding the N-terminal region of the *RP2* protein (figure 1.15a). However, two mutations have been described which located at the C-terminal region of the protein (R211H and L253R). The most common mutation is the Arg120 stop (Arg120X) mutation found in several families with different ethnicities (Voster *et al.*, 2004), resulting in no detectable protein in *RP2* patients lymphoblasts (Grayson *et al.*, 2002a). Currently there is no apparent correlation between genotype and patient phenotype (Pelletier *et al.*, 2007).

1.5.2. *RP2* protein

RP2 is a 350 amino acid protein with a predicted molecular weight 39 kDa and a pI 4.94. The protein consists of an N-terminal cofactor C (CoC) homology domain (1-228) and a C-terminal nucleoside diphosphate kinase (NDPK) homology domain (229-317) (Kuhnel *et al.*, 2006) (figure 1.15b).

a.



b.

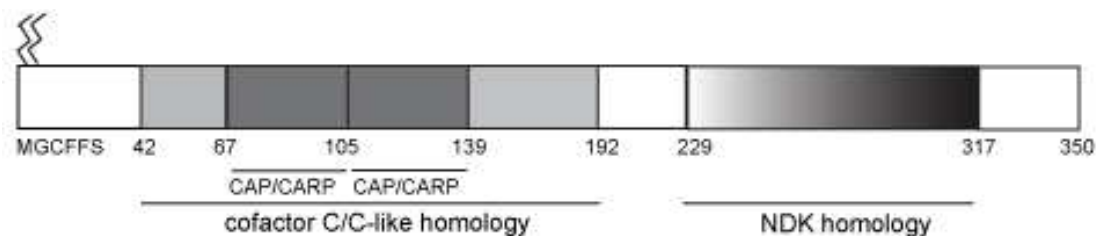


Figure 1.15. Position of pathogenic missense and nonsense mutations in the *RP2* gene and *RP2* protein domain organisation

a. Schematic of the human *RP2* gene. Exons are shown as boxes and are numbered as indicated. Introns are black lines. Shaded exon boxes indicate the coding regions and unfilled boxes are untranslated regions. Patient missense mutations identified are shown above the gene schematic and nonsense mutations are below. **b.** Schematic of the domain structure of *RP2* showing CoC homology domain (residues 42-192) and C-terminal NDPK homology domain (229-317). The N-terminal acylation motif (MGCFFS) is shown by two tags representing the myristoylation and palmitoylation that target *RP2* to the plasma membrane.

Intron/Exon	Position	Change	Consequence	Primary reference
All		Gene deletion		Pelletier <i>et al.</i> , 2007
Exon 1		Exon deletion		Bader <i>et al.</i> , 2003
Exon 1	16-18	3bp deletion	ΔS6	Schwann <i>et al.</i> , 1998
Exon 1	77/78	Insertion CA	Frameshift, 305 AA missing	Mears <i>et al.</i> , 1999
Intron 1		IVS1+3A>T	Splice site alteration	Sharon <i>et al.</i> , 2000
Intron 1		IVS1+3A>G	Splice site alteration	Breuer <i>et al.</i> , 2002
Intron 1		retrotransposition	Not known	Schwann <i>et al.</i> , 1998
Intron 1		IVS1-2A>G	Splice site alteration	Miano <i>et al.</i> , 2001
Exon 2	292	A insertion	G98fsX123	Pelletier <i>et al.</i> , 2007
Exon 2	297	5 bp insertion	S99fsX114	Pelletier <i>et al.</i> , 2007
Exon 2	305	T deletion	F102fsX11	Pelletier <i>et al.</i> , 2007
Exon 2	302	T insertion	F101fsX22	Miano <i>et al.</i> , 2001
Exon 2	330-342	12 bp deletion	C110fsX40	Mears <i>et al.</i> , 1999
Exon 2	350-351	2 bp deletion	F117fsX38	Breuer <i>et al.</i> , 2002
Exon 2	409	3 bp deletion	ΔI137	Sharon <i>et al.</i> , 2000
Exon 2	419-426	8 bp deletion	S140fsX151	Pelletier <i>et al.</i> , 2007
Exon 2	453	1 bp deletion	Y151fsX1	Schwann <i>et al.</i> , 1998
Exon 2	483/484	7 bp insertion	D161fsX13	Mears <i>et al.</i> , 1999
Exon 2	515	1 bp inserion	S172fsX1	Breuer <i>et al.</i> , 2002
Exon 2	538-539	2 bp deletion	V180fsX38	Pelletier <i>et al.</i> , 2007
Exon 2	670	1 bp insertion	R225 fsX9	Breuer <i>et al.</i> , 2002
Exon 2	688-692	5 bp deletion	Q229fsX2	Hardcastle <i>et al.</i> , 1999
Exon 2	723	1 bp deletion	F241fsX12	Thiselton <i>et al.</i> , 2000
Intron 2		IVS2-1G>A	Splice site alteration	Pelletier <i>et al.</i> , 2007
Exon 3	796-799	4bp deletion	V265fsX3	Thiselton <i>et al.</i> , 2000
Exon 3	801-804	4 bp deletion	T267fsX4	Pelletier <i>et al.</i> , 2007
Exon 3	834	2 bp inserion	Q278fsX15	Mashima <i>et al.</i> , 2000
Exon 3	853	1 bp insertion	F284fsX4	De Luca <i>et al.</i> , 2001
Exon 4		Exon deletion		Schwann <i>et al.</i> , 1998
Exon 4	925/926	2 bp insertion	V308fsX7	Mears <i>et al.</i> , 1999
Exon 4	929	1 bp insertion	E309fsX18	Hardcastle <i>et al.</i> , 1999
Intron 4		IVS4+3A>G	Splice site alteration	Sharon <i>et al.</i> , 2003

Table 1.6. Reported pathogenic mutations in *RP2*

1.5.2.1. Cofactor C homology domain

As the majority of patient missense mutations are located in the N-terminus of RP2 suggesting its importance for XLRP pathogenesis. The N-terminal β -helix domain from residue 42 to 192 shares 30.4 % of sequence identity and 43.7 % similarity with cofactor C (CoC) (figure 1.16) (Bartolini *et al.*, 2002). This parallel β -helix domain has a rectangular barrel shape and consists of three stacked β -sheets numbered PB1, PB1a and PB2 according to the nomenclature for β -helix domains (Kuhnel *et al.*, 2006) (figure 1.17). The fold of this region of RP2 is similar to that of C-terminal domain of cyclase associated protein (368-508) (C-CAP) of *S. cerevisiae* despite only 11 % of sequence identity (Dodatko *et al.*, 2004, Evans *et al.*, 2005). However, the proteins differ in their *in vitro* oligomerisation states; CAP forms a homodimer whereas RP2 is monomeric (Kuhnel *et al.*, 2006). Within the CoC homology region of RP2 lie two potential actin-binding domains known as CARP (figure 1.15b). Tandem repeats of such domains are found in the C-terminal region and CAPs are known to be involved in the regulation of actin polymerisation (Stevenson and Theurkauf, 2000; Ponting *et al.*, 2001). The presence of these CAP domains suggests the potential ability of RP2 and its homologue CoC to bind actin. However, there is no experimental evidence to support this hypothesis.

1.5.2.2. Nucleoside diphosphate kinase homology domain

The C-terminal α/β domain has a ferredoxin-like fold and forms a three layered $\alpha+\beta$ sandwich (figure 1.17) (Kuhnel *et al.*, 2006). This domain is structurally similar to the nucleoside diphosphate kinase (NDPK) domain (figure 1.18) with 22 % of the sequence identity. NDPK catalyses phosphorylation of nucleoside diphosphates to triphosphates and thus, is involved in a variety of cellular processes (Morera *et al.*, 1994a). However, the alignment of RP2 to NDPK indicates that the active catalytic residue His 122 is not conserved in RP2 (figure 1.18) and RP2 failed to bind ADP or GDP *in vitro* (Kuhnel *et al.*, 2006).

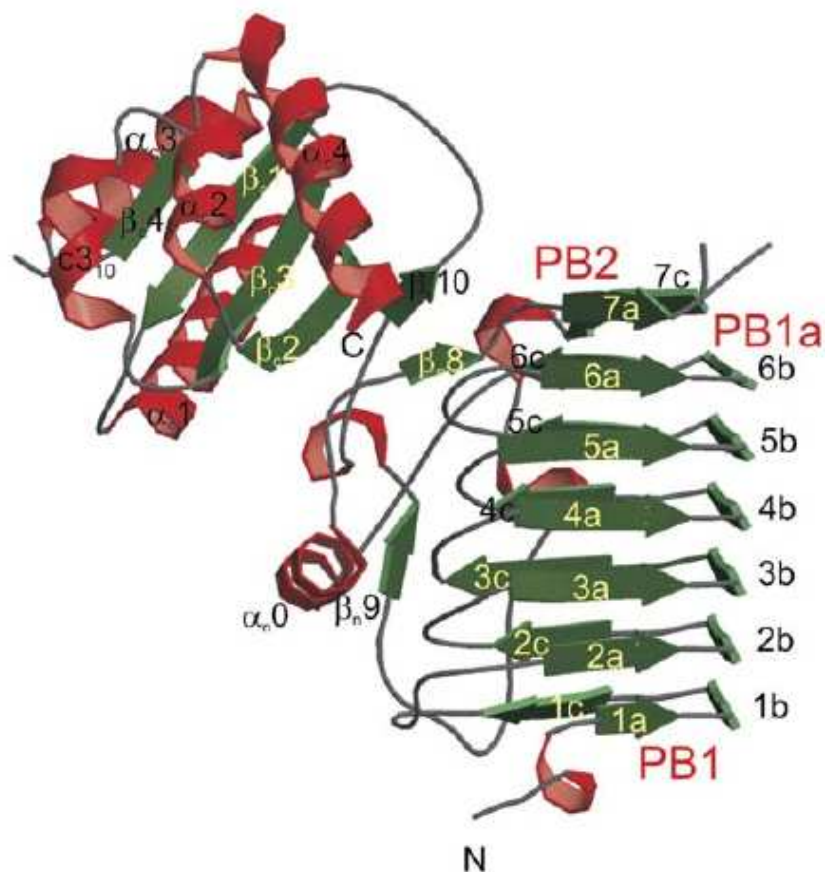
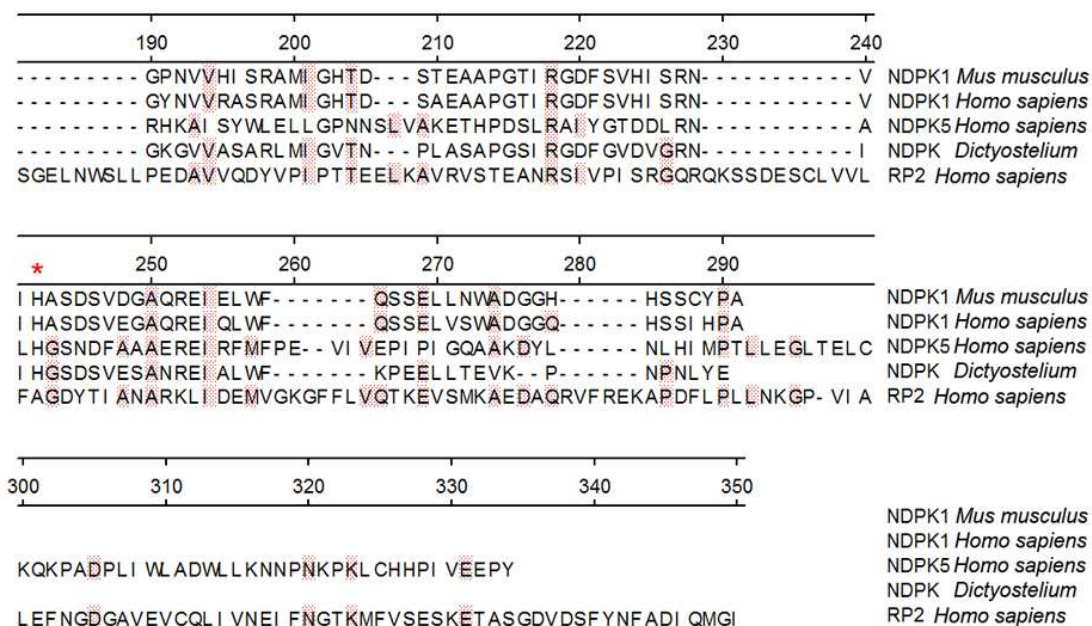


Figure 1.17. Structure of the human RP2 protein

Ribbon diagram of RP2 with β strands shown in green, red α helices, and grey loop regions. In the N-terminus strands a, b and c that form β sheets PB1, PB1a and PB2 are indicated. The structural model includes residues 34-347 (from Kuhnel *et al.*, 2006).

a.



b.



c.

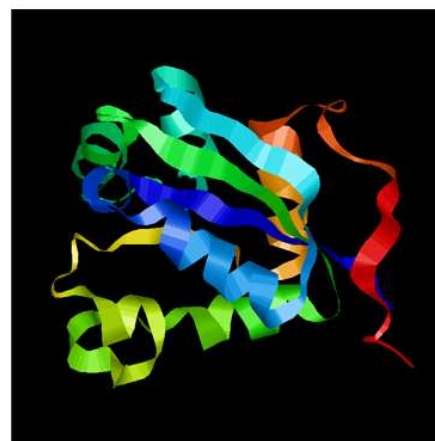


Figure 1.18. Comparison of the C-terminus of RP2 with NDPK

a. Protein sequence alignment of the C-terminal region of human RP2 (200-350) with mouse NDPK1, human NDPK1, testis specific human NDPK5 and NDPK of *Dictyostelium discoideum*. The residues that match RP2 are shadowed in red. Asterisk highlights the catalytic His in NDPK. The alignment is performed by Clustal W. **b.** Crystal structure of the C-terminus of human RP2 (AA 229-350) showing structural homology to NDPK (PDB [2BX6](#), Kuhnel *et al.*, 2006). **c.** Crystal structure of NDPK of *Dictyostelium discoideum* (PDB [1NPK](#), Morera *et al.*, 1994b).

1.5.3. Localisation of RP2 protein

RP2 has a MGCXXS motif at its N-terminus, which facilitates myristoylation at position G2 and palmitoylation at position C3 resulting in dual acylation. As a result RP2 protein is targeted predominantly to the plasma membrane (figure 1.19) (Chapple *et al.*, 2000; Chapple *et al.*, 2002; Grayson *et al.*, 2002b). It has been demonstrated that a patient mutation Δ S6 prevented normal targeting of RP2 to the plasma membrane (Chapple *et al.*, 2000), suggesting the importance of acyl modifications for XLRP pathogenesis. Mutation of G2 for alanine (G2A) abolished the plasma membrane localisation of RP2 (Chapple *et al.*, 2000). This residue was later reported to be mutated in XLRP patients with the substitution for valine (G2V) (Pelletier *et al.*, 2007). In the retina, RP2 was predominantly localised to the plasma membrane in all retinal cells, including photoreceptors (figure 1.19) (Grayson *et al.*, 2002b). However, many patient mutations outside of the acylation motif, such as R118H, did not alter the plasma membrane localisation of RP2 (figure 1.19, Chapple *et al.*, 2000).

Recently Li *et al.* (2004) in their flagella and basal body proteome study suggested that the *C. elegans* homologue of RP2 was localised to the basal body (described in section 1.2.2.3) along with other proteins involved in ciliary and basal body biogenesis, such as Arl3, RPGRIP and Unc119. However, the *C. elegans* RP2 lacks a myristoylation signal (G2) and therefore is unlikely to be targeted to the plasma membrane like human RP2. A trypanosome homologue of CoC and RP2, also lacking a myristoylation motif, was localized to the region around the basal body of the flagellum and appeared to recruit carboxyl-tyrosinated α tubulin to the basal body. This protein, named tbRP2, was suggested to act as a chaperone to monitor the quality of tubulin prior to cilia assembly (Stephan *et al.*, 2007).

Therefore, RP2 could cause XLRP through lack of plasma membrane targeting and potentially impaired chaperoning of components of the primary cilia. This hypothesis requires further investigation and currently does not explain why RP2 mutations do not lead to syndromic forms of retinitis pigmentosa.

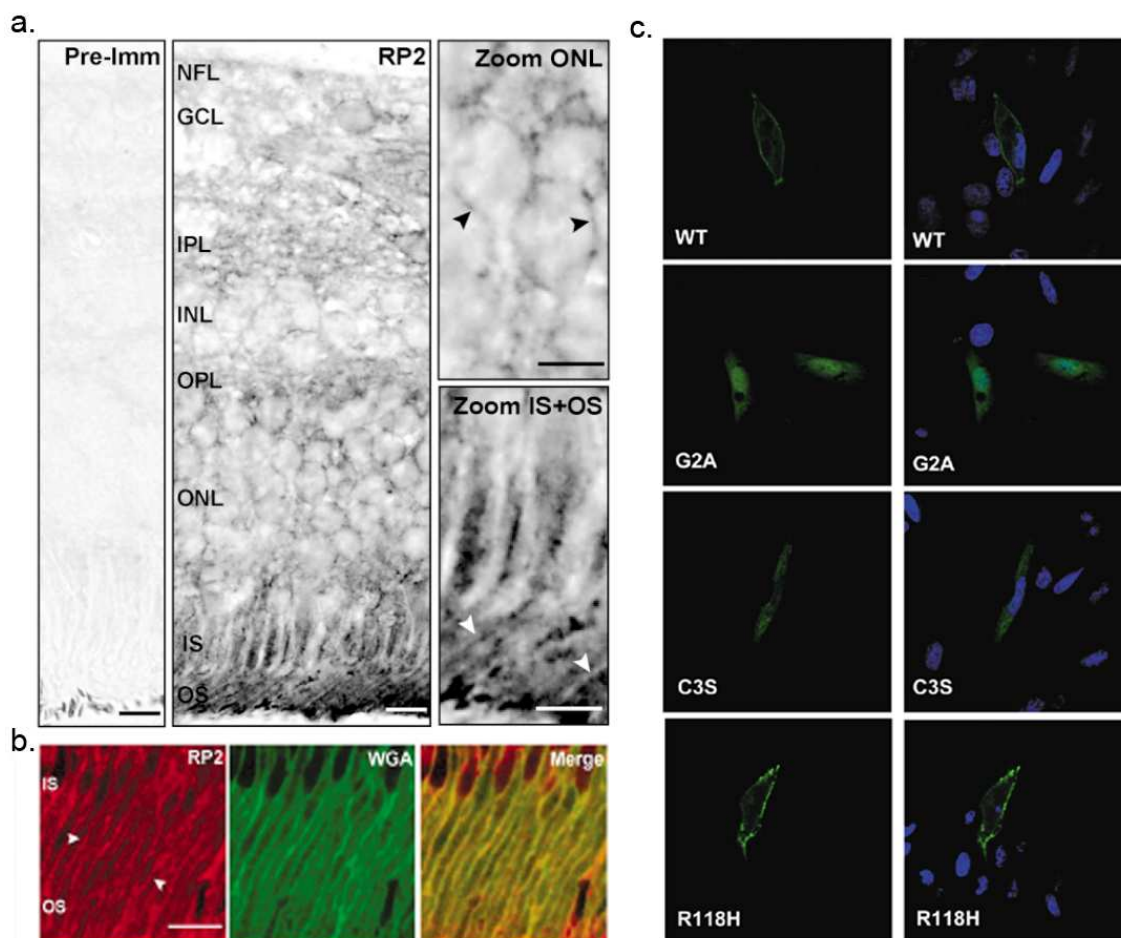


Figure 1.19. Localisation of RP2 protein

a. Immunohistochemistry of RP2 in human retina using anti-RP2 antibody. NFL, nerve fibre layer; GCL, ganglion cell layer; IPL, inner plexiform layer; INL, inner nuclear layer; OPL, outer plexiform layer; ONL, outer nuclear layer; IS, inner segments; OS, outer segments. Arrowheads highlight the plasma membrane localization. Scale bar is 10 mm (from Grayson *et al.*, 2002b). **b.** RP2 is localised predominantly at the plasma membrane of retinal cells. Confocal microscopy image of peripheral human retina using anti-RP2 antibody (red) and wheat germ agglutinin (WGA, green). IS, inner segments; OS, outer segments (from Grayson *et al.*, 2002b). **c.** Mutations of N-acylation motif, but not R118H mutation, alter the subcellular localisation of RP2 protein. Confocal microscopy images of CHO cells transfected with wild type RP2-GFP and its mutants as indicated. The images are 102 μm x 102 μm (from Chapple *et al.*, 2000).

1.5.4. RP2 function

RP2 protein function is unknown. The role of RP2 in different intracellular compartments is not clear. However, the strongest clue to the RP2 function lies in its homology to CoC and NDPK. RP2 was shown to exhibit functional homology to CoC. It was found that RP2 stimulates the GAP activity of tubulin in combination with CoD and thus, substituting for CoC in this function (Bartolini *et al.*, 2002). As described above, the N-terminus of RP2 and CoC have conserved Arg residues (figure 1.16). When these arginines on CoC (Arg262) and RP2 (Arg118) were mutated in both proteins, their tubulin GAP activity was abolished (Bartolini *et al.*, 2002). Such Arg residue is commonly called an “arginine finger” and it is often found in other GTPase activating proteins (GAPs) (Rittinger *et al.*, 1997; Vetter and Wittinghofer, 2001, Pan *et al.*, 2006), suggesting that RP2 is a GAP.

Due to a structural homology of the C-terminus of RP2 to NDPK, a functional overlap between these two proteins has also been suggested. RP2 has been reported to exhibit exonuclease activity, similar to NDPK (Yoon *et al.*, 2006).

Possibly, the key to uncovering of RP2 may also lie in its interactions. The only published interacting partner for RP2 is ADP-ribosylation factors (Arf)-like 3 (Arl3) (described below in 1.6) (Bartolini *et al.*, 2002).

1.5.4.1. Interaction of RP2 with Arl3

The interaction of RP2 with a small GTPase Arl3 was discovered in 2002 by Bartolini and colleagues who demonstrated that RP2 bound to the GTP-locked conformation of Arl3 (Q71L substitution). Several studies revealed that pathogenic mutations of RP2 could decrease the affinity of this interaction (Bartolini *et al.*, 2002, Evans *et al.*, 2005, Kühnel *et al.*, 2006), highlighting its importance.

Arl3 binds to the N-terminal CoC homology domain of RP2 (described in 1.5.2.1). The interaction occurs via the PB1 sheet of RP2 and includes β -strands 5a and 6a. Residues that are responsible for binding have been identified, including residues mutated in XLRP, such as Glu138 (Veltel *et al.*,

2008a). It was also revealed that RP2 contacts the bound nucleotide of Arl3 by four other residues including the catalytically important Arg118 (Bartolini *et al.*, 2002; Veltel *et al.*, 2008a). Biochemical studies demonstrated that Arl3's slow intrinsic GTP hydrolysis rate upon addition of RP2 was accelerated 1400-fold (Veltel *et al.*, 2008a). In the same study it was shown that an "arginine finger" mutation in RP2 (R118A) and another pathogenic mutation E138G drastically reduced the GTP hydrolysis stimulation.

Interestingly, CoC was able to act as a GAP towards Arl3 even at a low concentration, although with slightly less efficiency than the wild type RP2 (Veltel *et al.*, 2008a). Therefore, the functional overlap between RP2 and CoC to act as a GAP seems to be reciprocal.

1.6. ADP-ribosylation factors (ARF)-like GTPases

The ADP-ribosylation factors (Arf)-like GTPases (Arl) family of proteins are part of the Ras family of small GTPase proteins (Fan *et al.*, 2004). There are currently eight members of this family described, Arl1-8. Mammalian Arls have up to 40-60 % of protein sequence identity with Arfs, however they do not share function and are separated in two families. For instance Arf proteins are able to activate cholera-toxin catalysed ADP ribosylation, activate phospholipase D and complement the lethal *arf1*-/*arf2*- mutation in *S.cerevisiae*, whereas Arls do not possess such characteristics (Tamkun *et al.*, 1991; Amor *et al.*, 2001). Only Arl1 is an exception, which has a weak ability to act as an Arf (Hong *et al.*, 1998).

Small GTPases are known to adopt two conformational states that depend on the bound nucleotide. They adopt an "active" conformation when GTP bound and "inactive" when bound with GDP (Burd *et al.*, 2004). Arfs are known to have a myristoylation site, targeting protein to the plasma membrane. It has been shown that Arl1, Arl4 and Arl5 undergo such a posttranslational modification (Lee *et al.*, 1997; Randazzo *et al.*, 1995).

The *in vivo* functions of members of the Arl family are relatively unexplored. Arl 4, 6 and 7 are suggested to belong to a sub-group, characterised by a nuclear subcellular localisation and a nucleotide exchange rate higher than other Arls

(Jacobs *et al.*, 1999). Disruption of *Arl4* in mice causes retardation in normal germ cell development, showing that *Arl4* is required for the progression of cells through meiosis (Lin *et al.*, 2000; Schurmann *et al.*, 2002). *Arl5* also is localised to the nuclei and nucleoli and is developmentally regulated (Lin *et al.*, 2002).

Arl6 is known to be a causative gene for BBS type 3 (described in section 1.3.3.2) (Fan *et al.*, 2004). It was shown that the worm orthologue of *Arl6* is expressed in sensory neurons and is proposed to traffic along cilia by intraflagellar transport (IFT) (Fan *et al.*, 2004). A role for *Arl6* in ciliary functions has also been suggested by at least two comparative genomic searches (Li *et al.*, 2004; Avidor-Reiss *et al.*, 2004). These searches identified genes implicated in ciliogenesis or ciliary function that included both *Arl3* and *Arl6*. Together, these results point to a role for *Arl6* in cilia or flagella function. The presence of *Arl6* in flagella was confirmed in a study of the flagellar proteome of the biflagellated green alga *Chlamydomonas* (Pazour *et al.*, 2005).

1.6.1. *Arl3*

Arl3 has 45 % identity to *Arf1* protein and structural analysis revealed that *Arl3*-GDP is very similar to *Arf1*-GDP and *Arl1*-GDP (Amor *et al.*, 1994). *Arl3* was found to be a microtubule associated protein (MAP) (Grayson *et al.*, 2002b). *Arl3* was co-purified with microtubules from bovine brain, exhibited enhanced microtubule decoration upon tubulin stabilisation with taxol and redistributed to the nuclear membrane when the tubulin was depolymerised. The localisation of *Arl3* in the retina was also studied and it was revealed that *Arl3* was enriched in the photoreceptor connecting cilium of both rod and cone cells (Grayson *et al.*, 2002b).

There is further evidence for connecting cilium localisation of *Arl3* and its importance. A study in *Leishmania* demonstrated that over expression of an *Arl3* homologue (*LdArl3A*) was required for normal flagella development (Cuvillier *et al.*, 2000). However, *LdArl3A* is different to mammalian *Arl3* due to myristoylation (Randazzo *et al.*, 1995). Several cilia proteome studies (Li *et al.*, 2004; Avidor-Reiss *et al.*, 2004) have identified *Arl3* as a component of the

basal body structure, thus confirming the data of Grayson and colleagues (2002a).

A recent report of Arl3 knock-out mice further implicated Arl3 as a cilia protein (Schrick *et al.*, 2006). These mice exhibited abnormal development of renal, hepatic, and pancreatic epithelial tubule structures, which is characteristic of the renal-hepatic-pancreatic dysplasia found in autosomal recessive polycystic kidney disease (Zerres *et al.*, 1998). Absence of Arl3 was also associated with abnormal epithelial cell proliferation and cyst formation. Moreover, mice lacking Arl3 exhibited photoreceptor degeneration as early as postnatal day 14. These results demonstrated involvement of Arl3 in a ciliary disease similar to BBS (Schrick *et al.*, 2006). Furthermore, a proteomic screen of the photoreceptor mouse cilium detected Arl3 in this structure (Liu *et al.*, 2007).

1.6.2. Arl2

Arl2 is the closest homologue of Arl3 and they share 56 % identity however a recent study suggested different microtubule-associated roles for Arl2 and Arl3 (Zhou *et al.*, 2006). As described in section 1.4.4, Arl2 modulates the tubulin GAP activity of cofactors C and D and thus has a role in regulating tubulin dynamics (figure 1.16). Arl2 is essential for tubulin biogenesis (Steinborn *et al.*, 2002; Antoshechkin *et al.*, 2002). Genetic studies of a putative yeast homologue demonstrated that lack of Arl2 affected microtubule stability (Stearns *et al.*, 1990; Hoyt *et al.*, 1990). Interestingly, Arl2 has not been detected in the photoreceptor cilium proteome unlike Arl3, suggesting Arl3 and Arl2 may have divergent functions in this specialised cytoskeletal compartment (Liu *et al.*, 2007a). Arl2 has been identified with a number of interactors, and Arl2 shares some of these with Arl3.

1.6.3. Interacting partners of Arl2 and Arl3

Arl3 and Arl2 have been shown to interact with the ubiquitously expressed proteins such as the δ subunit of cGMP phosphodiesterase (PDE δ) and BART1 (Linari *et al.*, 1999; Sharer *et al.*, 1999). Both Arls were demonstrated to bind PDE δ predominantly in their GTP-bound “active” state (Hanzal-Bayer *et al.*,

2002). PDE δ in turn was shown to increase the affinity of Arl3 to GTP (van Valkenburgh *et al.*, 2001).

Although PDE δ function is not fully understood yet, it is suggested to be an effector of Arls (Hanzal-Bayer *et al.*, 2002). It has also been proposed that PDE δ has a more general function as a prenyl binding protein interacting with several other small GTPases which are prenylated (Zhang *et al.*, 2004). However, Arl3 and Arl2 have not been reported to be prenylated, suggesting that prenylation is not essential for Arl3 binding to PDE δ (Zhang *et al.*, 2004).

Arl3 and Arl2 have been shown to interact with Unc119 (HRG4) (described in section 1.3.4.1) (van Valkenburgh *et al.*, 2001; Kobayashi *et al.*, 2003). The C-terminus of Unc119 shares 30 % identity and 40 % similarity to PDE δ . Recently, the crystal structure of a ternary complex formed by Arl3, Unc119 and RP2 was described (Veltel *et al.*, 2008b). It was revealed that Arl3 is able to bind both Unc119 and RP2 at the same time, although RP2 and Unc119 residues that would interact directly were not found. Thus, the formation of the ternary complex and its role in the retina need further investigation.

Arl3 has also been shown to interact with Golgin-245, a GRIP domain protein recruited to trans-Golgi network (van Valkenburgh *et al.*, 2001) and the function of this interaction remains unclear.

1.7. Potential mechanisms of XLRP caused by RP2

The key to one of the possible mechanisms of XLRP caused by *RP2* mutations may lie in the disruption of RP2 GAP activity towards Arl3. As described in 1.6.1.1 and 1.6.1.3., Arl3 has retina specific interacting partners and is localised to the photoreceptor cilium, suggesting a potential pathogenic mechanism. However, Arl3 knockout mice exhibited a syndromic form of retinitis pigmentosa, unlike RP2 patients with the retina restricted phenotype. Moreover, due to the functional overlap in the catalytic activity of RP2 and CoC it is unclear whether disruption of RP2 GAP activity to Arl3 is the crucial step in the pathogenesis of XLRP since CoC does not compensate for loss of RP2 function in patients (Grayson *et al.*, 2002a).

Another possible hypothesis of XLRP pathogenesis suggests that cilia function is compromised by *RP2* mutations. However, primary cilium is a ubiquitous structure (described in 1.2.2.3) and its dysfunction would cause a syndromic form of RP rather than the retina restricted phenotype.

Pathogenic mutations in acyl modifications motif of *RP2* have been shown to abolish *RP2* plasma membrane localisation, highlighting an important retina functional role for *RP2* on the plasma membrane.

1.8. Aims of this study

The aim of this study was to find retina specific interacting partners of *RP2*, which would link *RP2* with the retinal physiology.

For this purpose *RP2* was tested for protein-protein interactions using two approaches. The first approach employed yeast two-hybrid screening of *RP2* with the retinal cDNA library. The second method involved using of a proteomic affinity assay with mass spectrometry analysis of potential novel interactors. Other biochemical and molecular biology methods were also applied in order to verify novel putative *RP2* interactions. They were also used to elucidate the consequences of novel *RP2* interactions *in vivo*.

Another purpose of this study was to further investigate the role of potential chaperones in the retina by testing whether prefoldin 5 (*PFND5*) mutations could cause syndromic or non-syndromic retinal dystrophy.

Chapter II. Materials and methods

2.1. Basic molecular biology techniques

2.1.1. Polymerase chain reaction

The polymerase chain reaction (PCR) was used to amplify selected regions of DNA for subsequent cloning or sequencing. PCR uses *in vitro* enzyme-catalysed DNA synthesis to create copies of a specific region of DNA. The oligonucleotide primers are extended towards one another under chosen conditions by a thermostable DNA polymerase in a three step reaction: denaturation, primer annealing and extension.

For cloning a 25 µl PCR mix of 50 ng DNA, 2 µM of forward and reverse primer, 0.2 mM of each dNTP (Promega), 1.5 mM MgCl₂, 1 µl of Taq polymerase (GoTaq®, Promega) and distilled water. For *PFDN5* gene fragments amplification consisted of 12.5 µl of 2x Abgene® Master Mix (Appendix), 100 ng of DNA, 2 nM of each primer and distilled water. The sequences of primers with integrated restriction sites used for cloning are shown in table 2.1. The sequences of primers designed for amplifying and sequencing *PFDN5* exons are shown in table 5.1. PCRs were performed using Techne Genius PCR thermocycler (Jencons-PLS). When PCR was performed for subsequent cloning the conditions were as follows: initial denaturation at 95°C for 5 minutes followed by 12-15 cycles of 95°C for 30 sec, Ta°C for 30 sec and 72°C for 35 sec.

When PCR was carried out to amplify *PFDN5* fragments for further sequencing, the PCR conditions were as follows: initial denaturation at 95°C for 5 minutes and 30 cycles of 95°C for 30 sec, annealing temperature (Ta°C) incubation for 30 sec (see chapter 5.2.1, table 5.1) and 72°C for 45 sec with the final extension step at 72°C for 5 minutes. All the PCR products if stored were kept at -20°C.

Primer	Sequence 5'-3'	Restriction site	Ta (°C)
Arl3 F	<u>GAATTC</u> CGATGGGCTTGCTCTCAATTTG	<i>EcoRI</i>	58
Arl3 R	CGGTCGACTCCCGCAGCTCCTGCATC	<i>SalI</i>	
PFN5 F	<u>GAATTC</u> GGATCCATGGCGCAGTCTATT AACATCACG	<i>EcoRI</i> , <i>BamHI</i>	60
PFN5 R	GGATCCAAGCTTGAATTCTCAGGCCTTAGCAGTAGCCTG	<i>BamHI</i> , <i>HindIII</i>	
pMyr PFN5 F	<u>GAATTC</u> ATGGCGCAGTCTATTAAC	<i>EcoRI</i>	58
pMyr PFN5 R	CTCGAGTCAGGCCTTAGCAGTAG	<i>XhoI</i>	
pSos PFN5 F	<u>GGATCC</u> ATGGCGCAGTCTATTAAC	<i>BamHI</i>	58
pSos PFN5 R	<u>GTCGACT</u> CAGGCCTTAGCAGTAG	<i>SalI</i>	
pCMV 46 F	<u>CCCGGG</u> CAGGGCAGAACAAAGC	<i>SmaI</i>	55
pCMV 46 R	<u>GATATC</u> GGCACGAGGCCTGAC	<i>EcoRV</i>	

Table 2.1. Sequences of primers used in this study for cloning (the restriction sites are underlined)

Exon	Primer sequence	Ta(°C) used	Amplicon size
1 forward	5'TCTGGCCGAGCGAGGCCTG3'	58	243 bp
1 reverse	5'GGCGCGAGAGTACGCGTG3'		
2 forward	5'TATCCGATCCCAGGACCTG3'	58	288 bp
2 reverse	5'GGATTTTCTCGTTTCAGGTAAG3'		
3 forward	5'TAACGTCTTACGTTGGAGCC3'	55	197 bp
3 reverse	5'GAGAGGGTAATCTGAAGTAAT3'		
4 forward	5'GGCGGAATCATGGCTCATGC3'	60	438 bp
5 reverse	5'TGGTTCACACTGCAATCCATG3'		
6 forward	5'GTTAGTCGGTCGCCTGTCC3'	58	271 bp
6 reverse	5'AGACCAACATTCTGCCAGC3'		

Table 2.2. Sequences of primers used for *PFDN5* amplification and sequencing

2.1.2. TA cloning

PCR products were TA cloned into *pGEM® -T Easy* vector (Promega). *pGEM® -T Easy* vector is cut with *EcoRV* resulting in a 3' terminal thymidine (T) to both ends. These single 3'-T overhangs at the insertion site improve the efficiency of ligation of a PCR product into the plasmids by preventing recircularization of the vector and providing a compatible overhang for PCR products generated by certain thermostable DNA polymerases. These polymerases often add a single deoxyadenosine (A), in a template-independent fashion, to the 3'-ends of the amplified fragments.

A ligation reaction consisted of 10 units of T4 DNA ligase, 1 µl 10x rapid ligase buffer (0.3 M Tris-HCl (pH 7.8), 0.1 M MgCl₂, 0.1 mM DTT and 10 mM ATP), 1 µl of *pGEM® -T Easy* vector, 3 µl of PCR product and 4 µl of water. The reaction mix was then incubated overnight at 4°C.

2.1.3. *E.coli* transformation

100 µl of JM109 competent cells, high efficiency (Promega), were mixed with the ligation reaction and incubated on ice for 30 minutes, heat shocked at 42°C for 45 sec in a water bath and then incubated on ice for 2 min. After that, 900µl of 37°C SOC medium (Appendix) was added and the transformed cells were incubated at 37°C with shaking for 1 hour, followed by plating on 50 µg/ml ampicillin Luria Broth (LB) agar (Appendix) and incubation overnight at 37°C.

For *E.coli* transformation with a ligation reaction into *pGEM® -T Easy* vector, a colour selection method was used. The *pGEM® -T Easy* vector contains contain T7 and SP6 RNA polymerase promoters flanking a multiple cloning region within the α -peptide coding region of the enzyme β -galactosidase. Insertional inactivation of the α -peptide allows recombinant clones to be directly identified by color screening on indicator plates.

Such plates were prepared by spreading 50 µl of 1 M IPTG and 50 µl of 20 mg/ml X-Gal on LB plates with 50 µg/ml ampicillin. Transformed JM109 cells were then spreaded onto the plates and incubated overnight at 37°C. The white colonies were then selected for further experiments.

2.1.4. Plasmid purification and DNA quantification

Colonies from plates with cells transformed as described above were picked and used to inoculate 5 ml of LB with ampicillin (50µg/ml, Appendix) followed by incubation at 37°C with shaking for 16-18 hours. Cells from 1.5 ml of each culture were centrifuged at 6,000 *g* for 5 minutes and the DNA was extracted using GenElute Miniprep kit (Sigma) according to the manufacturer's instructions. The kit is based on alkaline lysis of bacteria with alkaline lysis buffer. The lysate is neutralised by addition of a neutralising buffer containing acid and centrifuged for 10 minutes at 16100 *g* at 22°C. The cleared lysate is loaded on a DNA - binding column and is passed through a DNA binding membrane of the column followed by washing of the column with the wash buffer, containing 70 % (v/v) ethanol. After that the DNA is eluted with 60 µl of sterile distilled water.

To determine the DNA concentration spectrophotometric analysis was used. The DNA was diluted in ddH₂O and the absorbance was measured in a quartz cuvette at 260 nm wavelength. To calculate the concentration of DNA in the sample, an absorbance of 1 indicates 50 µg/ml of DNA.

2.1.5. Restriction enzyme digestion

For analytical routine digests 250 ng of DNA was mixed with at least 1 unit of restriction enzyme in a 10 µl volume with the appropriate buffer as recommended and provided by the manufacturer. The reaction was incubated at 37°C for 1 hour. For excision of inserts from plasmid DNA for cloning, 2 µg of DNA was digested in a 25 µl reaction volume with at least 10 units of appropriate enzyme. The DNA was then digested for 2 hours at 37°C. A list of enzymes and buffers used for cloning of plasmids constructed during this study is shown in table 2.3.

2.1.6. Alkaline phosphatase vector treatment

Vectors used for cloning were treated with calf intestinal alkaline phosphatase (CIAP, Promega) to dephosphorylate the 5' end of the cut vector after restriction digest to prevent self-ligation.

A typical reaction consisted of 2 µg of digested DNA, 10 µl of 10x CIAP reaction buffer, 1 unit of CIAP and nuclease free water to a final volume of 100 µl. The reaction was incubated for 1 hour at 37°C. To remove CIAP so it would not interfere with subsequent ligation by acting on insert, DNA clean up was performed using QIAquick PCR Purification Kit (Qiagen) according to the manual. The kit involves using of a silica-membrane based purification of DNA.

2.1.7. Analysis of PCR products and restriction digests

Products of PCR and restriction digests were analysed by agarose gel electrophoresis and ethidium bromide staining. Generally, 1 % (w/v) agarose in 1X tris-acetate (TAE) buffer was used (Appendix). Samples were prepared for loading by adding 6X dye (0.4 % (w/v) orange G; 0.03 % (w/v) bromophenol blue, 0.03 % (w/v) xylene cyanol FF, 15 % (v/v) Ficoll® 400, 10mM Tris-HCl (pH 7.5) and 50mM EDTA (pH 8.0)) to a final concentration of 1X. Ethidium bromide was added to the TAE buffer to a final concentration of 0.5 µg/ml prior to loading the samples. The bands were visualised by ultraviolet irradiation using Gene Genius Bio imaging system with GeneSnap software (Syngene).

2.1.8. Vectors and constructs

The human Arl3 coding sequence was amplified as described in 2.1.1 from plasmids previously constructed in our lab containing mutants of Arl3 (T31N and Q71L) in *pCMV tag 3B* vector and specific primers (table 2.1). Human PFDN 5 coding DNA was amplified as in 2.1.1 with appropriate specific primers (table 2.1) from IMAGE clone 6458093 (Geneservice Ltd).

The PCR products were TA cloned as in 2.1.2. The *pGEM*® - *T Easy* plasmids were digested as described in 2.1.5 with enzymes as shown in table 2.4. The target vectors (table 2.3) were CIAP treated as in 2.1.6. Ligation and transformation procedures are the same as described in 2.1.2 and 2.1.3.

Vector	Company	Expression system	Fusion of tag	Antibiotic Selection
<i>pGem[®] - T Easy</i>	Promega	<i>E. coli</i>	-	Ampicillin
<i>pSos</i>	Stratagene	<i>S. cerevisiae</i>	N-terminal hSos	Ampicillin/ Leucine
<i>pMyr</i>	Stratagene	<i>S. cerevisiae</i>	N-terminal myristoylation	Chloramphenicol/ Uracil
<i>pCMV Tag 3a,b</i>	Stratagene	mammalian	N-terminal myc	neomycin/ kanamycin
<i>pEGFP C1</i>	Clontech	mammalian	N-terminal GFP	neomycin/ kanamycin
<i>pTrc His (-A)</i>	Invitrogen	<i>E. coli</i>	N-terminal 6Xhis	Ampicillin
<i>pGEX-2T</i>	Pharmacia	<i>E. coli</i>	N-terminal GST	Ampicillin

Table 2.3. Vectors used in this study and their characteristics

Plasmid	Enzyme I	Enzyme II
<i>pGex-2T Arl3 T31N</i>	<i>EcoRI</i>	<i>EcoRI</i>
<i>pGex-2T Arl3 Q71L</i>		
<i>pCMV-Tag 3a clone 46</i>		
<i>pCMV-Tag 3b PFN5</i>	<i>BamHI</i>	<i>HindIII</i>
<i>pGex-2T PFN5</i>	<i>BamHI</i>	<i>EcoRI</i>
<i>pTrc-HisA PFN5</i>		
<i>pMyr PFN5</i>	<i>EcoRI</i>	<i>XhoI</i>
<i>pSos PFN5</i>	<i>BamHI</i>	<i>SalI</i>
<i>pCMV-Tag 3(b) Unc119</i>	<i>EcoRI</i>	<i>SalI</i>
<i>pEGFP-C1 clone 46</i>	<i>HindIII</i>	<i>EcoRI</i>

Table 2.4. Plasmids made in this study

The enzymes labeled “I” were used for digest the insert at the 5’ end and “II” for the 3’ end.

Other plasmids used in this study were either constructed in our lab before or were purchased/ gifted (table 2.5).

Plasmid	Source	Expression	Tag
pSos RP2 constructs	Evans, 2007.	<i>S. cerevisiae</i>	N-terminal hSos
pSos MAFB	Stratagene	<i>S. cerevisiae</i>	N-terminal hSos
pMyr Lamin C, pMyr SB pMyr MAFB pMyr cDNA retinal library	Stratagene	<i>S. cerevisiae</i>	N-terminal myristoylation signal
pcDNA-FLAG G β ₁ , G β ₃ , G β ₅ and G β _{5L}	Missouri S&T cDNA Resource Center	Mammalian	N-terminal FLAG
pcDNA arrestin1 pcDNA arrestin 3	Dr. Vsevolod V. Gurevich	Mammalian	no tag
pcDNA arrestin 1 - FLAG pcDNA arrestin 3 - FLAG	Dr. Vsevolod V. Gurevich	Mammalian	C-terminal FLAG
pGEX-2T RP2	Prof. Michael Cheetham	<i>E.coli</i>	N-terminal GST
pEGFPN1RP2 constructs	Dr PJ Chapple Dr R Evans	Mammalian	C-terminal GFP

Table 2.5. Provided plasmids used in this study

2.1.9. Short interfering RNA

The siRNA to human Arl3 and RP2 were designed and synthesised by Dharmacon. All four siRNAs for Arl3 were mixed to create a combined pool of siRNA to achieve a good protein suppression level. A negative control scrambled siRNA was also obtained from Dharmacon. The RNA sequences are represented in table 2.6. The cells were then transfected with siRNA as described in 2.3.3.

siRNA	sequence 5'-3'
Arl3 siRNA 1	AAUUCGCUAGUCCUGACUU
Arl3 siRNA 2	UAUUAGCAAAGAUGAGCACUU
Arl3 siRNA 3	UAUGCAGGUUCAGUCCUUCUU
Arl3 siRNA 4	AUUUACAGAGGCCGUUAUCUU

Table 2.6. siRNA sequences used in this study

2.2. CytoTrap® yeast-two hybrid

2.2.1. Cdc25-H yeast strain long term storage and resuscitation

The *S.cerevisiae* cdc25-H yeast strain (MAT_{aura}3-52 his3-200 ade2-101 lys2-801 trp1-901 leu2-3 112 cdc25-2 Gal+) was obtained from Stratagene and spread onto an YPAD plate (Appendix) and grown for 96 hours at 24°C. To ensure that the yeast phenotype had not reverted to allow growth at the 37°C restrictive temperature, the strain was streaked out on YPAD plate, placed at 37°C and examined for growth after 144 hours of incubation.

To create a frozen stock of yeast culture, 12 ml of YPAD broth (Appendix) was inoculated with a single colony and grown at 24°C with 250 rpm shaking overnight until saturation ($OD_{600} > 1$). The cells were harvested by centrifuging at 3000 *g* for 2 minutes, the supernatant was discarded and the pellet was resuspended in 12 ml of YPAD broth, containing 50 % glycerol. 1 ml aliquots were immersed in liquid nitrogen for 5 minutes, then placed at -70°C and kept until needed. To resuscitate, defrosted cells were spread by a 10 µl loop onto YPAD agar plate and grown for 96 hours.

2.2.2. Yeast transformation

10 ml of YPAD broth was inoculated with a single colony of yeast and incubated overnight at 24°C with shaking at 250 rpm. This culture was used to inoculate 50 ml of YPAD broth in 250 ml flask to a final $OD_{600} = 0.2$ and incubated at 24°C with shaking until $OD_{600} = 1.0$. Cells were centrifuged at 3000 *g* for 2 min, washed with 10 ml of water, resuspended, centrifuged again under the same conditions and washed with 5 ml of LiOAc/TE (10 mM LiOAc in TE, Appendix). The pellet was resuspended in 250 µl of LiOAc/TE and incubated for 15 minutes at room temperature.

50 µl of the yeast suspension was added to 2 µg DNA of a 1:1 mixture of appropriate pSos and pMyr constructs (section 2.1.8), combined with 5 µl of DMSO (Sigma) and 5 µl of salmon sperm DNA boiled for 5 minutes (Stratagene). Next, 300 µl of 40 % PEG 4000 in LiOAc/TE (Appendix) was

added to the cells, mixed gently by several inversions and incubated for 1 hour at 24°C, followed by heat shock for 10 minutes at 42 °C in a water bath. The cells were then centrifuged at 800 g for 2 minutes, washed with water and resuspended in 200 µl of water. The cells were plated on SD / glucose agar with amino acids (BD Biosciences), but lacking uracil and leucine (-UL) (Appendix).

2.2.3. Library screening

Yeast cells were co-transformed with pSosRP2 or pSos1-200RP2 with pMyr bovine retinal cDNA library as in 2.2.2. For a positive control these pSos constructs were also co-transformed with a positive control pMyrSB and the negative control pMyr LaminC (section 2.1.8) in the same way as the library. An additional control of pMyr bovine retinal cDNA library was transformed into yeast and plated on SD / glucose agar (-U) to monitor the number of temperature revertants. Every screen consisted of 25-30 co-transformations which were plated on SD / glucose agar (-UL) and incubated for 36 hours at 24°C. The colonies were then replica-plated with a clear orientation mark onto a selective SD/galactose (-UL) plates and incubated at 37°C. A library control plate was replica plated on SD/galactose (-U) plate at 37°C. Visible colonies were picked up during the following 144-240 hours until more than 20 colonies appeared on the negative control plates.

2.2.4. Total yeast DNA isolation

To isolate total yeast DNA, each colony was resuspended in 3 ml of SD/glucose broth with amino acids without uracil added and incubated at 24°C for 48 hours with shaking at 250 rpm. The yeast cultures were then centrifuged at 1000 g for 2 min at room temperature, supernatants discarded and the pellets were resuspended in 100 µl of 3 % SDS in 0.2 N NaOH. The cells were lysed for 15 min at room temperature with occasional mixing. After this 500 µl of TE buffer was mixed with the lysate and 60 µl of 3 M sodium acetate added (Appendix). Next 600 µl of phenol/chloroform/isoamylalcohol (25:24:1) (Sigma) was added and the tubes were mixed using vortex for 2 min each at maximum speed.

The samples were then centrifuged at 16200 *g* for 2 min at room temperature, the upper layers of the supernatants were transferred into fresh tubes with 600 μ l of phenol/chloroform/isoamylalcohol, followed by vortexing at maximum speed for 2 minutes. After that the tubes were centrifuged at 16200 *g* again as above, upper layers were taken into clean tubes containing 600 μ l of ice-cold 100 % isopropanol (Sigma) and mixed. The samples were incubated for 20 min at -20°C with subsequent centrifugation for 5 min at 16200 *g*.

The supernatant was discarded, 100 μ l of 70 % (v/v) ethanol was added and the tubes were centrifuged for 5 min at 16200 *g*. All the supernatants were then carefully discarded and the pellets were air-dried and resuspended in 15 μ l of distilled water to solubilise the DNA from the pellet.

2.2.5. pMyr plasmids isolation

5 μ l of total yeast DNA from section 2.2.4 was used to transform *E.coli* JM109 competent cells as described in 2.1.2 section with the difference that the cells with added DNA were incubated for 40 min on ice before the heat pulse. The transformed cells were selected on LB agar plates with 34 μ g/ml chloramphenicol (Sigma) and incubated at 37°C for 16-18 hours.

A single colony from each plate was picked and grown at 37°C for 16-18 hours with shaking at 250 rpm. The cells were collected and the plasmid DNA was purified using GenElute™ Plasmid Miniprep kit (Sigma) according to section 2.1.4. To check that the plasmid DNA was pMyr with an insert, restriction enzyme digestion was used as described in 2.1.5.

2.2.6. Protein-protein interaction verification by yeast two-hybrid

To verify that isolated pMyr plasmids still allowed growth at 37°C only upon co-transformation with the pSos construct used for the library screening, they were co-transformed in yeast as described in 2.2.4. After transformation cells were plated on SD/glucose (-UL) media and incubated for 96 hours at 24°C. Several single medium size colonies were resuspended in 100 μ l of distilled water and 5 μ l of each suspension was spotted onto a SD/galactose (-UL) plate and

incubated at 37°C and 24°C. Growth was observed over the next 144-168 hours.

2.3. Cell based techniques

2.3.1. Cell culture maintenance and storage

ARPE19 human retinal pigment epithelial cells and SK-N-SH human neuroblastoma cell line from ATCC collection (Cat. № HTB-11) were grown in DMEM/NUT.MIX.F12 with Glutamax-I (Invitrogen), 10 % (v/v) heat inactivated foetal bovine serum (FBS), 50 U/ml penicillin and 50 µg/ml streptomycin (all from Invitrogen) in a humidified atmosphere of 6 % (v/v) CO₂ at 37°C. HeLa human cervical carcinoma cells were grown in DMEM with Glutamax-I, 10 % (v/v) heat inactivated FBS and 50 µg/ml gentamycin under the same conditions.

When confluent, cells were washed with Hank's Buffered Salt Solution (HBSS) (Invitrogen) and treated with enough trypsin to cover the cell monolayer (Invitrogen) at 37°C until cells changed shape under light microscopy examination. The reaction then was blocked by addition of full media and resuspension. Cell counts were performed using Neubauer chamber (Sigma) according to the manual. All cell lines were not subjected to more than 25 passages.

For storage 2×10^5 cells were resuspended in 0.5 ml of freezing media (20 % v/v FBS, 72 % v/v DMEM/NUT.MIX.F12, 8 % v/v dimethyl sulfoxide (DMSO)) and the tubes were then put at -70°C in an alcohol/ isopropanol bath (VWR) for 24 hours. After that the tubes were transferred to liquid nitrogen storage. To resuscitate the cells the aliquots were rapidly warmed to 37°C, washed with HBSS, appropriate media was added and cells were cultivated as above.

2.3.2. Transfection procedure

Cells were cultivated as in 2.2.1 and grown until 60 % confluence. The transfection of cells was performed using liposome DNA delivery. The proportion of reagents for transformation was as recommended by Invitrogen for the type of flasks (Falcon) or chamber slides (Lab-Tek™) (table 2.7).

Flask	Number of cells	Plus [®]	Lipofect amine [®]	DNA (µg)	Total mixture volume	Cultivation media volume
chamber slide well	2 X 10 ⁴	1 µl	0.5 µl	0.1	125 µl	250 µl
well of a 6 well plate	6 X 10 ⁵	6 µl	3 µl	0.5	800 µl	2 ml
25 ml flask	1 X 10 ⁶	12 µl	6 µl	1.5	1.5 ml	5ml

Table 2.7. Transfection of mammalian cells with DNA

For this purpose diluted in serum-free media DNA was combined with Plus[®] Reagent (Invitrogen) and incubated for 15 min at room temperature. After that Lipofectamine (Invitrogen) was added to the mixture of DNA and Plus[®] and incubated for 15 minutes at room temperature. Cells were then washed twice with HBSS and once with DMEM/NUT.MIX.F12/Glutamax-I. The transfection mixture was added to the cells and incubated for 3 hours in a humidified atmosphere of 6 % (v/v) CO₂ at 37°C.

After that the transfection mixture was discarded and the fresh 10 % FBS DMEM/NUT.MIX.F12/Glutamax-I was added. Cells were then incubated for 24 hours under the same conditions and then used for further experiments.

2.3.3. Transfection with short interfering RNA (siRNA)

Cells were cultivated in chamber slides as described in 2.3.1 and grown until 40-50 % of confluence. The cells were then washed twice with serum free and antibiotic free DMEM/NUT.MIX.F12/Glutamax-I media. 100 nM of each combined siRNA (table 2.5) in siRNA buffer (Appendix) was diluted 2 X in the serum free media and incubated for 5 minutes at room temperature. Dharmafect[®] reagent (Dharmacon) was diluted 20 X in the serum free media and incubated for 5 minutes at room temperature. Both reagent mixtures were combined, incubated for 15 minutes at room temperature and cultivating media was added up to a final volume 200 µl for each chamber slide well. The cells

were then incubated for 96 hours in a humidified atmosphere of 6 % (v/v) CO₂ at 37°C and analysed further as in 2.3.4.

2.3.4. Immunocytochemistry

Approximately 80000 cells per ml were cultivated on Permax™ chamber slides for 24 hours and then the cells underwent transfection procedure as in 2.2.2. Slides were washed with phosphate buffered saline (PBS) and fixed using two different methods (table 2.8).

First method was fixing with 3.7 % (v/v) paraformaldehyde (PFA) (Sigma) for 15 minutes at room temperature with subsequent permeabilising with 0.2 % Triton X 100 (v/v) for 10 minutes.

The second fixation method was incubation of cells with ice-cold 100 % methanol (Sigma) for 5 minutes at room temperature. After fixation the cells were washed and blocked in PBS with 10 % normal donkey serum (w/v) (Invitrogen) and 3 % bovine serum albumin (w/v) (Sigma) for 20 minutes at room temperature.

The primary antibodies were diluted in the blocking solution as in table 2.7, incubated for 1 hour at room temperature, discarded and wells were washed 3 times with PBS. The cells were incubated further with appropriate secondary antibody Cy2- or Cy3- conjugate (all raised in donkey, Jackson) diluted to 1:100 in the blocking solution for 1 hour at room temperature.

The cells were then washed with PBS and nuclei were stained with 4',6-diamidino-2-phenylindole (DAPI) (Sigma) 5 µg/ml in PBS for 15 minutes at room temperature. After the final double wash with PBS the cells were covered with a glass coverslip of the appropriate size using fluorescent mounting media (Dako).

Antibody name	Specificity	Raised in	Supplier	Titre	Fixation
Arl3-854	Arl3	rabbit	Gift Dr N.Cowan	1:250	PFA
S974	RP2	sheep	Our own	1:50	methanol
M2	FLAG	mouse	Sigma (F1804)	1:100	methanol
PK/35/30d/1k/1g	CCT6	rat	Gift Dr K. Willison	1:25	PFA, methanol
9E10	c-myc	mouse	Sigma (M4439)	1:500	methanol
Anti-arrestin	F4C1epitope	rabbit	Gift Dr V. Gurevich	1:100	methanol

Table 2.8. Primary antibodies used for immunocytochemistry

2.3.5. Microscopy

The staining was initially analysed using X 40 and X 60 oil immersion objectives of Nikon Eclipse 80i epifluorescent microscope with excitation filters used as recommended by the manufacturer for the fluorochrome type.

The cell images were taken using a Carl Zeiss LSM 510 laser scanning confocal microscope with the 63 X oil immersion objective. The following excitation/emission conditions were used in separate channels: DAPI 364/475-525nm, GFP 488/505-530 nm, Cy3 543/560 nm. For the software used see section 2.6.

2.3.6. Subcellular fractionation

To separate cytosolic, nuclear, membrane and cytoskeletal fractions of cells a general subcellular fractionation was used. All the recipes for buffers used in this method are described in Appendix.

Cells were cultivated as in 2.3.1 and transfected as in 2.3.2. After that cells were treated with trypsin as in 2.3.1, resuspended in the appropriate media and counted. 3×10^6 cells then were pelleted at 1000g for 3 minutes at room temperature, the supernatant discarded and the cells were resuspended in 300 μ l of cold buffer C. The suspension was incubated at 4°C with slow rotation for

20 minutes, passed through a syringe with a 27 gauge needle 60 times and centrifuged at 15000 g for 20 minutes at 4°C. The supernatant was collected and represented a cytosolic fraction.

To remove a possible contamination of the next fraction with cytosolic proteins, the pellet from this fraction was washed in 700 µl of buffer C and centrifuged at 15000 g for 20 minutes at 4°C. The supernatant was discarded. This pellet was resuspended in 150 µl of cold buffer N. The pellet was incubated at 4°C with slow rotation and centrifuged at 15000 g for 20 minutes at 4°C. The supernatant was collected and represented the nuclear fraction.

The pellet from the last fraction was recovered in 150 µl of cold buffer M and incubated with slow rotation at 4°C with subsequent centrifugation at 15000 g for 20 minutes at 4°C to obtain the supernatant (membrane fraction).

The fraction was collected and the pellet was resuspended in 75 µl of CS buffer per 10 million cells and incubated for 20 minutes with slow rotation at 22°C. Then the cytoskeleton proteins fraction was isolated by centrifuging at 15000 g for 20 minutes at 4°C. The pellet left from the last fraction was resuspended in Laemmli buffer (Appendix). All the proteins in other fractions were precipitated as described below in 2.4.1 (Appendix), and analysed further as in section 2.4.

2.3.7. Detergent resistant membrane fraction isolation

The cells were cultivated as in 2.1.1 or cultivated and transfected as in 2.1.2 in T25 flasks (Falcon). After a confluent monolayer had formed, cells were washed with ice-cold 25 mM Tris pH 7.5/ 150mM NaCl/ 5mM EDTA buffer and all other procedures were carried out at 4°C in a cold room with ice-cold reagents and equipment. The cells were scraped into 0.5 ml of the lysis buffer (25 mM Tris pH 7.5; 150mM NaCl; 5mM EDTA; 0.5 % triton X100 (v/v), protease inhibitor cocktail, phosphatase inhibitor cocktail (all from Sigma) and left for 15 minutes to lyse.

The lysate was mixed with 80 % (w/v) sucrose (Sigma) in MNE buffer (Appendix) and transferred into 5 ml centrifuge tubes (N344057) for a MLS-50 swinging bucket rotor (Optima™ MAX-XP Benchtop Ultracentrifuge, Beckman).

Above the sucrose/lysate mixture 1 ml of 27.5 % sucrose in MNE buffer (w/v) was layered on top. Without mixing with any of previous layers 0.5 ml of 5 % sucrose in MNE buffer (w/v) was applied. The tubes were centrifuged at average speed 200000 *g* for 18 hours at 4°C. Fractions of 180 µl were collected from the top of the gradient to the bottom and the fractionated protein was precipitated by trichlore acetic acid (TCA) as in 2.4.2 and analysed as in 2.4.1-2.4.4 sections of this chapter.

2.3.8. Retinal lysate preparation

Retinae were dissected from fresh porcine eyes (Cheal Meats) and washed with cold PBS at 4°C for 10 minutes three times with slow rotation. Excess buffer was removed and the retinae were placed in different ice-cold lysis buffers (see table 2.9), where they were mechanically homogenised by 10 passages in a cold Dounce homogeniser.

The lysates were centrifuged at 16200 *g* for 15 min at 4°C. The supernatants were collected and the protein concentration was measured by Bradford protein assay as in section 2.4.1. The lysates were stored at -80°C.

Buffer name	Buffer composition	Lysis conditions
Lysis buffer 1	25 mM Tris pH 7.5, 150mM NaCl, no detergents, Protease inhibitors coclail (PIC), phosphatases inhibitors cocktail (PhIC), 1 mM EDTA	Freeze-thawing
Lysis buffer 2	25 mM Tris pH 7.5, 150mM NaCl, 0,1 % Triton- X100, PIC, PhIC. 1 mM EDTA	15 min on ice
Lysis buffer 3	25 mM Tris pH 8.0, 150mM NaCl, 0,1 % Triton- X100, PIC, PhIC. 1 mM EDTA	15 min on ice
Lysis buffer 4	25 mM Tris pH 7,5, 150mM NaCl, 0.25 % deoxycholate, 1 % NP-40, PIC, PhIC. 1 mM EDTA	10 min on ice
Lysis buffer 5	25 mM Tris pH 7,5, 50mM NaCl, 0.25 % deoxycholate, 1 % NP-40, PIC, PhIC. 1 mM EDTA	10 min on ice
Lysis buffer 6	PBS (Appendix), 1 % n-Dodecyl-beta-D-maltoside (DM), PIC, PhIC.	15 min on ice
RIPA	RIPA (Appendix), PIC	15 min on ice

Table 2.9. Buffers and conditions used for cell and retinal lysis

2.4. Protein based techniques

2.4.1. Protein concentration determination

In order to determine the protein concentration of cell or retinal lysates the Bradford method was applied. Bradford technique is based on the observation of the absorbance shifts of an acidic solution of Coomassie Brilliant Blue G-250 from 465 nm to 595 nm when binding to protein. Both hydrophobic and ionic interactions stabilize the anionic form of the dye, causing a visible color change (Bradford, 1976). To measure the protein concentration 5 X Bradford reagent (Pierce) was diluted up to a final 1 X concentration and 200 μ l was added to each well of a 96 well plate (Starlab).

Protein concentration standards bovine serum albumin (BSA, Sigma) in a range from 100 ng to 1 mg were prepared in buffers used for cell or retinal lysis and added to the reagent. The buffer used for lysis, lysates and their dilutions were added to the reagent. Absorbencies were taken using a microplate reader Sapphire at 595 nm (Tecan, Germany GmbH). The calibration curve of absorbance to protein concentration was obtained using the BSA standards and the concentration in lysates was calculated.

2.4.2. Sample preparation and SDS-polyacrylamide gel electrophoresis (SDS-PAGE)

Protein for analysis after cell fractionation was precipitated from each fraction using trichloroacetic acid (TCA). For each fraction TCA was added to a final concentration of 5 % w/v and the tubes were incubated on ice for 10 minutes. After that the samples were centrifuged at 16200 g for 15 minutes at 22°C and the supernatants were discarded.

500 μ l of ice-cold ethanol was added to the pellets to remove residual TCA and the samples were centrifuged again as before. The ethanol was removed and the tubes left open for 10 minutes to evaporate residual ethanol. The dried pellet was resuspended in 30 μ l of 1 X Laemmli sample buffer (Appendix).

All other samples were prepared using 2 X or 4 X Laemmli sample buffer (Appendix) and heated at 98°C for 3 minutes. Gels were prepared using vertical BIO-RAD mini-protean II SDS-PAGE equipment or BIO-RAD, Protean®II xi Cell. An 11 % w/v resolving gel was used for most applications with a 3 % w/v stacking gel.

The samples were electrophoresed at 200 V until the bromphenol blue dye reached the bottom of the gel. The sizes of proteins, once detected, were compared to the protein ladder containing proteins of known molecular weights (PageRuler Prestained Protein Ladder, Fermentas).

2.4.3. Staining of protein gels using Coomassie Blue

Proteins separated by SDS-PAGE were fixed with methanol and glacial acetic and stained with 0.25 % w/v Coomassie brilliant blue R250 (Appendix). Gels were immersed in stain for 4 hours and then destained with a destain solution (Appendix) overnight. After that, gels were soaked in water with 20 % v/v glycerol for 1 hour and air dried between two pieces of cellulose film using Gel Drying Kit (Promega).

2.4.4. Silver stain of protein gels

All the solutions and washes were made with ultra-pure MilliQ water. The gel slab was fixed in two changes of 50 % v/v methanol with 5 % v/v acetic acid in water for 15 minutes each and followed by washing in 50 % methanol for 10 minutes. Then the gel was washed with water overnight to remove the remaining acid and methanol.

The gel was sensitised by a 1 min incubation in 0.02 % sodium thiosulfate (w/v), and rinsed with two changes of water for 1 min each. After rinsing the gel was submerged in chilled 0.1 % silver nitrate solution (w/v) and incubated for 20 min at 4°C. Then the silver nitrate was discarded and the gel slab was washed twice with water for 1 min, followed by the development in 0.04 % v/v formalin in 2 % w/v sodium carbonate with shaking.

Once the developer turned yellow, it was discarded and replaced with fresh solution since it is essential that the developing is carried out in an absolutely transparent solution.

After the desired intensity of staining was achieved, the development was terminated by discarding the reagent, followed by washing the gel with 5 % v/v acetic acid. Then the gel was rinsed with water twice for 30 min and the gel slab was stored in water at room temperature until analysed.

2.4.5. Western blotting

Proteins were transferred from SDS-PAGE gels to 0.45 μm pore size nitrocellulose membrane (Protran[®], Whatman) by semi-dry electrophoretic transfer (BioRad) at 15 V and 0.8 A for 2 mini gels for 20 minutes. Non-specific binding sites of the membrane were blocked by incubation in 3 % (w/v) Marvel Skimmed milk powder (Premier Brands) for 1 hour at room temperature.

The blots were hybridised with primary antibody (table 2.10) in blocking solution for 1 hour, washed 3 times for 5 minutes with 0.05 % Tween-20 (v/v) in PBS and subsequently incubated with appropriate horseradish peroxidase-conjugated (HRP) secondary antibody (table 2.11) in blocking solution and further washed with 0.05 % Tween-20 in PBS as before.

Immunoreactive bands were detected using an enhanced chemiluminescence reagent (ECL, GE Healthcare) according to the manufacturers protocol and visualised by exposing to X-ray film (Fuji Film).

Antibody name	Specificity	Raised in	Supplier	Titer for WB	Titer for IP
S974	RP2	sheep	our own	1:1000	1:50
Arl3 854	Arl3	rabbit	Gift Dr N.Cowan	1:2000	1:200
Anti-BART1	BART1	rabbit	Gift Dr R. Kahn	1:1000	-
PA1-725	Transducin β	rabbit	ABR	1:500	-
(C-16):sc-379	Transducin β	rabbit	Santa Cruz	1:1000	1:50
(K-20):sc-389	Transducin α	rabbit	Santa Cruz	1:2000	-
PDS1	Visual arrestin	mouse	Santa Cruz	1:500	-
F4C1	Pan arrestin	rabbit	Gift Dr V. Gurevich	1:2000	-
G8795	GAPDH	mouse	Sigma	1:40000	-
M0725	Vimentin	mouse	Dako	1:500	-
CNX	Calnexin	mouse	StressGen	1:10000	-
T4026	β -tubulin	mouse	Sigma	1:2000	-
M2	FLAG	mouse	Sigma	1:2000	1:100
NCL	Nucleolin	rabbit	Sigma	1:5000	-
BRM22	Hsp70/Hsc70	mouse	Sigma	1:1000	-
9E10	Myc	mouse	Sigma	1:2000	-

Table 2.10. Primary antibodies used for Western blotting and immunoprecipitation.

Specificity	Raised in	Supplier	Titre
Mouse IgG	donkey	Pierce	1:10000
Rabbit IgG			1:30000
Sheep IgG			1:7000

Table 2.11. HRP conjugated secondary antibody used for Western blotting.

2.4.6. Production of recombinant proteins

Prior to large scale production of GST- or His-tag fusion recombinant proteins, each of the constructs was checked in small-scale analytical expression studies and examined by SDS-PAGE. The expression studies were used to confirm that the bacteria efficiently expressed the recombinant proteins of the correct size and to optimise conditions for the preparation of each protein. For optimal protein expression and yield, all plasmids were transformed into OneShot TOP10 competent cells (Invitrogen) as described in 2.1.2 and two single colonies from each transformation were used to inoculate an overnight starting culture of 10 ml of LB (Appendix) with 50 µg/ml of ampicillin.

2.4.7. Preparation of recombinant proteins

The overnight cultures of transformed OneShot TOP10 cells were grown as described in 2.3.5. These cultures were used to inoculate 500 ml of LB with 50 µg/ml ampicillin for GST-Arl3s and His-PFDN5 and in 700ml for GST-RP2. The cells were grown in an orbital incubator at 37°C with 250 rpm shaking until OD₆₀₀ reached 0.6. The protein expression was induced by adding of isopropyl-beta-D-thiogalactopyranoside (IPTG) (Sigma) to a final concentration 1 mM and incubated further for 2-4 hours at 37°C or 35 °C, depending on the levels of protein expression determined by a scaled-down expression studies.

The cells were harvested by centrifugation at 6000 *g* for 15 minutes at 4°C and the pellet was resuspended in 15 ml of PBS, containing protease inhibitor cocktail for bacterial cultures (Sigma). The cells were then sonicated on ice 10 X 10 second pulses with 30 second cooling between them, using a 9 mm probe sonicator (MSE Soniprep 150). The resulting lysate was cleared by centrifugation at 14000 *g* for 30 min at 4°C. The supernatant was filtered through 45 µm membrane (Millipore) and the pellet was discarded.

2.4.8. Purification of GST-fused recombinant protein

The GST-fused recombinant proteins were purified by affinity chromatography using glutathione sepharose (GE Healthcare). All steps were performed using pre-chilled buffers and plastic ware to maintain protein stability. 200 µl of the

sepharose slurry was loaded onto each 10ml polypropylene column and washed with 2 ml of PBS once.

The clarified supernatants were added to the columns and allowed to pass through by gravity flow, collected and re-applied three times. After that the columns were washed with 50 ml of PBS using a peristaltic pump with a flow rate approximately 5 ml/ min. Proteins were left non-eluted from the columns.

2.4.9. GST pull-down

All steps were carried out at 4°C using pre-chilled buffers and plastic ware. The beads of glutathione-sepharose with GST-fused recombinant proteins bound to them were washed in 1.5 ml of the buffer which was used for cell lysis (table 2.8). The beads were transferred from columns into Eppendorfs and centrifuged at 500 *g* for 2 minutes. The supernatant was discarded and 500 µg of total protein from the mammalian cell lysates or retina lysates (table 2.8) was added to 50 µl of the beads. The reactions were incubated overnight with slow rotation. The samples were then centrifuged at 500 *g* and washed 4 times with appropriate lysis buffer without PIC and the detergents. Afterwards the beads were resuspended in 50 µl of 2 X Laemmli buffer and kept at -20°C until analysed.

2.4.10. Mass spectrometry

The samples from GST pull-down experiment were resolved by Protean®II xi Cell SDS-PAGE (as described in 2.4.2) with subsequent mass-spectrometry compatible silver stain (see 2.4.5). The unique bands were excised and digested in the gel, using a robotic system as described in Wait *et al.* (2001) by Dr. Robin Wait, Kennedy Institute of Rheumatology Division, Faculty of Medicine, Imperial College London. Tandem mass spectra were recorded using a Waters Q-ToF (Waters, Manchester, UK) interfaced to a Waters CapLC capillary chromatograph.

Samples were dissolved in 0.1 % v/v aqueous formic acid and injected onto a Pepmap C18 column (300 µm x 0.5 cm; LC Packings, Amsterdam, NL) and eluted with an acetonitrile/0.1 % formic acid gradient v/v (5 %-70 % acetonitrile

over 20 minutes) at a flow rate of 1 μ l per minute. The capillary voltage was 3500 V. A survey scan over the m/z range 400-1300 was used to identify protonated peptides with charge states of 2, 3 or 4, which were automatically selected for data-dependent MS/MS analysis, and fragmented by collision with argon.

The resulting product ion spectra were transformed onto a singly charged m/z axis (MaxEnt3, Waters) and proteins were identified by correlation of uninterpreted spectra to entries in the NCBI nr database using MASCOT (www.matrixscience.com).

2.4.11. Co-immunoprecipitation from mammalian cell or retinal lysates

Transfected cells or the retina lysate prepared with lysis buffer 4 (table 2.9) was pre-cleared with protein G sepharose to minimise non-specific binding. For each sample 50 μ l of protein G sepharose slurry was washed twice with 500 μ l of the appropriate lysis buffer (table 2.9), prepared without protease and phosphatase inhibitors, and centrifuged at 16200 g for 2 min at 4°C after each wash. These beads were incubated with 500 μ g of total protein in 500 μ l for 1 hour at 4°C with slow rotation.

The pre-cleared lysates were then incubated with the antibodies (table 2.6) at 4°C over night with slow rotation followed by binding with prepared protein G beads as above for 1 hour at 4°C with rotation. The tubes then were centrifuged for 2 min, the supernatants were removed and the beads were washed 5 times with 500 μ l of ice-cold appropriate buffer.

After the last wash the supernatants were aspirated and 50 μ l of 2 X Laemmli buffer was added to the pellets. The samples were incubated for 15 min at room temperature, boiled for 3 min, centrifuged at 16200 g for 2 min, resolved by SDS-PAGE and analysed by standard protein blotting techniques described in sections 2.4.2 - 2.4.5.

2.5. Automated DNA sequencing

Cycles of DNA denaturation, primer annealing and DNA synthesis with dNTPs and fluorescently labeled ddNTPs form the basis of automated sequencing. These ddNTPs lack an -OH residue at the 3' position of the deoxyribose, which prevents the formation of a phosphodiester bond when incorporated into elongating DNA, leading to chain termination. Thus reaction products contain a set of DNA segments of different lengths, each terminating with different labeled ddNTPs, which is detected by fluorescence signal in sequencer.

2.5.1. Genomic sequencing

For screening of the *PFDN5* gene, its exons were amplified by PCR as described in 2.1.1 section. Before sequencing, PCR products were purified to remove unincorporated nucleotides and primers by using 1 U of ExoSAP-IT® (USB), which contains Exonuclease I and Shrimp Alkaline Phosphatase in a specially formulated buffer. A 2 µl aliquot of each PCR product was diluted in 23 µl of water and treated with 1 U of ExoSAP-IT for 15 min at 37°C, followed by 80 °C for 15 min to inactivate the enzyme. The purified DNA was then used for sequencing: 13 µl of DNA, 5 µl of TM buffer (200 mM Tris pH 9.0, 5 mM MgCl₂), 1 µl of Big Dye® Terminator Version 3.1 and 1 nM of a specific forward or reverse primer (table 2.2).

The sequencing reaction consisted of 30 cycles of 96°C for 30 sec, 50 °C for 15 sec and 60 °C for 4 min and was carried out in Techne Genius PCR thermocycler. Sequencing reaction products were precipitated by adding 26 µl of precipitation solution (120 mM NaOAc in 95 % (v/v) ethanol) at -20°C for 10 min, centrifuged at 16000 g for 30 min and the supernatant was discarded, then the pellet was washed with 200 µl of 70 % (v/v) ethanol and centrifuged for 10 min at 16000 g. The supernatant was carefully removed and the pellets were dried at 65 °C for 5 min. The pellets were resuspended in 11 µl of formamide and loaded onto an ABI 3100 automated sequencer.

2.5.2. Plasmid sequencing

To identify putative interacting partners of RP2 identified during the yeast-two hybrid screen, 2µl aliquots of each pMyr plasmid miniprep DNA with an insert containing a potential interactor was sequenced. This was combined with 1.5 µl of TM buffer (200 mM Tris pH 9.0, 5 mM MgCl₂), 4 µl of Big Dye[®] Terminator Version 3.1 (Applied Biosystems) and 1 nM of a specific forward or reverse primer (table 2.12). The sequencing reaction consisted of 30 cycles of 96°C for 30 sec, 50 °C for 15 sec and 60 °C for 4 min and was carried out in Techne Genius PCR thermocycler.

Sequencing reaction products were added to 26 µl precipitation solution (120 mM NaOAc in 95 % (v/v) ethanol) and incubated at room temperature for 10 min, centrifuged at 16000 g for 10 min and the supernatant was discarded. The pellets were washed with 100 µl of 70 % (v/v) ethanol and centrifuged for 10 min at 16000 g. The supernatant was carefully removed and the pellets were dried at 65 °C for 1-5 min. The pellets were resuspended in 12 µl of formamide and loaded onto an ABI 3100 automated sequencer.

Primer name	Primer sequence 5'-3'
pMyr F	ACTACTAGCAGCTGTAATAC
pMyr R	CGTGAATGTAAGCGTGACAT
Bovine Arl3 F	ATGGGCTTACTCTCAATTC
Bovine Arl3 R	TTATTTCTTCTTTGCGCTGAC
Bovine Arl2 F	ATGGGGCTTCTGACCATACT
Bovine Arl2 R	TCAGTCGGCCATGAAGATGC
Clone 46 fragment 2 F	GCCAAACAGCTCGCTGACCAA
Nucleolin fragment 2 F	GCTCCTGAAGCCAAGAAAC
Nucleolin fragment 2 R	CTATCCCTTCTCTCCCTCTTC
Nucleolin fragment 3 F	GCAGCTCCTGAAGCCAAG
Nucleolin fragment 3 R	CCATGTACAAAACCATTTTTTTCC
Nucleolin fragment 4 F	CCATTTCTCTGTACTACACCG

Table 2.12. Primers used for sequencing of pMyr clones

2.6. Bioinformatics and software

For analysing of DNA sequences for the presence of internal restriction sites which could interfere with subcloning into vectors EditSeq and MapDraw applications of DNA star program® (DNA Star Inc) were used.

Carl Zeiss AIM software was used to analyse confocal microscopy images (2.3.5). Images were studied and exported using LSM Image browser (Carl Zeiss).

For the analysis of the data obtained from the mass spectrometry procedure the MASCOT program (www.matrixscience.com) was used in conjunction with NCBI nr database for peptide sequence identification.

To identify the sequences obtained from yeast two-hybrid screens the UCSC (University California Santa Cruz) genome bioinformatics site <http://genome.ucsc.edu> and the NCBI site (National Center for Biotechnology Information) <http://www.ncbi.nlm.nih.gov> were used for BLAST analysis of nucleotide and predicted protein sequence. Genomic alignments with the cDNA sequences were also compared.

For protein sequence prediction, computation of the theoretical pI (isoelectric point) and Mr the ExPASy Proteomics Server was used <http://www.expasy.org>. For the protein structure analysis Protein Data Bank with RasWin software was used (<http://www.rcsb.org/pdb> www.rasmol.org).

The SeqMan 4.03 tool of DNA star program® (DNA Star Inc) was employed for analysis of DNA sequencing reaction products since it allows the display of an ABI chromatogram and aligns sequences obtained using ABI sequencer. Other tools for DNA chromatogram reading such as BioLign 4.0.6 (Biosoft Net, <http://en.bio-soft.net>) were also used mainly for plasmid sequence analysis. For single nucleotide polymorphism identification the SNP database of NCBI was searched (<http://www.ncbi.nlm.nih.gov/projects/SNP>).

Figures were cropped, adjusted and annotated using Adobe Illustrator CS2 and Adobe Photoshop CS2.

Chapter III. Novel putative interacting partners of RP2 identified by yeast two-hybrid screening

3.1. Introduction

In order to find novel interacting partners of RP2, a yeast two-hybrid system was used. The system was developed almost 20 years ago by Fields and Song (1989). It was based on the principle that when two functional domains of a transcription factor (DNA binding domain and transcriptional activation domain) are separated and are able to exist independently. For the transcription factor to activate a reporter gene its two domains must be physically brought together. For this purpose the cDNA of a protein of interest, the “bait”, was fused with the DNA binding domain and putative interacting protein cDNA, the “prey”, with the transcriptional activation domain. When a “bait” protein interacts with a “prey” protein, two domains of the transcription factor are joined and the reporter gene is activated (β -galactosidase), which can then be detected by an appropriate assay.

Variations on this methodology have been developed since it was first published. In this study the Son of Sevenless (Sos) recruitment system was used. It is based on using a strain of yeast, *cdc25-H*, which contains a point mutation at position 1328 of *Cdc25* gene. The *cdc25* yeast protein is functionally homologous to human Sos (hSos). *Cdc25* and hSos proteins act as guanyl nucleotide exchange factors for Ras, which is required for yeast growth, and hSos is able to substitute this function of *cdc25* in mutant yeast (Broder *et al.*, 1998). The mutant strain is temperature sensitive and the yeast are able to grow only at 22-25°C (permissive temperature) but not at 37°C (restrictive temperature) (Aronheim *et al.*, 1994).

The protein of interest is fused with hSos and is used as a “bait”. The fusion protein hSos-“bait” can activate Ras, compensating the mutant *cdc25*, only when it is targeted to the membrane. For this study a bovine retina cDNA library

was used in the pMyr vector which attaches a myristoylation signal to the N-terminus of target proteins (Stratagene, CytoTrap®). When the “bait” physically interacts with the target protein expressed from the library, it recruits hSos to the plasma membrane. The Ras pathway becomes activated by hSos and the mutant yeast strain can grow at the restrictive temperature (Figure 3.1).

This system has several advantages compared to the one developed by Fields and Song in 1989. First, the proteins do not have to be transported into the nucleus, so it may be used for proteins which do not translocate easily. Second, it allows limited post-translational modifications that may occur in the cytoplasm and might be important for the interaction. A further advantage of CytoTrap® is the signal amplification by the cascade nature of the Ras activating pathway, which helps to reveal even weak interactions. This system was the most suitable one for detecting of potential RP2 interactors since RP2 is dually acylated and targeted to the cytosolic surface of the plasma membrane (see 1.5.3). As such, the localisation of a “prey” to the plasma membrane was considered to be closer to the normal physiological environment for RP2 than the nucleus.

However, this system also has problems that are typical for all yeast two hybrid strategies. One of them is false positive interacting partners, which are either able to activate the Ras pathway without recruiting hSos or are able to substitute yeast Ras and cause growth at 37°C. Another problem is that CytoTrap® uses a temperature sensitive strain which is prone to a phenomenon of reversion to the non-temperature sensitive phenotype. This phenomenon occurs when yeast start to compensate for the impaired Ras pathway by alternative pathways and become able to grow at 37°C (Huang *et al.*, 2001).

Despite these difficulties, the yeast two-hybrid system is suitable as a method for identifying protein-protein interactions. It has been used to successfully identify many protein-protein interactions including an interaction between GABAp1 and cellular retinoic acid binding protein (CRABP) (Song *et al.*, 2005).

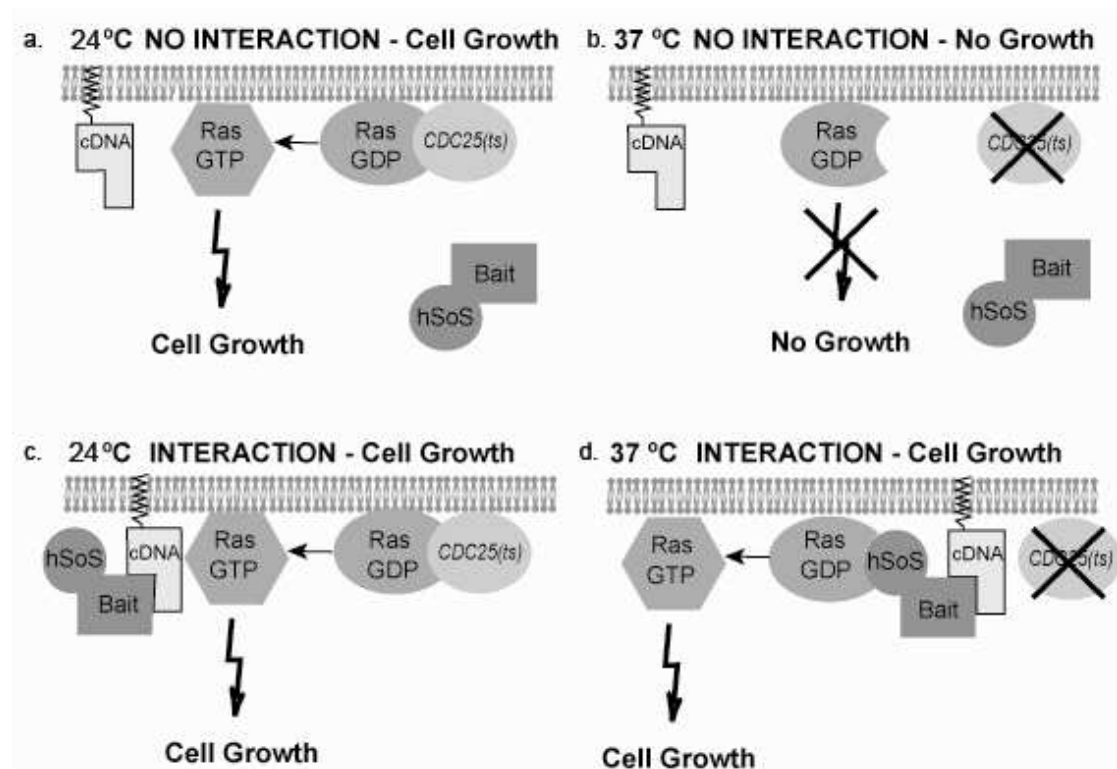


Figure 3.1. Schematic of yeast two-hybrid hSos recruitment system (CytoTrap®)

a. At a permissive temperature (24°C) the yeast are able to grow due to the *cdc25* mutation having no effect. **b.** At the restrictive temperature (37°C) when there is no interaction between the "bait" and the "target" yeast are not able to grow. This is due to the mutant strain being unable to convert Ras-GDP into Ras-GTP and thus growth at 37°C does not occur. **c.** At the permissive temperature the yeast grow whether there is an interaction or not. **d.** If there is an interaction, the loss of function of *cdc25* is compensated by the recruitment of hSos to the plasma membrane. This causes the conversion of Ras-GDP to a GTP bound form and the yeast cells are able to grow at the restrictive temperature (Evans *et al.*, 2005).

The interaction of RP2 and Arl3 was studied using the CytoTrap® method as an *in vivo* system (Evans *et al.*, 2005). During screening for RP2 interactors with a bovine retina cDNA library, 91 % of putative positive interactors were represented by Arl3 (Evans, 2007), indicating that this interaction *in vivo* is very abundant. Using CytoTrap® it was also revealed that RP2 was able to bind Arl2, although with a much lower affinity compared to Arl3. This interaction required full length RP2 and did not show any binding to the N-terminus of RP2 (1-200 AA) unlike Arl3 (Evans, 2007). RP2 and Arl2 have not been described as interactors (Bartolini *et al.*, 2002; Kuhnel *et al.*, 2006). However, in biochemical studies of GAP activity, Arl2 demonstrated a weak GTP hydrolysis upon incubation with RP2 at stoichiometric concentration (Veltel *et al.*, 2008a), indicating that the CytoTrap® system is highly sensitive to weak interactions. Moreover, several novel potential interacting partners binding to the C-terminus of RP2 (190-350 AA) were identified by this method during screening of RP2 with a bovine retina cDNA library (Evans, 2007).

One of the novel interactors was a small GTPase RAN (Evans, 2007). RAN protein (CAG 29343) is a small GTPase of Ras superfamily that localises predominantly in the nucleus (Macara, 2001; Kornbluth *et al.*, 1994). Studies into RAN function suggested involvement in the nucleo-cytoplasmic transport of proteins (Ribbeck *et al.*, 1998; Yoneda *et al.*, 1999) and mitotic spindle formation (Kalab and Heald, 2008). The role of the interaction of RP2 with RAN is unclear. The L253R mutant of RP2, along with misfolding mutants (C67T and C86T) disrupted the interaction. Interestingly, the interaction of RP2 and RAN was stronger when RAN was in a GDP-locked conformation.

Another of the identified interacting partners was p27 (cyclin dependent kinase inhibitor 1, BAA25263). High levels of p27 are associated with different types of cancer (Curry *et al.*, 2008; Caldon *et al.*, 2006). This protein is involved in cell cycle control progression from G1 to S phase (Caldon *et al.*, 2006). It was demonstrated that RAN is involved in p27 nuclear export (Connor *et al.*, 2003). Transportin 3 from importin- β family (TNPO3, NP036602), which was also identified in the CytoTrap® screen along with RAN and p27, is mainly involved in the transport of proteins into the nucleus. It takes part in transport of SR

proteins and splicing regulators to the nucleus in conjunction with RAN (Lai *et al.*, 2001). Thus, these three putative interacting proteins found during CytoTrap® screening by Dr. R.J. Evans (2007) belong to one nuclear transport pathway, possibly involving RP2. The mechanism of nuclear transport could potentially be involved in RP2 retina degeneration pathogenesis. There are numerous mutations in genes encoding splicing factors which cause retinal degeneration, such as PRPF31 (Chakarova *et al.*, 2002), PRPF8 and 3 (Gamundi *et al.*, 2008). Potentially their impaired transport to the nucleus could cause retinal degeneration.

To date, the putative novel interacting partners of RP2 found during CytoTrap® screening were proteins with a ubiquitous expression pattern which bound to the C-terminal region of RP2 (amino acids 190 to 350) (Evans, 2007). This region includes the NDK homology domain and a short linker region between this domain and the N-terminus (see 1.5.2). However, most of pathogenic mutations in *RP2* are found in the N-terminal region and the only known interacting partner for the N-terminus of RP2 is Arl3. Therefore, it was important to identify and confirm novel interacting partners of RP2 that would shed light on RP2 function in the retina.

Yeast two-hybrid screening has been successfully used to identify retina specific interacting partners for other retinal degeneration related proteins. For example, the screening of a ubiquitously expressed protein causing X-linked retinitis pigmentosa, RPGR, was performed by Boylan and Wright (2000) and Roepman *et al.* (2000). The RCC1 domain of this protein was used as “bait” for screening a retinal cDNA library, which resulted in identification of a retina-specific protein, RPGRIP1. This protein was subsequently found to be a causative gene for Leber congenital amaurosis (Dryja *et al.*, 2001; Gerber *et al.*, 2001).

Therefore, CytoTrap® was chosen for further screening for new interactions using the full-length RP2 and its domains as “bait”. A schematic of the fragments of RP2 used for screening, domain mapping and the RP2 mutants tested for interaction are shown in figure 3.2.

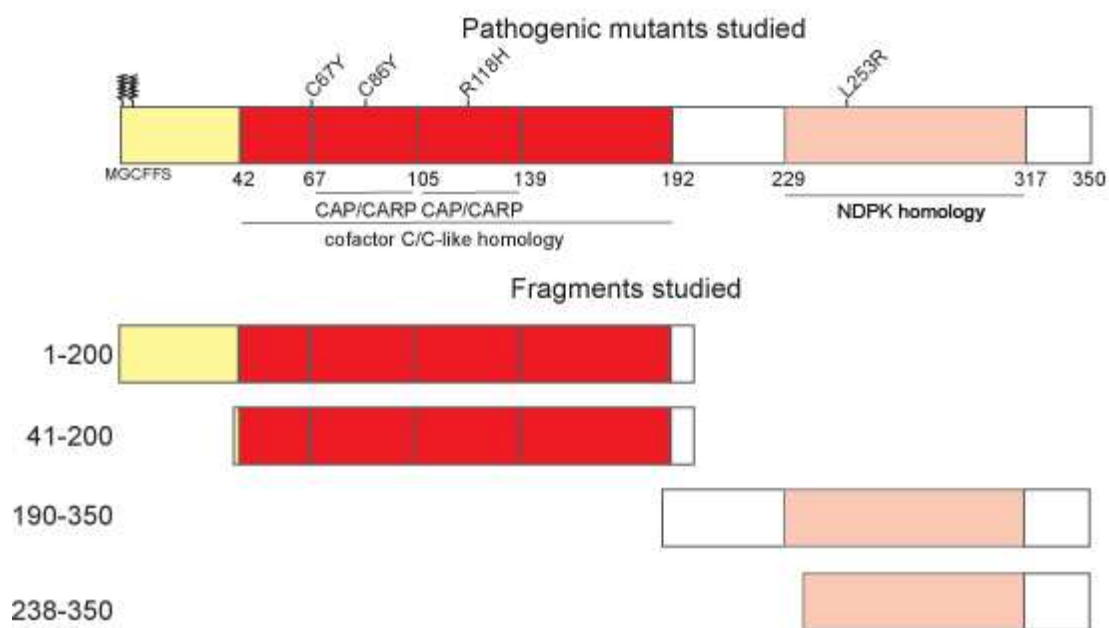


Figure 3.2. Schematic of fragments and mutants of RP2 used in CytoTrap®

The top panel represents a schematic of the domain structure of the RP2 protein. The N-terminal acylation motif is shown by two tags representing the myristoylation and palmitoylation posttranslational modifications. The position of introduced pathogenic amino acid substitution mutations is indicated. Panels below show the fragments used in CytoTrap®. Yellow boxes illustrate the very N-terminal region, red boxes highlight the cofactor C homology domain, pink boxes correspond to the NDPK homology domain.

3.2. CytoTrap® system characterisation

The CytoTrap® system was first tested with positive and negative control plasmids, provided by the manufacturer (Stratagene). The yeast strain *cdc25-H* was maintained as described in 2.2.1. The yeast cells were co-transformed with pSos RP2 or its fragments and mutants (figure 3.2, described in section 2.1.8) and pMyrSB as a positive control (hSos-binding). This plasmid contains Sos binding protein as a “prey” and therefore when it is targeted to the membrane by the myristoylation signal it binds to hSos, activating the Ras pathway and thus, yeast are able to grow at 37°C. For the negative control all RP2 constructs were co-transformed with pMyr LaminC since Lamin C protein does not interact with hSos or RP2.

Upon co-transfection with RP2 constructs and the positive control plasmid, yeast exhibited growth at 24°C on the selective media after 72 hours of incubation. After replating several yeast colonies from each transformation (as in 2.2.6) it was found that yeast cells were able to grow at 37°C on selective media. The intensity of yeast growth when using the same positive control plasmid as a “prey” directly corresponds to the expression level of the hSos fusion construct (Evans, 2007).

It was revealed that the positive control (pMyr SB) with wild type pSos and 1-200 RP2, 190-350 RP2 fragment fusions with hSos co-transfected grew on the first day of incubation at the restrictive temperature (37°C) on selective media, indicating a high expression level of RP2 and these fragments (figure 3.3a). The intensity of yeast growth was higher in yeast transformed with the wild type RP2 than any of the domain deletions. Yeast expressing RP2 fragments 42-200 and 238-350 and hSos binding protein exhibited growth only after 72 hours of incubation at 37°C, suggesting low expression level of these RP2 fragments (figure 3.3a).

The hSos-RP2 constructs were tested in the system with the negative control plasmid pMyr LaminC (Figure 3.3b). It was found that after 144 hours of incubation at 37°C on the selective media, none of the constructs exhibited visible growth. However, after incubation longer than 144 hours weak growth

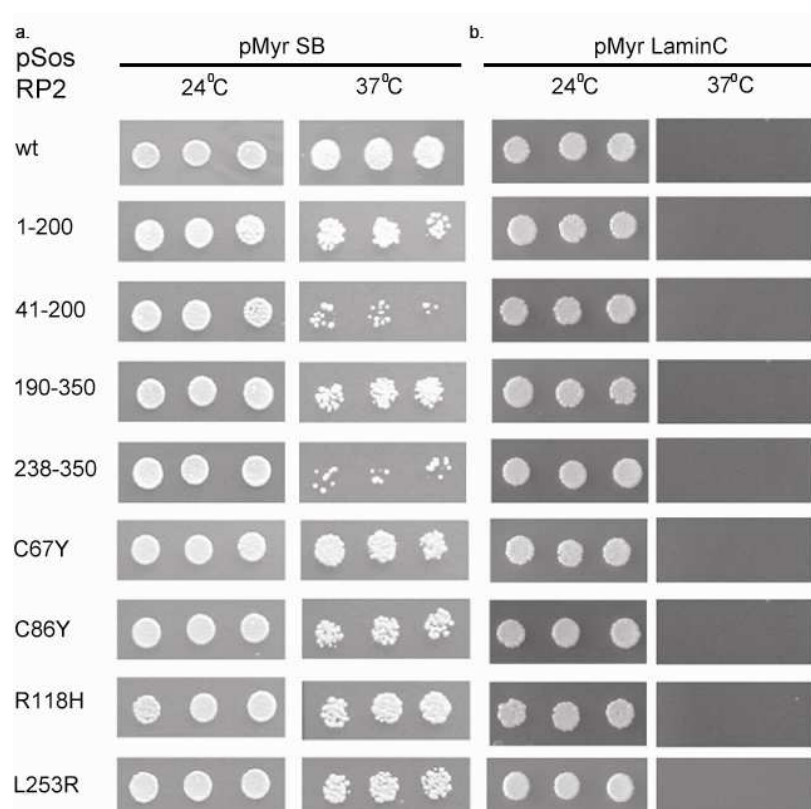


Figure 3.3. Interaction of hSos-RP2 constructs with positive and negative controls

Three different colonies for each transformation were spotted onto selective media as described in 2.2.6. The growth observed after incubation at the non-restrictive temperature (24°C) for 96 hours and at the restrictive temperature (37°C) for 144 hours is shown. Each saturated spot contains approximately 1×10^8 yeast cells. **a.** Growth of yeast co-transformed with pSos RP2 constructs and a positive control plasmid pMyr SB. **b.** Co-transformation of yeast with pSos RP2 constructs and the negative control plasmid pMyr LaminC resulted in growth only at 24°C and not at 37°C.

was observed in yeast co-transformed with pMyr Lamin C and full-length pSos RP2 or pSos 190-350 RP2 fragment. The yeast growth was more pronounced after 168 hours of incubation (data not shown) therefore indicating a low level of transactivation. Results for the full length RP2 and its 190-350 fragment were therefore evaluated after a maximum 144 hours of incubation at the restrictive temperature on the selective media.

3.3. Screening of the bovine retinal cDNA library with the full length human RP2

Cdc25-H yeast cells were co-transformed with the pSos RP2 construct and a bovine retinal cDNA library as described in 2.2.2. The co-transformed yeast cells were incubated on the selective media at 24°C. The colonies from each transformation were counted for analysis of the number of “prey” plasmids screened and yeast transformation efficiency. The plates were then replica-plated and incubated at 37°C restrictive temperature on the selective media with galactose to activate the library vector promoter and induce expression (as in 2.2.3).

Single colonies which exhibited growth under such conditions after 144 hours were picked and cultivated (2.2.4). Total yeast DNA from selected colonies was isolated as described in 2.2.4. Bacterial cells were then transformed with isolated total yeast DNA to derive pMyr plasmids of putative interacting partners as described in section 2.2.5.

The cdc-25H yeast strain is prone to produce temperature resistant revertants (described in 3.1), causing yeast cells to grow at 37°C. Such yeast, being transformed with empty pMyr or pMyr containing “prey”, would exhibit growth on the selective media at 37°C, giving a false positive result.

This problem was overcome two ways. First, the number of revertants from each transformation was monitored at 37°C on non-selective media (as in 2.2.5). When this number was more than 30 revertants per plate, the transformation was considered not successful and was not analysed further.

Secondly, verification of a putative interaction was performed by re-transformation from another batch of *cdc25-H* yeast with newly isolated pMyr clone and pSos RP2 or pSos. This would eliminate false positive interacting partners binding to Sos or Ras pathway activators. At least three colonies for each pMyr clone were then tested for growth on the selective media at 37°C to ensure that the isolated pMyr clones caused yeast growth at 37°C on the selective media in the presence of pSos RP2(2.2.6).

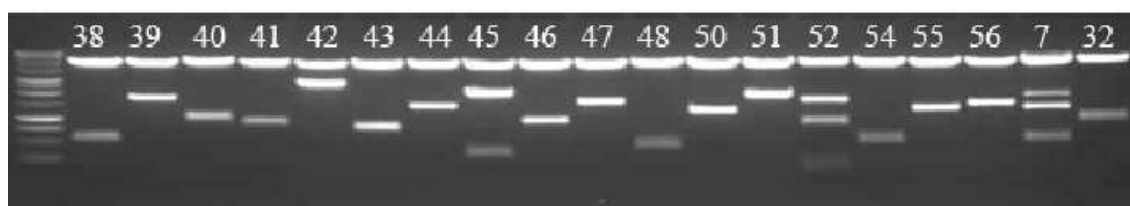
Approximately 250,000 colonies of yeast transformants were obtained during the screening of pSos RP2 with the retinal library, which were able to grow on selective media at 24°C permissive temperature. After screening for the ability to grow at 37°C (as described in 2.2.3), 135 putative positive colonies were isolated and checked for the presence of pMyr clone inserts by restriction with *EcoRI* and *SaI* (figure 3.4).

Upon analysis of clones which grew in the first 48 hours of library screening, it was revealed that most of them (124) did not demonstrate any growth, suggesting they were revertants. 9 colonies exhibited growth upon re-transformation with pSos RP2 at 37°C on the selective media. The pMyr cDNA inserts were sequenced as in 2.5.2 and bioinformatic analysis revealed that the open reading frames of these nine pMyr plasmids corresponded to in frame *Arl3* coding sequence (data not shown).

The other three clones that exhibited growth in the re-transformation test (as in 2.2.5) grew at a slower rate with colonies visible between 48 and 144 hours of incubation at 37°C. The inserts of these cDNA were sequenced as in 2.5.2 and clone 28 contained an open reading frame encoding *TNPO3* (data not shown). This interacting partner has been reported previously (Evans, 2007).

The other two clones that exhibited growth at 37°C on the selective media during interaction verification were sequenced and it was identified that open reading frames of these clone contained coding sequences of novel putative interacting partners of RP2. The screen summary is shown in figure 3.4b.

a.



b.

	Full length RP2 as "bait"	1-200 RP2 fragment as "bait"
No. Colonies screened	~224,000	~60,000
No. potential interactors	135	86
No. interactors analysed	135	69 (first 17 excluded)
No. revertants/ False positives (%)	124 (91.8 %)	62 (89 %)
No. Interactors	12	7
No. Arl3 clones	9	2
No. of TNPO3 clones	1	0
Novel putative interactors	2	5

Figure 3.4. Summary of CytoTrap® screening performed in this study

a. Examples of analytical restriction digest with *EcoRI* and *SaI* of isolated pMyr plasmids of putative interacting partners. The lane on the left represents a 1kb DNA ladder. Clone numbers are as indicated. **b.** Tabulated summary of CytoTrap® screening of pSos RP2 and pSos 1-200 RP2 fragment with a bovine retinal cDNA library.

3.3.1. Nucleolin

Clone 30 was verified for interaction upon re-transformation with pSos RP2. This pMyr clone proved negative for the interaction with an empty pSos vector (figure 3.5). Clone 30, when co-transformed with full-length RP2, demonstrated visible growth after 48 hours of incubation at 37°C on the selective media (figure 3.5).

The plasmid was sequenced and the electropherogram was interpreted as described in 2.5.2 and 2.6. The open reading frame of pMyr clone 30 had 100 % identity to cDNA of nucleolin (NCL) (figure 3.6a).

The protein sequence was predicted by bioinformatics tools (2.6) using the insert in frame DNA sequence and it was revealed that the protein contained 573 amino acids with a molecular weight 62.6 kDa and calculated pI 4.57. The protein sequence was used to search for matches against the NCBI database (2.6) and it was found that the protein sequence of clone 30 had 100 % identity to bovine NCL isoform 1 ([XP_614626](#)) (figure 3.6c).

The identity between clone 30 and NCL began at clone 30 residue 67 and extended to the C-terminus (amino acid 720) including predicted RNA recognition motif (RRM) domains of the NCL protein (figure 3.6). The first 66 amino acids did not match any proteins in the databases searched (2.6), but the DNA showed 100 % identity to an in frame region of the intron 4 of the bovine *NCL* gene suggesting either alternate or incomplete splicing (figure 3.6a).

3.3.1.1. Characterisation of NCL interaction with RP2 in CytoTrap®

Clone 30 was tested further by CytoTrap® to determine which domain of RP2 takes part in binding to NCL and whether RP2 mutants were able to affect this interaction.

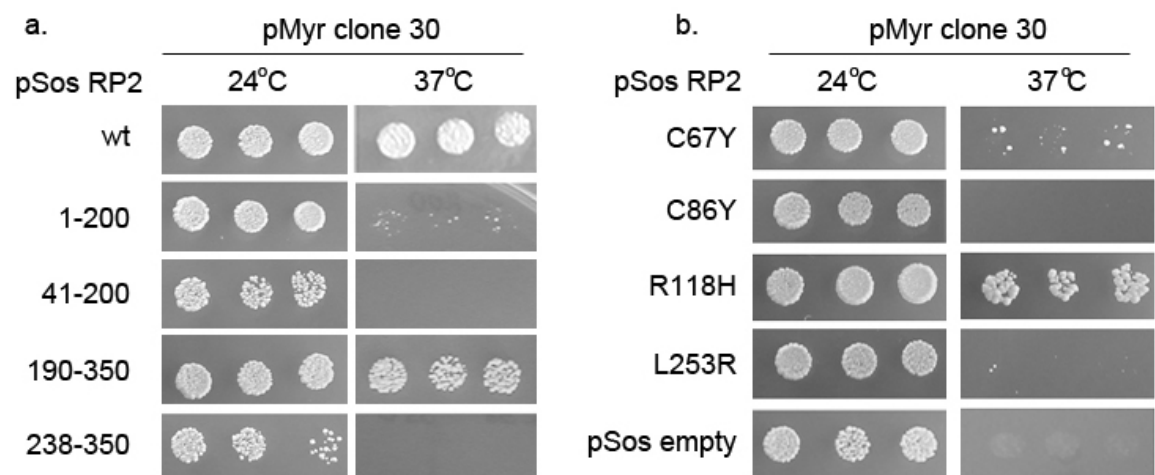


Figure 3.5. Interaction of clone 30 with RP2 in CytoTrap®

a. Growth of yeast co-transformed with pMyr clone 30 and wild type (wt) pSos RP2 and RP2 fragments as indicated. Three different colonies were used for each transformation and were tested at the permissive (24°C) after 96 hours of incubation on the selective media, and at the restrictive temperature (37°C) after 144 hours. **b.** Yeast growth when co-transformed with pMyr clone 30 and pSos RP2 mutants as indicated. Yeast tested for growth at two temperatures on the selective media with pSos empty vector negative control.

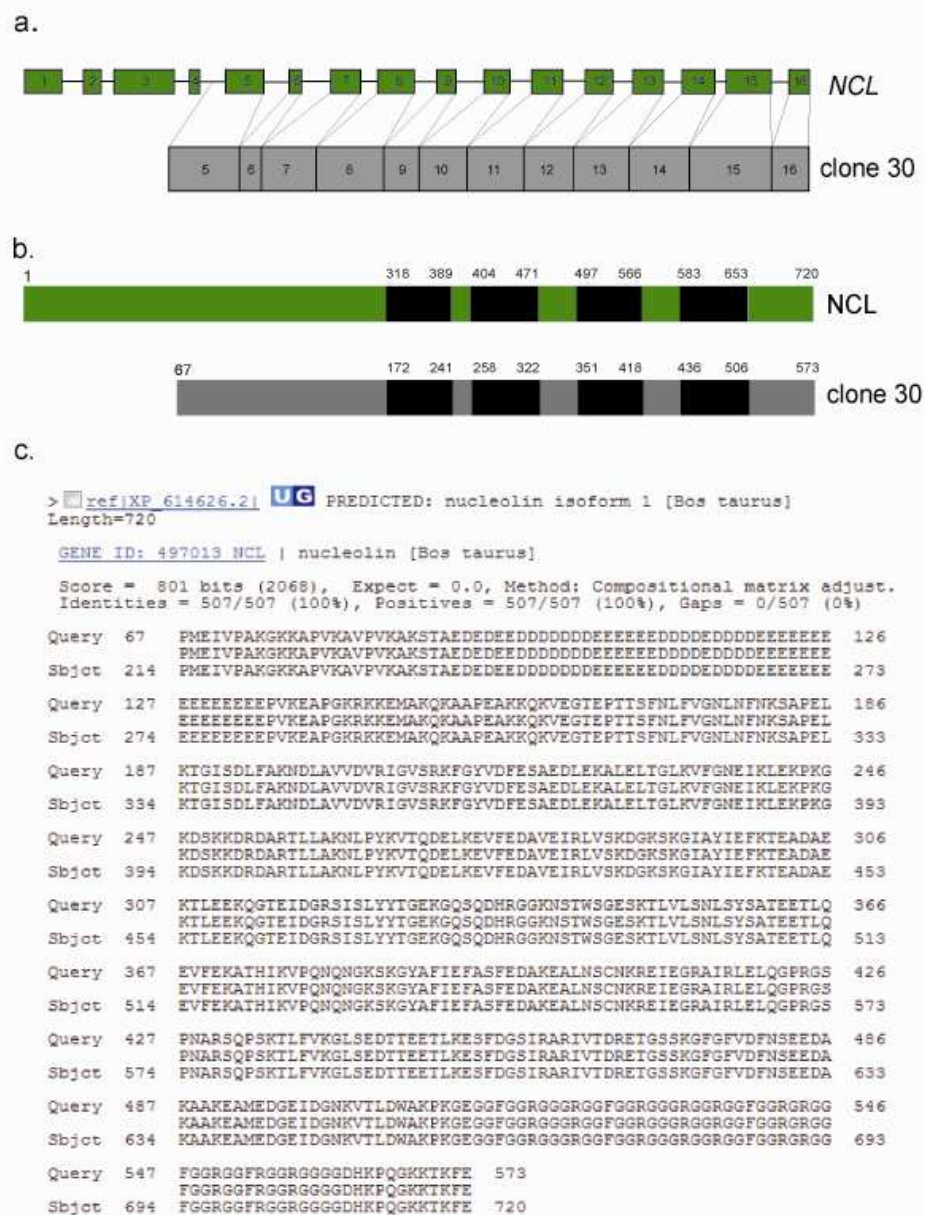


Figure 3.6. Characterisation of clone 30

a. Alignment of clone 30 to the bovine *NCL* gene. The exons of bovine *NCL* are in green and numbered as indicated, black horizontal lines correspond to introns. Regions of clone 30 corresponding to exons of *NCL* are in grey with vertical lines highlighting these regions. **b.** Comparison of the protein domain structure of bovine *NCL* (green) with a predicted domain structure of clone 30 protein (grey). Black boxes with numbers above indicate the position of RNA-binding RRM domains. **c.** Alignment of the predicted protein sequence from the open reading frame of pMyr clone 30 (Query) to the protein sequence of bovine *NCL* (Sbjct) performed using BLAST at NCBI (2.6).

Upon co-transformation of the pMyr NCL plasmid with RP2 fragments yeast growth was mainly observed with RP2 fragment amino acids 190-350 but not other fragments, including a smaller C-terminal RP2 fragment of amino acids 238-350 (figure 3.5a). RP2 fragment 1-200 resulted in weak yeast growth after 120 hours of incubation at 37°C upon co-transformation with pMyr NCL fragment, but not with RP2 41-200 fragment. However, yeast co-transformed with RP2 41-200 plasmid and the positive control pMyr SB had exhibited poor growth before (figure 3.3), suggesting a lower expression level of this fragment of RP2 protein. Therefore, in this case the absence of growth cannot be interpreted. These data suggest that the NCL protein fragment binds the C-terminal region of RP2 with the region essential for binding defined as amino acid 190 to 350.

The NCL fragment was also tested for its ability to bind mutants of RP2. It was revealed that NCL, when co-transformed with pSos RP2 misfolding mutants such as C67Y and C86Y, significantly slowed yeast growth (figure 3.5b). C67Y co-transformed yeast were able to grow only after 120 hours of incubation at 37°C and cells co-expressing C86Y mutant with pMyr clone 30 did not exhibit growth after 144 hours. However, this mutant has a lower expression level compared to other constructs (described in section 3.2). The pathogenic C-terminal mutation L253R caused slower growth of yeast compared to the full length wild type pSos RP2. The “arginine finger” mutation (R188H) did not noticeably affect yeast growth, which was observed after 48 hours of incubation at 37°C as was growth for the full length wild type RP2 (figure 3.5b).

Thus, it was shown that in CytoTrap® the NCL fragment preferably interacts with the C-terminus of RP2 and that misfolding mutations in the N-terminus and the C-terminal mutation L253R could affect this interaction. As the cDNA does not represent the full length NCL, it is possible to suggest that the potential interaction of the full length NCL with RP2 is not mediated by the 1-214 N-terminal region of NCL.

3.3.2. Drebrin-like protein

Re-transformation of clone 20 resulted in yeast growth with pSos RP2 and not with the empty pSos vector at the restrictive temperature on selective media (figure 3.7d). The insert sequence was obtained and interpreted as described in 2.5.2 and 2.6. The insert sequence of pMyr clone 20 had 95 % identity to 7 exons of the drebrin-like protein (*DBNL*) gene positioned at chr22:62,002-80,241 of bovine genome (figure 3.7a).

The in frame open reading frame (ORF) of pMyr clone 20 was translated into a protein sequence using bioinformatic tools (2.6) and used for BLAST analysis. The predicted clone 20 protein sequence had 95 % identity to bovine DBNL protein isoform 2 ([XP_001092440](#)) (figure 3.7b and c). Clone 20 protein aligned to DBNL starting from amino acid 171 to the C-terminus but did not include a region between amino acids 240 to 250 of DBNL. This region of 10 amino acids corresponds to the sequence of exon 8 of the bovine *DBNL* gene (figure 3.7b). These data suggest that this exon was spliced out producing a DBNL isoform different to isoform 2. This region does not include known functional domains of DBNL or disrupts the reading frame. Clone 20 is predicted to contain the SH3 conserved domain but lack the actin depolymerisation factor/cofilin-like domain (ADF) of DBNL (figure 3.7b).

3.3.2.1. RP2 domain mapping of the interaction with clone 20

To investigate further which part of RP2 binds to the DBNL fragment, the CytoTrap® assay was performed with RP2 fragments. It was revealed that pMyr clone 20 when co-transformed with full-length RP2 exhibited growth only after 96 hours of incubation at 37°C on the selective media. Upon co-transformation of pMyr clone 20 with pSos RP2 fragments (figure 3.2) the yeast growth was observed only for the C-terminal 190-350 pSos RP2 fragment after 120 hours of incubation at 37°C on the selective media (figure 3.7d). These data suggest that clone 20 protein binds the C-terminus of RP2.

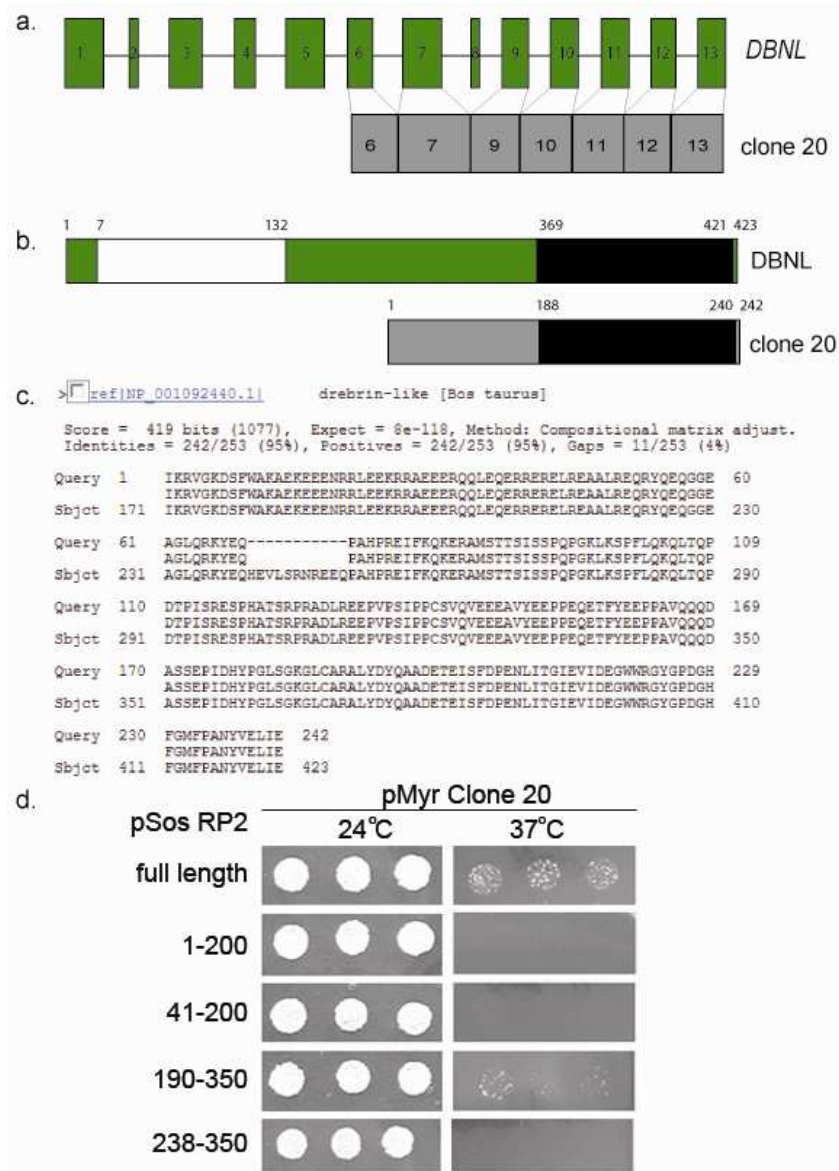


Figure 3.7. Clone 20 characterisation and its interaction with RP2

a. Comparison of clone 20 (grey boxes) sequence to the exon organisation of the bovine *DBNL* gene (green boxes are exons, black horizontal lines as introns). Exon 8 of *DBNL* was not present in the clone 20 sequence. **b.** Comparison of the domain structure of bovine *DBNL* protein (green) to the predicted domains of clone 20 (grey). White box represents the actin depolymerisation factor (ADF) domain and the black box is the SH3 domain. **c.** Alignment of clone 20 protein sequence to bovine *DBNL* performed using BLAST at NCBI (2.6). **d.** Three different colonies of yeast co-transformed with pMyr clone 20 pSos RP2 or RP2 fragments after incubation on the selective media at permissive (24°C) and restrictive temperature (37°C) after 144 hours.

3.3.3. Unc119

Clone 58 only resulted in a low level of yeast growth upon re-transformation with pSos RP2. The yeast did not exhibit growth compared to the pMyr Lamin C negative control after 144 hours of incubation at 37°C. However, after incubation for 156 hours at 37°C yeast co-transfected with pMyr clone 58 and pSos RP2 exhibited growth slightly above the level of pSos RP2 transactivation (data not shown). This growth indicated a possibility of a low affinity interaction and therefore, the pMyr clone 58 insert was sequenced and analysed by BLAST searching as described in 2.5.2 and 2.6. pMyr clone 58 cDNA sequence had 100 % identity to all 5 exons of the bovine *Unc119* gene positioned at chr19:19,894,298-19,909,204 of the bovine genome (figure 3.8a). The in frame sequence of clone 58 was translated into protein sequence and it was revealed that the protein contained 222 amino acids and was predicted to have a molecular weight 25.3 kDa with pI 5.33. Clone 58 protein aligned to bovine *Unc119* ([NP_001029817.1](#)) from amino acid 19 to the C-terminus and contained GMP PDE δ domain of *Unc119* (figure 3.8b, c).

Further study of this putative interacting partner was attempted due to the fact that *Unc119* is a retinal specific protein involved in pathogenesis of cone-rod dystrophy and has been reported to form a ternary complex with Arl3 and RP2 (Kobayashi *et al.*, 2000; Veltel *et al.*, 2008b). However, the clone 58 - pSos RP2 interaction was not reproducible in CytoTrap® and no yeast growth was observed when pMyr 58 was co-transformed with pSos RP2 fragments (data not shown).

The DNA insert of clone 58 was directly subcloned from the pMyr vector into the mammalian expression vector pCMV Tag 3(b) as described in sections 2.1.5-2.1.8 and table 2.3. SK-N-SH cells were transfected (as in 2.3.2) with pCMV Tag 3(b) *Unc119* construct and co-transfected with RP2-GFP to test for an overlap in their subcellular localisation. After visualising expressed myc-*Unc119* with anti tag antibody, no overlap with RP2-GFP localisation was observed (figure 3.9). Thus, it is unclear whether the potential interaction between *Unc119* and RP2 occurs.

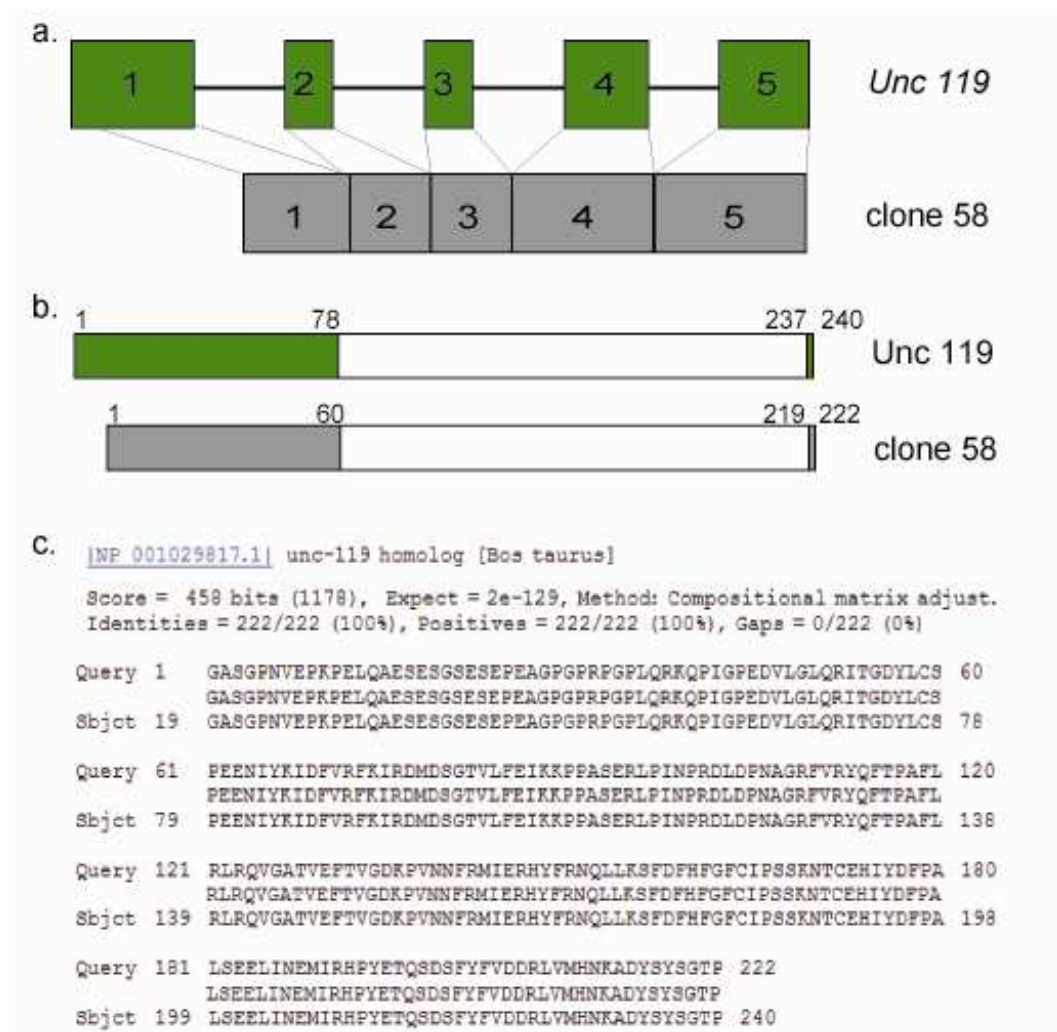


Figure 3.8. Characterisation of clone 58

a. Schematic of exon structure of the bovine *Unc 119* gene (green boxes) and corresponding DNA sequence of clone 58 (grey boxes). The corresponding regions are indicated by black vertical lines. **b.** Domain structure of bovine *Unc 119* protein (green) and the predicted protein translated from the open reading frame of pMyr 58 (grey) with a white box indicating the GMP PDE δ domain. **c.** Alignment of predicted protein sequence of the open reading frame of clone 58 to bovine *Unc119* performed using BLAST (NCBI) as described in 2.6.

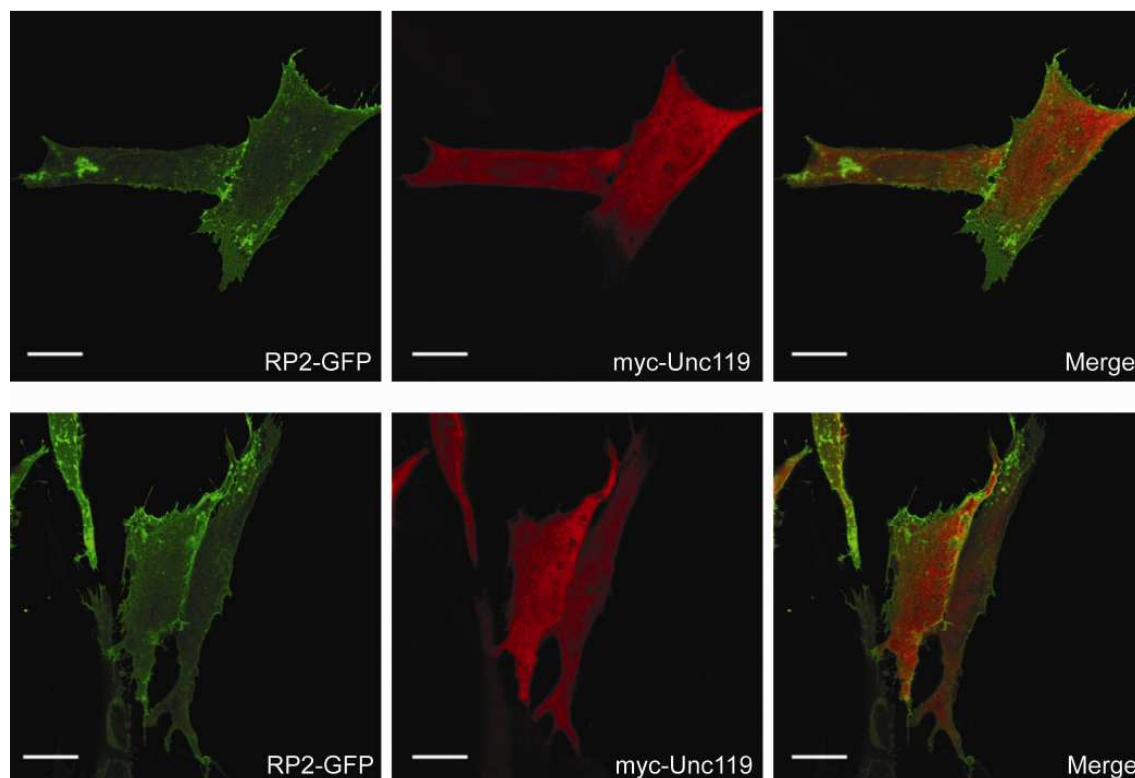


Figure 3.9. Subcellular localisation of Unc119

Confocal microscopy images of representative SK-N-SH cells co-transfected with RP2-GFP (green) and myc-Unc119, visualised with anti-myc antibody (red). Scale bars are 10 μ m.

3.4. Screening of the N-terminus of RP2 using CytoTrap®

Novel interacting partners identified during the screening of full-length RP2 with a retinal cDNA library exhibited binding to the C-terminus of RP2. Moreover, the difficulty of the screening protocol was enhanced by the transactivation of the pSos RP2 construct after incubation for longer than 144 hours at 37°C, which probably resulted in losing low affinity interacting proteins.

Therefore, the retinal cDNA library was further screened using an N-terminal fragment of RP2. The 1-200 fragment was chosen since it was demonstrated to have a good expression level compared to 41-200 fragment (figure 3.3a). The pSos 1-200 RP2 construct did not transactivate the CytoTrap® system after incubation for longer than 240 hours (data not shown) and thus, allowed longer incubation times and potentiated detection of low affinity interactions.

After yeast transformation (performed as described in 2.2.1-2.2.2) approximately 60,000 colonies were obtained, which were able to grow on the selective media at 24°C permissive temperature. These colonies were then replica-plated (as in 2.2.3) and tested for ability to grow at 37°C on selective media. As a result, 86 putative positive colonies were selected and plasmids were isolated (summary of the screening is shown in figure 3.4b).

Based on the previous experience of the screening of the full-length RP2 (described in section 3.2.3), colonies which appeared to grow on the second day (starting at colony number 17) and until 192 hours of incubation at 37°C were selected. This was done to avoid revertants or clones containing the high affinity interacting partner Arl3.

The remaining 67 clones were analysed by restriction digest to determine the presence and size of the insert. Two pMyr clones (clone 8 and clone 10) released a fragment of about 550 bp. After re-transformation with pSos 1-200 RP2 for interaction verification clones 8 and 10 exhibited growth on the first day of incubation at 37°C on selective media. The pMyr inserts of clones 8 and 10 were sequenced (as in 2.5.2) and it was revealed that these clones contained

the full coding sequence of bovine Arl3 as the open reading frame (data not shown). Other plasmids released inserts of different sizes and were therefore re-transformed with pSos 1-200 RP2 for verification. It was found that only 5 out of 65 pMyr clones exhibited growth at 37°C on the selective media. These pMyr clones inserts were sequenced and it was found that they represented novel putative interacting partners of RP2. The summary of the screening is shown in figure 3.4b.

3.4.1. Rod arrestin

pMyr clone 46 was verified by re-transformation with pSos 1-200 RP2 fragment. This “prey” demonstrated yeast growth after 120 hours of incubation at 37°C (figure 3.9). It was also tested for yeast growth when co-transformed with an empty pSos vector to ensure that clone 46 did not bind hSos (figure 3.10).

pMyr clone 46 insert was sequenced (as in 2.5.2) and the electrophoregram was interpreted using bioinformatic tools described in 2.6. The DNA sequence of the open reading frame of clone 46 had 100 % identity to 11 exons of a gene positioned at chr3:120,315,637-120,373,305 of bovine genome that corresponds to the bovine s-antigen SAG gene (figure 3.11a).

Bioinformatic tools (section 2.6) were used to translate the in frame DNA of pMyr clone 46 insert into protein sequence which was predicted to contain 282 amino acids with a molecular weight of approximately 31.5 kDa and a calculated pI 5.26. This protein sequence was searched against the NCBI database (2.6) and it was found that clone 46 protein had 100 % identity to the bovine rod arrestin protein isoform p48 (1CF1) starting from amino acid 123 to amino acid 404 (figure 3.11c). Clone 46 protein contained a part of the “Arrestin N” conserved domain at the N-terminus and the full C-terminal “Arrestin N” domain (figure 3.11b).

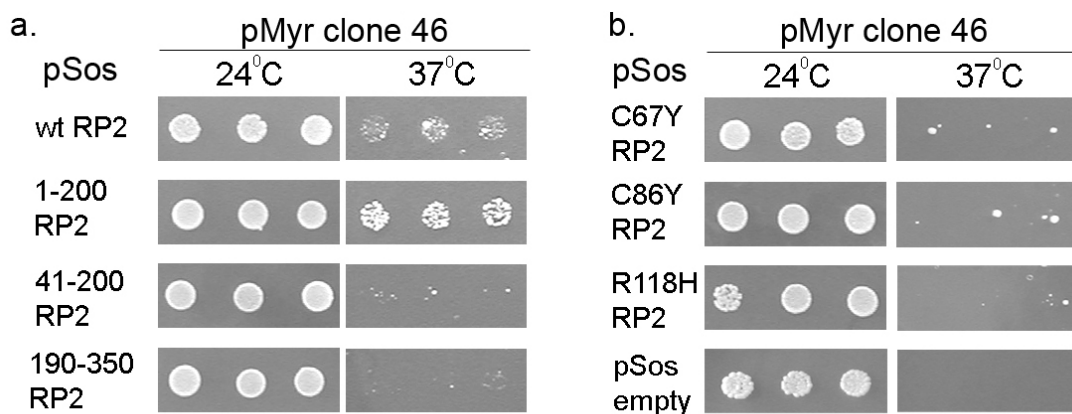


Figure 3.10. Interaction of clone 46 with RP2 in CytoTrap®

Yeast growth when co-transformed with pMyr clone 46 and wild type pSos RP2, RP2 fragments “a.” and RP2 mutants “b.” as shown. pSos empty panel shows the negative control for pMyr 46 clone with the pSos vector. Three different colonies were used for each transformation and were tested at the non-restrictive temperature (24°C) for 96 hours and at the restrictive temperature (37°C) for 168 hours.

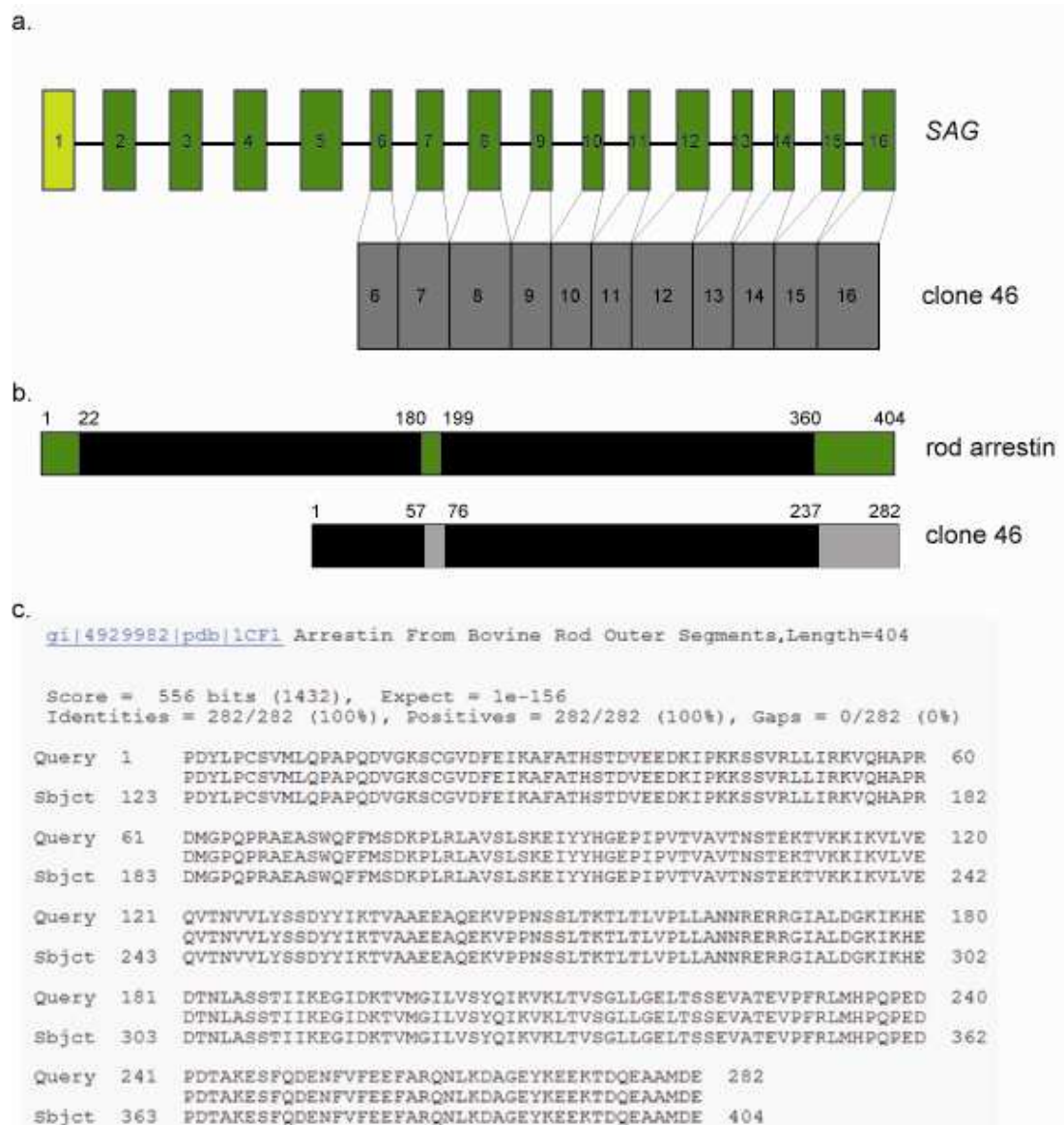


Figure 3.11. Comparison of clone 46 to bovine rod arrestin

a. Alignment of the DNA insert of clone 46 to the bovine rod arrestin gene (SAG). Exon 1 is a non-coding exon and is in light green. Other SAG exons are shown as green boxes and regions of clone 46 corresponding to SAG exons are in grey. **b.** The domain structure of the bovine rod arrestin protein (green) and a predicted domain structure of clone 46 protein (grey) with black boxes showing position of two Arrestin_N domains. **c.** The protein sequence predicted by translation of the in frame sequence of pMyr clone 46 insert DNA using bioinformatic tools (2.6). Alignment of the predicted protein sequence of clone 46 (Query) and the protein sequence of bovine rod arrestin (Sbjct) performed using BLAST analysis at NCBI (2.6).

3.4.1.1. Characterisation of RP2-rod arrestin interaction by CytoTrap®

pMyr clone 46 was investigated further with the yeast two-hybrid system. The ability to interact with the full-length RP2 and RP2 fragments was examined (figure 3.10a). It was revealed that yeast growth was slower with the full-length protein rather than with 1-200 fragment. The two other fragments of pSos RP2 did not exhibit growth and the small single colonies which appeared after 168 hours of incubation at the restrictive temperature are more likely to be temperature resistant revertants (3.1). The co-transformation of pMyr clone 46 with RP2 mutants did not result in detectable yeast growth after 120 hours of incubation at 37°C suggesting no interaction occurred (figure 3.10b). Therefore, the putative interaction of rod arrestin fragment with RP2 required further investigation.

3.4.1.2. Expression of rod arrestin fragment in SK-N-SH cells

The open reading frame of clone 46 was subcloned from the pMyr vector into a *pCMV-Tag3b* vector to facilitate mammalian expression of N-terminally myc-tagged rod arrestin fragment (as in 2.1.1-2.1.8). It was also subcloned into the *pEGFPC1* vector to produce N-terminally tagged GFP fusion protein. The primers used for subcloning into the vectors are shown in table 2.3. However, the internal *Sall* and *EcoRI* sites of TA-cloned pGEM-T Easy® clone 46 were used to construct pCMV-Tag3b-clone 46. To produce a GFP fused clone 46 protein, two *EcoRI* restriction sites of *pGEM-T Easy®* were used with subsequent check for correct orientation in *pEGFPC1* frame by restriction digest using *HindIII* and *Sall*.

SK-N-SH human neuroblastoma cells were transfected as described in 2.3.2 with the rod arrestin fragment expression plasmids. The cells were incubated for 24 hours and fixed using different protocols (2.3.4). The expression of pEGFPC1 clone 46 construct was not detectable with fluorescent microscopy of live cells or of either paraformaldehyde or methanol fixed cells. It was not detected in cell lysates by Western blotting with an anti GFP antibody (data not shown). Transfection of SK-N-SH cells with pCMV-Tag3b clone 46 followed by immunostaining with anti-myc antibody revealed that the myc-tagged protein formed intracellular inclusions (figure 3.12a). The inclusions varied in size and

number per cell. The subcellular localisation of the myc-rod arrestin fragment did not change when it was co-transfected with human RP2-GFP (figure 3.12a, b). Also transfection with myc-rod arrestin fragment did not change RP2-GFP localisation compared to the previously reported subcellular localisation of RP2 (described in 1.5.3) (figure 3.12c).

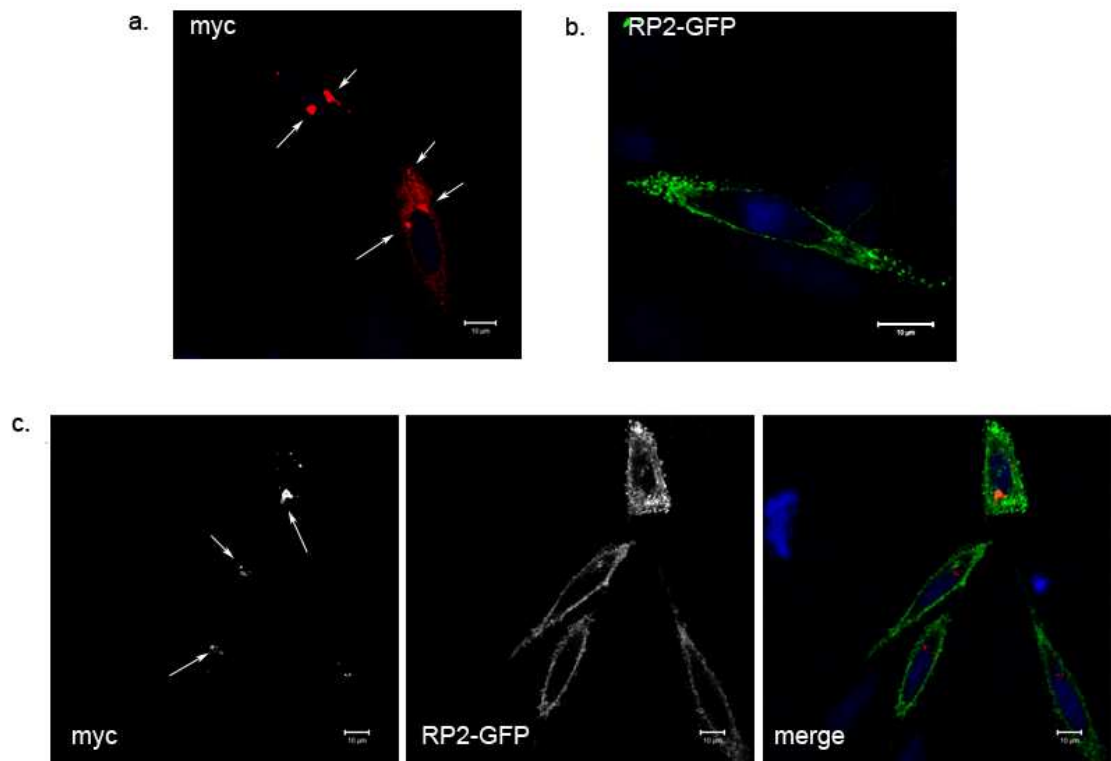


Figure 3.12. Subcellular localisation of myc-rod arrestin fragment and RP2-GFP

Confocal microscopy images of SK-N-SH cells immunostained with anti-myc antibody (red). Nuclei were visualised with DAPI (blue). **a.** Cells transfected with myc-rod arrestin fragment (red) exhibit formation of large and small intracellular inclusions (indicated with arrows). **b.** Representative image of cells transfected with RP2-GFP exhibit the previously observed RP2 localisation predominantly on the plasma membrane. **c.** Cells expressing both myc-rod arrestin fragment and RP2-GFP proteins demonstrate no overlap of RP2-GFP localisation, with inclusions formed by myc-rod arrestin fragment (indicated by arrows). The scale bars are 10 µm.

3.4.1.3. Specific binding of rod arrestin to RP2

For further investigation of the RP2-rod arrestin interaction, a complementary immunoprecipitation (IP) method was applied. SK-N-SH human neuroblastoma cells were chosen for the IP experiment. These cells were considered to be most suitable for transfection with RP2 constructs since they had been previously shown to have an undetectable level of endogenous RP2 (data not shown). Cells were treated and co-transfected as described in 2.3.2 with human RP2-GFP and full length both bovine rod arrestin-FLAG plasmid or β -arrestin-2-FLAG constructs (Dr S. Gurevich, section 2.1.8, table 2.4).

β -arrestin-2 was used to test whether RP2 was able to discriminate between rod arrestin and a ubiquitous arrestin. β -arrestin-2 is expressed ubiquitously with a higher expression level in the central nervous system and is involved in quenching of β -adrenoreceptor-2 (Attramadal *et al.*, 1992).

An alignment of protein sequences that compares rod arrestin with β -arrestin-2 is shown in figure 3.13. The proteins share 55 % identity in their amino acid sequences and have similar functions. Therefore, the efficiency of co-IP between human RP2-GFP co-transfected with bovine rod arrestin and human RP2-GFP co-expressed with bovine β -arrestin-2 was tested.

The transfected cells were lysed with RIPA buffer (table 2.8), incubated with anti-FLAG antibody (table 2.9) and all subsequent procedures were performed as described in 2.4.11. To control for non-specific binding, the lysates were incubated with mouse IgG and treated the same way as the samples with anti-FLAG antibody. The protein G sepharose eluates were resolved by SDS-PAGE and analysed by Western blotting (as in sections 2.4.2 and 2.4.5). The results are shown in figure 3.14.

The F4C1 anti pan-arrestin antibody (table 2.9) detected bands of approximately 45 kDa, corresponding to both FLAG tagged rod arrestin and β -arrestin-2 in the input lanes. The β -arrestin-2 immunoreactive band appeared to be less intense (figure 3.14).

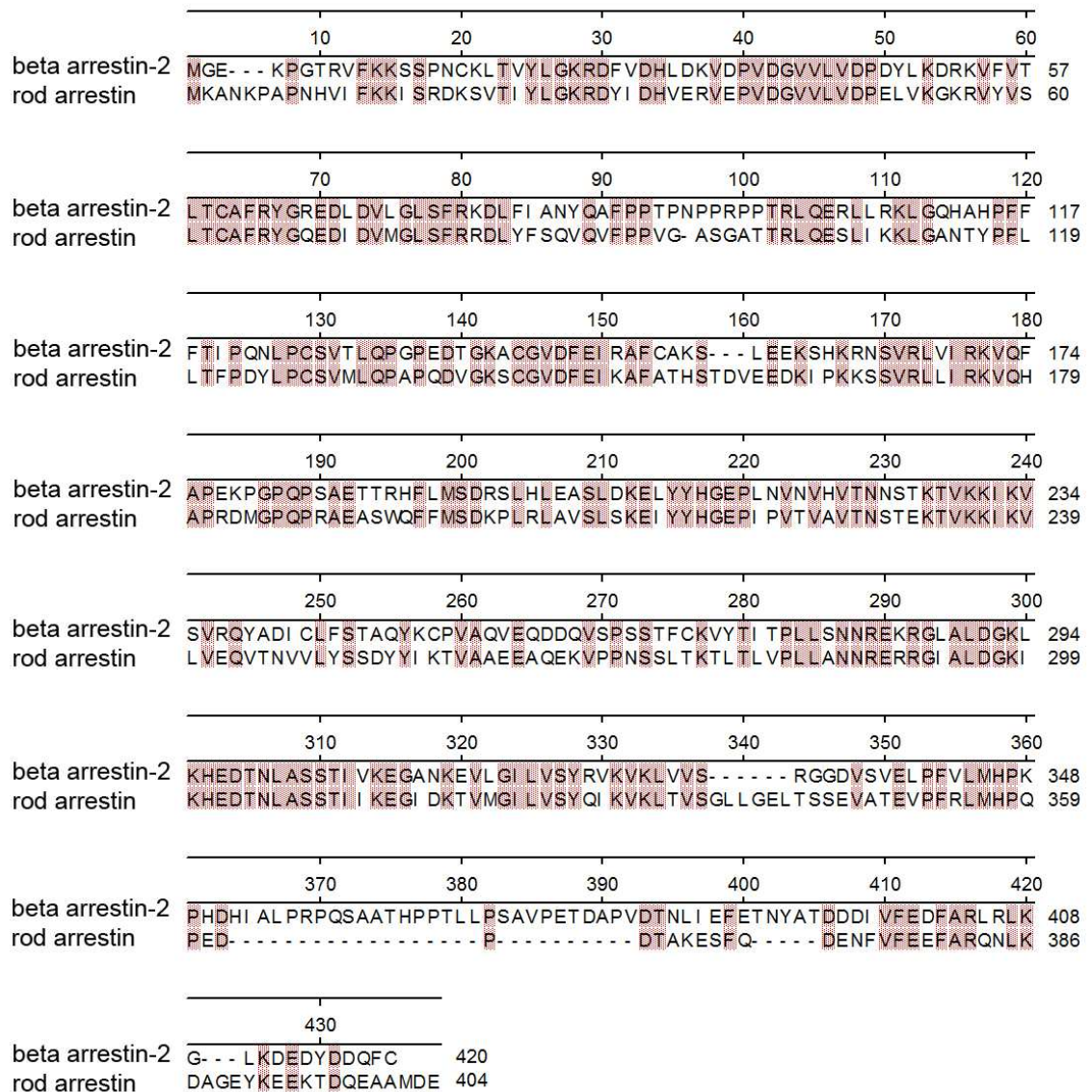


Figure 3.13. The alignment of bovine rod arrestin to bovine β -arrestin-2 protein sequences

The protein sequences of bovine β -arrestin-2 and bovine rod arrestin are aligned using Clustal W. The red shaded residues indicate identities between rod arrestin and β -arrestin-2.

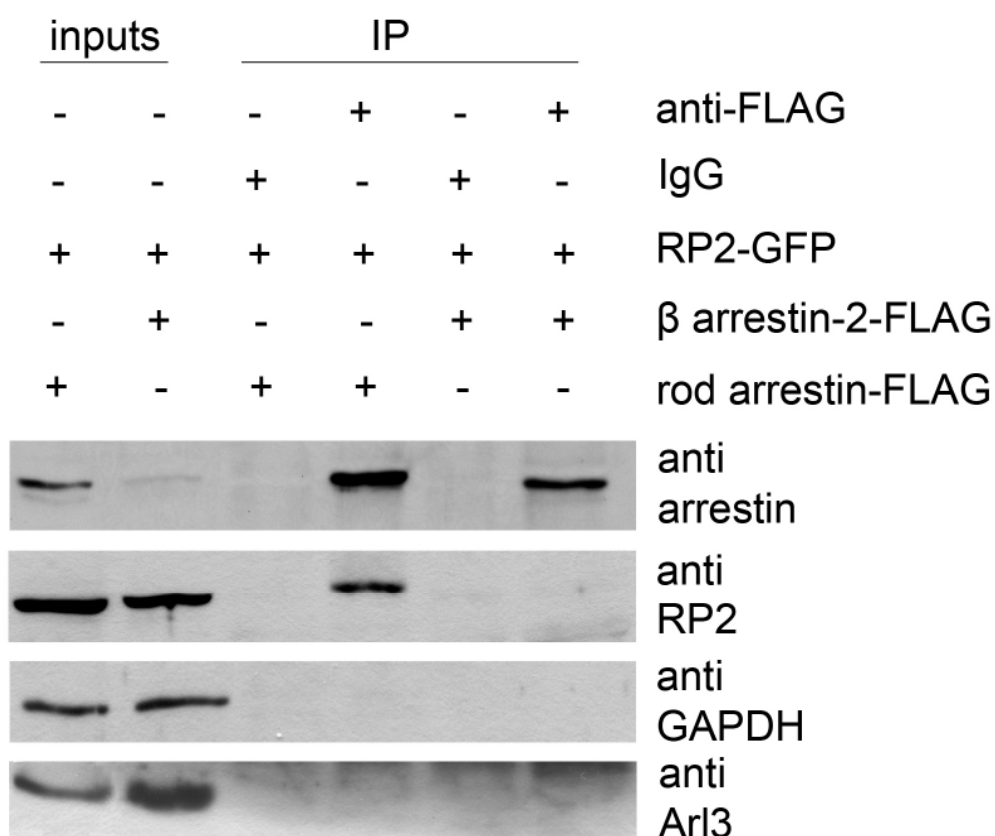


Figure 3.14. Co-immunoprecipitation of rod arrestin-FLAG with RP2-GFP

Western blots of the immunoprecipitation (IP) of rod arrestin-FLAG and β -arrestin-2-FLAG using anti-FLAG antibody are shown. The first panel shows the blot immunostained with anti-pan arrestin antibody detecting bands of approximately 45 kDa, the second blot is immunostained with anti-RP2 antibody and shows the RP2-GFP bands at the predicted molecular weight 66 kDa. Western blot immunostained with anti-GAPDH antibody shows endogenous GAPDH of approximately 36 kDa in the cell lysates and no detectable signal in the IP lanes. The bottom Western blot shows endogenous Arl3 of approximately 20 kDa in the input lanes, but not in the lanes with IP.

The anti-FLAG antibody immunoprecipitated both FLAG conjugated arrestins, showing the bands of appropriate size (45kDa) on the Western blot. In samples where the lysates were incubated with mouse IgG no arrestin bands were detected. Upon immunostaining with an anti-RP2 antibody (table 2.10) it was found that RP2-GFP was detected as a band of 66kDa in the input lanes of both types of lysates.

Importantly, in the lanes from the FLAG immunoprecipitation samples, the RP2-GFP band was detected only in the presence of rod arrestin-FLAG. There were no bands detected in IgG negative control samples for both types of lysates. This suggested that the binding of RP2-GFP to rod arrestin was specific.

No band corresponding to RP2-GFP was detected with anti-FLAG antibody incubated with the lysate in which cells co-expressed β -arrestin-2-FLAG with RP2-GFP, suggesting no interaction occurred. The RP2-GFP band in the lane with rod arrestin co-IP appeared to have a slightly slower mobility (about 68 kDa) compared to the RP2-GFP band in the input lane, suggesting potential protein modifications.

The Western blot was also probed with anti GAPDH antibody (table 2.10) to control equal loading of inputs, and the specificity of IP experiment. GAPDH analysis showed that this was achieved. Thus, IP demonstrated that RP2 specifically bound to rod arrestin and not to β -arrestin-2.

3.4.1.4. Arrestins and endogenous Arl3

An anti Arl3 antibody (table 2.9) was used to test if endogenous Arl3 was co-precipitated with arrestin proteins. Arl3 bands were detected only in the inputs but not in any of the IPs suggesting that no co-IP occurred (figure 3.14). However, the band in the lane of the input containing rod arrestin-FLAG was less intense compared to the one in the input with β -arrestin-2-FLAG. The significance of difference in the Arl3 band intensity is not clear.

3.4.1.5. Co-Immunoprecipitation of rod arrestin with RP2 mutants

Co-IP it was then used to confirm the previous yeast two-hybrid results of disruption of the interaction by RP2 mutations. For this purpose SK-N-SH cells were transfected (described in 2.3.2) with bovine rod arrestin-FLAG and RP2-GFP mutants: C67T, C86T, R118H and L253R (section 2.1.8, table 2.4). The experiment was performed as described before, but in this case only bovine rod arrestin-FLAG was used for IP for all lysates and RP2-GFP constructs were varied as described above.

Western blotting confirmed that the anti-FLAG antibody immunoprecipitated rod arrestin-FLAG from the lysates (figure 3.15). The expression level in the inputs of cell lysates was inconsistent. However, the bands of precipitated rod arrestin-FLAG demonstrated a similar intensity in all the IPs (figure 3.15).

Western blotting with anti-RP2 antibody demonstrated that the expression level of the RP2 constructs differed. The lowest expression level was observed for C67Y and L253R mutants. The highest expression level was exhibited with wild type RP2, with moderate expression level for the R118H mutant. Co-immunoprecipitated RP2-GFP variants were detected at a similar level in all lanes (figure 3.15). Importantly, the bands of co-precipitated RP2-GFP and the mutants appeared to run slower on SDS-PAGE compared to RP2-GFP in the input lanes.

Thus, the co-IP experiment did not show any disruption of rod arrestin interaction with tested RP2 mutants. However, an SDS-PAGE mobility shift of RP2-GFP precipitated by rod arrestin was observed once more, suggesting that RP2 undergoes changes upon binding to rod arrestin.

3.4.1.6. RP2 is a putative calcium binding protein

To test whether the shift in RP2-GFP SDS-PAGE mobility was caused by its binding to calcium, a calcium mobility shift assay was performed (Maruyama and Nonamura, 1984). This method is based on the ability of proteins bound to calcium to resolve faster on SDS-PAGE due to becoming more positively charged.

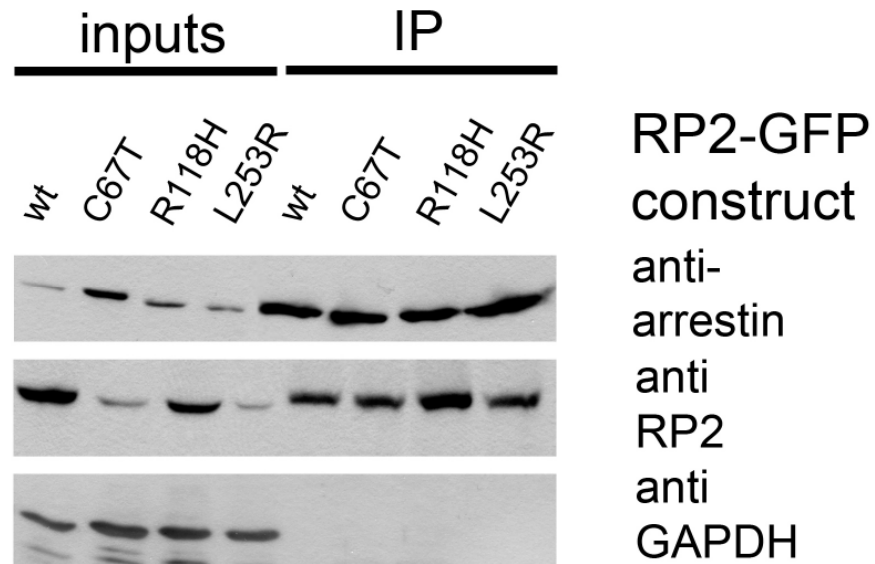


Figure 3.15. Co-IP of rod arrestin-FLAG with wild type RP2-GFP and RP2 mutants

Western blot showing IP of rod arrestin-FLAG with different RP2-GFP mutants as indicated. The first panel shows bands of 45 kDa size which correspond to rod arrestin-FLAG protein in the inputs and IP lanes. The bands of co-precipitated RP2-GFP are shown on IP lanes. Their mobility was slower compared to expected and corresponded to approximately 68 kDa. The bands in inputs of different RP2-GFP demonstrated the expected mobility for this protein of approximately 66 kDa. The expression level of RP2-GFP constructs was reflected by their band intensity in input lanes in comparison to GAPDH control for a house keeping protein (bottom panel).

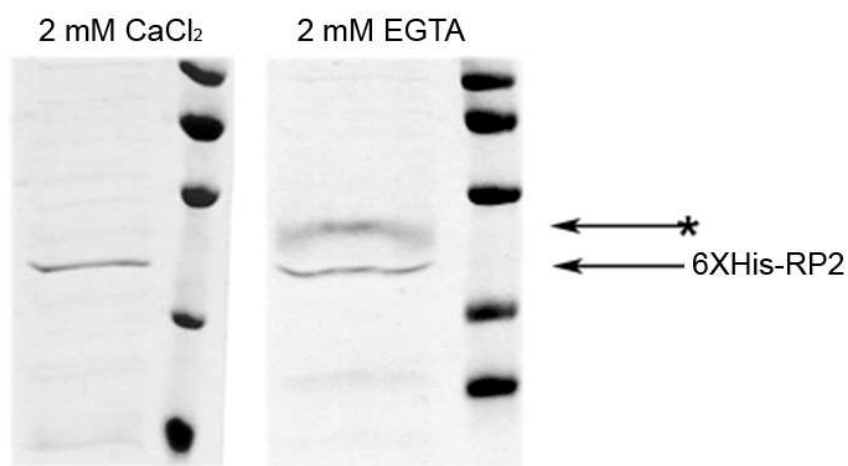


Figure 3.16. RP2 is a putative calcium binding protein

Coomassie stained SDS-PAGE of 6xHis-RP2 in the presence of 2mM CaCl₂ or 2mM EGTA as indicated. Arrow shows the mobility of 6xHis-RP2 and arrow with asterisk indicates a band with a lower mobility which corresponds to potential calcium free 6xHis-RP2.

Purified 6xHis-RP2 protein (provided by Dr N. Schwarz) was resolved by SDS-PAGE (as described in 2.4.2) under two conditions: 2 mM CaCl₂ or 2 mM EGTA was added to Laemmli sample buffer and SDS-PAGE running buffer. 500 ng of 6xHis-RP2 for each SDS-PAGE condition was resolved and the protein was visualised with Coomassie blue stain.

It was observed that in the presence of 2 mM EGTA 6xHis-RP2 appeared to separate into two bands, whereas in the presence of 2 mM CaCl₂ only one band was observed (figure 3.16). The size of the single band on the gel resolved in the presence of 2 mM CaCl₂ corresponded to the lower band of 6xHis-RP2 in the presence of 2 mM EGTA, suggesting enhanced mobility of calcium bound 6xHis-RP2. The upper band on the gel resolved in the presence of 2 mM EGTA exhibited slower electrophoretic mobility compared to the lower band, suggesting the presence of calcium free protein. As a slower mobility 6xHis-RP2 band was observed in the previous immunoprecipitation experiments, these data suggest that RP2 might release calcium upon binding to rod arrestin.

3.4.1.7. Subcellular localisation of rod arrestin and RP2

To investigate the nature of the putative interaction of RP2 with rod arrestin further, immunocytochemistry was employed. SK-N-SH cells were transfected with full length rod arrestin alone or co-transfected with rod arrestin and RP2 constructs. Rod arrestin constructs were designed to express this protein without a tag, with FLAG tag and GFP fused (Dr S. Gurevich, section 2.1.8 and table 2.4).

After 24 hours the cells were methanol fixed and immunostained using anti RP2, anti pan-arrestin and anti FLAG antibody as in table 2.7 (as described in 2.3.4). Rod arrestin exhibited predominantly cytoplasmic localisation with a less intense staining in the nucleus. In most of the cells, rod arrestin did not decorate any particular cellular structures (figure 3.17). Upon co-transfection with RP2-GFP it was observed that the rod arrestin staining pattern did not change compared with rod arrestin alone and did not overlap with RP2 localisation. RP2 localisation did not show any changes from previously reported (figure 3.18).

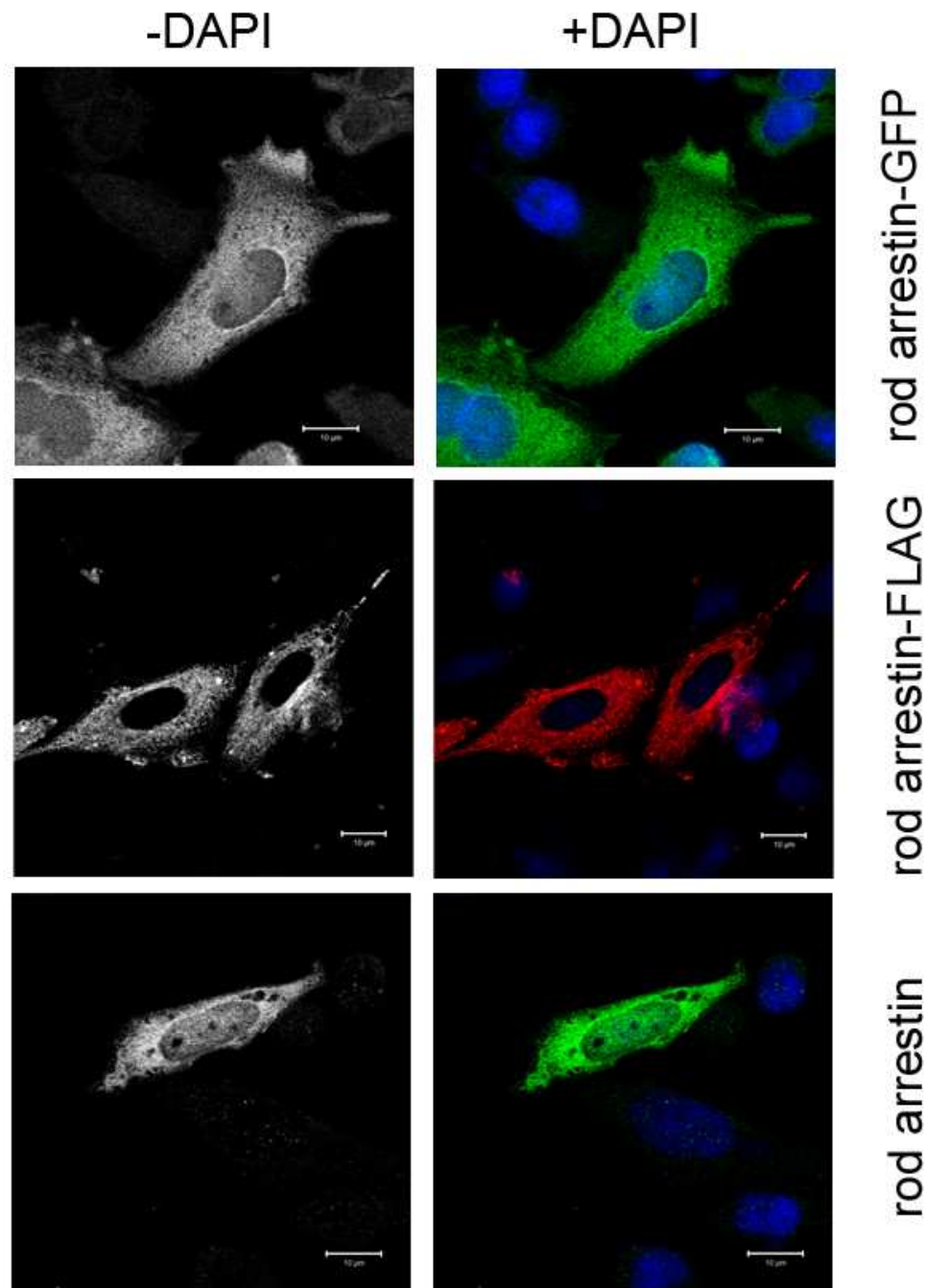


Figure 3.17. Subcellular localisation of bovine rod arrestin in SK-N-SH cells

Immunofluorescence of cells transfected with different constructs of bovine rod arrestin expression. C-terminal GFP tagged rod arrestin demonstrated some nuclear staining and diffuse cytoplasmic, as did the untagged construct when visualised with anti pan-arrestin (F4C1) antibody. The cell nuclei were visualised with DAPI staining on the right panels (blue). The scale bars are 10 μ m.

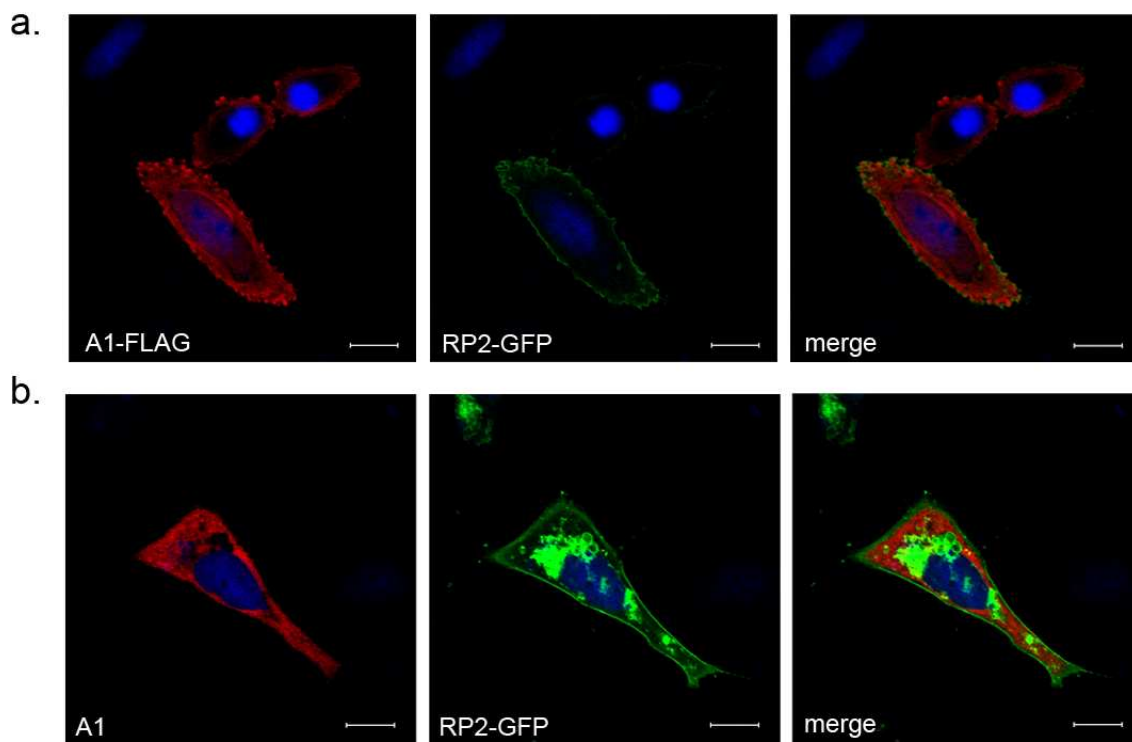


Figure 3.18. Subcellular localisation of bovine rod arrestin and human RP2 in SK-N-SH cells

Immunofluorescence of cells co-transfected with various constructs as follows:

- a.** Cells co-transfected with arrestin-FLAG (A1-FLAG, red) and RP2-GFP (green). **b.** untagged rod arrestin (A1) visualised with anti pan-arrestin antibody (F4C1) (red) and RP2-GFP (green). The scale bars are 10 μ m.

3.4.2. Other novel interacting partners identified in CytoTrap® screening of the N-terminal fragment of RP2

Several other potential interacting partners for the N-terminus of RP2 were found during the screening (section 3.4). Isolated pMyr clones from yeast colonies number 43, 44, 48, 55 were verified by re-transformation with the N-terminal fragment of RP2. All four clones grew at the 37°C restrictive temperature. The clones were also checked for growth when co-transformed with an empty pSos vector to test for false positives binding to hSos without RP2 “bait”. These interactors corresponded to chaperones and components of the ubiquitin – proteasome system (UPS).

3.4.2.1. Chaperones as putative interacting partners of RP2

3.4.2.1.1. Hsc70

pMyr clone 44 exhibited growth after 96 hours of incubation at 37°C with pSos 1-200 RP2, and no growth upon co-transfection with the empty pSos vector negative control (figure 3.19e). The plasmid was sequenced (as in 2.5.2) and analysed using bioinformatic tools (2.6). The DNA sequence had identity with three exons of a gene at position chr15:32,343,661-32,354,150, which was a part of the bovine *HSPA8* gene (figure 3.19a).

The in frame translation of pMyr clone 44 insert sequence to a predicted amino acid sequence and BLAST analysis revealed that it was 100 % identical to the bovine Hsc70 protein ([AAI54390](#)) spanning the region from amino acid 463 to the C-terminal amino acid 650 (figure 3.19d). The predicted protein was calculated to have a molecular weight of 20.4kDa and a pI 4.85.

To confirm Hsc70 protein expression the yeast cells of clone 44 were grown (section 2.2.5) and the total protein from the culture was extracted (2.2.7). The protein was analysed by Western blotting using an anti-Hsp/Hsc70 antibody (table 2.10). The yeast culture expressing Arl3 in pMyr vector was used as a control for non-specific antibody reactivity.

It was found that clone 44 expressed a protein of the expected size (approximately 20 kDa) corresponding to a part of the substrate binding domain at the C-terminus of Hsc70 (figures 3.19b, c). Weak cross-reactive bands of endogenous yeast Hsc70 exhibited gel mobility of approximately 70 kDa (figure 3.19c).

Clone 44 was tested for interaction with full-length RP2, 41-200 and 190-350 RP2 fragments and the N-terminal mutants (figure 3.2). It was found that co-transformation of clone 44 with the full length RP2 resulted in much slower growth of the *cdc25-H* strain at 37°C compared to the 1-200 RP2 fragment (figure 3.19e).

When the cells were co-transformed with the 41-200 fragment, almost no growth was observed. The missense mutations in the N-terminus of RP2 were tested for interaction with pMyr clone 44. No growth was observed in this experiment with any of the mutants tested, suggesting that they might weaken or disrupt the interaction (figure 3.19e).

3.4.2.1.2. Cytosolic chaperonin subunit 6A (CCT6A)

pMyr clone 55 resulted in yeast growth upon co-transformation of *cdc25-H* strain with the RP2 “bait” (as in 2.4.6) after 120 hours of incubation at 37°C and no growth upon co-transfection with the empty pSos vector (figure 3.20). The insert was sequenced as in 2.5.2 and analysed using bioinformatic tools (2.6). The insert DNA sequence aligned to a position on chr25:29,531,890-29,577,699 of the bovine genome where the *CCT6A* gene mapped (figure 3.20a).

Analysis of the translated protein sequence of pMyr clone 55 revealed that the first methionine in clone 55 protein was at amino acid position 33, which corresponds to the methionine start codon of *CCT6A* ([NP_001029714](#)) (figure 3.20b). The insert DNA encoding the first 32 amino acids showed 100 % to the DNA sequence of 5'UTR of bovine *CCT6A* gene, and allowed in frame translation of *CCT6A* with the pMyr tag.

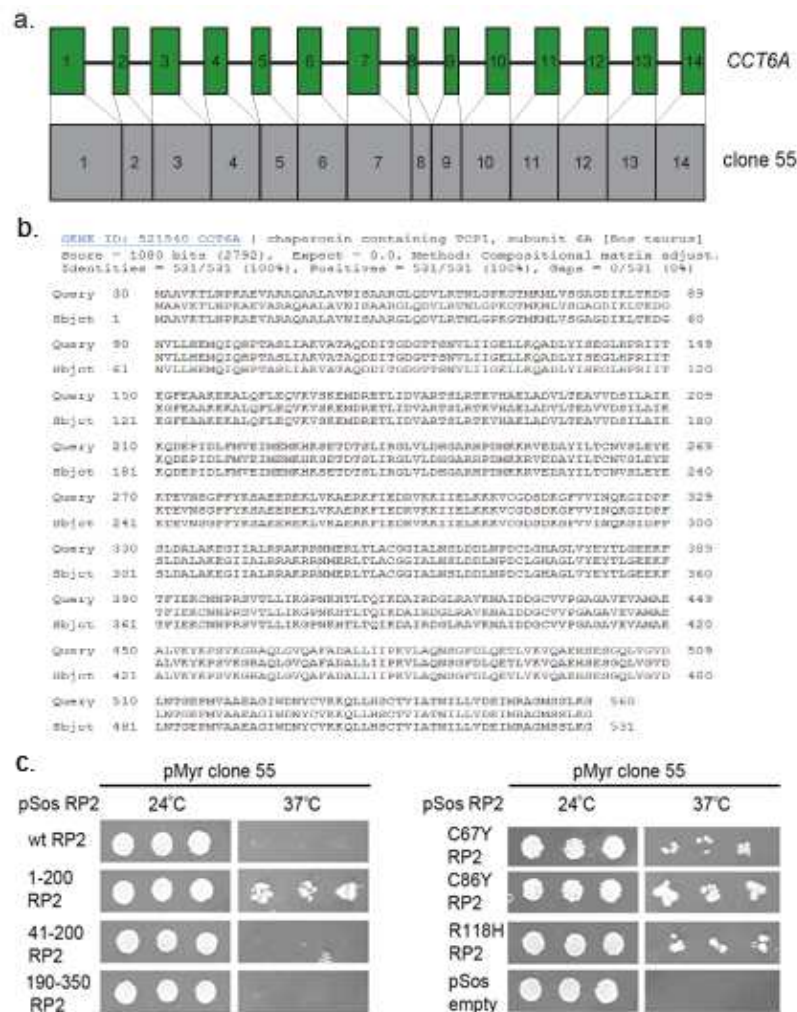


Figure 3.20. Characterisation of clone 55

a. Schematic of the bovine *CCT6A* gene. Exons are indicated with green boxes. The DNA sequence of clone 55 is grey with lines indicating corresponding regions of *CCT6A*. **b.** Alignment of protein sequence of the open reading frame of clone 55 (Query) to bovine *CCT6A* (Sbjct) using BLAST at NCBI (section 2.6). **c.** Yeast growth of cells co-transformed with pMyr clone 55 and pSos RP2 constructs as indicated. Three different colonies are shown for each transformation incubated at 24°C for 96 hours and 37°C for 156 hours on the selective media.

The clone containing bovine CCT6A subunit was tested for its ability to interact with the full-length RP2 by yeast two-hybrid. Surprisingly, no growth was observed when this clone was tested with the full-length pSos RP2 (figure 3.20c). However, the yeast co-transformed with a 1-200 RP2 fragment as “bait” exhibited growth after 144 hours of incubation. None of the other RP2 fragments demonstrated growth (figure 3.20c). The missense mutations in the N-terminus of RP2 were also tested for the interaction with CCT6A. Similar growth was observed with all of the RP2 mutants with the highest intensity of growth for the C86Y mutant which is predicted to be misfolded (figure 3.20c).

3.4.2.2. 26S proteasome non-ATPase subunit 4 (PSMD4)

Co-transformation of “bait” (pSos 1-200 RP2) with the isolated pMyr clone 43 resulted in yeast growth after 48 hours of incubation at 37°C (figure 3.21). No growth was observed when clone 43 was co-transfected with the empty pSos vector. The insert was sequenced (as in 2.5.2) and analysed using bioinformatic tools (2.6). The insert DNA sequence had 98 % identity to 8 exons of the 26S proteasome non-ATPase subunit 4 *PSMD4* gene at position chr3:21,068,954-21,072,236 (figure 3.21a) of the bovine genome.

The open reading frame of pMyr clone 43 was translated into a protein (2.6) and BLAST analysis revealed 98 % identity to the bovine PSMD4 isoform 1 ([AAI19965](#)) from amino acid 57 to the C-terminus (figure 3.21b, c). Clone 43 protein compared to PSMD4 had an amino acid substitution (L61P) and three extra amino acids inserted at residue 252 of PSMD4 (figure 3.21c). The protein expressed in the open reading frame of clone 43 was predicted to have molecular weight 35.1 kDa with pI 4.72 and to contain a partial von Willebrand A (VWA) 26S proteasome conserved domain (figure 3.21b).

Clone 43 was tested for interaction with the full-length RP2, RP2 fragments and RP2 mutants. Yeast co-transformed with full-length RP2 exhibited growth after 36 hours of incubation at 37°C. Growth was observed with fragment 1-200 RP2 after 48 hours. Much slower growth was demonstrated with the other RP2 fragments after 120 hours of incubation at 37°C (figure 3.21d).

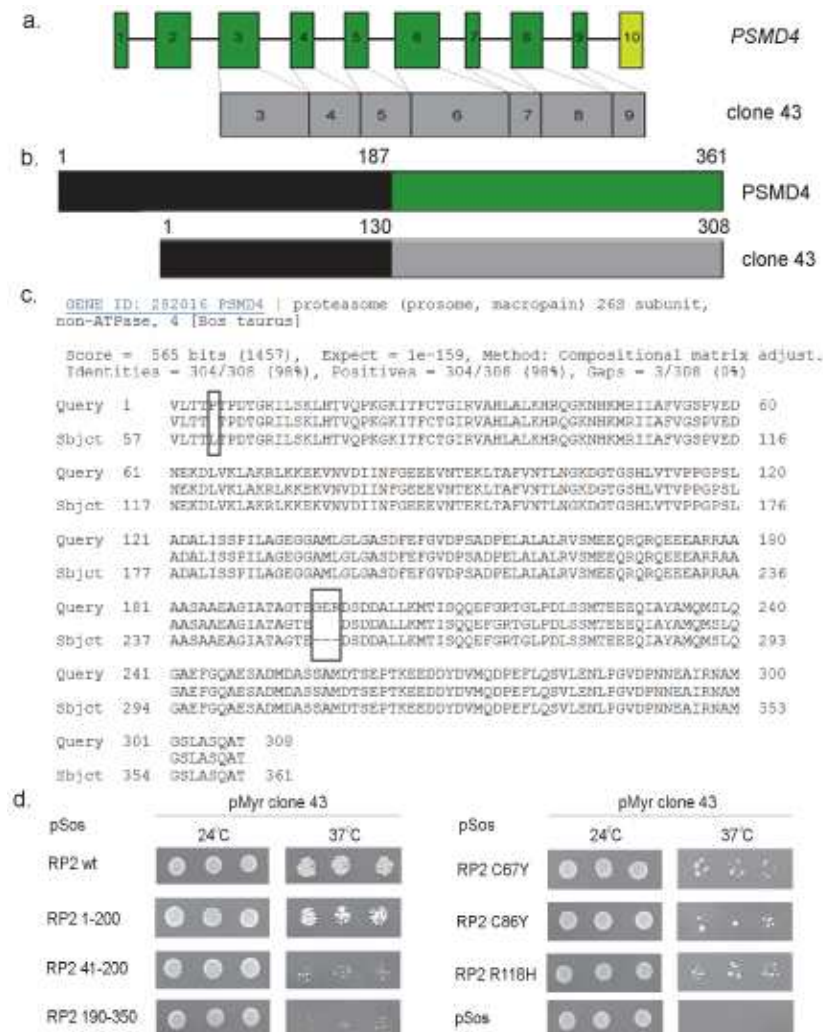


Figure 3.21. Characterisation of clone 43 and its interaction with RP2

a. Schematic of the bovine *PSMD4* gene. Exons are indicated with green boxes with a non-coding exon 10 in light green. Clone 43 is shown in grey boxes with lines indicating corresponding regions of *PSMD4*. **b.** Domain structure of bovine *PSMD4* protein (green) and the predicted domains of the protein translated from clone 43 open reading frame. VWA 26S proteasome subunit domain is shown by a black box. **c.** Alignment the predicted protein sequence of clone 43 (Query) to bovine *PSMD4* (Sbjct) using BLAST at NCBI (section 2.6). Regions of mismatch are boxed. **d.** Yeast growth of cells co-transformed with pMyr clone 43 and pSos RP2 constructs as indicated. Three different colonies shown for each transformation were incubated at 24°C for 96 hours and 37°C for 144 hours on the selective media.

Missense mutations in the N-terminus of RP2 were tested for interaction with pMyr clone 43. Slower growth was observed with all of the mutants tested after 144 hours of incubation at 37°C on the selective media (figure 3.21d) compared to the wild type, suggesting a weaker interaction.

3.5. Discussion

3.5.1. Screening a retinal cDNA library with RP2

Despite the large number of false positive putative interactors (~91 %), CytoTrap[®] yeast two-hybrid technique has proven to be a relatively efficient method for detecting potential novel interactions of RP2. As a result one previously reported interacting partner, Arl3, and one as yet unpublished interactor, TNPO3, were confirmed. Seven novel potential interactors were identified. However, when comparing the two strategies of screening with the full length RP2 or the 1-200 RP2 fragment it was found that screening with the fragment was more efficient for finding novel interactors. This higher efficiency could be due to the 1-200 RP2 fragment not transactivating the CytoTrap[®] system after incubation for longer than 144 hours at the restrictive temperature. Incubation of yeast with “bait” and “prey” for long time periods provided the opportunity to detect comparably low affinity interactions such as binding of RP2 to rod arrestin.

On the other hand, using full-length RP2 to screen a retinal cDNA library allowed identification of two novel interacting partners that bind to the C-terminus of RP2. One of them, nucleolin, exhibited a high affinity interaction in CytoTrap[®].

3.5.2. Nucleolin

Clone 30 contained nearly full length nucleolin (NCL) which is one of the major and most extensively studied nucleolar proteins. NCL is highly conserved. The N-terminus is composed of highly acidic regions, the central region has multiple phosphorylation sites and the C-terminus is known to have four RNA recognition motif (RRM) domains. The NCL protein fragment identified in this study represents part of the acidic region in the N terminus, with all the C-terminal containing RRM domains. A bioinformatic search for NCL isoforms similar to the fragment did not result in any matches, suggesting it is partial clone and not a result of alternative splicing.

NCL is a multifunctional protein that is highly phosphorylated (Lapeyre *et al.*, 1986), and this modification varies during the cell cycle and regulates kinetochore formation (Morimoto *et al.*, 2007; Ma *et al.*, 2007). Thus, there is a functional overlap between NCL and other newly identified interactors of RP2 such as RAN and p27 (Evans, 2007) which have a role in cell cycle regulation and spindle formation (Kalab *et al.*, 2006).

Interestingly, NCL was recently shown to interact with lebercilin (LCA5) protein. Mutations in *LCA5* gene encoding this protein lead to Leber congenital amaurosis (LCA) (described in section 1.3.6), which is a severe form of congenital blindness. Lebercilin is widely expressed throughout development and is localised to the connecting cilia of photoreceptors, microtubules and primary cilia (den Hollander *et al.*, 2007, Gerber *et al.*, 2007).

Another protein which causes X-linked retinitis pigmentosa, RPGR, (described in 1.3.2.1.1) is tethered to the cilia via its interacting partner RPGRIP (Hong *et al.*, 2000, Shu *et al.*, 2005) and they interact with nucleophosmin, which is a nucleolar protein similar to NCL (Shu *et al.*, 2005). NCL and nucleophosmin were also shown to interact by yeast two-hybrid (Li *et al.*, 1996).

Thus, the interaction of RP2 with NCL places RP2 in a pathway with other retinal degeneration related proteins, such as RPGR and lebercilin not only because of cilia localisation, but also by the protein interaction network.

Thus, the putative interaction of NCL with RP2 could potentially be significant for its retinal function. The pathogenic misfolding mutants of RP2 and the C-terminal L253R mutation decreased the interaction affinity which highlights its importance. However, attempts to confirm this interaction by methods other than CytoTrap[®], such as GST pull-down with the retinal lysate and immunoprecipitation, which involved mammalian endogenous NCL were not successful (data not shown). This could be due to RP2 binding shorter isoforms of NCL rather than full length NCL since the clone identified in this study is only partial NCL.

Therefore, subcloning NCL fragments and of the full length NCL in mammalian expression vectors with subsequent biochemical experiments, such as IP is essential to confirm the interaction.

3.5.3. Drebrin-like protein

Clone 20 exhibited a low affinity interaction with RP2 in CytoTrap® specifically binding to the C-terminus of RP2. Clone 20 represents part of bovine drebrin-like gene (*DBNL*) but with exon 8 spliced out. This exon is present in all bovine *DBNL* sequences on the UCSC database. Analysis of the predicted protein sequence encoded by clone 20 showed that the protein contained the central region of *DBNL* and the C-terminus with a SH3-domain but lacked the ADF domain, which is responsible for binding to F-actin (Larbolette *et al.*, 1999). Thus, the protein expressed in clone 20 is unlikely to have the actin-binding function of *DBNL*.

DBNL was demonstrated to bind dynamin, a GTPase responsible for endocytosis regulation via its SH3 domain (Kessels *et al.*, 2001). The deficiency of *DBNL* in mice leads to impaired synaptic endocytosis and failure of recycling of the synaptic vesicles (Connert 2006). *DBNL* was identified in the mouse cilia proteome (Liu *et al.*, 2007a), suggesting a potential overlap in localisation of *DBNL* and RP2. The role of the potential interaction of *DBNL* and RP2 has yet to be elucidated. The region where *DBNL* binds to RP2 lies within the RP2 C-terminus. However, whether the mutations of RP2 could affect this interaction needs to be investigated further using CytoTrap® and biochemical methods.

Thus, two novel putative interacting partners identified by screening a retinal library with the full length RP2 were not retina specific. However, their ubiquitous expression pattern does not indicate that they are not important for retinal function. Further investigation into whether these interactions are biologically significant *in vivo* would be important to reveal the pathways RP2 could be implicated in.

3.5.4. Unc119

Clone 58 encoded Unc119, missing the first 19 amino acids. Unfortunately, this interaction required longer than 144 hours incubation time at the restrictive temperature and therefore was difficult to verify using CytoTrap[®]. However, this potential interaction is worth further investigation because Unc119 is a retina specific protein associated with cone-rod dystrophy (described in 1.3.5.1).

Despite CytoTrap[®] being designed as a system for binary complex identification, there is the possibility that a ternary complex formation between “bait”, “prey” and a yeast endogenous protein could result in growth at the restrictive temperature. It has been reported that Arl3 can bind Unc119 (Van Valkenburgh *et al.*, 2001). Recently a crystal structure of the ternary complex formed by Arl3, RP2 and Unc119 was described. However, RP2 and Unc119 were not found to have residues that interacted directly, as they were brought together by Arl3 (Veltel *et al.*, 2008b).

Yeast homologue of Arl3, Cin4 (YMR138W), has 42.5 % identity with human Arl3 and 6 residues are conserved between yeast and human Arl3 that are responsible for binding to RP2 (figure 3.22). Thus, it is possible that endogenous yeast Arl3 homologue could mediate interaction of RP2 with Unc119 in yeast cells during CytoTrap[®] screening. This mediation by Cin4 could result in low level yeast growth observed upon co-transformation of clone 58 with RP2, indicating the high sensitivity of the CytoTrap[®] system. This hypothesis could be tested further by CytoTrap[®] using Cin4 knock-out yeast strain. The growth of Cin4 knock out temperature sensitive *cdc25-H* strain co-transformed with pMyr Unc119 and pSos RP2 would indicate that the interaction is direct and not mediated by Cin4.

3.5.5. Rod arrestin

It was shown in this study that RP2 binds rod arrestin in CytoTrap[®] with low affinity. The interaction was then confirmed by IP, where it was demonstrated that RP2 specifically bound rod arrestin and not β -arrestin-2. Thus, the interaction detected in this study potentially provides a link between the phototransduction cascade and RP2 function.

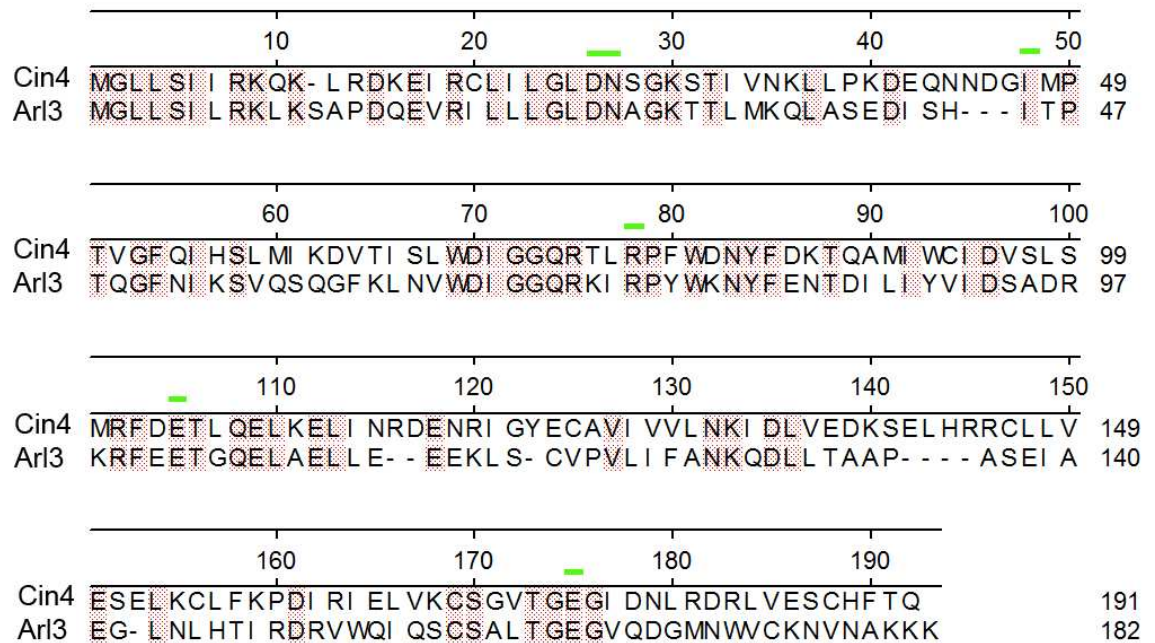


Figure 3.22. Alignment of yeast Cin4 protein sequence to human Arl3

Comparison was performed using Clustal W alignment. Residues conserved between human Arl3 and Cin4 are highlighted by red shadow. The residues responsible for the interaction with RP2, conserved between these two proteins are highlighted with green lines.

Mutations in rod arrestin have been shown to cause retinitis pigmentosa (see section 1.3.2) and therefore, the interaction identified in this study places RP2 in a pathway with other retinal disease causing proteins.

The importance of the rod arrestin interaction with RP2 in the retina is supported by the finding that RP2 does not bind β -arrestin-2. Rod arrestin and β -arrestin-2 proteins have 55 % identity and are considered to be highly similar (figure 3.12). As seen from the alignment the proteins have regions of high and low similarity in both N-terminal and C-terminal regions.

The protein expressed in clone 46 is not the full length rod arrestin as it lacks a part of the N-terminal Arrestin_N domain. The region of significant dissimilarity between proteins of clone 46 and β -arrestin-2 spans amino acids 244-282. This is a potential binding site of rod arrestin for binding to RP2. Construction of rod arrestin fragments and testing the fragments for their ability to bind RP2 in IP and CytoTrap® would identify the region of rod arrestin responsible for the interaction.

The retinal cDNA library screening was performed using the N-terminus (AA 1-200) of RP2 as “bait”, delineating this conserved RP2 domain as mediating rod arrestin binding. This region of RP2 has been described to contain the vast majority of pathogenic RP2 mutations (see section 1.5.1). It was shown in this study that misfolding mutants, C67Y and C86Y, did not interact with rod arrestin. These two mutants have been shown to abolish most interactions in CytoTrap®, even those mediated by the C-terminus of RP2 (Evans, 2007).

The pathogenic R118H RP2 mutation did not disrupt any of interactions in CytoTrap® apart from rod arrestin. These data indicate the potential importance of this interaction for the pathogenesis of XLRP. Nevertheless, this disruption of interaction was not confirmed in biochemical experiments and therefore, needs further investigation by other methods testing protein-protein affinity such as GST pull-down assays and other techniques, such as surface plasmon resonance (Biacore).

Experiments involving mammalian expression of clone 46 protein were not very successful due to the myc tagged protein forming intracellular inclusions and such inclusions did not recruit co-expressed RP2 and vice versa. This could be due to the rod arrestin fragment being misfolded, which would affect binding site presentation to RP2. Sub-cloning in other mammalian expression vectors such as GFP did not result in detectable protein expression.

Full length rod arrestin appeared to be soluble but when co-expressed with RP2 it was found that they did not co-localise. A possible clue to this phenomenon is in the rod arrestin structure and its ability to self-associate into a stable tetramer. The K_d for the dimer/tetramer equilibrium is lower than for monomer/dimer (Hanson *et al.*, 2008). Therefore, in the retina or when expressed in yeast or mammalian cell lines rod arrestin predominantly exists as a tetramer. The self-association described by Waker and colleagues (1987) is by N-N and C-C terminus interaction and the function of the tetramer is yet to be identified but is suggested to be a storage form of arrestin (described in section 1.2.3.5) (Hanson *et al.*, 2008).

Clone 46 found in this study is perhaps more likely to remain as a monomer/dimer due to its predicted inability to form a N-N connection since it lacks a significant part of rod arrestin N-terminus. Therefore clone 46 protein with an attached myristoylation tag from the pMyr expression vector is expected to remain in a monomeric state when it binds to RP2 in CytoTrap®.

In immunoprecipitation experiments, rod arrestin could be monomerised by the RIPA buffer, which contains SDS (Appendix) disrupting non-covalent bonds. Thus, it is feasible to hypothesise that in the two methods, where RP2 and rod arrestin demonstrated binding, rod arrestin was presented for binding as a monomer.

In immunofluorescence experiments, arrestin would be expected to exist as a tetramer, therefore no co-localisation would be observed with RP2, suggesting that the rod arrestin tetramer does not bind RP2. This hypothesis would need to be investigated further. It could be explored by IP using non-denaturing, SDS free buffers to find whether RP2 still binds to rod arrestin. Under SDS-free conditions, rod arrestin would be expected to stay as a tetramer due to the high

concentrations when overexpressed in mammalian cells, and would show no interaction with RP2. Creation of soluble rod arrestin oligomerisation mutants and testing for co-localisation with RP2 in cells and by IP would shed light on such a hypothesis.

Thus, the data obtained in this study suggest that RP2 preferentially binds to rod arrestin monomer rather than a tetramer. It has been demonstrated that only monomeric arrestin is able to quench phosphorylated rhodopsin, but not the tetramer (Hanson *et al.*, 2007), highlighting the potential importance of the RP2 and rod arrestin interaction for retina function.

However, both RP2 and rod arrestin have high affinity interacting partners, creating competition for binding. RP2 interacts with Arl3 whereas rod arrestin binds activated phosphorylated rhodopsin (PhRho*) (sections 1.2.3.3). Nonetheless, such high affinity interaction as arrestin - (PhRho*) occurs only when light strikes the retina suggesting that other interactions with arrestin could occur in the dark adapted state.

RP2 binding to Arl3 is mediated via the N-terminus of RP2, which was also shown to bind rod arrestin in this study. However, GDP bound Arl3 has been shown to have a very low affinity for RP2 and they do not co-localise when co-expressed in mammalian cells (Bartolini *et al.*, 2002; Evans, 2007). Additionally, Arl3 is thought to exist predominantly in a GDP bound state in the retina, allowing other interactions mediated by the N-terminus of RP2 to potentially occur (Prof Mike Cheetham, personal communication). Importantly, it has been demonstrated in biochemical assays that Arl3 preferably binds RP2 when RP2 is not myristoylated (Bartolini *et al.*, 2002). Therefore the interaction of rod arrestin and RP2 is more likely to happen when RP2 is myristoylated.

An interesting finding of this study was a change in the mobility of the wild type RP2 and its mutants in the rod arrestin IP lanes when compared to input lanes on the Western blot. Proteins are known to change SDS-PAGE mobility depending on post-translational modifications, such as myristoylation, or binding to ions, such as calcium. Therefore, the observed mobility shift in RP2 bands could be due to RP2 being myristoylated or bound to calcium.

It is proposed in this study that RP2 could change its mobility due to a potential calcium binding ability since the gel mobility shift was observed in the presence of a calcium chelator, EGTA. Usually calcium binding proteins have one or several so-called EF hands, which are composed of a region of about 12 or more amino acids with structural composition helix-loop-helix (Swan *et al.*, 1987; Reddy *et al.*, 2004). An EF hand is also known to have a conserved X*Y*Z-Y*X**Z motif with Glu as an essential component at position Z.

Although RP2 lacks the typical structure of calcium binding proteins, it has similarity to an EF hand at the C-terminus, which is composed of two helices roughly perpendicular to each other (figure 3.23a). They are connected by a loop-strand region rich in Glu, which would be able to provide oxygen ions for calcium binding (figure 3.23a).

On the other hand, rod arrestin demonstrated change in RP2 bands mobility upon binding in IP experiments and showed binding to the N-terminus of RP2 in CytoTrap®. Thus, it is possible to suggest that potential calcium binding residues are located within the N-terminal region. The acidic region in the N-terminus of RP2 is located at amino acids position 14-34 (figure 3.23b). The structure of this region is not solved by X-ray diffraction due to the fact that the first 34 amino acids including the dual acylation signal are hidden inside the cavity formed by β -sheets (Kuhnel *et al.*, 2006).

It is feasible to suggest that an unknown stimulus changes RP2 protein conformation so the myristoylation motif becomes exposed, leading to RP2 membrane localisation. Therefore, structural studies are needed to test whether calcium binding changes RP2 conformation by the suggested way, similar to a calcim-myristoyl switch mechanism (described in section 1.2.3.6.3). Site directed mutagenesis can also be used to identify residues responsible for potential calcium binding.

The calcium binding ability of RP2 and its consequences for the protein remain to be elucidated. Therefore, the role of calcium in the interaction of RP2 with rod arrestin is unclear. A potential role of the RP2 interaction with rod arrestin is in the phenomenon of light dependent translocation (described in 1.5.3) and this

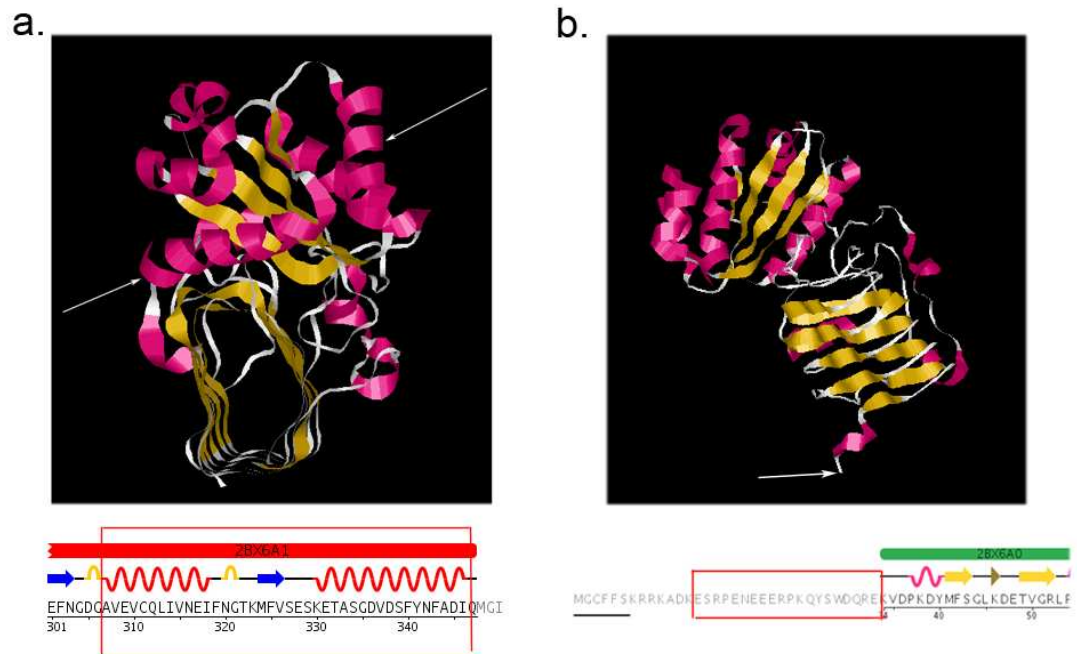


Figure 3.23. Potential calcium binding sites in the RP2 protein

a. Top view of the crystal structure of RP2 (PDB 2bx6). Helix regions are shown in pink and extended strands are yellow. Arrows indicate the two helices nearly perpendicular to each other. Below the secondary structure a putative calcium binding Glu rich region is highlighted by the red box. **b.** Side view of the crystal structure of RP2 (PDB 2bx6). Helix regions are shown in pink and extended strands are yellow. Arrow indicates the N-terminal fragment where another putative calcium binding region starts. The N-terminal RP2 sequence below contains the suggested calcium binding region with multiple Glu and is highlighted with a red box. The double acylation motif of RP2 is underlined with a black line.

could be tested as this process is important for the retina and could be the pathway disrupted in XLRP.

RP2 has been suggested to be a cilia-related protein and as suggested in this study its intracellular localisation could be regulated by a calcium-myristoyl switch. Other cilia-localised calcium binding proteins, centrin, have been demonstrated to contribute to the translocation of another phototransduction cascade component, transducin $\beta\gamma$ (Giessl *et al.*, 2006). Another pathway, where RP2 and rod arrestin could act together is nuclear transport. As shown in this study, a small amount of rod arrestin was detected in the nucleus. It has been shown that different arrestins, including rod arrestin, can bind JNK3 and MDM2 and relocalise these proteins from the nucleus to the cytoplasm (Song *et al.*, 2006).

RP2 is potentially involved in the nuclear transport pathway via interaction with TNPO3 and RAN (Evans *et al.*, 2007). However, nuclear transport mediated by arrestin is directed to the cytoplasm, whereas the suggested nuclear transport involving RP2 proceeds in the opposite direction. Thus, the involvement of nuclear transport in the pathogenesis of XLRP from the standpoint of the RP2 interaction with rod arrestin is unclear.

3.5.6. Other potential interacting partners identified by yeast two hybrid

Several other interacting partners with a ubiquitous expression were identified by CytoTrap® screening with the N terminus of RP2. One of them was the C-terminus of Hsc70.

As described in this study, a fragment of Hsc70 can bind to the N-terminus of RP2. Since the cDNA encodes part of the substrate binding domain of Hsc70 it seems possible that the binding occurred due to Hsc70 chaperone activity, representing binding to partially misfolded RP2 or its fragment. This is supported by data showing more yeast growth with the 1-200 RP2 fragment compared to the full length RP2. Binding to the RP2 mutants, especially the misfolded mutants, such as C67Y and C86Y, was expected to be stronger if this interaction was due to Hsc70 chaperone function. However, the interaction was disrupted by RP2 mutations suggesting that the interaction of RP2 with Hsc70 could be functional. Moreover, the clone expressing the Hsc70 fragment contains an important co-chaperone binding EEVD motif (Freeman *et al.*, 1995). It is possible that RP2, being a putative chaperone, is involved in one of the Hsc70 pathways.

One of these pathways could be the proteasomal degradation pathway. It has been shown that Hsc70, together with co-chaperones such as BAG1, could promote proteasomal degradation of misfolded proteins (Elliott *et al.*, 2007). In this study RP2 appeared to interact with the 26S proteasome subunit 4 (PSMD4). This subunit is a key component for the recruitment of ubiquitinated substrates to the 26S proteasome (Ferrell *et al.*, 1996). PSMD4 has been demonstrated to bind NEDD8 and NEDD8 ultimate buster 1 (NUB1) (Kamitani *et al.*, 2001), which interact with another retinal disease causing protein, AIPL1, mutations in which cause Leber congenital amaurosis (LCA) (Sohocki *et al.*, 2000). Thus, this interaction places RP2 in another pathway implicated in retina degenerations.

In this study it was shown that PSMD4 has a high affinity for the N-terminus of RP2 as well as full length RP2. Slow yeast growth was observed with the 41-

200 fragment of RP2 with PSMD4 therefore suggesting first 41 amino acids of RP2 are not essential for this interaction. The N-terminal mutants of RP2 demonstrated almost no effect on the PSMD4 and RP2 interaction in this study suggesting that this binding is unlikely to be affected during the XLRP pathogenesis. However, this interaction is still interesting for general RP2 functional investigation.

Another chaperone identified in the CytoTrap® screen was cytosolic chaperonin subunit 6 (CCT6). CCT6 is part of a large multisubunit chaperone cytosolic chaperonin complex (CCT), described in section 1.4.2. This clone represented the full length protein but appeared to interact only with the N-terminus of RP2 and demonstrated no interaction with the full length protein. Surprisingly, the interaction with the mutants of RP2 had affinity as high as the binding to the N-terminus. These data suggest that CCT6A, being a chaperone, bound a partially misfolded 1-200 RP2 fragment and misfolding RP2 mutants. It is unlikely that this subunit, expressed in pMyr vector, which attaches a myristoylation signal, became recruited in yeast homologue of CCT due to targeting of the clone to the plasma membrane. These data indicate that this subunit of the CCT chaperone complex may be able to act independently on other members of the complex.

Potentially, if mutants of RP2 bind CCT6 with high affinity, it could lead to its lack of function in photoreceptors, causing cytoskeletal protein misfolding by altering the CCT complex chaperone function. As described in section 1.3.3.2, mutations in homologues of the CCT complex subunits have been shown to cause a ciliopathy with retinitis pigmentosa, Bardet-Biedl syndrome (BBS). On the other hand, XLRP patients with RP2 mutations have not been reported to exhibit generalised ciliopathy to date.

Thus, using CytoTrap® system allowed identification of several novel potential interacting partners of RP2. However, using only one method for searching for interactors is unlikely to result in identifying all potential protein interactors. Moreover, CytoTrap® is known to have several disadvantages. Many interactions in higher protein complexes may be too weak to be detected by two-hybrid methods (Mendelsohn and Brent, 1999). Moreover, potential

interactors of those membrane proteins are unlikely to be identified by this method. It also does not allow posttranslational modifications of the bait, and therefore modification-dependent interaction will not be identified. CytoTrap® system used in this study is designed for binary complexes identification and therefore higher complex formations could be missed. Thus, another method described in the following chapter was also applied to identify RP2 potential interacting partners.

Chapter IV. Transducin- β subunit as a putative interacting partner of RP2

4.1. Introduction

Previous work described in chapter 3 and PhD studies of Evans (2007) have identified novel RP2 interactors through the use of a yeast two-hybrid system, potentially shedding light on RP2 function. However, due to several CytoTrap® disadvantages, many putative interactions could potentially be missed. To make possible identification of potential interactors of membrane bound proteins, those mediated by post translational modifications or by forming higher complexes a variant of a protein affinity assay, GST pull-down, with the retinal lysate was applied. Protein affinity assays with subsequent mass-spectrometry analysis have been extensively used previously and have proved themselves an efficient tool for identifying novel protein-protein interactions.

For such experiments the protein of interest needs to be expressed and purified. In order to identify protein-protein interactions in prokaryotes or yeast, gel filtration is often used for co-purification of “bait” complexes directly from the cells which express “bait” (Pinto *et al.*, 2005). In contrast, when identifying mammalian protein-protein interactions, a “bait” can be fused with a tag suitable for expression in an *E.coli* system and purified using affinity chromatography. Immobilised in this way, the purified protein can be incubated with mammalian cell lysate containing “prey” proteins, which are captured and then identified by mass-spectrometry. Some systems allow mammalian expression of tagged bait protein making possible co-purification of endogenous complexes (Jones *et al.*, 2008).

The most common tags used for *E.coli* expression and purification are 6xHis and glutathione S-transferase (GST). Vectors for protein expression with these tags provide high expression level and easy purification. Six histidine residues at the N-terminus or C-terminus act as a metal binding domain of a fusion protein and therefore it can be purified by metal affinity chromatography with Ni²⁺ or Co²⁺ resins. This technique has some disadvantages such as low protein

solubility and can involve using buffers with non-physiological compounds. The His tag is rarely used for a pull-down as proteins containing polyhistidine motifs can bind non-specifically to the resin.

GST pull-down has been successfully used for identification of novel interacting partners of many proteins involved in retinal degeneration. For instance, it was found that a protein mutated in arRP, TULP1, interacted with F-actin (Xi *et al.*, 2005). The GST tag expression system is known to result in a good expression level with high protein solubility. Protein purification is based on GST affinity to glutathione, immobilised on sepharose. The GST tag also allows a flexible choice of buffers for protein purification and incubation with prey proteins.

Prey proteins can be obtained from multiple sources including recombinant purified proteins, cell lysate or *in vitro* transcription/translation reactions. Proteins bound to bait can be visualised by SDS-PAGE with detection methods depending on the sensitivity required. Such methods include Coomassie or silver staining, Western blotting and radioisotopic detection. Bands corresponding to potential interacting proteins can be excised and analysed by mass-spectrometry (Muzio *et al.*, 1996).

This technique identifies compounds on the basis of mass-to charge ratio (Q/m) of charged particles, which occurs by passing the particles through electric and magnetic fields in a mass spectrometer. It has been more than a century since mass spectrometry experiments were described for the first time by Eugen Goldstein in 1886. Some of the modern techniques of mass spectrometry were devised by A. Dempster and F. Aston in 1920s (reviewed in Budzikiewicz and Grisby, 2006).

Mass-spectrometry was widely used for gas compound analyses. However with the development of matrix-assisted laser desorption/ionisation (MALDI) by Hillenkamp and colleagues (1990) and electrospray ionisation (ESI), invented by Fenn and colleagues (1989), it has been used for protein analysis. Proteins could be analysed intact or enzymatically digested with proteases resulting in a collection of peptides (Shevchenko *et al.*, 1996). Most commonly, ESI is coupled with liquid chromatography (LC) that separates compounds chromatographically and introduces the ion source.

After ionisation by MALDI or ESI, charged particles are separated by mass analysers according to Q/m . It is known that the speed of a charged particle can be altered when it is passing through a magnetic field, where its speed and trajectory gets deflected depending on Q/m . There are several types of mass analysers. A sector field mass-analyser uses electric and/or magnetic field to affect the path and velocity of a charged particle (Badman *et al.*, 2000). The time-of-flight (TOF) analyser uses an electric field as well but measures the time a charged particle takes to reach the detector. Quadripole analysers apply a radio frequency oscillating field to selectively destabilise/stabilise ions and act as mass-selective filters (Badman *et al.*, 2000). The final element of any mass-spectrometer is a detector that records the ion charge when it passes or hits the detector's surface. Recently, tandem mass spectrometry has been widely used for protein identification. In this method the first mass analyser isolates a peptide and the second analyser stabilises the ions while they collide with a gas, causing them to fragment (collision induced dissociation). The third mass analyser then sorts the fragments produced from the peptides.

Mass spectrometry produces various types of data. The most common data representation is the mass spectrum. The interpretation of mass spectra requires a combined use of techniques and is usually software assisted (Wilm *et al.*, 1996). A characteristic pattern of peptides is used for protein identification in a peptide fingerprinting database, it is called peptide mass fingerprinting (PMF) (Iborra *et al.*, 1979). If the identification is performed after using tandem MS it can be termed as *de novo* sequencing (Dancik *et al.*, 1999, Horn *et al.*, 2000). Such sequences are used to compare to a database of predicted proteins encoded by an organism's genome.

Therefore, GST pull-down was attempted to investigate novel RP2 interacting partners, which could be present with RP2 in complexes important for retina function. Additionally, this assay was also used to look for the guanine-exchange factor (GEF) for Arl3. As described in the general introduction (Velitel *et al.*, 2008a), RP2 is a GAP for Arl3, but a GEF of Arl3 has yet to be discovered. Presumably, the GEF for Arl3 is upstream of RP2 and is important for the retina. It has been shown that amino acid substitutions in Arl3, T31N and Q71L, mimic Arl3 conformations when bound to GDP or GTP respectively

(Bartolini *et al.*, 2002). Such a GDP- or GTP-“locked” condition can be used in a proteomic affinity assay to compare protein complexes which preferentially bind one form.

4.2. Results

4.2.1. Expression and purification of recombinant GST-Arl3 and GST-RP2 in *E.coli*

To perform GST pull-down experiments bait proteins first need to be produced and purified using affinity chromatography.

Two forms of GST-Arl3 were constructed, expressed and purified, T31N and Q71L. These amino acid substitutions alter the Arl3 conformation and emulate the conformations of the GDP- or GTP-bound states respectively. Coding DNA sequences for these constructs were amplified by PCR (as in 2.1.1) using specific primers (table 2.1) from pCMV Tag3a Arl3 T31N and Q71L plasmids previously constructed in our lab. They were then TA-cloned into pGEM-T®easy and sub-cloned into *pGEX-2T* expression vector (2.1.2 and 2.1.8) using *EcoRI* restriction sites. The correct orientation of the insert was checked by protein expression. Several single colonies of pGEX-2T Arl3s were used to inoculate 5 ml of LB and incubated as in 2.4.6, induced with IPTG at $OD_{600} \geq 0.2$ and lysed after 2 hours of incubation. The total and soluble fractions of cells were resolved by SDS-PAGE and visualised by Coomassie staining (2.4.2-2.4.3).

Clones expressing GST-Arl3 exhibited a unique band of 46 kDa, which corresponded to the expected mobility for a GST-Arl3 fusion protein (data not shown). Western blotting (2.4.5) with anti Arl3 antibody (table 2.10) of clones expressing the 46 kDa protein showed specific bands of this size, confirming the identity of this band as GST-Arl3. It was found that the GTP form (Q71L) was expressed at higher levels than the GDP one (T13N) after 4 hours of incubation. However, after 2 hours of incubation with IPTG the expression level of both mutants was similar and therefore this time point was chosen for future cell harvests (figure 4.1a). The expression level of a previously constructed GST-RP2 plasmid (table 2.5) was checked in BL-21(DE3) pLysS *E.coli* strain. Several colonies were used to inoculate 5 ml of LB, induced with IPTG, lysed and analysed by SDS-PAGE as described for GST-Arl3. It was found that GST-RP2 was expressed and was partly soluble after 4 hours of incubation at 37°C (figure 4.1b).

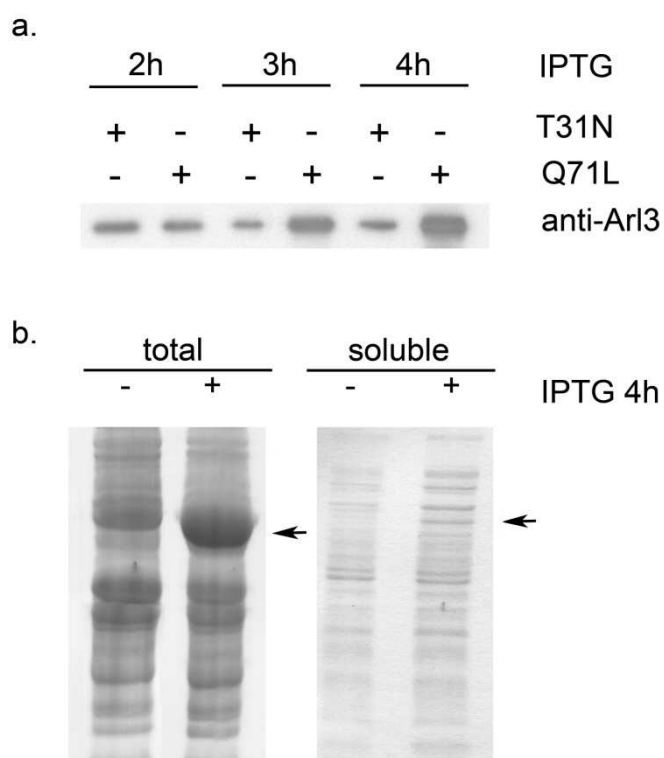


Figure 4.1. Expression and solubility of GST-Arl3 and GST-RP2

a. Western blot with anti-Arl3 antibody of soluble fractions of cells lysates, expressing GST-Arl3 T31N or GST-Arl3 Q71L after different incubation periods with IPTG as indicated. Immunostaining with anti Arl3 antibody (Arl3 854, table 2.10) showed specific bands of 46kDa. **b.** Coomassie stained SDS-PAGE gel of soluble and total fractions of cells lysates expressing GST-RP2 in response to incubation with IPTG for 4 hours. Arrows indicate bands of approximately 65 kDa which correspond to the predicted size of GST-RP2.

The small-scale experiments were scaled-up and GST-Arl3 and GST-RP2 proteins were purified as in described 2.4.8. The purified GST-fusion proteins were left bound to glutathione-sepharose beads to use as an affinity “trap”. To control for non-specific binding of “prey” proteins to the beads alone and/or GST bound glutathione sepharose was essential. Therefore, GST was expressed in the same strain of *E.coli* using an empty *pGEX-2T* vector (table 2.3). GST was then purified on glutathione-sepharose beads using the same techniques as for GST-fused RP2 and Arl3.

4.2.2. GST pull-down optimisation.

In order to find the optimal conditions for protein-protein binding in GST pull-down, the system was tested to identify conditions for the known interaction of RP2 with Arl3 to occur. A variety of factors such as pH, salt concentration and presence of detergents can influence protein-protein interaction affinity. On the one hand harsh conditions, such as high salt concentration or too high/low pH can disrupt interactions. On the other hand mild conditions (low salt or pH close to physiological) can lead to non-specific binding to the “bait” protein and give false positive results. Therefore, a balance between these two conditions needs to be found. The presence of detergent could affect the potential interaction affinity as well, however, in many cases detergents are essential for efficient extraction of many proteins, for example those having trans-membrane domains or cytoskeletal proteins. Thus, the right choice of buffer was crucial for the success of the experiment.

Several kinds of mammalian cell lysis buffers were tested to find the optimal one for the RP2-Arl3 interaction in GST pull-downs. For this purpose T31N and Q71L forms of GST-Arl3 were bound to the beads as described above in 4.2.1. They were then incubated with different HeLa cell lysates prepared using buffers from table 2.9, incubated with the beads bound to GST-Arl3 or GST and washed with the buffer used for cell lysis (described in section 2.4.9).

Proteins from the beads were eluted with Laemmli buffer and the samples were resolved by SDS-PAGE, stained with Coomassie (as in 2.4.2 and 2.4.3) to visualise the equality of loading. Western blotting was performed with anti-RP2

antibody to detect endogenous RP2 protein bound to GST-Arl3s (section 2.4.5; table 2.10).

It is known that GTP-bound Arl3 binds to RP2 stronger than GDP-Arl3 (described in section 1.5.4.1), therefore it was expected that the Q71L mutant Arl3 would preferentially bind to endogenous RP2. This was observed by using buffer 3, which had pH 8.0 and 0.1 % Triton X-100 (table 2.9). Buffer 2 had the same detergent as buffer 3 but a lower pH (7.5) and such a change caused RP2 to bind GST-Arl3 T21N and even, to a lesser extent, the GST negative control lane. Using buffer at pH 7.5 but without detergent for the GST-Arl3 pull-down did not demonstrate any binding of RP2 to Arl3, presumably due to poor RP2 protein extraction (figure 4.2a).

Lysis buffer 3, which was found to be optimal for GST-Arl3 binding to RP2, was then tested in the reciprocal experiment. GST-RP2 was used as “bait” protein for binding endogenous Arl3 from human cells and porcine retina lysates. For this purpose HeLa cells and isolated pig retinae were lysed in buffer 3. They were then incubated with aliquots of GST-RP2 glutathione-sepharose beads with all the procedures performed as described above for GST-Arl3 pull-down and in section 2.4.9. The samples were then analysed by SDS-PAGE with Coomassie stain and Western blotting (2.4.2-2.4.6).

The eluates from the GST-RP2 pull-downs were visualised by SDS-PAGE and a strong unique band was observed in the lane where GST-RP2 was incubated with the pig retina lysate compared to the one incubated with HeLa cell lysate (figure 4.2b). It had mobility similar to GST. It is possible that it was a porcine GST (predicted Mw 23 kDa) bound by glutathione-sepharose beads. These data suggest that the sepharose beads were not saturated by the recombinant protein and therefore, endogenous GST from the library of “prey proteins” was captured.

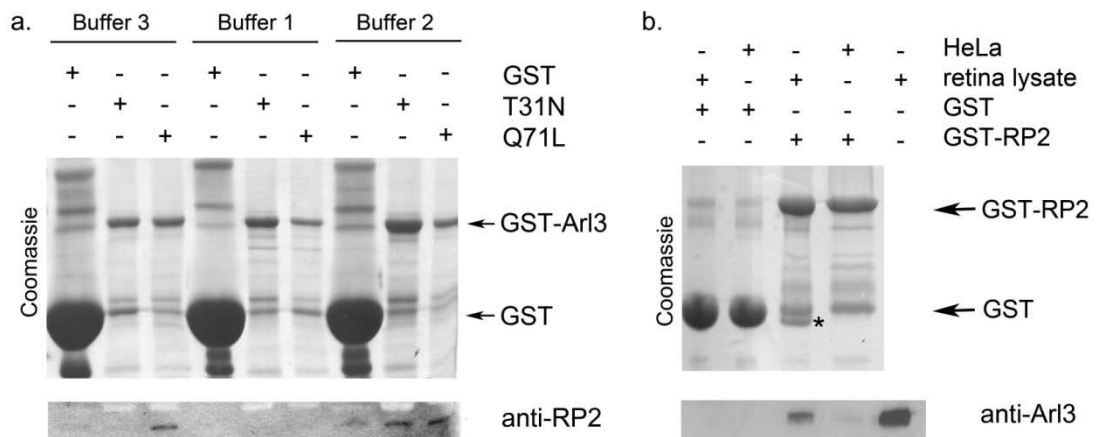


Figure 4.2. GST pull-down with GST-Arl3 and GST-RP2

a. Coomassie stained gel of the samples of the GST pull-down experiment of GST-Arl3 T31N and Q71L with HeLa cell lysates lysed using different buffers as in table 2.9. Eluate from GST bound beads (24 kDa) was used as a control for non-specific binding. Both GST-Arl3 forms showed the expected mobility at around 46 kDa. Western blot immunostained with anti RP2 antibody below the gel demonstrates specific bands of the bound endogenous RP2 (39kDa) from HeLa cell lysates. **b.** Coomassie stained gel of the GST pull down experiment using GST-RP2 as “bait” with HeLa cells and pig retina lysate (as indicated). The arrows indicate the mobility of GST-RP2 at 65 kDa and GST at 24 kDa. An asterisk indicates the position of a 23 kDa potential porcine GST band. The Western blot below is immunostained with anti Arl3 antibody demonstrating 20 kDa specific bands.

It was shown by Western blotting that under the chosen conditions the interaction of GST-RP2 with endogenous Arl3 from both HeLa cell lysate and the retinal lysate occurred (figure 4.2b). At the same time there were no bands observed in the GST negative control lane, demonstrating the specificity of binding of GST-RP2 to Arl3 in this assay. The Arl3 band from the pull-down with the retinal lysate appeared to be stronger than the one in the lane with the HeLa cell lysate. This difference could be due to the different concentration of Arl3 in these lysates possibly due to different expression level (data not shown).

4.2.3. Identification of transducin- β subunit as a potential RP2 interacting partner

The optimal conditions for the interaction of RP2 with Arl3 were used for further experiments aimed at identifying novel interacting partners of RP2 and to identify a GEF for Arl3 by GST pull-down followed by mass-spectrometry.

For this purpose beads with GST, GST-RP2, and both forms of GST-Arl3 were incubated with porcine retinal lysate in buffer 3 and all the experimental procedures were performed as in section 2.4.9. As an additional negative control for possible bacterial protein contamination, GST-RP2 or GST-Arl3 beads were incubated in buffer 3 but without retinal lysate added and treated as all other samples. The beads were eluted with 100 μ l of Laemmli buffer and 80 μ l of each eluate was resolved using a Midi-Vertical SDS-PAGE (2.4.2) in order to achieve a maximal concentration of protein for each sample and for better band separation. The proteins on the gel were visualised with mass-spectrometry compatible silver stain as described in section 2.4.4.

In the lanes with GST-Arl3 T31N and GST-Arl3 Q71L pull-down there were no bands observed which appeared to be unique to T31N mutant and likely to be a GEF, therefore no bands were excised from GST-Arl3 pull-down lanes (figure 4.3). However, as seen from figure 4.3 the loading of GST-Arl3 T31N protein was not equal to GST-Arl3 Q71L on the beads, therefore this experiment would need further optimisation.

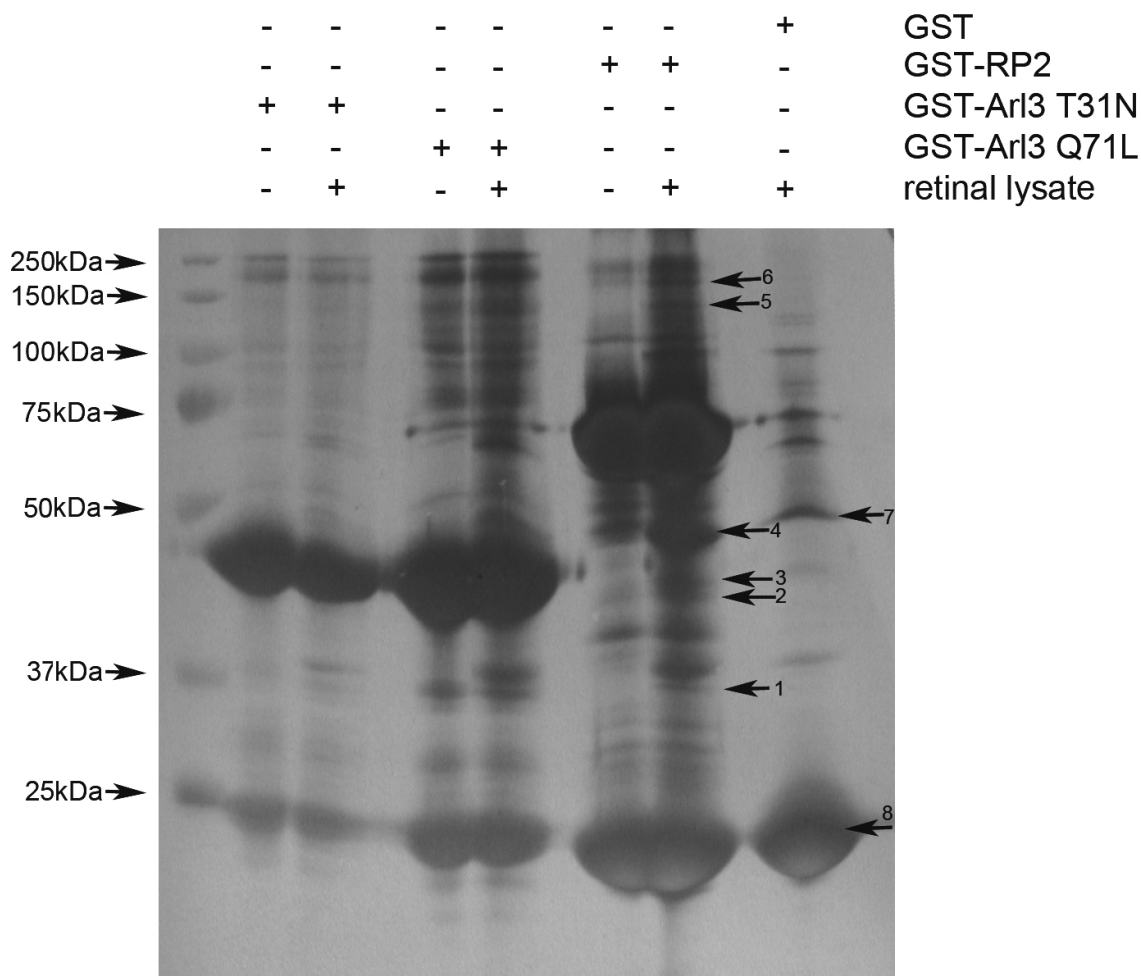


Figure 4.3. Pull-down assay of GST-RP2 and GST-Arl3 mutants with porcine retinal lysate

Silver stained midi-vertical SDS-PAGE gel of the GST pull-down experiment. The experimental lanes are as indicated above the gel. The numbered arrows on the gel (1-8) indicate the bands that were excised from the gel for mass-spectrometry analysis. The arrows on the left of the gel show the mobility of bands of the pre-stained molecular weight standard (see section 2.4.2).

In the GST-RP2 pull-down with the retinal lysate lane there were six unique bands found that were not apparent in the GST negative control lane or GST-RP2 beads control lane. The bands were of the following approximate sizes: about 37 kDa (1), 45kDa (2), 47kDa (3), 49kDa (4), 130 kDa (5), 180 kDa (6).

These bands were excised (figure 4.3) and further analysed by ESI-MS/MS as described in section 2.4.10 by Dr. R Wait (Kennedy Institute of Rheumatology Division, Imperial College, London). Two other bands were excised from the GST negative control lane – one at approximately 50 kDa (band 7) and the band 8, corresponding to GST (25 kDa), and these were analysed the same way.

The data obtained after ESI-MS/MS was analysed with the MASCOT program and searched for matching peptides in the NCBI nr database (section 2.6). Proteins were considered “identified” when they were represented by at least two unique peptides with a MASCOT ion score >35, or at least one peptide with MASCOT ion score >70 and that manual interpretation confirmed agreement between spectra and peptide sequence (analysis performed by Dr R. Wait).

Most of the bands did not show any significant match to known proteins but RP2, GST and enolase, which is frequently observed as a contaminant in pull-down assays with mammalian cell lysates (personal communication, Dr R Wait). The protein sequences obtained from each band are represented in table 4.1 and MS/MS data are attached to the thesis (compact disc).

Only one band (figure 4.3, band 1) resulted in five peptides with a MASCOT score >35. The comparison was performed based on the similarity between species due to the fact that the database for *Sus scrofa* is incomplete. ESI-MS/MS analysis of the band number 1 resulted in three peptides with significant ions score (35, 43 and 55). Three peptide sequences matched across species to a highly conserved protein, transducin- β (figure 4.4a). Other peptides from this band corresponded to either RP2 or GST.

Band	~Mw (kDa)	Proteins identified by at least two peptides with mascot score>35	Eukaryotic proteins predicted from unmatched peptides (mascot score<35)	Bacterial proteins predicted from unmatched peptides (mascot score<35)
1	37	transducin- β 37 kDa gi 6680045		ABC transporter transmembrane ATP-binding protein
		GST 25 kDa gi 84402		
		RP2 39 kDa gi 5902060		
2	45	enolase 49 kDa gi 119338	RP2 39 kDa	flagellar biosynthesis protein; NERD domain protein; ankyrin repeat domain protein;
		GST 25 kDa gi 84402	RAD10 domain protein (Mw range 32- 42 kDa)	
3	47	actin, ~42 kDa gi 113292	enolase 49 kDa	TufB domain protein; inorganic pyrophosphatase
		GST 25 kDa gi 84402		
4	49	enolase 49 kDa gi 119338	PolyA polymerase (testis specific) 112 kDa	squalene photoene synthase; DNA helicase; serine/threonine transferase; DHH family protein
		GST 25 kDa gi 84402		
5	130	enolase 49 kDa gi 119338	CAATT-binding protein (<i>Drosophila</i>) ~120 kDa	ribonucleotide transferase; phytoene desaturase; oxidoreductase;
		GST 25 kDa gi 84402	RP2 39 kDa	
6	180	GST 25 kDa gi 84402	hypothetic protein DDBDRAFT 0184139	aspartyl tRNA synthase; serine/threonine transferase squalene photoene synthase
			TIP120 ~140kDa	
7	50	enolase 49 kDa gi 119338	GST 25 kDa	β -gluconase; 50S ribosomal protein; squalene photoene synthase
8	25	GST 25 kDa gi 84402		

Table 4.1. The proteins and peptides identified in ESI-MS/MS analysis of GST-RP2 pull-down with the retinal lysate

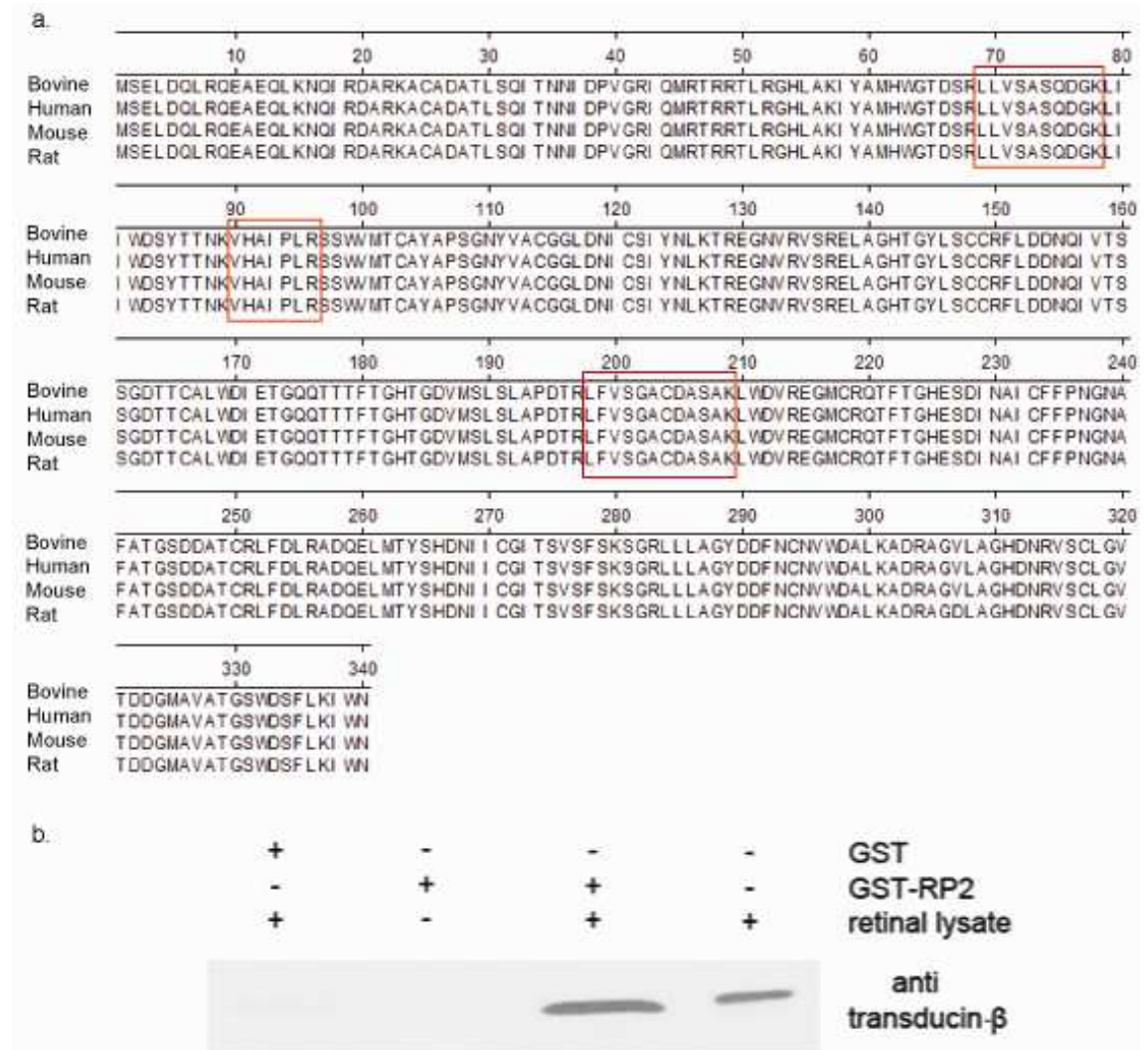


Figure 4.4. Transducin- β subunit identification

a. The peptides highlighted in red boxes were obtained from ESI-MS/MS of band 1 (collaboration with Dr R Wait) correspond to highly conserved transducin- β sequences from different species as indicated (the sequences are aligned using Clustal W). **b.** Western blot with anti transducin- β antibody (table 2.9) of the GST pull-down experiment showing presence of a 37 kDa transducin- β band in the GST-RP2 pull-down lane and not in the negative control GST pull-down lane.

4.2.4. Confirmation of transducin- β interaction with RP2 in retinal lysate

To test whether the protein in band 1 identified by mass spectrometry did correspond to porcine transducin- β , the aliquots of the samples from the experiment described above in 4.2.3 were resolved by mini SDS-PAGE with subsequent Western blotting (2.4.2 and 2.4.5). Immunostaining with anti transducin- β antibody revealed an immunoreactive 37 kDa specific bands in lanes with GST-RP2 pull-down and the retinal lysate input. There was no transducin- β band observed with the negative control GST alone pull-down with the retina lysate, demonstrating the specificity of binding (figure 4.4b). The mobility of the transducin- β band on the Western blot complemented the Mr of band 1 from the silver stained gel (section 4.2.3, figure 4.3), suggesting that the excised band did correspond to porcine transducin- β .

4.2.5. Interaction of transducin- β with RP2 in immunoprecipitation assay

In order to test whether transducin- β was a potential interacting partner of RP2, co-immunoprecipitation (IP) assays were used as a complementary technique.

SK-N-SH human neuroblastoma cells with an undetectable level of endogenous RP2 were chosen for the IP experiment. Cells were co-transfected (as described in 2.3.2) with human RP2-GFP and human FLAG-transducin- β plasmid (Missouri S&T cDNA Resource Center, section 2.1.8, table 2.5). The transfected cells were lysed with buffer 7 (table 2.8), which had been shown to be optimal for co-IP of Tctex-1 and transducin- β (Sachdev *et al.*, 2007), and incubated with anti-FLAG antibody (table 2.10). The co-IP was then incubated with Protein G sepharose, washed and eluted with Laemmli buffer (described in section 2.4.11). To control for non-specific binding the cell lysates were incubated with mouse non-specific IgG and treated the same way as the samples with anti-FLAG antibody. The eluates obtained from protein G sepharose were resolved by SDS-PAGE and analysed by Western blotting (as in sections 2.4.2 and 2.4.5).

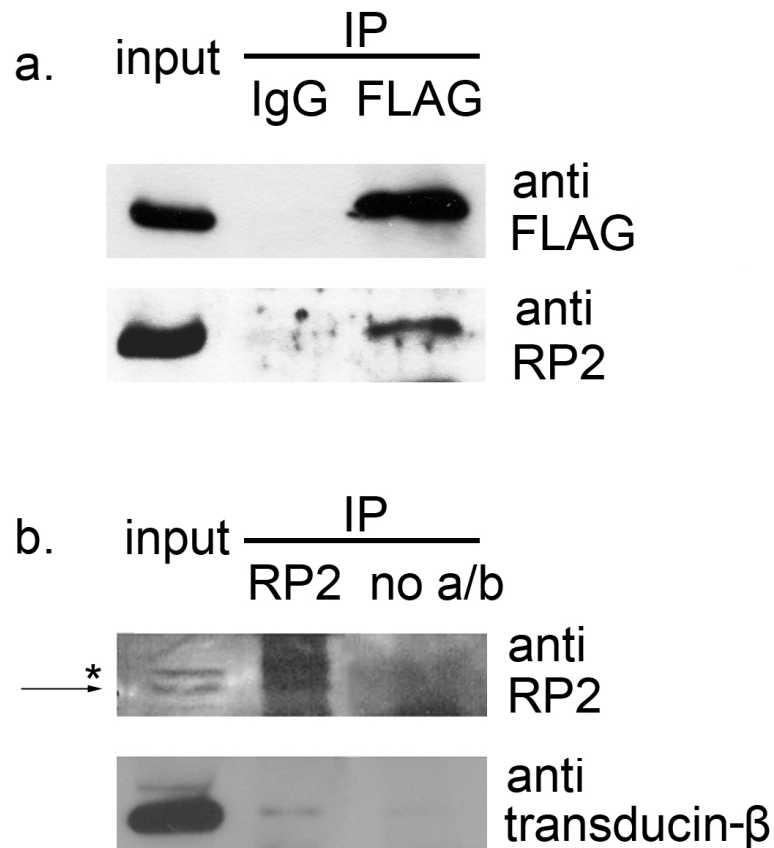


Figure 4.5. Interaction of transducin- β with RP2

a. Western blots of immunoprecipitation (IP) with anti-FLAG of FLAG-transducin- β and RP2-GFP, expressed in SK-N-SH cells. The upper panel shows a Western blot immunostained with M2 anti-FLAG (table 2.10) antibody detected a 37 kDa specific band of FLAG-transducin- β . The lower panel represents a Western blot stained with anti-RP2 antibody (S974, table 2.10) showing a specific band of 66 kDa in the input and FLAG IP lanes but not in the IgG negative control lane. **b.** Western blots of IP of endogenous RP2 from pig retinal lysate using anti-RP2 antibody detected two specific bands of approximately 39 kDa (indicated with arrow) and 40 kDa (indicated with asterisk) (upper panel). The lower panel shows a Western blot with anti transducin- β of transducin- β co-precipitated with RP2 from the retinal lysate using anti-RP2 antibody as above and immunostained with anti- transducin- β antibody (table 2.10) detected a 37 kDa transducin- β band in the input lane and RP2 IP lane.

It was observed that the anti-FLAG antibody successfully precipitated FLAG-transducin- β from the cell lysate and that FLAG-transducin- β was able to co-precipitate RP2-GFP whereas the non-specific IgG did not (figure 4.5a), suggesting that an interaction between transducin- β and RP2 had occurred.

Several attempts were made to precipitate an endogenous complex of transducin- β with RP2 from the pig retina lysate. However, the result was inconsistent and the antibodies to RP2 or transducin- β either failed to precipitate appropriate proteins or precipitated hardly detectable amounts (an example is shown in figure 4.5b). This problem did not allow the detection of Arl3 co-precipitated with RP2 from the retinal lysate (data not shown). Thus, it remains to be clarified whether an endogenous complex of RP2 with transducin- β is formed in retina lysates.

4.2.6. The effect of RP2 mutations on the interaction with transducin- β

The binding of transducin- β to mutants of RP2 was tested by co-IP. SK-N-SH cells were transfected with the wild type RP2 or the four mutants (C67Y, C86Y, R118H and L253R) and the FLAG-transducin- β construct (table 2.4, section 2.1.8). The experiment was performed as described above. β -arrestin-2-FLAG was chosen as a negative control as it was shown in chapter 3 (section 3.3) that RP2-GFP did not bind this protein in co-IP.

The results of the experiment are shown in figure 4.6. It was shown by Western blot with anti GAPDH antibody (table 2.9) that the protein concentration loading was roughly equal in all the input lysates. The IP samples did not demonstrate any bands of contamination with GAPDH. The anti-FLAG antibody precipitated equal amounts of FLAG-transducin- β from all the lysates despite different expression level. The β -arrestin-2-FLAG was expressed at comparable levels; however, the band of precipitated protein was likely to be covered by the band of anti-FLAG IgG heavy chains.

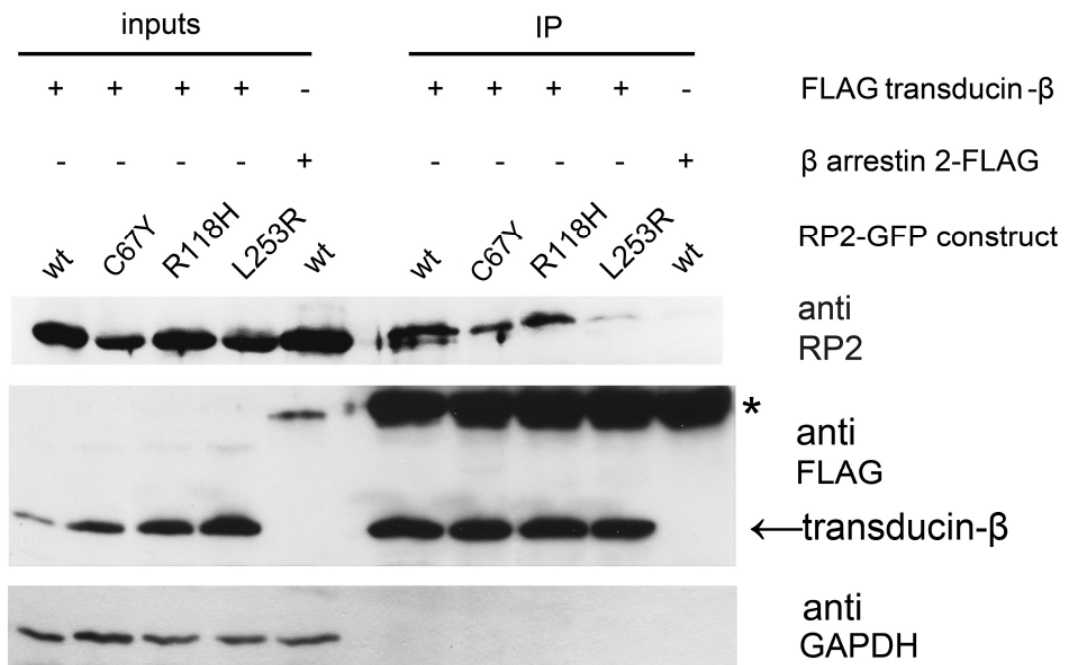


Figure 4.6. Interaction of RP2 mutants with transducin- β .

Western blots of IP of FLAG-transducin- β with wild type RP2-GFP and its mutants as indicated. The upper panel represents a Western blot immunostained with anti-RP2 antibody (S974, table 2.10) demonstrating 66 kDa RP2-GFP bands of different intensity in input lanes and in co-IP lanes. Middle panel shows Western blot stained with M2 anti-FLAG antibody (table 2.10), the bands of 37 kDa of FLAG-transducin- β and a 46 kDa band of β -arrestin 2-FLAG in lanes as indicated. The asterisk shows the position of mouse IgG heavy chain. The bottom panel shows bands of 36 kDa on the Western blot with anti GAPDH antibody (table 2.10).

The Western blot immunostained with anti-RP2 antibody showed specific bands of 66 kDa in most input and IP lanes but the negative control β -arrestin-2-FLAG lane, indicating that binding of RP2-GFP to FLAG-transducin- β occurred.

The expression of wild type RP2-GFP and the R118H mutant was higher than the other RP2 constructs. RP2-GFP C67Y and L253R mutants had a lower expression level compared to the wild type RP2 (figure 4.6). Wild type RP2 appeared to be co-precipitated with FLAG-transducin- β by the anti-FLAG antibody. However, in the lane where transducin- β was co-transfected with C67Y the RP2 specific band appeared to be weaker compared to the wild type RP2 and the R118H mutant.

There was a very weak band observed in the IP lane with the L253R RP2 mutant, suggesting that this mutation in the C-terminus of RP2 could disrupt the interaction with transducin- β . The R118H “arginine finger” mutation did not demonstrate significant disruption of the transducin- β interaction (figure 4.6).

4.2.7. The subcellular localisation of transducin- β and RP2 overlap

To investigate the nature of putative interaction of RP2 with transducin- β , these proteins were studied in cell culture using immunofluorescence. SK-N-SH cells were transfected with GFP or RP2-GFP and FLAG-transducin- β (as in 2.3.1 and 2.3.2). The cells were then fixed, immunostained with anti-FLAG antibody as described in 2.3.4 and table 2.8. Cells were analysed by confocal microscopy (2.3.5).

It was observed that in cells co-transfected with FLAG-transducin- β and an empty GFP vector the staining of transducin- β was predominantly cytoplasmic with small cytosolic and often perinuclear intracellular inclusions (figure 4.7a). Some cells exhibited predominant plasma membrane localisation of transducin- β (figure 4.7b) and cell counting estimated the proportion of such cells at 33 % of the population (figure 4.10a). There was no similarity in the staining pattern of transducin- β and GFP (figure 4.7a, b).

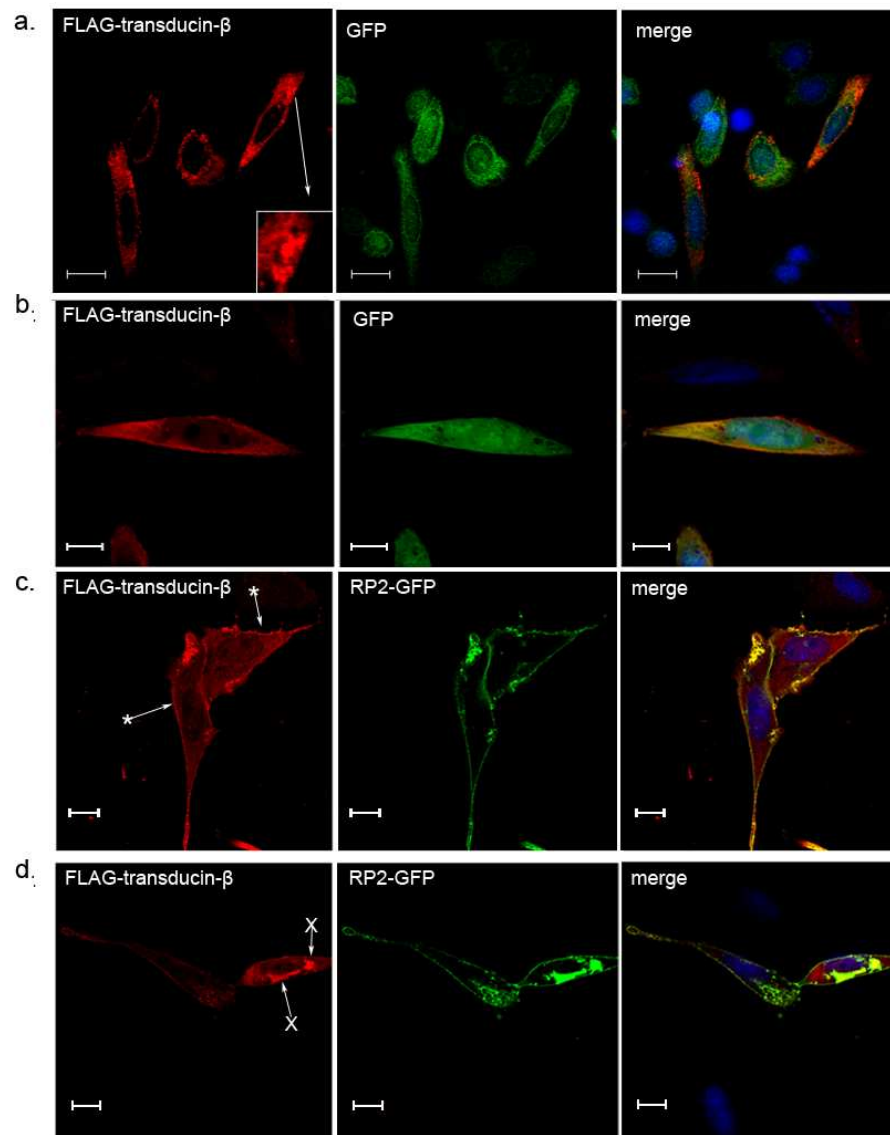


Figure 4.7. Subcellular localisation of transducin- β and RP2

Confocal microscopy images of SK-N-SH cells co-transfected with FLAG-transducin- β and empty GFP (**a**, **b**) or RP2-GFP (**c**, **d**), immunostained with anti-FLAG antibody. FLAG-transducin- β is shown in red whereas GFP or RP2-GFP is in green. Arrows on panel **a** highlight intracellular inclusions formed by FLAG-transducin- β when co-transfected with GFP (zoomed inset). **b** shows an example of a cell expressing FLAG-transducin- β without inclusion formation with some localisation on the plasma membrane. Arrows with asterisks on panel **c** shows plasma membrane localisation of FLAG-transducin- β in the presence of RP2-GFP. Panel **d** shows intracellular FLAG-transducin- β and RP2-GFP co-localisation as indicated with arrows with crosses. Scale bars are 10 μ m.

Upon co-transfection of FLAG-transducin- β with RP2-GFP, a change in the localisation of transducin- β was observed. In 68 % of co-transfected cells transducin- β was localized predominantly on the plasma membrane together with RP2-GFP (figure 4.7c, d). This observation was highly reproducible and quantified in at least three independent experiments (figure 4.10). It had been shown previously that RP2, when over-expressed, can form intracellular inclusion-like structures (Evans, 2007). This phenomenon was observed in some cells transfected with RP2-GFP and when RP2-GFP was co-transfected with FLAG-transducin- β . It was found that FLAG-transducin- β was recruited to RP2-GFP intracellular inclusions in 88 % of cells with such inclusions (figures 4.7d and 4.10c).

4.2.8. Subcellular localisation of other G β proteins and RP2

To reveal whether the potential interaction of RP2 with transducin- β was specific to transducin- β and not other types of G β proteins, SK-N-SH cells were co-transfected with RP2-GFP and different N-terminally FLAG-tagged constructs of G β 3, G β 5 and G β 5L proteins (cDNA Resource Center, table 2.5) as described in section 2.3.2. The cells were then fixed with methanol and immunostained with anti-FLAG antibody with subsequent confocal microscopy (table 2.7 and section 2.3.5).

The staining of G β 3 protein was predominantly cytoplasmic with occasional intracellular inclusions. This staining pattern did not overlap with RP2-GFP distribution on the membrane or in occasional intracellular inclusions formed by RP2 (figure 4.8). G β 5L was observed mostly on the plasma membrane with a relatively small portion in the cytoplasm and the staining overlapped with RP2-GFP localisation on the membrane. However, when RP2-GFP formed inclusions, they did not appear to co-localise with G β 5L staining (figure 4.8). Co-transfection of RP2-GFP with G β 5 protein resulted in the same pattern as described for its longer isoform G β 5L (figure 4.8). Thus, the localisation of RP2-GFP and other G β proteins did not seem to overlap as closely as transducin- β .

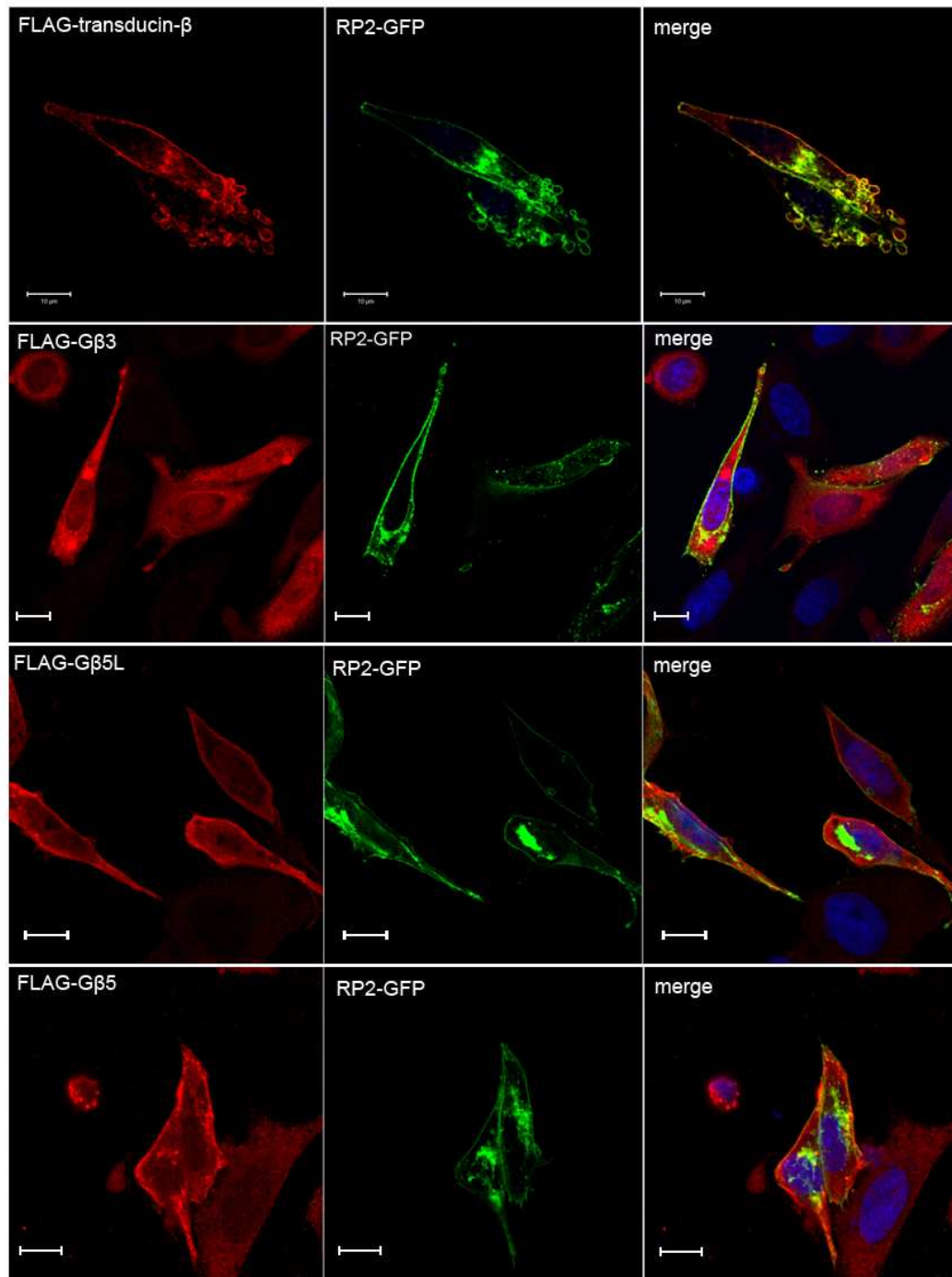


Figure 4.8. Subcellular localisation of transducin- β , G β 3, G β 5L, G β 5 and RP2-GFP in SK-N-SH cells

Confocal microscopy images of SK-N-SH cells co-transfected with different G β proteins and RP2-GFP as indicated. After methanol fixation cells were stained with M2 anti-FLAG antibody (table 2.10) to visualise N-terminally FLAG tagged G β proteins (red). RP2-GFP is shown in green. Scale bars are 10 μ m.

4.2.9. L253R mutation in the C-terminus of RP2 affects transducin- β co-localisation with RP2

To confirm the previous data that suggested that the pathogenic L253R RP2 mutation decreased the affinity of the transducin- β interaction with RP2, immunofluorescence was used to study this interaction further.

SK-N-SH cells were co-transfected with FLAG-transducin- β and the wild type RP2-GFP or its mutants (C67Y, C86Y, R118H and L253R) as described in sections 2.3.1-2.3.2. After methanol fixation and staining with anti-FLAG antibody the cells were analysed using confocal microscopy (table 2.7 and section 2.3.5).

The co-transfection of cells with FLAG-transducin- β and wild type RP2-GFP demonstrated a shift in localisation FLAG-transducin- β from the cytoplasm to the plasma membrane as described in 4.2.8, indicating that the data were reproducible (figure 4.9). Upon transfection with the C67Y RP2-GFP mutant, the formation of large intracellular inclusions was observed and cells appeared to be significantly smaller in size with abnormal nuclei.

Therefore when the cells were co-transfected with the FLAG-transducin- β and C67Y RP2 mutant, the result was difficult to assess due to such changes. However, in some cells staining of FLAG-transducin- β and RP2-GFP mutants overlapped. Unfortunately, correct counting of the overlap incidence was not feasible due to poor anti-FLAG antibody penetration into the inclusions formed by C67Y RP2-GFP mutant (figure 4.9).

Co-transfection of cells with the R118H RP2 mutant and FLAG-transducin- β resulted in no change in localisation compared to wild type RP2-GFP. Transducin- β was present on the plasma membrane and co-localised with R118H RP2-GFP. Some cells, where intracellular staining of R118H RP2-GFP was observed, showed overlap in staining of intracellular transducin- β with R118H RP2-GFP (83 %) (figure 4.10 b, c). This overlap was comparable to the wild type RP2-GFP (88 %) (figure 4.10c).

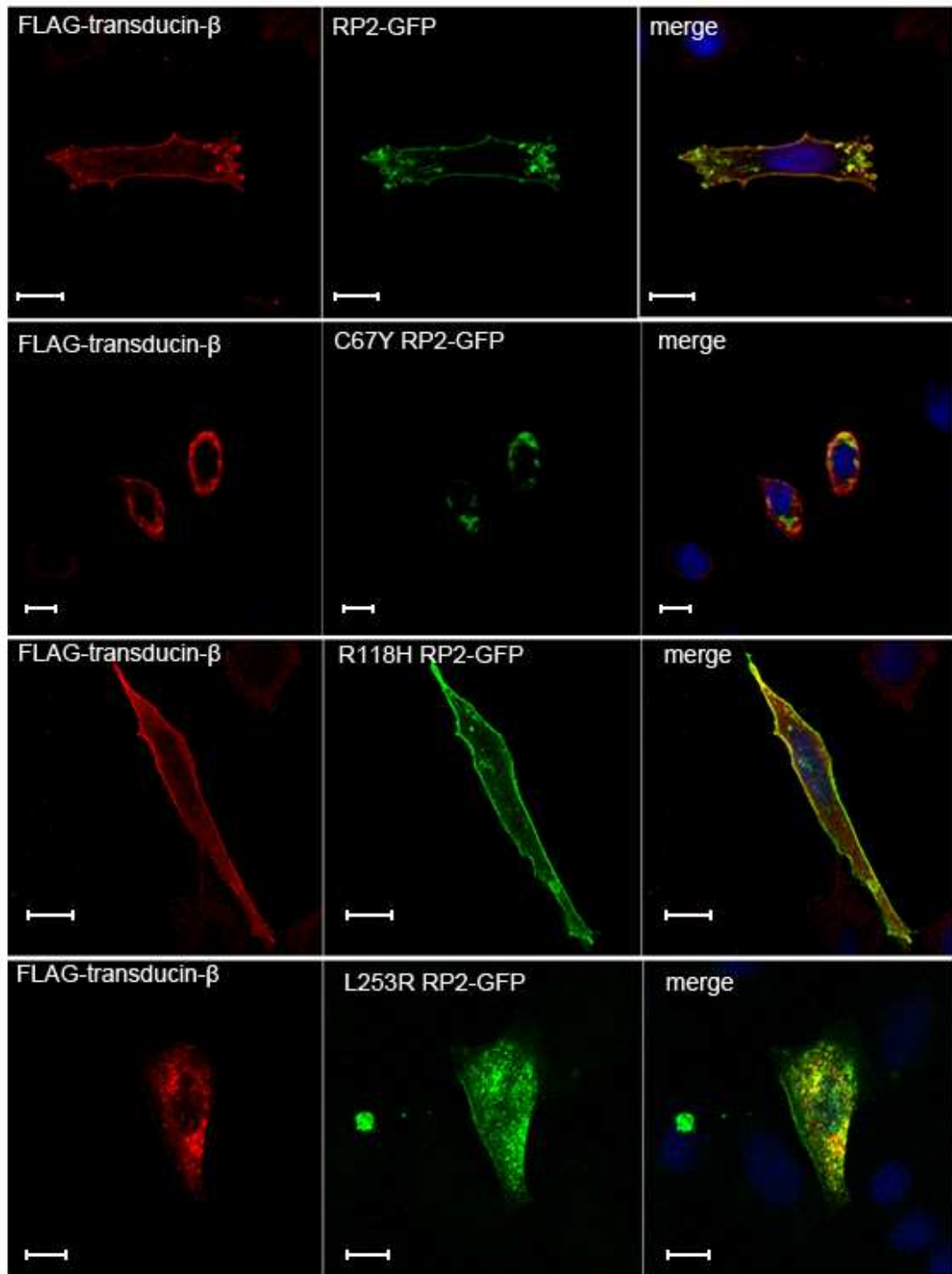


Figure 4.9. Effect of RP2 mutations on transducin- β intracellular staining

Confocal microscopy images of cells co-transfected with wild type (wt) RP2-GFP or the RP2-GFP mutants (green) and FLAG-transducin- β (red). Scale bars are 10 μ m.

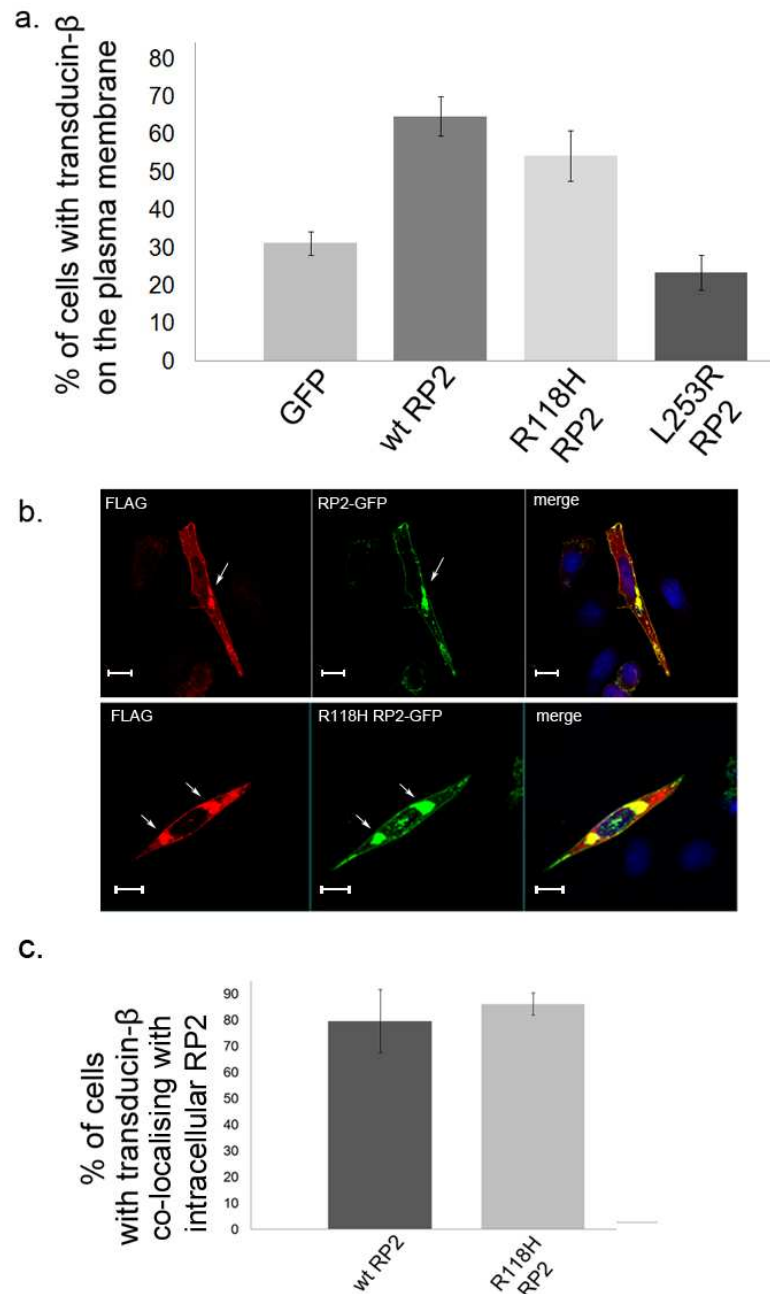


Figure 4.10. Effect of RP2 mutants on transducin- β localisation

a. The graph represents the percent of cells with FLAG-transducin- β staining localised predominantly on the plasma membrane when co-transfected with different RP2-GFP plasmids as indicated on the x axis. Error bars show standard deviation (± 1 SD) **b.** Confocal images of cells co-transfected with FLAG-transducin- β and RP2-GFP or R118H RP2-GFP mutant with intracellular staining indicated with arrows. **c.** Graph showing the percent of cells with coincidence of overlap in the intracellular staining of RP2-GFP/R118RP2-GFP and transducin- β . Error bars are standard deviation (± 1 SD).

Cells transfected with the L253R RP2-GFP mutant exhibited some plasma membrane staining with small intracellular inclusions. In cells co-transfected with this mutant and FLAG-transducin- β , the L253R mutant did not change its localisation (data not shown). However, FLAG-transducin- β staining was observed predominantly in the cytoplasm and was similar to cells co-transfected with FLAG-transducin- β and GFP alone (figure 4.9). In 20 % of cells, transducin- β staining was still observed on the plasma membrane (figure 4.10a). Therefore, the L253R C-terminal mutation of RP2 was found to have a strong effect on the RP2 interaction with transducin- β .

4.2.10. Subcellular fractionation assay of transducin- β localisation upon co-transfection with RP2

In order to confirm the translocation of transducin- β from the cytoplasm to the plasma membrane upon co-transfection with RP2, subcellular fractionation was used to test whether there was a shift in transducin- β into the membrane fraction when co-transfected with RP2.

SK-N-SH cells were co-transfected with FLAG- transducin- β and empty GFP vector to test which fraction FLAG-transducin- β was present. A parallel SK-N-SH cell population was co-transfected with FLAG-transducin- β and RP2-GFP to determine whether RP2 is able to change FLAG-transducin- β subcellular localisation.

The cells were then fractionated using the protocol described in section 2.3.6. This technique separates cells into cytosolic, membrane, cytoskeletal and SDS-insoluble proteins (pellet) fractions. For the extraction of the cytosolic proteins, the plasma membrane was disrupted mechanically to release proteins into the buffer. After the cytosolic fraction was isolated, Triton X 100 was included in the next extraction buffer to solubilise membrane-bound proteins. When the membrane protein fraction is collected, the next buffer uses SDS to solubilise cytoskeletal proteins. The pellet fraction obtained after the final extraction represents cell proteins that are not soluble in SDS.

However, it is not possible to accept that the cytoskeletal fraction contains only cytoskeleton components. The buffer for extraction of proteins for this fraction

contains SDS, which solubilises not only cytoskeletal proteins, but also those, which are insoluble in Triton X100 of the membrane extraction buffer. Thus, the fraction is conditionally called “cytoskeletal” although this name does not refer to its content exclusively.

When performing the cell fractionation technique it is possible to contaminate the cytosolic fraction with membrane proteins and vice versa. Therefore, the efficiency of fraction separation was checked. GAPDH was chosen as a marker for soluble cytosolic proteins and the endoplasmic reticulum (ER) chaperone calnexin for membrane proteins.

Each fraction was resolved by SDS-PAGE and analysed by Western blotting. It was shown that fraction separation was achieved (figure 4.11) and there was no contamination of the membrane and subsequent fractions with soluble cytosolic proteins as GAPDH was present only in the cytosolic fractions. However, a minor contamination of cytosolic and cytoskeletal fractions with calnexin was observed. This contamination was equal in both GFP and RP2-GFP transfected cells lysates and was considered not a significant problem for this experiment.

RP2-GFP showed a predominant localisation in the membrane fraction although a small amount was also present in cytoskeletal and pellet fractions (figure 4.11).

When co-transfected with empty GFP, FLAG-transducin- β was mainly present in the cytoskeletal and the pellet fractions with a trace amount in the membrane fraction. There was no band detected in the soluble cytosolic protein fraction. Upon co-transfection of FLAG-transducin- β with RP2-GFP, it was found that transducin- β was present only in the membrane protein fraction with a significant amount of transducin- β retained in the stacking gel as seen in figure 4.11.

Thus, this experiment showed that the majority of transducin- β shifted from the “cytoskeletal” fraction to the membrane fraction upon co-transfection with RP2.

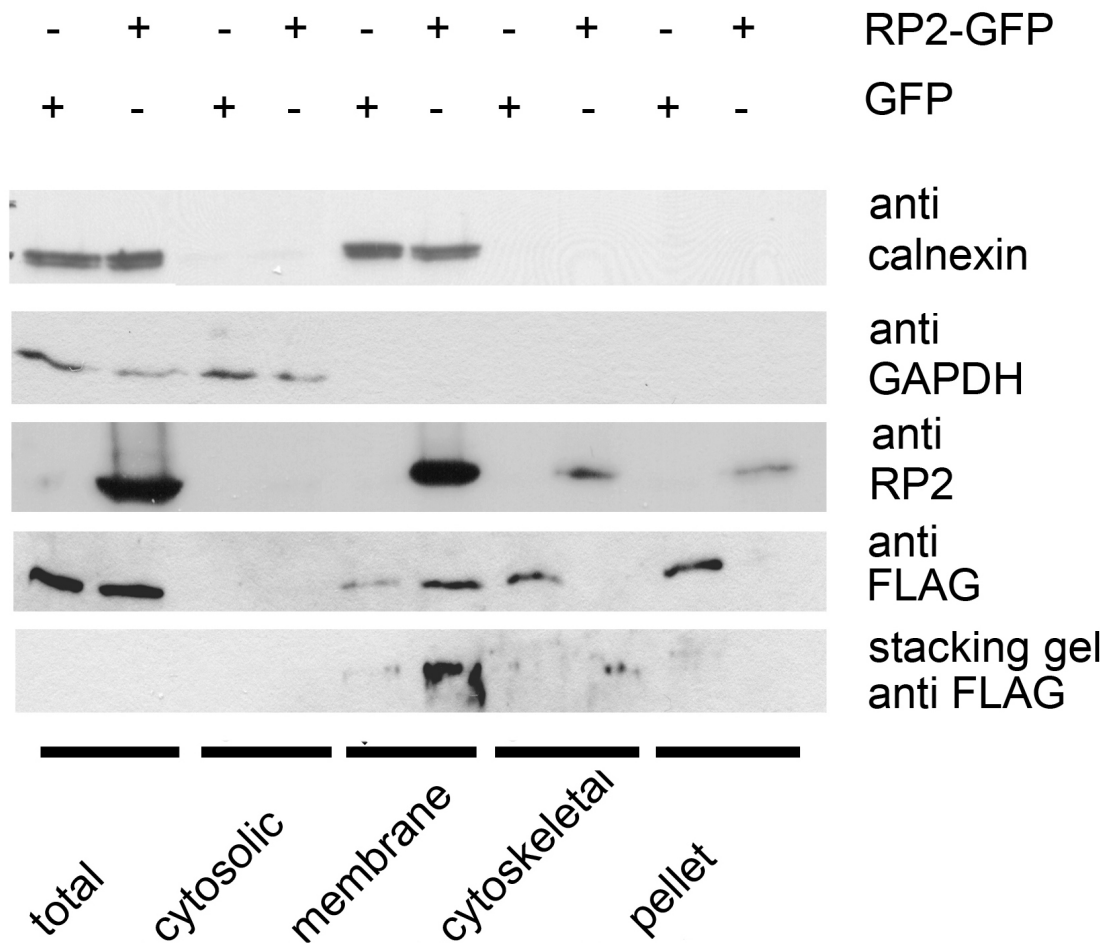


Figure 4.11. Changes in the subcellular localisation of transducin- β upon co-transfection with RP2

Western blots of subcellular fractions of cells co-transfected with FLAG-transducin- β and GFP or RP2-GFP. The upper panel shows the predominant presence of endogenous calnexin in the membrane fraction. The next panel demonstrates the presence of GAPDH in the cytosolic fraction only. Western blot of fractions immunostained with anti RP2 antibody showed its fractionation mainly with the membrane fraction. The last two panels show Western blots of the resolving and stacking parts of the SDS-PAGE gel of fractions stained with anti-FLAG antibody, demonstrating higher intensity bands of FLAG-transducin- β in the membrane fraction upon co-transfection with RP2-GFP.

4.2.11. Detergent resistant membrane isolation from cells co-transfected with transducin- β and RP2

It has been shown that RP2 is partly localised to detergent resistant membranes (DRM) (Chapple *et al.*, 2003). In order to test if RP2 recruits transducin- β to DRM, the membrane fraction isolation was performed.

First the procedure was tested for the optimal conditions such as gradient density and buffers. Thereby, a protocol of sucrose gradient fractionation described in section 2.3.7 was developed and a test fractionation of ARPE19 cells was performed.

GM₁ was used as a marker for the DRM fraction, which was detected by binding to HRP-conjugated cholera-toxin subunit B. It was found that fractions 3-5 of the gradient contained DRM (figure 4.12). Calnexin was chosen as a marker for detergent soluble membranes and was co-fractionated with fractions 7-12 and the pellet.

Western blotting for endogenous RP2 revealed that RP2 gradient distribution was similar to calnexin, with the difference that RP2 was also present in fractions 3-5, which contained DRM (figure 4.12). Endogenous Arl3 was present in fractions 10-12 only, as previously described (Chapple *et al.*, 2003).

ARPE19 cells were co-transfected with FLAG-transducin- β and empty GFP or RP2-GFP. After that the cells were lysed in buffer 2 (table 2.8) and the sucrose gradient fractionation was performed as described above. However, the antibody to RP2, GFP and FLAG could not detect the transfected proteins in the Western blot after sucrose gradient fractionation. This could be a consequence of the expression level being too low for the dilution by the fractionation procedure. Another possibility is that the tested proteins were not solubilised in Laemmli buffer after TCA precipitation (as described in section 2.4.2). The potential effect of RP2 on DRM recruitment of transducin- β needs to be investigated further.

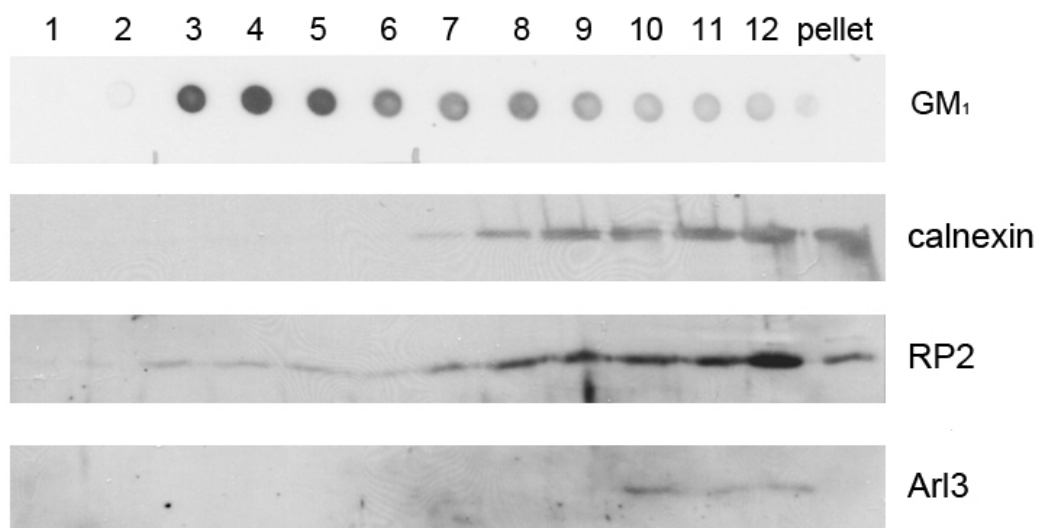


Figure 4.12. Detergent resistant membrane fractionation of ARPE19 cells

Lanes 1-12 represent sucrose gradient cell lysate separation. The number of each fraction indicates collection from top to the bottom of the gradient. The first panel shows a dot-blot of the gradient obtained after DRM isolation, incubated with HRP-cholera-toxin subunit B to bind GM₁. Fractions 3-5 contain the highest concentration of GM₁. Western blot with anti-calnexin antibody revealed specific bands of 90 kDa calnexin in fractions 7-12 and in the pellet. The next panel shows Western blotting with anti-RP2 antibody showing 39 kDa bands of endogenous RP2 in lanes 3-12. The Western blot stained with anti Arl3 antibody showed specific bands of 20 kDa of endogenous Arl3 in fractions 10-12.

4.2.12. Arl3 siRNA does not alter the overlap in subcellular co-localisation of transducin- β and RP2

In order to check if RP2 and transducin- β form a binary complex or RP2 acts together with Arl3 in this interaction, a GST-pull down assay of porcine retinal lysate with GST-Arl3 was performed. The experiment showed presence of specific transducin- β bands in the lanes of both GST-Arl3 fusion proteins with a stronger intensity band with the GST-Arl3 Q71L mutant elution (figure 4.13a). This result indicated the possible involvement of Arl3 in the RP2 interaction with transducin- β .

In order to test if Arl3 was required for the interaction of RP2 with transducin- β , siRNA for Arl3 was used reduce Arl3 expression. SK-N-SH cells were chosen for this experiment as previous experiments on the RP2 interaction with transducin- β were performed using this line (sections 4.2.5-4.2.10).

Cells were transfected with siRNA for Arl3 or a negative control of scrambled siRNA as described in 2.3.3. After 76 hours of incubation with siRNA, the cells were co-transfected with RP2-GFP and FLAG-transducin- β constructs and incubated for another 24 hours. The cells were then fixed with methanol and immunostained with anti-FLAG antibody (table 2.6) as in section 2.2.4. Cells transfected with scrambled and Arl3 siRNAs were immunostained with anti Arl3 antibody to confirm that the Arl3 expression level was decreased (figure 4.13b).

The efficiency of endogenous Arl3 knock down was assessed using epifluorescent microscopy with software as described in 2.3.5 section. The images of the negative control with scrambled siRNA and Arl3 siRNA were taken on the same microscope using identical exposure settings. It is shown in figure 4.13b that the Arl3 staining was less intense in cells transfected with siRNA Arl3 compared to scrambled siRNA control. Arl3 siRNA had been tested in our lab before by Western blotting and had demonstrated up to 70 % decrease in Arl3 protein compared to the scrambled siRNA negative control (data not shown).

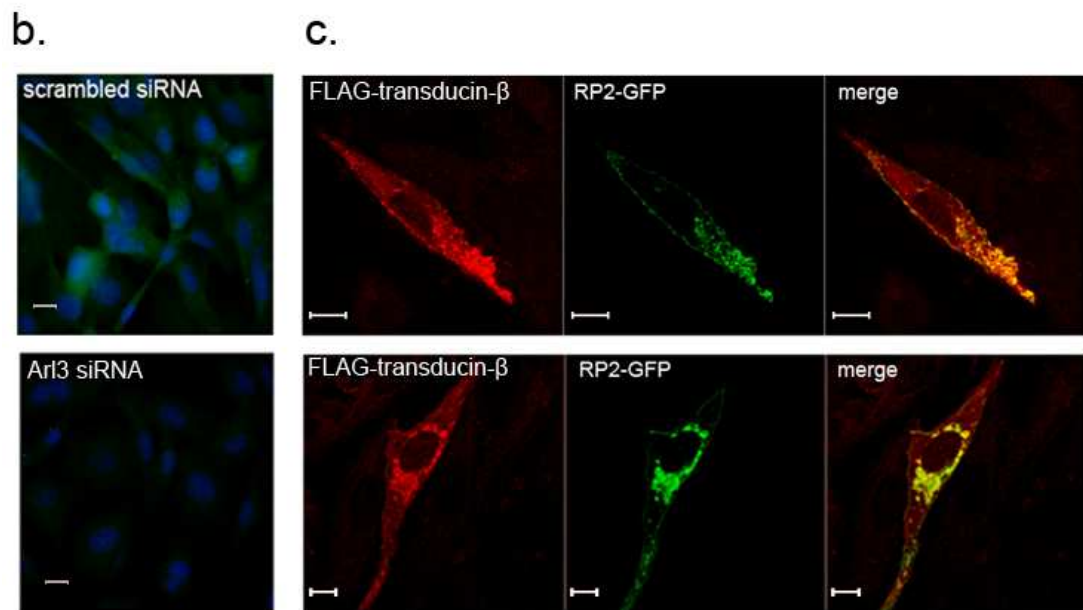
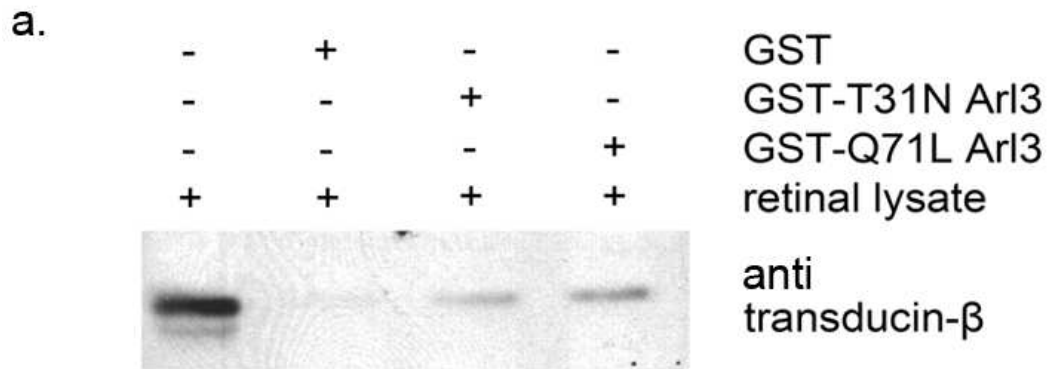


Figure 4.13. GST-Arl3 pull down with retina lysate and the effect of Arl3 siRNA on RP2 co-localisation with transducin- β

a. Western blot of GST pull-down using T31N and Q71L forms of GST-Arl3 with pig retinal lysate. The 37 kDa porcine transducin- β bands were detected with GST-Arl3 pull-down but not in GST negative control pull-down. **b.** Epifluorescent microscopy images of SK-N-SH cells transfected with scrambled siRNA or Arl3 siRNA immunostained with anti-Arl3 antibody (green). The nuclei are visualised with DAPI (blue). Scale bars are 10 μ m. **c.** Confocal images of SK-N-SH cells co-transfected with scrambled siRNA (top) or Arl3 siRNA (lower), RP2-GFP and FLAG-transducin- β . Cells were immunostained with anti-FLAG antibody visualising transducin- β (red), RP2-GFP is in green. Scale bars are 10 μ m.

No difference in cells with or without Arl3 expression knock-down was observed (figure 4.13c). Thus, Arl3 siRNA does not appear to affect the intracellular co-localisation of RP2 with transducin- β .

4.2.13. Arl3 is able to alter co-localisation of RP2 with transducin- β

In order to test if over expression of GDP- or GTP-bound conformations of Arl3 can influence the overlap in localisation of RP2 and transducin- β , SK-N-SH cells were co-transfected with FLAG-transducin- β , RP2-GFP and non-tagged T31N or Q71L Arl3. After 24 hours the cells were fixed with methanol and immunostained with anti-FLAG antibody to visualise transducin- β (section 2.3.4, table 2.6).

It was observed that T31N Arl3 did not change the overlap in plasma membrane localisation of FLAG-transducin- β with RP2-GFP (figure 4.14). Q71L Arl3 caused RP2-GFP to partially localise to a perinuclear region within the cell, an effect that had been observed previously (Evans, 2007). Similar effect was observed with transducin- β co-transfected with RP2-GFP and GTP-Arl3. The subcellular localisation of transducin- β changed to a more intracellular staining pattern but this did not appear to overlap with the intracellular localisation of RP2-GFP (figure 4.14).

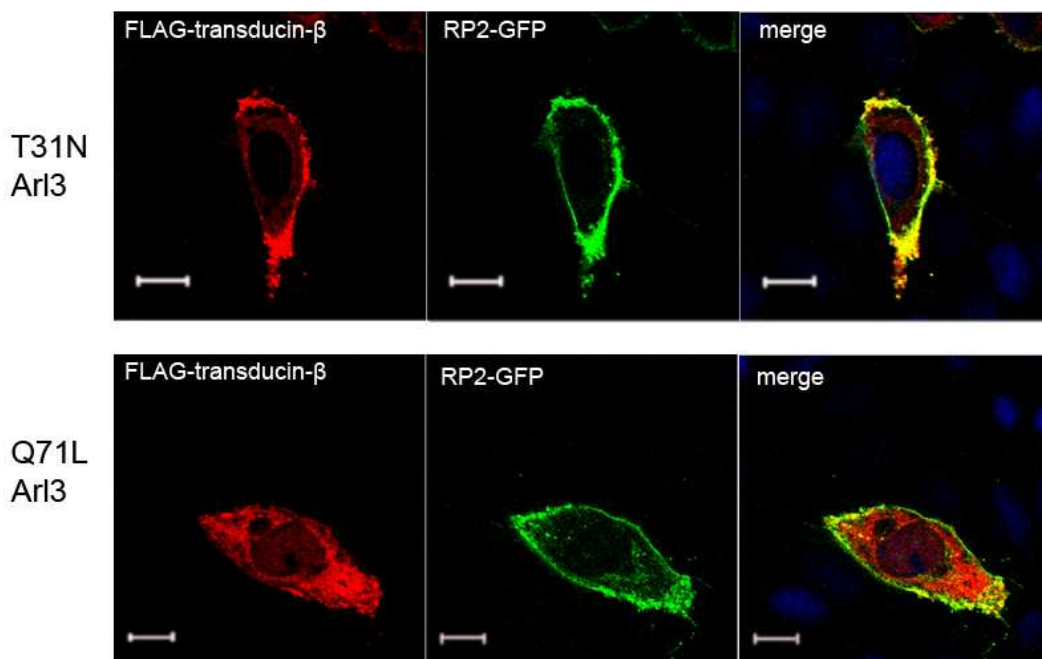


Figure 4.14. Subcellular localisation of transducin- β and RP2 upon co-transfection with Arl3

Confocal microscopy images of SK-N-SH cells co-transfected with FLAG-transducin- β , RP2-GFP and GDP- or GTP conformational forms of Arl3 as indicated. Cells were immunostained with M2 anti-FLAG antibody to visualise transducin- β (red). RP2 is shown in green and the nuclei are visualised with DAPI (blue). Scale bars are 10 μ m.

4.3. Discussion

This chapter demonstrates that a GST pull-down protein affinity approach was an efficient tool for finding of interacting partners for RP2. Using such an approach another potential novel interacting partner for RP2, transducin- β , was identified. Transducin- β is a subunit of the transducin heterotrimeric complex that takes part in the phototransduction cascade (described in section 1.2.3.3). The identification of this protein was possible due to mass spectrometric analysis of three peptides of transducin- β . However, two of these peptides were identical to another G protein β subunit involved in β -adrenoreceptor signalling, G β 3, but one peptide demonstrated identity to transducin- β and not to other G β proteins (figure 4.15). Thus, transducin- β was another putative interacting partner identified in this study that puts RP2 in a retina specific pathway.

However, this experiment was not reproducible possibly due to the pig retinal lysate properties varied from different pig eyes delivery. Attempts to detect the endogenous complex of these proteins in retinal lysates using immunoprecipitation were not successful. When the anti-RP2 antibody used for the IP appeared to precipitate RP2 protein from the pig retinal lysate, this recovery was of low yield and therefore not sufficient for detection of any proteins which could have been co-precipitated, including Arl3. The staining of porcine retina cryosections with anti-RP2 antibody and/or anti transducin- β antibody was also not successful (data not shown). It is possible that the anti-RP2 antibody did not cross-react well with the pig protein. Delay in harvesting of pig retinas could also affect the result. Therefore this experiment could be improved by using retinal lysate from other species, such as mouse.

Despite these concerns the RP2- transducin- β interaction was confirmed by immunoprecipitation assays when transducin- β and RP2 were overexpressed in a cell culture, which showed that RP2 specifically bound transducin- β . This study also demonstrated that co-localisation of RP2 and transducin- β was specific to transducin- β rather than other G β family proteins tested, such as G β 3.

1	MSELDQLRQE	<u>AEQLKNQIRD</u>	ARKACADATL	SQITNNIDPV	transducin β
1	MGEMEQLRQE	<u>AEQLKKQIAD</u>	ARKACADVTL	AELVSGLEVV	G β 3
54	NETLASLKSE	<u>AE SLKGKLEE</u>	ERAKLHDVEL	HQVAERVEAL	G β 5L
8	NETLASLKSE	<u>AE SLKGKLEE</u>	ERAKLHDVEL	HQVAERVEAL	G β 5
41	<u>GRIQMRTRRT</u>	<u>LRGHLAKIYA</u>	<u>MHWGTD</u> SRLL	<u>VSASQDGKLI</u>	transducin β
41	<u>GRVQMRTRRT</u>	<u>LRGHLAKIYA</u>	MHWATDSKLL	<u>VSASQDGKLI</u>	G β 3
95	<u>GQFVMKTRRT</u>	<u>LKGHGKLVLC</u>	MDWCKDKRRI	<u>VSSSQDGKVI</u>	G β 5L
49	<u>GQFVMKTRRT</u>	<u>LKGHGKLVLC</u>	MDWCKDKRRI	<u>VSSSQDGKVI</u>	G β 5
81	<u>IWDSYTTNKV</u>	<u>HAIPLRSSWV</u>	MTCAYAPSGN	<u>YVACGGLDNI</u>	transducin β
81	<u>VWDSYTTNKV</u>	<u>HAIPLRSSWV</u>	MTCAYAPSGN	<u>FVACGGLDNM</u>	G β 3
135	<u>VWDSFTTNKE</u>	<u>HAVTMPCTIWV</u>	MACAYAPSGC	<u>AIACGGLDNK</u>	G β 5L
89	<u>VWDSFTTNKV</u>	<u>RHCSQPRYRG</u>	FRIPAYLKVL	<u>WSSCPALS..</u>	G β 5
121	<u>CSIYNLKTRE</u>	<u>GNVRVSRELA</u>	GHTGYLSCCR	<u>FLDDNQIVTS</u>	transducin β
121	<u>CSIYNLKSRE</u>	<u>GNVKVSRELS</u>	AHTGYLSCCR	<u>FLDDNNIVTS</u>	G β 3
175	<u>CSVYPLTFDK</u>	<u>NENMAAKKKS</u>	VAMHTNYLSA	<u>CSFTNSDMQI</u>	G β 5L
.....	G β 5
161	SGDTT...CA	<u>LWDIETGQQT</u>	<u>TFIGHTGDV</u>	<u>MSLSLAPDTR</u>	transducin- β
161	SGDTT...CA	<u>LWDIETGQQK</u>	<u>TVFVGHGDC</u>	<u>MSLAVSPDFN</u>	G β 3
215	LTASGDGTCA	<u>LWDVESGQLL</u>	<u>QSFHGHGADV</u>	<u>LCLDLAPSET</u>	G β 5L
.....	G β 5
198	<u>LFVSGACDAS</u>	<u>AKL..WDVRE</u>	<u>GMC</u> RQTFIGH	<u>ESDINAICFF</u>	transducin β
198	<u>LFISGACDAS</u>	<u>AKL..WDVRE</u>	<u>GIC</u> RQTFIGH	<u>ESDINAICFF</u>	G β 3
255	<u>GNTFVSGGCD</u>	<u>KKAMVWDMRS</u>	<u>GQC</u> VQAFETH	<u>ESDINSVRY</u>	G β 5L
.....	G β 5
236	<u>PNGNAFATGS</u>	<u>DDATCR</u> LFDL	<u>RADQE</u> LMTYS	<u>HDNI</u> ICGITS	transducin β
236	<u>PNGEAICTGS</u>	<u>DDASCR</u> LFDL	<u>RADQE</u> LICFS	<u>HESI</u> ICGITS	G β 3
295	<u>PSGDAFASGS</u>	<u>DDATCR</u> LYDL	<u>RADRE</u> VAIYS	<u>KESI</u> IFGASS	G β 5L
.....	G β 5
276	<u>VFSKSGRLL</u>	<u>LAGYDD</u> FNCN	<u>VWDAL</u> KADRA	<u>GVL</u> AGHDNRV	transducin β
276	<u>VAFSLGRLL</u>	<u>FAGYDD</u> FNCN	<u>VWDSM</u> KSERV	<u>GILS</u> GHDNRV	G β 3
335	<u>VDFSLGRLL</u>	<u>FAGYND</u> YTIN	<u>VWDVL</u> KGSRV	<u>SILF</u> GHENRV	G β 5L
.....	G β 5
316	<u>SCLGVTDDGM</u>	<u>AVATGS</u> WDSF	<u>LKIWN</u>		transducin β
316	<u>SCLGVTADGM</u>	<u>AVATGS</u> WDSF	<u>LKIWN</u>		G β 3
385	<u>STLRVSPDGT</u>	<u>AFCSGS</u> WDHT	<u>LRVWA</u>		G β 5L
.....		G β 5

Figure 4.15. Alignment of transducin- β protein to other G β proteins

Multiple sequence alignment of human protein sequences of transducin- β , G β 3, G β 5 and G β 5L. Residues highlighted in red demonstrate identity; conserved WD repeats are shown in green. Transducin- β shares approximately 40 % of amino acid identity with other G β proteins (Alignment was performed by ClustalV). The peptides identified in this study in GST pull-down experiment are underlined in transducin- β sequence with the red line highlighting the peptide specific to transducin- β .

A SNP in the *GNB3* gene is associated with essential hypertension and obesity (Dong *et al.*, 2004). G β 5 is found predominantly in brain but its longer isoform, G β 5L, is expressed in the retina where it forms a complex with RGS9 taking part in phototransduction (described in section 1.2.3.3; He *et al.*, 2000). All G β proteins are structurally similar (figure 4.15), especially transducin- β and G β 3, but my data show that RP2 was unlikely to interact with G β 3, however this hypothesis needs to be investigated further by biochemical tests, such as IP. Construction of transducin- β fragments and testing them using IP and immunofluorescence would be useful to identify the binding site responsible for binding to RP2.

It was revealed that transducin- β was translocated from the cytoplasm to the plasma membrane upon RP2 co-expression. This effect was quantified and proved to be statistically significant. It was also reproduced using a biochemical method that demonstrated a shift in transducin- β co-fractionation into the membrane fraction.

It is known that transducin complex subunits shuttle rapidly between the plasma membrane and Golgi apparatus membranes (Chisari *et al.*, 2007). This process is vesicle-independent and can be inhibited by the palmitoylation and myristoylation inhibitor 2-bromopalmitate. Transducin- β has not been found to be myristoylated or palmitoylated and can translocate independently of transducin- α . Transducin- γ was suggested to mediate the translocation since it has been described to be prenylated but this modification cannot be blocked by 2-bromopalmitate treatment, therefore transport by transducin- γ does not seem to be a possible mechanism (Chisari *et al.*, 2007).

As described in sections 1.5.2-1.5.3, RP2 is myristoylated and palmitoylated and there are pathogenic mutations described in this motif which affect RP2 membrane localisation (Chapple *et al.*, 2002). The G β 5L-RGS9 complex is anchored to the photoreceptor disc membranes by R9AP protein, and its knock down in mice leads to a slow light response (Keresztes *et al.*, 2004). Therefore, RP2 may act in a similar way with transducin- β .

Thus, it is possible to suggest that RP2 is a protein which mediates transducin- β translocation to the plasma membrane and possibly into detergent resistant membranes (DRM). A test of whether there was a translocation of transducin- β into the detergent resistant membranes fraction in the presence of RP2 was attempted. However, the experiment was not successful due to transfected RP2 or transducin- β protein not being expressed at a high enough level to be detected. Thus, the hypothesis of RP2 dependent transducin- β translocation into DRM needs to be investigated further by optimising the sucrose gradient protocol, increasing the transfection efficiency and trying different antibodies.

The pathogenic mutation L253R in the C-terminus of RP2 caused significant decrease of the RP2-transducin- β interaction affinity by IP. It was revealed by immunocytochemistry that this mutation did not result in targeting of transducin- β to the plasma membrane. Transducin- β staining in such cells resembled the FLAG-transducin- β intracellular distribution in the absence of RP2, suggesting no interaction occurred. RP2 mutations located at the N-terminus did not demonstrate any significant effect on the interaction by both IP and ICH. Therefore, it is likely that the region for binding of transducin- β lies within the C-terminus of RP2, which is homologous to nucleoside diphosphate kinase (NDPK) (Kuhnel *et al.*, 2006). Interestingly, NDPK can interact with the transducin- $\beta\gamma$ complex and intermediately phosphorylate His266 in transducin- β (Cuello *et al.*, 2003) (figure 4.16). This promotes the formation of GTP on the transducin- α subunit and results in transducin- $\alpha\beta\gamma$ complex dissociation. This mechanism is proposed to be regulatory for the basal effector activity (Wieland, 2007).

RP2 does not share homology with NDK in the His122 catalytic residue therefore it is doubtful that this interaction results in an NDPK-like effect on the transducin complex. On the other hand, RP2 acts as a GAP for Arl3 (Veltel *et al.*, 2008a) and there is a possibility that the phosphate from the Arl3 catalysis by RP2, could be transferred to His 266 of transducin- β and thus, activates transducin complex. If transducin- β binds to the C-terminus of RP2, the N-terminus of RP2 could be free for binding to Arl3 and therefore, form a ternary complex.

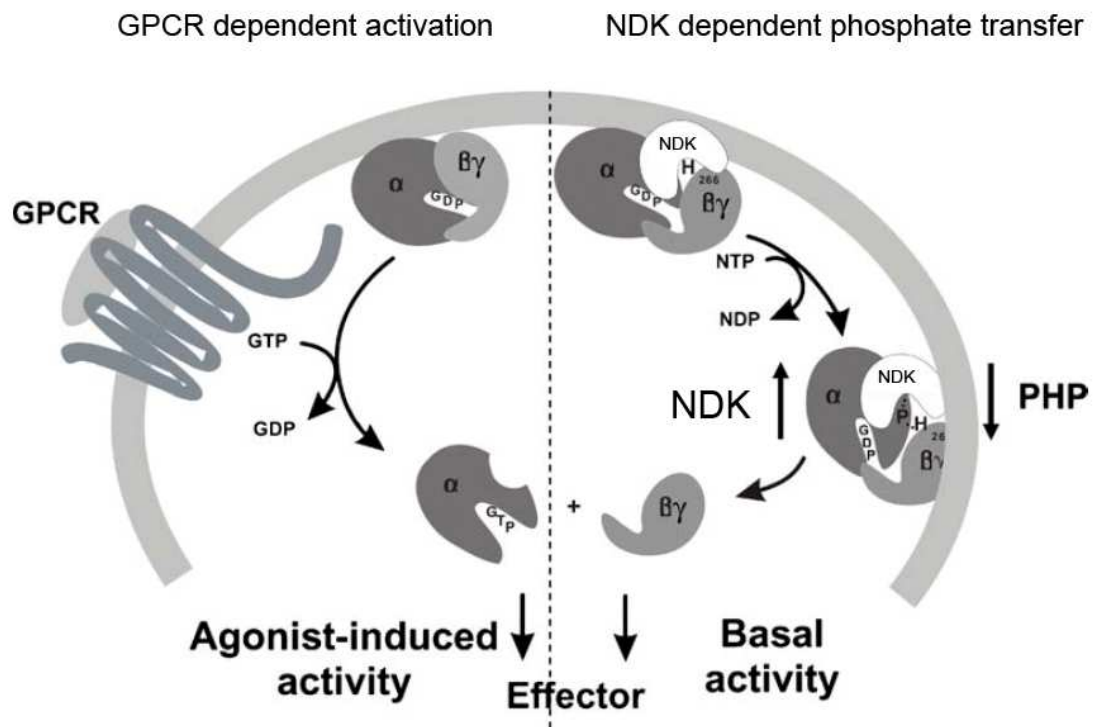


Figure 4.16. G protein coupled receptor dependent and alternative NDK dependent G protein activation

Schematic of two possible mechanisms modulating the G protein activation pathway are shown. Agonist binding to a G protein coupled receptor (GPCR) triggers GDP/GTP exchange on G α and release of G $\beta\gamma$, leading to effector responses (left side). When heterotrimeric G proteins complexes with NDK, a phosphotransfer onto His266 of G β promotes the formation of GTP, leading to GPCR-independent G protein activation and thus, regulation of basal effector activity (right side). Phosphohistidine phosphatase (PHP), which can specifically dephosphorylate G β , is a potential counter regulator of NDP dependent G protein activation (from Wieland, 2007).

This hypothesis is already supported by the data obtained in a GST pull-down assay with GST-Arl3 and the retinal lysate. On the other hand, the gene silencing of Arl3 did not change the overlap in co-localisation of RP2 with transducin- β , indicating that this protein may be unlikely to mediate the interaction or is not essential. However, siRNA techniques do not lead to an absolute knock-down, therefore there is still some protein produced. Possibly, even a small amount of Arl3 is sufficient to form a ternary complex.

On the other hand, data obtained in GTP-Arl3 overexpression experiments with RP2 and transducin- β suggest that Arl3 did not form a ternary complex but competed with RP2 for binding with transducin- β and caused it to re-localise to the cytoplasm. As no overlap was observed in intracellular localisation of RP2 with transducin- β upon GTP-Arl3 expression, there is a possibility that RP2 becomes bound to GTP-Arl3 and therefore is less available for the interaction with transducin- β . However, immunofluorescence studies are not sufficient to fully understand the role of Arl3 in the RP2/transducin- β interaction. Biochemical studies of transducin complex dissociation in the presence of RP2 with/without Arl3 are needed to test the effects of Arl3.

The role of the RP2 interaction with transducin- β in the retina still remains to be investigated. Functional studies, such as transducin complex dissociation by activated rhodopsin in the absence/presence of RP2, would potentially demonstrate whether RP2 affects phototransduction cascade activation. Studies on how activated transducin activates the PDE complex in the presence/absence of RP2 with or without Arl3, which is known to bind PDE δ (van Vekelenburgh *et al.*, 2001), would be another way of answering the question about RP2 involvement in transducin function.

Experiments to investigate the dynamics of these proteins in the retina could be performed. The hypothesis of light dependent translocation of transducin could be explored. It has been shown that transducin subunits translocate upon light exposure and this process is considered to be mediated by cilia proteins (Giesl *et al.*, 2006). Thus, RP2 and Arl3 might be the proteins that mediate such a translocation. This translocation has been suggested to be essential for the

retinal physiology (Slepek *et al.*, 2008) and therefore, disruption of this mechanism could cause retinal degeneration.

Chapter V. Prefoldin 5 as a candidate gene for retinal degeneration

5.1. Introduction

It has been reported that a homozygous point mutation (L110R) in *Pfdn5* in mice could lead to abnormal outer segment development and severe retinal degeneration (Lee *et al.*, 2005). Mice appeared to have thinner outer and inner segments. Rhodopsin and ROM-1 were mislocalised, indicating that their transport via the connecting cilium to the outer segment might be impaired. The phenotype was apparently not restricted to the retina as mice exhibited hydrocephaly, Purkinje cell degeneration and male infertility (Lee *et al.*, 2006). These findings suggest that mutant *Pfdn5* mice could have a syndromic type of retinal degeneration.

5.1.1. The human *PFDN5* gene

The human *PFDN5* gene maps to chromosome 12q12 spanning approximately 4 kb of genomic sequence and consists of at least 6 coding exons. *PFDN5* is alternatively transcribed with 5 reported isoforms (figure 5.1). The largest reported isoform of PFDN5 represents a fusion transcript containing a region of chromosome 14 at the 5' end (Hagio *et al.*, 2006) and probably represents a cloning artefact. Other isoforms, PFDN5 α , β , γ and δ , are derived from chromosome 12q12 (figure 5.1).

5.1.2. PFDN5 protein

The α isoform of PFDN5 (NP 002615) is a protein of 167 amino acids with a molecular weight (Mw) of approximately 17 kDa and pI 5.94. It has a common domain for other PFDN complex subunits structure of two coiled-coils connected by a linker region with five loops and four extended strands (figure 5.2). This protein has been shown to bind c-myc (Mori *et al.*, 1998), p73 (Watanabe *et al.*, 2002) and PFDN6 (Simons *et al.*, 2004).

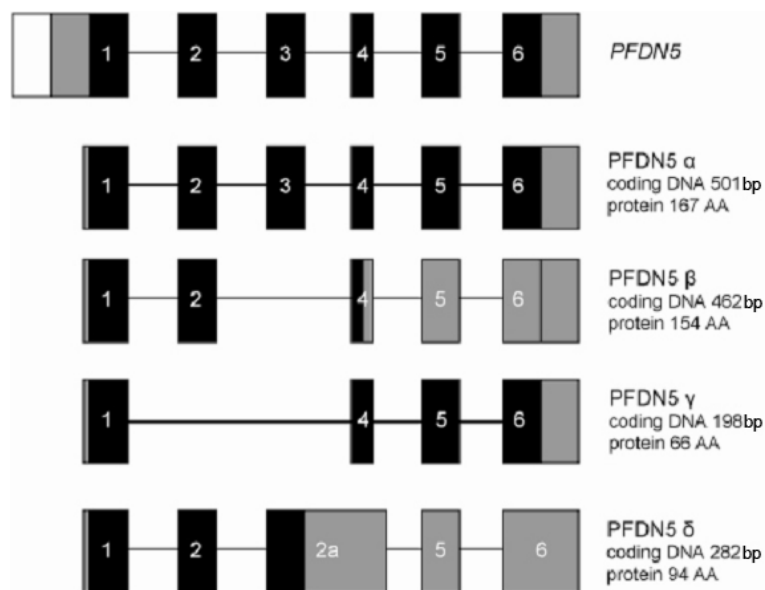


Figure 5.1. Organisation of human PFDN 5 isoforms

Schematic of the reported isoforms (PFDN5, PFDN5 α , β , γ and δ) is shown. Exons are represented as boxes with the coding regions as black. Untranslated regions are shown with grey boxes. The numbers on the boxes indicate the exon number. The length of the coding sequence and of the protein product is indicated (modified from Hagio *et al.*, 2006 and UCSC database as described in 2.6).

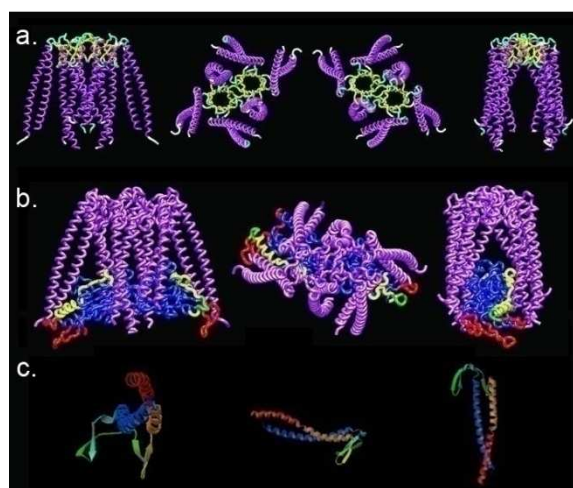


Figure 5.2. Proposed model of the PFDN complex structure

a. Three dimensional diagram of archeal PFDN (PDB: [1FXK](#)). **b.** Model of interaction of PFDN complex with denatured actin (Martin-Benito *et al.*, 2002). **c.** PFDN5 subunit structure (Siegert *et al.*, 2000).

5.1.3. PFDN5 as a part of a chaperone complex

Prefoldin (PFDN), alternatively called Gim complex (GimC), is a chaperone that works in conjunction with the cytosolic chaperonin (CCT) in assisting with the folding of actin and tubulin in archaea and eukaryotes (described in chapter 1.4.3.2). PFDN is composed of six different subunits, which are able to assemble spontaneously into a complex (figure 5.2) (Leroux *et al.*, 1999). The prefoldin 5 subunit (PFDN5), one of the most evolutionary conserved in the complex, has been shown to be essential for PFDN complex association. It was able to form intermediates with prefoldin 6 subunit and this sub-complex was shown to donate subunits for the PFDN assembly reaction. Moreover, it was demonstrated that the prefoldin complex with a truncated prefoldin 5 subunit failed to bind its target substrate tubulin and therefore was important for actin/tubulin PFDN folding function (Simons *et al.*, 2004).

It is known that the archeal prefoldin complex is able to replace the function of Hsp70 in archaea (reviewed in Macario and Conway di Macario, 2001). The mammalian prefoldin complex has been demonstrated to assist in not only the folding of actin and tubulin, but misfolded proteins, such as amyloid β . It was demonstrated that prefoldin was able to solubilise β -sheet-rich fibrils formed by amyloid β peptides into a soluble state (Sakono *et al.*, 2008). However, it has been suggested that such soluble misfolded peptides are more toxic for neurons (Klein *et al.*, 2001).

5.1.4. PFDN5 as a candidate gene for retinal degeneration.

There is evidence that subunits of prefoldin could be involved in cilia-related retina degeneration. Recently it was demonstrated that PFDN1 deficient mice develop severe abnormalities including ciliary dyskinesia, loss of neuron tracts in the brain, and defects in B and T cell development (Cao *et al.*, 2008).

Another PFDN complex subunit, PFDN3, is also known as von Hippel-Lindau binding protein 1 (VBP1), binds the tumor suppressor von Hippel-Lindau protein (pVHL) which mutated in the disease of the same name (OMIM [300133](#)) (Tsuchiya *et al.*, 1996). VHL is characterised by highly vascularised malignant

tumors in many organs and form renal clear-cell carcinomas (RCCs). pVHL is localised to the cilium, although not exclusively, and is thought to have multiple functions, such as polyubiquitination, regulation of hypoxia-inducible factors (HIF1a, HIF2a) and cell cycle control via cyclin D (reviewed in Shehata *et al.*, 2008). However, the most important role is now considered to be regulation of cilia formation in kidneys (Thoma *et al.*, 2007, Lolkema *et al.*, 2008). It was shown that RCCs in patients develop from renal cysts which are believed to be the most serious VHL manifestation (Kim *et al.*, 2005). Therefore, PFDN3 protein acts as a chaperone as a part of PFDN complex and also has another role via the interaction with pVHL.

Non folding roles for PFDN5, which may also be important for fundamental cell biology and retinal function, have also been suggested. PFDN5, also referred to as MM-1 (Myc Modulator-1), was isolated as a c-myc interacting protein in yeast two-hybrid screening (Mori *et al.*, 1998). C-myc is a transcription factor that plays pivotal roles in cell proliferation, differentiation and apoptosis regulation (Dang *et al.*, 2006). PFDN5 was shown to repress the E box-dependent transcription activity of c-myc by itself or by recruiting HDAC1 via TIF1, a co-repressor. This pathway targets another proto-oncogene c-fms (Satou *et al.*, 2001, 2004).

Further, it was revealed that PFDN5 could bind the p73 tumour suppressor protein and b-myc, an N-terminal homologue of c-myc (Watanabe *et al.*, 2002, Burton *et al.*, 2006). These data suggest that prefoldin 5 may function as a tumour suppressor protein. This hypothesis is supported by the genetic survey made by Fijioaka and colleagues (2001) suggesting that an A157R sequence change in PFDN5 was associated with leukaemia and lymphoma.

Tumourigenesis involves numerous pathways and one of them is wnt signalling which is now considered to be a potential therapeutic target for cancer (reviewed in Ewan *et al.*, 2008). Recently prefoldin 5 was shown to negatively regulate the wnt signalling pathway by inhibiting of the expression of the *wnt4* gene (Yoshida *et al.*, 2008). The wnt pathway is a network of proteins which is involved in a large variety of processes including retinal degeneration (Yi *et al.*, 2007). Wnt proteins are a family of secreted growth factors. The signal triggered

by these factors can be transmitted in two ways – the canonical or non-canonical pathways (figure 5.3).

The canonical epithelial pathway is also known as wnt/ β -catenin pathway (figure 5.3). In differentiated cells, β -catenin is associated with adherens junctions at the cell membrane. In the absence of wnt proteins β -catenin is complexed with axin, glycogen synthase kinase-3 β (GSK-3 β), and adenomatous polyposis coli (APC) (Liu *et al.*, 2002, Amit *et al.*, 2002). This large complex prevents accumulation of β -catenin in the cytoplasm through proteasomal degradation (Liu *et al.*, 2002). Wnt proteins bind to the receptor Frizzled (Bhanot *et al.*, 1996), which protects complex formation between β -catenin, GSK-3 β , axin and APC. The cytoplasmic non-phosphorylated β -catenin then translocates to the nucleus and acts as a transcription factor for several genes, such as c-myc, c-jun and cyclin D1 (reviewed in Sakanaka *et al.*, 2000). It was demonstrated that stabilisation of β -catenin causes onset of cancer and it was found to be the most common cause of colorectal cancer (Karim *et al.*, 2004).

The non-canonical wnt pathway (figure 5.3), or wnt/Ca²⁺, is important for dictating the plane of the epithelium to be perpendicular to the cells' apical–basal axis and the orientation of the mitotic spindle (Gong *et al.*, 2004). When wnt ligand binds its receptor, an early event involving a protein called dishevelled (Dsh) determines whether canonical or non-canonical wnt signalling is initiated.

Several studies have implicated cilia and ciliary proteins to be involved in this regulation (Corbit *et al.*, 2008, Mans *et al.*, 2008). For example inversin is expressed upon increase of intracellular Ca²⁺ caused by mechanosensation of cilia by fluid flow (Kishimoto *et al.*, 2008). Mutations in the gene encoding inversin are suggested to causes nephronophthisis (Simons *et al.*, 2005). A group of cilia-localised proteins, mutations in which have been shown to cause BBS, also involve the wnt signalling pathway.

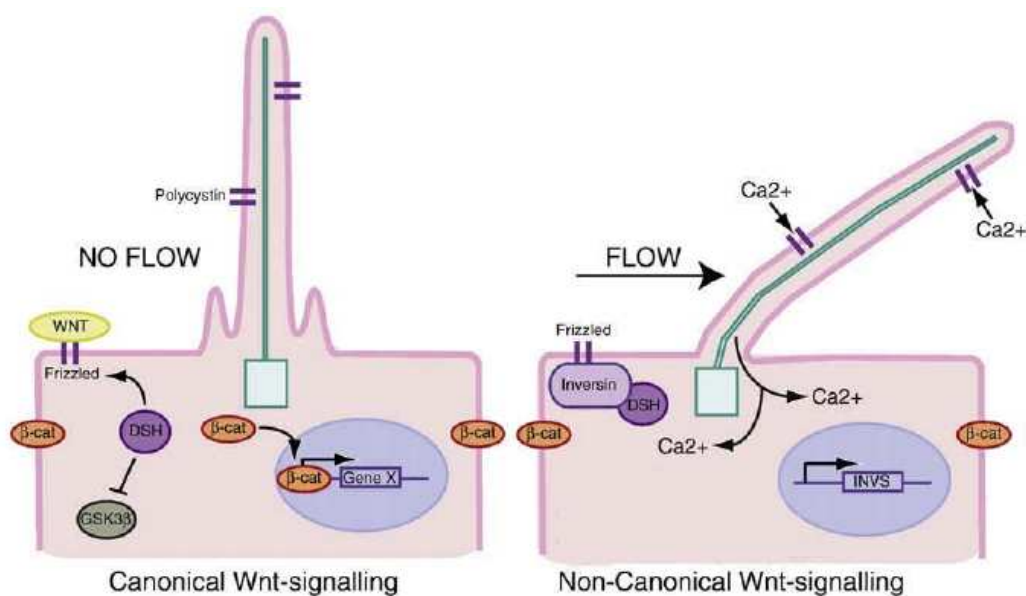


Figure 5.3. Schematic of the wnt signaling pathway in a ciliated cell

In the absence of flow (left panel), canonical wnt signalling can occur when the ligand binds the frizzled receptor, thereby recruiting dishevelled (DSH) and inactivating GSK3 β . β -catenin (β -cat) becomes subsequently stabilized and translocates to the nucleus where it acts as a transcriptional co-activator. Upon mechanosensation by fluid flow (right panel) the increased level of intracellular Ca²⁺ triggers expression of inversin that binds DSH. Thus, β -catenin is guided for degradation by axin, adenomatous polyposis coli (APC) and GSK3 β and therefore does not act as a transcription factor (Mans *et al.*, 2008).

Numerous studies in mouse mutants for BBS proteins 1, 4, and 6 display a strikingly similar array of developmental defects as mutants in the *wnt/Ca²⁺* signalling pathway. When BBS4 heterozygous healthy mice were crossed with the *wnt/Ca²⁺* signalling component van Gogh-like-2 (VANGL2) heterozygous mice, the heterozygous offspring for both genes displayed the same severe phenotype as homozygous *wnt/Ca²⁺* (Ross *et al.*, 2005). In another study using zebrafish, suppression of *bbs4* in *vangl2* mutant embryos similarly resulted in a phenotype typically caused by defective *wnt/Ca²⁺* signalling (Badano *et al.*, 2006). Together, these *in vivo* data strongly argue for a functional link between *wnt/Ca²⁺* signalling and ciliary function.

In the study of Yoshida and colleagues (2008) it was demonstrated that PFDN5 was able to down regulate the *wnt/β-catenin* pathway. Cells knocked down for expression of PFDN5 protein had increased expression levels of the *wnt4* gene, accumulation and translocation of β-catenin and upregulation of TCF/Lef-1, one of the target proteins of *wnt/β-catenin* pathway. It was shown that, together with the zinc-finger protein Egr-1, PFDN5 down-regulated the promoter activity of the *wnt4* gene.

Additionally it has been suggested that PFDN5 could be involved in the non-canonical pathway regulation. Henkel and colleagues (2001) have shown that the yeast homologue of PFDN5, Bob1, interacts with the MAP kinase kinase (MAPKK) Byr1 and regulates sexual differentiation in fission yeast. This kinase is one of the target genes for *wnt* signalling regulated by *wnt4* via the non-canonical pathway (Chang *et al.*, 2007b). Therefore it is feasible to suggest that PFDN5 may act as one of the proteins modulating the *wnt* signalling pathway via both canonical and non-canonical pathways.

Thus, PFDN5 is suggested to have multiple functions – on one hand it is an important transcription repressor of *c-myc* pathway, on the other hand PFDN5 plays an important role in cytoskeleton biogenesis as a part of the PFDN complex. At the same time PFDN5 is shown to regulate the *wnt* signalling pathway, which is involved in the pathogenesis of Bardet-Biedl syndrome. A mutation in *PFDN5* could potentially affect one of these pathways and result in syndromic or non-syndromic retinal degeneration.

A study into whether mutations in *PFDN5* cause retinal degeneration in human patients has not been reported to date, and therefore forms the basis of this chapter.

5.2. Results

5.2.1. Screening of patients with non-syndromic and syndromic forms of retinal degeneration

A panel of 96 DNA samples from patients with an early onset form of retinal degeneration (EORD) was obtained from Moorfield's Eye Hospital (provided by Prof. Anthony T. Moore). These unrelated patients were diagnosed with severe non-syndromic, early onset, retinal degeneration and were from different age groups. Most of the patients presented as children of 2-10 years age (39 %); two large groups were formed by patients of age from 10 to 20 years (27 %) and 20-40 years (26 %). The smallest age group screened was represented by DNA from people older than 40 years (8 %). All the patient samples had proved negative in a variety of previous LCA and RP disease gene mutation screens.

Another panel of 48 DNA samples from patients with a recessive syndromic form of retinitis pigmentosa was donated by Prof. Phillip L. Beales (Institute of Child Health, UCL). All these patients were diagnosed with Bardet-Biedl Syndrome (BBS, described in section 1.3.3.2) of unknown aetiology. The age range and sex was not known, however, all 48 patient samples were negative in reported BBS gene mutation screens.

In order to obtain PCR products of each *PFDN5* exon for subsequent DNA sequencing, specific primers were designed approximately 60 bp from the exon/intron boundaries (figure 5.4a). An aliquot of patient DNA (50 ng) was PCR amplified using exon specific primers (table 2.2) as described in section 2.1.1. Following amplification, each PCR product (5 µl) was electrophoresed on an agarose gel (as in 2.1.7). Examples are represented in figure 5.4b, which shows that all specific primer pairs resulted in the amplicons of the expected size. Each PCR product was purified and sequenced bidirectionally (section 2.5.1). The resulting ABI electrophoregrams were read using DNA sequence analysis tools as described in section 2.6. The presence of sequence changes was identified by comparison to the reference sequence of the *PFDN5* gene, obtained from UCSC database (section 2.6).

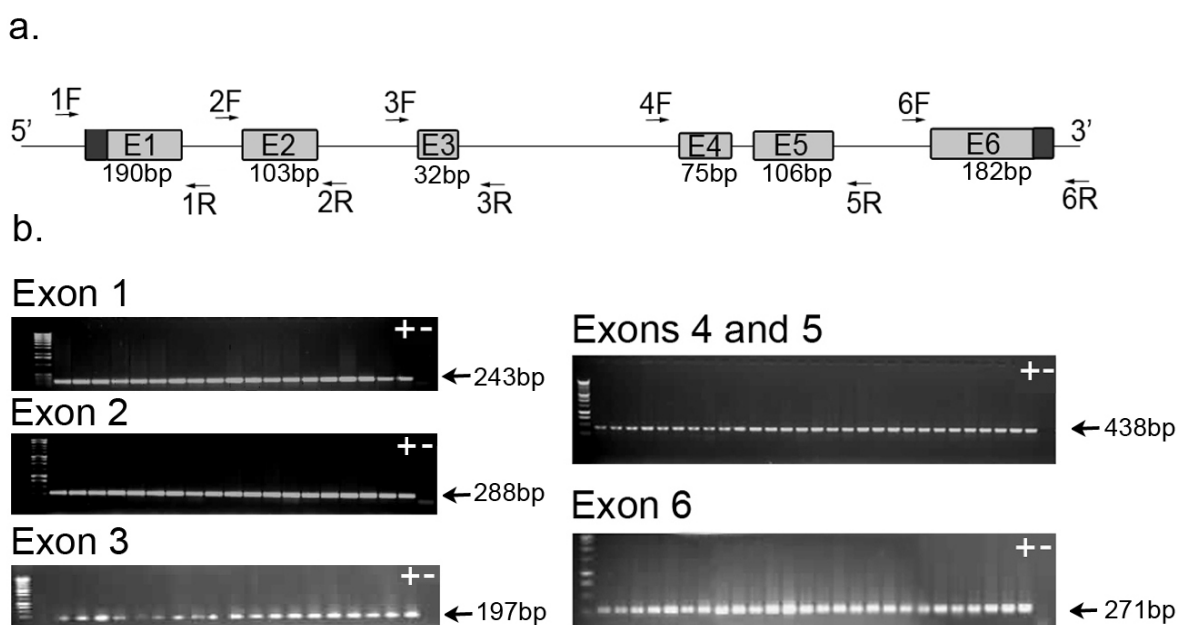


Figure 5.4. Primer design for *PFDN5* screening and examples of PCR products amplified from patient DNA samples

a. Exons are shown as grey boxes with E1 to E6 representing the exon number and untranslated regions as black boxes. The size of each exon is shown below exons. The position of intronic primers designed to amplify the gene are shown by arrows. **b.** Patient DNA amplification of *PFDN5* fragments as indicated. The first lane on each of the agarose gels is a 1 kb DNA size marker. “+” represents PCR products obtained with positive control DNA, “-” represents negative control PCR without DNA. The size of the amplicons for each *PFDN5* fragment is indicated with arrows.

Upon analysis of exon 1, the electropherogram of patient 30 DNA from the EORD panel showed the presence of two alleles in the 5' untranslated region 21 bp upstream of the start codon. The reference sequence and the control DNA sequence have a C at this position, whereas patient 30 DNA had a C allele and a T allele. This finding indicates that the patient is heterozygous (figure 5.5a).

Examining the data for exon 2, a sequence change was detected in intron 1 of patient 55 DNA of the EORD panel. The change was 27 bp upstream of the splice acceptor site of exon 2. The electropherogram of the control DNA and the reference sequence have a T allele but in patient 55 DNA this was a C. This finding suggests that this sequence change is present on both alleles and represents a homozygous sequence change. However, it is possible that this sequence change is present on one allele and the other allele could be deleted (figure 5.5 b). The SNP database was examined for the sequence changes identified in the EORD panel (NCBI, section 2.6) and these changes have not been previously annotated as SNPs.

All the other 94 DNA samples from the EORD panel and 48 from the BBS panel appeared to have no sequence changes in any of the fragments of the *PFDN5* gene screened.

5.2.2. PFDN5 protein purification

To initiate investigation of the biological properties of the PFDN5 protein a recombinant protein was produced. For this purpose the coding sequence of the PFDN5 α isoform (NM 002624) was amplified by PCR from an I.M.A.G.E. clone as described in section 2.1.1 and using primers from table 2.1.

The obtained PCR product was analysed by agarose gel electrophoresis which showed a single band of the expected size of approximately 470 bp (2.1.1). This amplicon was then subcloned into the *E. coli* expression vectors *pGEX-2T* and *pTrc-HisA* (2.1.7) to produce GST and His tag constructs as described in sections 2.1.2-2.1.5.

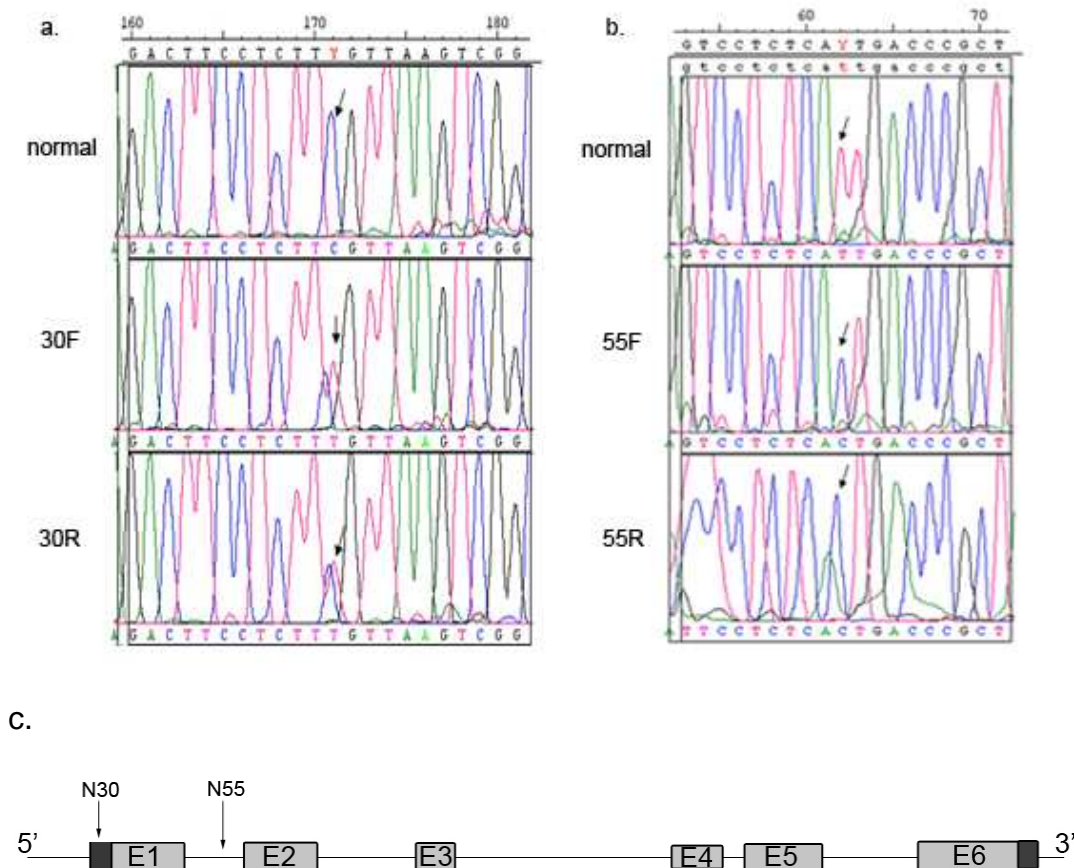


Figure 5.5. Sequence changes found in the *PFDN5* gene in patients with retinal degeneration

a. Heterozygous sequence change (C to T) in the 5' UTR of patient 30 DNA is shown on the electropherogram obtained using 1F forward (30F) or 1R reverse (30R) primers and is highlighted by an arrow. **b.** Homozygous sequence change (T to C) in intron 1 of patient 55 DNA is highlighted with an arrow on the electropherogram obtained using 2F forward or 2R reverse primers (55F and 55R respectively). **c.** Approximate position of the sequence changes identified in patient 30 DNA and patient 55 DNA in *PFDN5* gene. Exons are shown as grey boxes (E1-E6) and untranslated regions as black boxes.

The competent *E. coli* were then transformed with the plasmid DNA and induced with IPTG to activate the promotor (section 2.4.6-2.4.7). The PFDN5 protein expression level was analysed by SDS-PAGE with Coomassie stain (section 2.4.2. and 2.4.3) of total and soluble fractions of lysates of cells expressing either GST-PFDN5 or His-PFDN5. The expression of the protein was compared to the control lysates of non-transformed *E.coli* cells. The size of proteins was determined by comparison to a prestained protein ladder. The PFDN5 protein had a predicted molecular weight 17 kDa and therefore the expected molecular weight for PFDN5 with a His tag was approximately 20 kDa and for GST-fused protein approximately 43 kDa.

His-PFDN5 protein appeared in the total fraction but not in the soluble fraction and all attempts at purification failed (data not shown). GST-PFDN5 appeared to be present in the soluble fraction as well as in total. The procedure was optimised for expression level in One-Shot Top10® cells. The solubility of GST-PFDN5 was improved by incubating at 33°C for 5 hours after induction with IPTG rather than at 37°C (Figure 5.6a). Tag free PFDN5 was purified by on-column thrombin cleavage with subsequent passing through benzamidine-sepharose column to remove the thrombin as described in section 2.4.7 (figure 5.6b).

5.2.3. GST pull-down with mammalian cell lysates

To reveal whether PFDN5 could act independently of other PFDN complex subunits by binding substrates, or whether it could interact with other proteins which are known to be involved in cytoskeleton biogenesis, a GST pull-down assay was performed as described in section 2.4.9. GST tagged PFDN5 was expressed as described above in *E.coli*. Glutathione sepharose beads were then used to bind recombinant GST-PFDN5 from the bacterial lysate. The purified protein was left on the column and used for incubation and pull-down of interacting proteins from mammalian cell lysates.

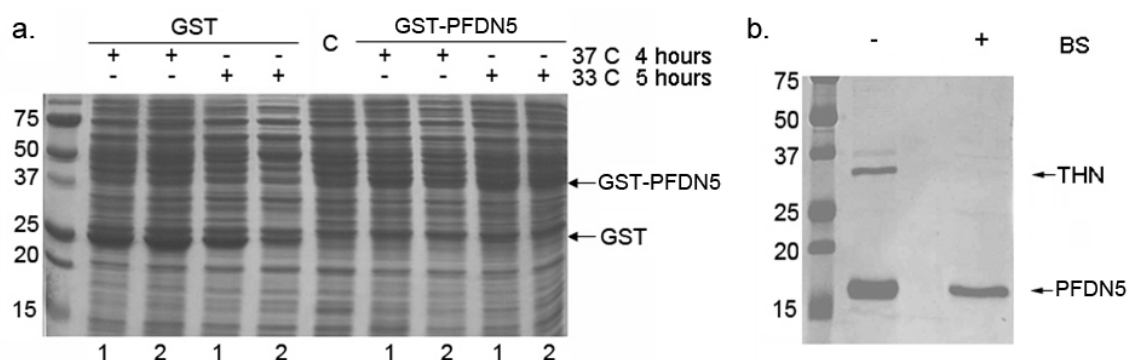


Figure 5.6. PF DN5 protein purification

a. Coomassie stained SDS-PAGE gel showing *E.coli* cell lysate soluble fractions transformed with two different clones (1 and 2) for pGEX2T alone and pGEX2T-PF DN5 incubated at different times and temperatures after IPTG induction as indicated. The position of the expected mobility of GST and GST-PF DN5 are highlighted with arrows. Molecular weight markers are on the left with Mr in kDa as indicated. **b.** Coomassie stained SDS-PAGE gel of purified PF DN5 (predicted Mr 17 kDa) after on-column cleavage with thrombin (THN, predicted Mr 35 kDa). The first lane shows GST-free PF DN5 and thrombin in the eluate after overnight thrombin cleavage. The second lane represents purified PF DN5 (GST free and thrombin free) after passing through benzamide-sepharose (BS). Molecular weight markers are on the left with Mr in kDa as indicated.

Two cell lines, HeLa and SK-N-SH (treated as described in section 2.3.1) were used for extraction of soluble protein using 0.1 % Triton X100 in PBS (table 2.8). The lysates were then incubated with GST- or GST-PFDN5 beads. The bound proteins were eluted and analysed by Western blotting as shown in figure 5.7 (described in sections 2.4.2 and 2.4.5). GST- bound resin, incubated with the same lysates, was used as a control for non-specific binding. Analysis with anti β -tubulin antibody showed specific bands of the 50 kDa expected size only in the lanes where GST-PFDN5 was incubated with the lysates and in the lane with a HeLa lysate control, but not in any other lanes (figure 5.7). Western blotting of this GST pull-down for other proteins, such as Arl3 or RP2, did not show any specific binding (data not shown).

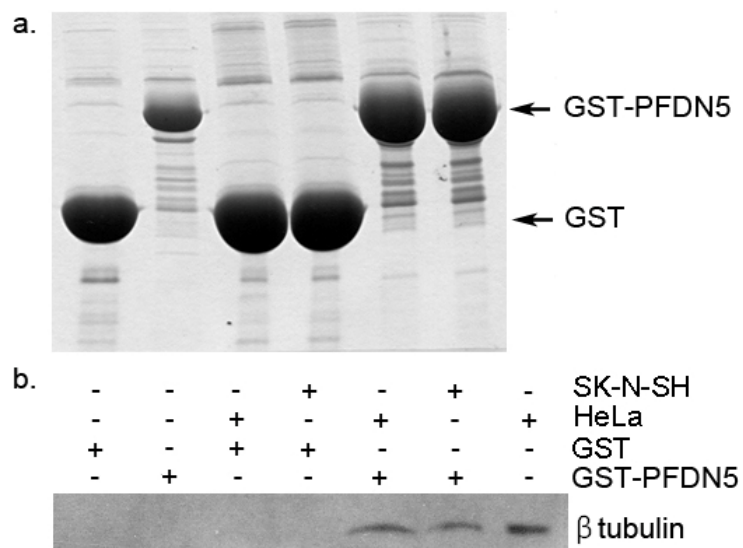


Figure 5.7. Binding of β -tubulin by GST-PFDN5 in an affinity pull-down assay.

a. Coomassie stained gel of a GST pull-down assay with extracts of SK-N-SH and HeLa cells. The position of expected mobility of GST and GST-PFDN5 is indicated with arrows. **b.** Western blot of the samples from the same experiment immunostained for beta-tubulin is shown. The last lane shows 25 μ g/ml of HeLa total lysate input.

5.2.4. PFDN5 in CytoTrap®

The tubulin folding pathway is facilitated by a variety of chaperones including PFDN and tubulin folding cofactors (section 1.4.4). The yeast two-hybrid approach, CytoTrap®, described in chapter 3.1.1, was chosen as an *in vivo* system for studying potential interactions of PFDN5. This experiment was performed with the aim of determining whether PFDN5 could interact with other proteins taking part in tubulin biogenesis such as RP2, Arl3, Arl2 or Arl6.

For this purpose PFDN5 α coding sequence was amplified from an I.M.A.G.E. clone with specific primers (table 2.1) resulting in an amplicon of the expected size of 470 bp. This PCR product was then cloned into pSos and pMyr vectors following the protocols described in 2.1.2-2.1.8. Cdc25-H yeast cells were cultivated as described in 2.2.1 and then transformed (2.2.2). Yeast growth was tested at two temperatures – the permissive temperature (24 °C) and the restrictive temperature (37 °C) on the appropriate selective media (described in 2.2). Growth at the restrictive temperature (37°C) indicated a protein-protein interaction had occurred. If growth was not observed after 168 hours of incubation at 37°C on the selective media, the proteins were considered not to interact. Examples of positive and negative growth are shown in figure 5.8.

Yeast transformed with PFDN5 in pSos and the positive control (pMyr SB) exhibited quick growth and formed colonies after only 96 hours of incubation under restrictive conditions. This control was interpreted as a high affinity binding interaction and that hSos-PFDN5 was expressed and the hSos moiety was functional. The negative control, pMyr LaminC, upon co-transformation with pSosPFDN5 did not result in yeast growth at 37 °C for 240 hours of incubation on the selective media. These data demonstrate that hSos-PFDN5 did not transactivate the system. For the protein interaction assay of PFDN5 with other proteins of interest, yeast cells were co-transformed with pSos-PFDN5 and the candidate interacting proteins in pMyr vector: Arl3, Arl2, Arl6 and RP2 (sections 2.2, 2.1.8). The experiment showed that no growth at the restrictive temperature was observed and therefore no interaction occurred. The results of this analysis are represented in table 5.1.

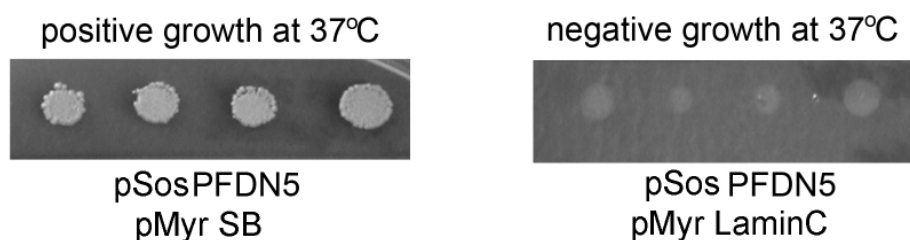


Figure 5.8. PFDN5 in the CytoTrap® system

Illustration of positive and negative yeast growth of four different colonies from each transformation after 144 hours of incubation on galactose –UL selective media. The yeast were transformed with pSos-PFDN5 and pMyr Sos binding protein (SB) for a positive control, or pMyr Lamin C for a negative control.

pSOS	pMyr	24°C (72h)	37°C (168h)
Sos	Myr	+++	-
Sos	PFDN5	+++	-
RP2	Myr	+++	-
RP2	PFDN5	+++	-
PFDN5	Myr	+++	-
PFDN5	Arl3	+++	-
PFDN5	Arl2	+++	-
PFDN5	RP2	+++	-
PFDN5	SB	+++	+++
PFN5	Arl6	+++	-

Table 5.1. Summary of PFDN5 CytoTrap® results

Growth was examined after incubation at 24°C on glucose –UL selective media and galactose –UL selective media. Positive growth is labelled “+++” when yeast formed saturated colonies. Negative growth is indicated by “-” in case no colonies were observed after 168 hours of incubation. The absence of growth suggests that no interaction occurred in this system.

5.3. Discussion

It was demonstrated in this chapter that sequence changes in the *PFDN5* gene were not associated with severe early onset retinal degeneration or Bardet-Biedl syndrome. However, a mouse model with a homozygous point mutation in *Pfdn5* was described with a syndromic form of retinal degeneration (Lee *et al.*, ARVO 2005), these data have never been published so it is difficult to discuss them in detail.

However studies in mice deficient in another subunit of the PFDN complex, PFDN1, exhibited a syndrome with ciliary dyskinesia and thus, support possible involvement of PFDN in retinal degeneration (Cao *et al.*, 2008). The mice developed hydrocephaly and respiratory mucus accumulation. Unlike PFDN5, the PFDN1 subunit has not been found to be crucial for the binding of the PFDN complex with tubulin (Simons *et al.*, 2004).

PFDN5 mutations would be predicted to affect cilia more severely than PFDN1. Our study demonstrated for the first time that PFDN5 was able to bind beta tubulin, a substrate for the whole PFDN complex, independently from other PFDN complex subunits. These data are supported by the previous finding that the PFDN complex with truncated PFDN5 failed to bind tubulin (Simons *et al.*, 2004). These new data indicate the importance of the PFDN5 subunit function of the PFDN complex. It is also possible that null-mutations in such an important subunit would be lethal and this could be one of the reasons why a mutation of this kind was not identified in this study.

On the other hand, it has been previously reported that a sequence change in exon 6 (A157R) was associated with cancer in humans. *PFDN5* was screened in 57 cultured cancer cells and 90 tissues from cancer patients. This sequence change was present in about 50–60 % of leukemia/lymphoma cells and in more than 75 % of squamous cell carcinomas of the tongue (Fujioka *et al.*, 2001). This sequence change was not found during our screening of 144 patients suggesting that it is more likely to be a mutation rather than a polymorphism. The A157R mutation abrogated the function of PFDN5 towards *c-myc* *in vitro*, proposing that it could be a tumor suppressor protein. The involvement of

PFDN5 in anti-oncogenic pathways has been shown previously (described in 5.1.4) (Mori *et al.*, 1998). PFDN5 is able to regulate several proto-oncogenes, such as c-myc, b-myc and c-fms directly, or via the wnt pathway. Thus, there is a possibility that amino acid substitution mutations in the C-terminus decrease the ability of PFDN5 to down regulate c-myc.

The DNA sequence changes found in patients with EORD were located in regions which are not predicted to directly affect the protein sequence. On the other hand, in our study, only *PFDN5* exons and short regions of introns within 60 bp from the acceptor/donor splice sites were screened. Therefore there is a possibility that large deletions or insertions within intronic regions could cause disease and would not be identified by this method. Intronic deletions/insertions have been shown to affect protein synthesis e.g. in the Parkinson's disease causing gene *NURR1* and in *SCN5A* that mutations result in Brugada syndrome (Hong *et al.*, 2005; Nickols *et al.*, 2004). However, such mutations are usually located around splice sites like those described for *LCA5* and *TULP1* (Ramprasad *et al.*, 2008; Abbasi *et al.*, 2008). Promoter region mutations can affect the binding to RNA polymerase II or numerous regulatory co-factors (Spek *et al.*, 1995), and this region was not screened in our study either. Thus, these potential ways of affecting of the protein synthesis of PFDN5 could be investigated further by screening of promoter regions and all PFDN5 introns.

The sequence changes found during the screening of *PFDN5* in this study have not been described in the SNP database and therefore are likely to be mutations. There is a possibility that a homozyous sequence change at a position 27 bp upstream from the splice site of exon 2 in DNA 55 in EORD panel could affect the protein synthesis if there was a potential cryptic splice site. However, sequence analysis does not support this hypothesis.

Another possibility is that this sequence change could disrupt a potential interaction with DNA binding proteins, which could potentially modulate *PFDN5* splicing. In order to prove this hypothesis, the protein expression analysis of PFDN5 in blood samples from patient 55 could be used. To perform such a study it is essential to make an antibody to PFDN5, which is possible since a

tag free protein has been successfully purified and is ready for an animal immunisation procedure.

Investigation of PFDN5 interactions with other proteins important for cytoskeleton biogenesis did not reveal any binding in CytoTrap®. This assay has proved useful for RP2 screening for novel interacting partners. Proteins tested for interaction with PFDN5 in CytoTrap® were not checked for expression level, therefore it is possible that this method was not optimal. To investigate interactions further, a GST pull-down could be used since this affinity assay was efficient for identifying the binding of β -tubulin by PFDN5.

Recently, an additional exon 2a was reported and this was not screened in this study since the reported mouse *Pfdn5* mutation was in exon 4 which is absent in the PFDN5 δ isoform that contains exon 2a (figure 5.1) (Hagio *et al.*, 2006). However, there is a possibility that this isoform is important for the retina and thus, alterations in this exon would be crucial. Therefore a study into which isoform of PFDN5 is expressed in the retina using RT-PCR and isoform specific antibody would be informative. Thus, the importance of PFDN5 for the retina is yet to be revealed.

Chapter VI. Discussion and future work

Inherited retinal dystrophies represent a major cause of blindness of which retinitis pigmentosa is the most prevalent. Retinitis pigmentosa is both clinically and genetically heterogeneous and the pathogenesis has yet to be clearly defined. The ultimate goal of studies into the disease associated genes is the possibility of developing new and effective therapies. However, before that may be achieved, the function of the causative gene and its role in the retina needs to be established.

RP2 is a protein with a ubiquitous expression pattern and the reason why its mutations cause retinal degeneration is unknown (Schwann *et al.*, 1998). RP2 has been suggested to localise in the cilium (described in 1.5.3), a ubiquitous structure which dysfunction is known to cause mainly syndromic forms retinal degeneration (reviewed in Klysik, 2008). RP2 is suggested to be partially localised to the cilia (described in section 1.5.3). However RP2 mutations have not been shown to cause a cilia related disorder suggesting redundancy of RP2 function in the cilium. Moreover, the RP2 plasma membrane localisation through dual acylation has been shown to be important for the disease pathogenesis (Chapple *et al.*, 2000; Chapple *et al.*, 2002; Grayson *et al.*, 2002).

The possible clues to RP2 function may be in its interactions with other proteins. At the start of this study, RP2 was believed to have only one interacting partner, the ubiquitous cilia and microtubule localised ADP ribosylation factor-like Arl3 (sections 1.6 and 1.7). Recent studies revealed several other potential interacting partners, suggesting the involvement of RP2 intracellular transport mechanisms and cell cycle regulation. All of them are ubiquitous proteins and bind to the C-terminus of RP2, presumably competing with each other (Evans, 2007).

In this study two proteins taking part in the phototransduction cascade, rod arrestin and transducin- β , have been identified to bind to RP2. These two novel interacting partners, for the first time, provided a direct link between RP2 and retinal physiology. Moreover, mutations in rod arrestin are known to cause autosomal recessive retinitis pigmentosa (arRP) and Oguchi disease

(Nakazawa *et al.*, 1998), suggesting the similarity of pathogenic pathways with XLRP. Pathogenic RP2 mutations were demonstrated to disrupt both identified interactions, supporting their potential importance for XLRP pathogenesis.

The role of these new interactions remains to be elucidated. Importantly, functional studies need to be performed to test whether RP2 is directly involved in phototransduction cascade regulation. Thus, a variety of experiments including studies of transducin complex dissociation by activated rhodopsin and PDE complex activation in the presence of RP2 would improve our understanding of the role of RP2 interactions with transducin- β . Tests of the ability of rod arrestin to quench activated phosphorylated rhodopsin in the presence of RP2 could be performed to investigate the consequences of RP2-rod arrestin interaction for the phototransduction cascade. The effect of pathogenic mutants of RP2 in such studies could be also explored.

Another hypothesis that could be investigated is the involvement in the phenomenon of light-dependent translocation that has been described for both rod arrestin and transducin (described in section 1.2.3.6). Light dependent translocation mechanism for another protein, recoverin, has been proposed to be connected with a calcium-myristoyl switch mechanism (Tanaka *et al.*, 1995; Strissel *et al.*, 2005), but the mechanism of translocation for rod arrestin and transducin remains to be elucidated. RP2 may be one of the proteins that mediate such translocation (figure 6.1).

It is unknown if RP2 itself is able to translocate between photoreceptor segments upon light exposure. This could be tested by staining of sections of the dark and light adapted retina with anti-RP2 antibody. It is possible to predict that this movement would be similar to the one described for recoverin from OS to IS upon light exposure due to their similarity in posttranslational modification. Therefore the hypothesis of calcium-myristoyl switch mechanism should be explored as RP2 was suggested to bind calcium in a calcium mobility shift assay. It is not clear which residues of RP2 are potentially responsible for calcium binding, whether it is the region in the N-terminus following the myristoylation motif or it is the C-terminal residues that resemble an EF-hand.

In order to develop this hypothesis studies into the calcium binding ability of RP2 and its role in RP2 function could be explored. This question is especially important for the retinal specific function of RP2 due to the drop in calcium concentration upon phototransduction cascade activation. Calcium concentration in the retina is known to regulate a variety of processes (section 1.2.3.3). For example, other calcium binding proteins, centrin, recently have been suggested to be gatekeepers of transducin translocation (Wolfrum *et al.*, 2002; Giessl *et al.*, 2006). Centrin isoforms are differently localised at the basal body and in the cilium. When activated by calcium, centrin isoforms were demonstrated to bind transducin $\beta\gamma$, suggesting that the complex may regulate the transducin movement through the connecting cilium (Giessl *et al.*, 2006).

Another possible role of RP2 interaction with rod arrestin and transducin- β is their targeting to the membranes. This was demonstrated in this study, that in vitro RP2 localised transducin β to the plasma membrane. It is known that the transducin β subunit, as other β subunits of the G protein family of heterotrimeric proteins, does not undergo posttranslational modifications which would target it to the membrane. It is proposed that it is brought there by the prenylated γ subunit (McGudden *et al.*, 2005). However, recent data argue against this hypothesis showing that a block of palmitoylation and myristoylation but not prenylation inhibited transducin- β membrane localisation (Saini *et al.*, 2007). This report suggested that transducin- β has a palmitoylated and myristoylated adaptor that tethers it to the membrane. RP2 is known to have a dual acylation motif (Chapple *et al.*, 2000) and thus, such a role for RP2 seems possible (figure 6.1).

The consequence of RP2 interaction with rod arrestin and transducin β remains to be revealed. As proposed in this study, RP2 may bind to rod arrestin when it is a monomer but not a tetramer (Hanson *et al.*, 2008). Therefore, elucidation of the effect of RP2 binding to rod arrestin could be investigated using mutants, which would support rod arrestin binding to a monomer state. It is important to confirm the hypothesis of the interaction of RP2 with the rod arrestin monomer as it is an active form quenching activated rhodopsin whereas the tetramer is considered to be a storage form (Hanson *et al.*, 2007; Hanson *et al.*, 2008).

Interestingly, both transducin and isoform 44 of rod arrestin are found in detergent resistant membranes (DRM) of photoreceptors upon light illumination and RP2 has been shown to localise to DRM in cells (Nair *et al.*, 2002; Chapple *et al.*, 2003). Therefore, the experiments that would show whether RP2 is present in DRM of the photoreceptors in the dark adapted or light adapted retina could be performed. In this aspect it is also important to test if RP2 binds to the p44 isoform of rod arrestin and whether this interaction is essential for p44 localisation in DRM.

Another putative interacting partner of RP2, retina specific protein Unc119, was identified in this study using yeast two-hybrid screening with a retinal library. This finding complements the recent report of Veltel and colleagues (2008b) showing that RP2 is able to form a ternary complex with Unc119 via Arl3. Thus, the weak interaction observed in yeast two-hybrid may suggest that the system is able to detect even ternary complexes via endogenous yeast proteins.

Another interacting partner that would put RP2 in a pathway with other retinal dystrophies is nucleolin (NCL). NCL is known to bind the lebercilin protein (LCA5) which is localised to the connecting cilium and which failure causes Leber Congenital Amaurosis (LCA, described in section 1.3.6) (den Hollander *et al.*, 2007). NCL is also reported to be involved in the pathogenesis of retinal dystrophies caused by mutations in RPGR via the interaction of the cilia localised RPGR interacting protein (via RPGRIP1) with nucleophosmin (NPM) (Shu *et al.*, 2005). Both NCL and NPM interact with each other and are multifunctional chaperones that shuttle between the nucleoli and the cytoplasm and have been associated with centrosomal division (Ugrinova *et al.*, 2007; Cha *et al.*, 2004). Thus, cilia localised RP2, LCA5 and RPGR are put in one pathway not only by their localisation but by shared interacting partners. The physiological significance of NCL and NPM interaction for retinal dystrophies is unknown (figure 6.1).

The interaction of RP2 with NCL can be hypothesised to be transient during cell cycle progression while NPM and NCL shuttle between the nucleus and the cytoplasm. It has been proposed that such nuclear proteins are released by importin in the presence of centrosomal RAN-GTP (Cha *et al.*, 2004).

Moreover, RPGR is known to have RCC1 domain in its structure highly homologous to RCC1 protein, a GEF for RAN. Thus, there is a possibility that the interactions of RP2 with NCL and RPGR with NPM are a consequence of relationships with RAN.

Other ubiquitous interacting partners of RP2 were identified using the yeast two-hybrid approach. Among them were chaperones, a part of the substrate binding domain of Hsc70 and a subunit of cytosolic chaperonin, CCT6. These two interactors were identified during the screening with the N-terminal fragment of RP2 and at first sight this data suggested that the fragment used for the screening was at least partly misfolded. This hypothesis was supported by results obtained during characterisation of interaction with CCT6, which demonstrated binding of this chaperone subunit only to the fragment of RP2 and its mutants. However, the interaction with Hsc70 was disrupted with pathogenic mutations in RP2, suggesting that this interaction, unlike the one with CCT6, may be functional. Moreover, recently the interacting partner of RP2, Arl3, was identified as one of the proteins of the Hsp90 interactome, providing another link between RP2 and chaperone machinery (McClellan *et al.*, 2007).

The role of the RP2 interaction with Hsc70 is to be elucidated. Hsc70 is a multifunctional protein and involved in a variety of cellular pathways (described in 1.4.1.1). One of them is the degradation by the proteasome and this function requires the assistance of co-chaperones such as CHIP. This study suggests that RP2 could be involved in 26S proteasomal degradation pathway due to one of the identified RP2 interacting partners being a non ATPase subunit 4 of 26S proteasome, PSMD4. Thus, the hypothesis that RP2 may act as a co-chaperone of Hsc70 in protein degradation machinery could be explored.

A study into whether mutation in another putative chaperone, subunit 5 of prefoldin complex (PFDN5), could cause retinal degeneration was performed. The trigger for this project was a conference report of Lee and colleagues (2005) about a novel retinal dystrophy causing gene in mice, *Pfdn5*. However, upon screening of two panels of patients with syndromic and non-syndromic retinal degeneration no mutations were identified in this gene. There could be

several reasons for the absence of mutations. It has been three years since a point mutation in gene was first reported, however these data have not been published, arising a question whether data of Lee and colleagues (2005) was correct.

There is another possibility that mutations in PFDN5 could be lethal in humans and therefore is not possible to identify in patients. This hypothesis is supported by the finding of this study demonstrating that PFDN5 protein is able to bind tubulin, a substrate of PFDN complex, independently on other complex subunits. Thus, PFDN5 subunit is proposed to be essential for the complex function and therefore correct cytoskeleton elements folding (described in section 1.4.4).

Thus, the aims of this study have been achieved. At least two retina specific putative interacting partners of RP2 protein have been identified; however the role of these interactions still remains to be elucidated. Other interactors of RP2 were also identified suggesting its involvement in other cellular processes such as 26S proteasomal degradation and nuclear transport pathway (figure 6.1). Therefore, this study suggested future ways of exploring of RP2 function in the retinal physiology.

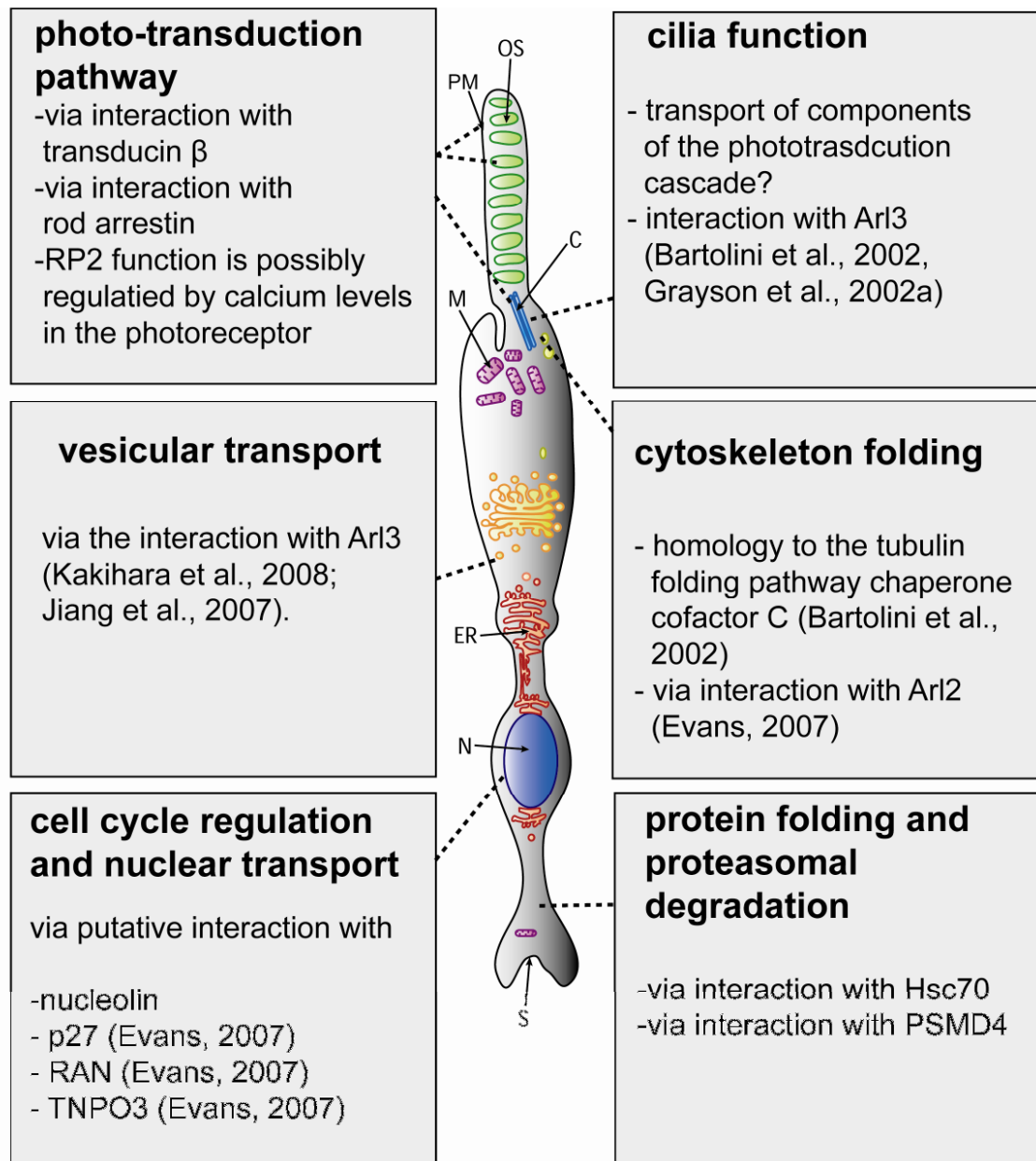


Figure 6.1. A schematic of potential pathways where RP2 may function

S – synapse, N – nucleus, ER – endoplasmic reticulum, M – mitochondrion, C – cilium, OS – outer segment, PM – plasma membrane.

References

Abbasi,A.H., Garzozzi,H.J., and Ben Yosef,T. (2008). A novel splice-site mutation of TULP1 underlies severe early-onset retinitis pigmentosa in a consanguineous Israeli Muslim Arab family. *Mol. Vis.* 14, 675-682.

Aleman,T.S., Cideciyan,A.V., Volpe,N.J., Stevanin,G., Brice,A., and Jacobson,S.G. (2002). Spinocerebellar ataxia type 7 (SCA7) shows a cone-rod dystrophy phenotype. *Exp. Eye Res.* 74, 737-745.

Ames,J.B., Ishima,R., Tanaka,T., Gordon,J.I., Stryer,L., and Ikura,M. (1997). Molecular mechanics of calcium-myristoyl switches. *Nature* 389, 198-202.

Amit,S., Hatzubai,A., Birman,Y., Andersen,J.S., Ben Shushan,E., Mann,M., Ben Neriah,Y., and Alkalay,I. (2002). Axin-mediated CKI phosphorylation of beta-catenin at Ser 45: a molecular switch for the Wnt pathway. *Genes Dev.* 16, 1066-1076.

Amor,J.C., Horton,J.R., Zhu,X., Wang,Y., Sullards,C., Ringe,D., Cheng,X., and Kahn,R.A. (2001). Structures of yeast ARF2 and ARL1: distinct roles for the N terminus in the structure and function of ARF family GTPases. *J. Biol. Chem.* 276, 42477-42484.

Anderson,D.H., Fisher,S.K., and Steinberg,R.H. (1978). Mammalian cones: disc shedding, phagocytosis, and renewal. *Invest Ophthalmol. Vis. Sci.* 17, 117-133.

Anfinsen,C.B. (1973). Principles that govern the folding of protein chains. *Science* 181, 223-230.

Ansley,S.J., Badano,J.L., Blacque,O.E., Hill,J., Hoskins,B.E., Leitch,C.C., Kim,J.C., Ross,A.J., Eichers,E.R., Teslovich,T.M., Mah,A.K., Johnsen,R.C., Cavender,J.C., Lewis,R.A., Leroux,M.R., Beales,P.L., and Katsanis,N. (2003). Basal body dysfunction is a likely cause of pleiotropic Bardet-Biedl syndrome. *Nature* 425, 628-633.

Antoshechkin,I. and Han,M. (2002). The *C. elegans* *evl-20* gene is a homolog of the small GTPase ARL2 and regulates cytoskeleton dynamics during cytokinesis and morphogenesis. *Dev. Cell* 2, 579-591.

Arnold-Schild,D., Hanau,D., Spehner,D., Schmid,C., Rammensee,H.G., de la,S.H., and Schild,H. (1999). Cutting edge: receptor-mediated endocytosis of heat shock proteins by professional antigen-presenting cells. *J. Immunol.* 162, 3757-3760.

Aronheim,A., Engelberg,D., Li,N., al Alawi,N., Schlessinger,J., and Karin,M. (1994). Membrane targeting of the nucleotide exchange factor Sos is sufficient for activating the Ras signaling pathway. *Cell* 78, 949-961.

Arshavsky,V.Y. and Bownds,M.D. (1992). Regulation of deactivation of photoreceptor G protein by its target enzyme and cGMP. *Nature* 357, 416-417.

Arshavsky,V.Y. and Pugh,E.N., Jr. (1998). Lifetime regulation of G protein-effector complex: emerging importance of RGS proteins. *Neuron* 20, 11-14.

Arshavsky,V.Y., Lamb,T.D., and Pugh,E.N., Jr. (2002). G proteins and phototransduction. *Annu. Rev. Physiol* 64, 153-187.

Arts,H.H., Doherty,D., van Beersum,S.E., Parisi,M.A., Letteboer,S.J., Gordon,N.T., Peters,T.A., Marker,T., Voesenek,K., Kartono,A., Ozyurek,H., Farin,F.M., Kroes,H.Y., Wolfrum,U., Brunner,H.G., Cremers,F.P., Glass,I.A., Knoers,N.V., and Roepman,R. (2007). Mutations in the gene encoding the basal body protein RPGRIP1L, a nephrocystin-4 interactor, cause Joubert syndrome. *Nat. Genet.* 39, 882-888.

Asea,A. (2008). Hsp70: a chaperokine. *Novartis. Found. Symp.* 291, 173-179.

Asea,A., Rehli,M., Kabingu,E., Boch,J.A., Bare,O., Auron,P.E., Stevenson,M.A., and Calderwood,S.K. (2002). Novel signal transduction pathway utilized by extracellular HSP70: role of toll-like receptor (TLR) 2 and TLR4. *J. Biol. Chem.* 277, 15028-15034.

Attramadal,H., Arriza,J.L., Aoki,C., Dawson,T.M., Codina,J., Kwatra,M.M., Snyder,S.H., Caron,M.G., and Lefkowitz,R.J. (1992). Beta-arrestin2, a novel member of the arrestin/beta-arrestin gene family. *J. Biol. Chem.* 267, 17882-17890.

Avidor-Reiss,T., Maer,A.M., Koundakjian,E., Polyanovsky,A., Keil,T., Subramaniam,S., and Zuker,C.S. (2004). Decoding cilia function: defining specialized genes required for compartmentalized cilia biogenesis. *Cell* 117, 527-539.

Badano,J.L., Ansley,S.J., Leitch,C.C., Lewis,R.A., Lupski,J.R., and Katsanis,N. (2003). Identification of a novel Bardet-Biedl syndrome protein, BBS7, that shares structural features with BBS1 and BBS2. *Am. J. Hum. Genet.* 72, 650-658.

Badano,J.L., Leitch,C.C., Ansley,S.J., May-Simera,H., Lawson,S., Lewis,R.A., Beales,P.L., Dietz,H.C., Fisher,S., and Katsanis,N. (2006). Dissection of epistasis in oligogenic Bardet-Biedl syndrome. *Nature* 439, 326-330.

Bader,I., Brandau,O., Achatz,H., Apfelstedt-Sylla,E., Hergersberg,M., Lorenz,B., Wissinger,B., Wittwer,B., Rudolph,G., Meindl,A., and Meitinger,T. (2003). X-linked retinitis pigmentosa: RPGR mutations in most families with definite X linkage and clustering of mutations in a short sequence stretch of exon ORF15. *Invest Ophthalmol. Vis. Sci.* 44, 1458-1463.

Badman,E.R. and Graham,C.R. (2000). Miniature mass analyzers. *J. Mass Spectrom.* 35, 659-671.

Banerjee,P., Kleyn,P.W., Knowles,J.A., Lewis,C.A., Ross,B.M., Parano,E., Kovats,S.G., Lee,J.J., Penchaszadeh,G.K., Ott,J., Jacobson,S.G., and Gilliam,T.C. (1998). TULP1 mutation in two extended Dominican kindreds with autosomal recessive retinitis pigmentosa. *Nat. Genet.* 18, 177-179.

- Bartolini,F., Bhamidipati,A., Thomas,S., Schwahn,U., Lewis,S.A., and Cowan,N.J. (2002). Functional overlap between retinitis pigmentosa 2 protein and the tubulin-specific chaperone cofactor C. *J. Biol. Chem.* 277, 14629-14634.
- Bartolini,F., Tian,G., Piehl,M., Cassimeris,L., Lewis,S.A., and Cowan,N.J. (2005). Identification of a novel tubulin-destabilizing protein related to the chaperone cofactor E. *J. Cell Sci.* 118, 1197-1207.
- Bayes,M., Giordano,M., Balcells,S., Grinberg,D., Vilageliu,L., Martinez,I., Ayuso,C., Benitez,J., Ramos-Arroyo,M.A., Chivelet,P., and . (1995). Homozygous tandem duplication within the gene encoding the beta-subunit of rod phosphodiesterase as a cause for autosomal recessive retinitis pigmentosa. *Hum. Mutat.* 5, 228-234.
- Beales,P.L., Elcioglu,N., Woolf,A.S., Parker,D., and Flinter,F.A. (1999). New criteria for improved diagnosis of Bardet-Biedl syndrome: results of a population survey. *J. Med. Genet.* 36, 437-446.
- Bergsma,D.R. and Brown,K.S. (1975). Assessment of ophthalmologic, endocrinologic and genetic findings in the Bardet-Biedl syndrome. *Birth Defects Orig. Artic. Ser.* 11, 132-136.
- Bessant,D.A., Payne,A.M., Mitton,K.P., Wang,Q.L., Swain,P.K., Plant,C., Bird,A.C., Zack,D.J., Swaroop,A., and Bhattacharya,S.S. (1999). A mutation in NRL is associated with autosomal dominant retinitis pigmentosa. *Nat. Genet.* 21, 355-356.
- Bhamidipati,A., Lewis,S.A., and Cowan,N.J. (2000). ADP ribosylation factor-like protein 2 (Arl2) regulates the interaction of tubulin-folding cofactor D with native tubulin. *J. Cell Biol.* 149, 1087-1096.
- Bhanot,P., Brink,M., Samos,C.H., Hsieh,J.C., Wang,Y., Macke,J.P., Andrew,D., Nathans,J., and Nusse,R. (1996). A new member of the frizzled family from *Drosophila* functions as a Wingless receptor. *Nature* 382, 225-230.
- Bhattacharya,S.S., Wright,A.F., Clayton,J.F., Price,W.H., Phillips,C.I., McKeown,C.M., Jay,M., Bird,A.C., Pearson,P.L., Southern,E.M., and . (1984). Close genetic linkage between X-linked retinitis pigmentosa and a restriction fragment length polymorphism identified by recombinant DNA probe L1.28. *Nature* 309, 253-255.
- Bird,A.C. (1975). X-linked retinitis pigmentosa. *Br. J. Ophthalmol.* 59, 177-199.
- Bomont,P. and Koenig,M. (2003). Intermediate filament aggregation in fibroblasts of giant axonal neuropathy patients is aggravated in non dividing cells and by microtubule destabilization. *Hum. Mol. Genet.* 12, 813-822.

- Bomont,P., Cavalier,L., Blondeau,F., Ben Hamida,C., Belal,S., Tazir,M., Demir,E., Topaloglu,H., Korinthenberg,R., Tuysuz,B., Landrieu,P., Hentati,F., and Koenig,M. (2000). The gene encoding gigaxonin, a new member of the cytoskeletal BTB/kelch repeat family, is mutated in giant axonal neuropathy. *Nat. Genet.* 26, 370-374.
- Bosch,E., Horwitz,J., and Bok,D. (1993). Phagocytosis of outer segments by retinal pigment epithelium: phagosome-lysosome interaction. *J. Histochem. Cytochem.* 41, 253-263.
- Bowne,S.J., Daiger,S.P., Hims,M.M., Sohocki,M.M., Malone,K.A., McKie,A.B., Heckenlively,J.R., Birch,D.G., Inglehearn,C.F., Bhattacharya,S.S., Bird,A., and Sullivan,L.S. (1999). Mutations in the RP1 gene causing autosomal dominant retinitis pigmentosa. *Hum. Mol. Genet.* 8, 2121-2128.
- Boylan,J.P. and Wright,A.F. (2000). Identification of a novel protein interacting with RPGR. *Hum. Mol. Genet.* 9, 2085-2093.
- Brann,M.R. and Cohen,L.V. (1987). Diurnal expression of transducin mRNA and translocation of transducin in rods of rat retina. *Science* 235, 585-587.
- Breitwieser,G.E. (2004). G protein-coupled receptor oligomerization: implications for G protein activation and cell signaling. *Circ. Res.* 94, 17-27.
- Breuer,D.K., Yashar,B.M., Filippova,E., Hiriyanna,S., Lyons,R.H., Mears,A.J., Asaye,B., Acar,C., Vervoort,R., Wright,A.F., Musarella,M.A., Wheeler,P., MacDonald,I., Iannaccone,A., Birch,D., Hoffman,D.R., Fishman,G.A., Heckenlively,J.R., Jacobson,S.G., Sieving,P.A., and Swaroop,A. (2002). A comprehensive mutation analysis of RP2 and RPGR in a North American cohort of families with X-linked retinitis pigmentosa. *Am. J. Hum. Genet.* 70, 1545-1554.
- Broder,Y.C., Katz,S., and Aronheim,A. (1998). The ras recruitment system, a novel approach to the study of protein-protein interactions. *Curr. Biol.* 8, 1121-1124.
- Broekhuysen,R.M., Tolhuizen,E.F., Janssen,A.P., and Winkens,H.J. (1985). Light induced shift and binding of S-antigen in retinal rods. *Curr. Eye Res.* 4, 613-618.
- Bruckert,F., Chabre,M., and Vuong,T.M. (1992). Kinetic analysis of the activation of transducin by photoexcited rhodopsin. Influence of the lateral diffusion of transducin and competition of guanosine diphosphate and guanosine triphosphate for the nucleotide site. *Biophys. J.* 63, 616-629.
- Budzikiewicz,H. and Grigsby,R.D. (2006). Mass spectrometry and isotopes: a century of research and discussion. *Mass Spectrom. Rev.* 25, 146-157.
- Burd,C.G., Strohlic,T.I., and Gangi,S., Sr. (2004). Arf-like GTPases: not so Arf-like after all. *Trends Cell Biol.* 14, 687-694.

- Burton,R.A., Mattila,S., Taparowsky,E.J., and Post,C.B. (2006). B-myc: N-terminal recognition of myc binding proteins. *Biochemistry* 45, 9857-9865.
- Caldon,C.E., Daly,R.J., Sutherland,R.L., and Musgrove,E.A. (2006). Cell cycle control in breast cancer cells. *J. Cell Biochem.* 97, 261-274.
- Calvert,P.D., Strissel,K.J., Schiesser,W.E., Pugh,E.N., Jr., and Arshavsky,V.Y. (2006). Light-driven translocation of signaling proteins in vertebrate photoreceptors. *Trends Cell Biol.* 16, 560-568.
- Cao,S., Carlesso,G., Osipovich,A.B., Llanes,J., Lin,Q., Hoek,K.L., Khan,W.N., and Ruley,H.E. (2008). Subunit 1 of the prefoldin chaperone complex is required for lymphocyte development and function. *J. Immunol.* 181, 476-484.
- Carmi,R., Rokhlina,T., Kwitek-Black,A.E., Elbedour,K., Nishimura,D., Stone,E.M., and Sheffield,V.C. (1995). Use of a DNA pooling strategy to identify a human obesity syndrome locus on chromosome 15. *Hum. Mol. Genet.* 4, 9-13.
- Carter-Dawson,L.D. and LaVail,M.M. (1979). Rods and cones in the mouse retina. I. Structural analysis using light and electron microscopy. *J. Comp Neurol.* 188, 245-262.
- Carver,L.A. and Bradfield,C.A. (1997). Ligand-dependent interaction of the aryl hydrocarbon receptor with a novel immunophilin homolog in vivo. *J. Biol. Chem.* 272, 11452-11456.
- Cha,H., Hancock,C., Dangi,S., Maignel,D., Carrier,F., and Shapiro,P. (2004). Phosphorylation regulates nucleophosmin targeting to the centrosome during mitosis as detected by cross-reactive phosphorylation-specific MKK1/MKK2 antibodies. *Biochem. J.* 378, 857-865.
- Chakarova,C.F., Hims,M.M., Bolz,H., Abu-Safieh,L., Patel,R.J., Papaioannou,M.G., Inglehearn,C.F., Keen,T.J., Willis,C., Moore,A.T., Rosenberg,T., Webster,A.R., Bird,A.C., Gal,A., Hunt,D., Vithana,E.N., and Bhattacharya,S.S. (2002). Mutations in HPRP3, a third member of pre-mRNA splicing factor genes, implicated in autosomal dominant retinitis pigmentosa. *Hum. Mol. Genet.* 11, 87-92.
- Chang,H.C., Tang,Y.C., Hayer-Hartl,M., and Hartl,F.U. (2007). SnapShot: molecular chaperones, Part I. *Cell* 128, 212.
- Chang,J., Sonoyama,W., Wang,Z., Jin,Q., Zhang,C., Krebsbach,P.H., Giannobile,W., Shi,S., and Wang,C.Y. (2007). Noncanonical Wnt-4 signaling enhances bone regeneration of mesenchymal stem cells in craniofacial defects through activation of p38 MAPK. *J. Biol. Chem.* 282, 30938-30948.
- Chapple,J.P., Grayson,C., Hardcastle,A.J., Bailey,T.A., Matter,K., Adamson,P., Graham,C.H., Willison,K.R., and Cheetham,M.E. (2003). Organization on the plasma membrane of the retinitis pigmentosa protein RP2: investigation of association with detergent-resistant membranes and polarized sorting. *Biochem. J.* 372, 427-433.

- Chapple,J.P., Hardcastle,A.J., Grayson,C., Spackman,L.A., Willison,K.R., and Cheetham,M.E. (2000). Mutations in the N-terminus of the X-linked retinitis pigmentosa protein RP2 interfere with the normal targeting of the protein to the plasma membrane. *Hum. Mol. Genet.* **9**, 1919-1926.
- Chapple,J.P., Hardcastle,A.J., Grayson,C., Willison,K.R., and Cheetham,M.E. (2002). Delineation of the plasma membrane targeting domain of the X-linked retinitis pigmentosa protein RP2. *Invest Ophthalmol. Vis. Sci.* **43**, 2015-2020.
- Cheetham,M.E., Jackson,A.P., and Anderton,B.H. (1994). Regulation of 70-kDa heat-shock-protein ATPase activity and substrate binding by human DnaJ-like proteins, Hsj1a and Hsj1b. *Eur. J. Biochem.* **226**, 99-107.
- Chen,J., Wu,M., Sezate,S.A., and McGinnis,J.F. (2007). Light threshold-controlled cone alpha-transducin translocation. *Invest Ophthalmol. Vis. Sci.* **48**, 3350-3355.
- Chen,J., Wu,M., Sezate,S.A., Matsumoto,H., Ramsey,M., and McGinnis,J.F. (2008). Interaction of glyceraldehyde-3-phosphate dehydrogenase in the light-induced rod alpha-transducin translocation. *J. Neurochem.* **104**, 1280-1292.
- Chen,Y. and Struhl,G. (1996). Dual roles for patched in sequestering and transducing Hedgehog. *Cell* **87**, 553-563.
- Chiang,A.P., Beck,J.S., Yen,H.J., Tayeh,M.K., Scheetz,T.E., Swiderski,R.E., Nishimura,D.Y., Braun,T.A., Kim,K.Y., Huang,J., Elbedour,K., Carmi,R., Slusarski,D.C., Casavant,T.L., Stone,E.M., and Sheffield,V.C. (2006). Homozygosity mapping with SNP arrays identifies TRIM32, an E3 ubiquitin ligase, as a Bardet-Biedl syndrome gene (BBS11). *Proc. Natl. Acad. Sci. U. S. A* **103**, 6287-6292.
- Chisari,M., Saini,D.K., Kalyanaraman,V., and Gautam,N. (2007). Shuttling of G protein subunits between the plasma membrane and intracellular membranes. *J. Biol. Chem.* **282**, 24092-24098.
- Cole,D.G., Diener,D.R., Himelblau,A.L., Beech,P.L., Fuster,J.C., and Rosenbaum,J.L. (1998). Chlamydomonas kinesin-II-dependent intraflagellar transport (IFT): IFT particles contain proteins required for ciliary assembly in *Caenorhabditis elegans* sensory neurons. *J. Cell Biol.* **141**, 993-1008.
- Connert,S., Wienand,S., Thiel,C., Krikunova,M., Glyvuk,N., Tsytsyura,Y., Hilfiker-Kleiner,D., Bartsch,J.W., Klingauf,J., and Wienands,J. (2006). SH3P7/mAbp1 deficiency leads to tissue and behavioral abnormalities and impaired vesicle transport. *EMBO J.* **25**, 1611-1622.
- Connor,M.K., Kotchetkov,R., Cariou,S., Resch,A., Lupetti,R., Beniston,R.G., Melchior,F., Hengst,L., and Slingerland,J.M. (2003). CRM1/Ran-mediated nuclear export of p27(Kip1) involves a nuclear export signal and links p27 export and proteolysis. *Mol. Biol. Cell* **14**, 201-213.

Corbit,K.C., Shyer,A.E., Dowdle,W.E., Gaulden,J., Singla,V., Chen,M.H., Chuang,P.T., and Reiter,J.F. (2008). Kif3a constrains beta-catenin-dependent Wnt signalling through dual ciliary and non-ciliary mechanisms. *Nat. Cell Biol.* 10, 70-76.

Cremers,F.P., van de Pol,D.J., van Driel,M., den Hollander,A.I., van Haren,F.J., Knoers,N.V., Tijmes,N., Bergen,A.A., Rohrschneider,K., Blankenagel,A., Pinckers,A.J., Deutman,A.F., and Hoyng,C.B. (1998). Autosomal recessive retinitis pigmentosa and cone-rod dystrophy caused by splice site mutations in the Stargardt's disease gene ABCR. *Hum. Mol. Genet.* 7, 355-362.

Cuello,F., Schulze,R.A., Heemeyer,F., Meyer,H.E., Lutz,S., Jakobs,K.H., Niroomand,F., and Wieland,T. (2003). Activation of heterotrimeric G proteins by a high energy phosphate transfer via nucleoside diphosphate kinase (NDPK) B and Gbeta subunits. Complex formation of NDPK B with Gbeta gamma dimers and phosphorylation of His-266 IN Gbeta. *J. Biol. Chem.* 278, 7220-7226.

Curcio,C.A., Sloan,K.R., Kalina,R.E., and Hendrickson,A.E. (1990). Human photoreceptor topography. *J. Comp Neurol.* 292, 497-523.

Curry,J.L., Richards,H.W., Huttenbach,Y.T., Medrano,E.E., and Reed,J.A. (2008). Different expression patterns of p27(KIP1) and p57(KIP2) proteins in benign and malignant melanocytic neoplasms and in cultured human melanocytes. *J. Cutan. Pathol.*

Cuvillier,A., Redon,F., Antoine,J.C., Chardin,P., DeVos,T., and Merlin,G. (2000). LdARL-3A, a Leishmania promastigote-specific ADP-ribosylation factor-like protein, is essential for flagellum integrity. *J. Cell Sci.* 113 (Pt 11), 2065-2074.

Daiger,S.P., Bowne,S.J., and Sullivan,L.S. (2007). Perspective on genes and mutations causing retinitis pigmentosa. *Arch. Ophthalmol.* 125, 151-158.

Dancik,V., Addona,T.A., Clauser,K.R., Vath,J.E., and Pevzner,P.A. (1999). De novo peptide sequencing via tandem mass spectrometry. *J. Comput. Biol.* 6, 327-342.

Dandekar,S.S., Ebenezer,N.D., Grayson,C., Chapple,J.P., Egan,C.A., Holder,G.E., Jenkins,S.A., Fitzke,F.W., Cheetham,M.E., Webster,A.R., and Hardcastle,A.J. (2004). An atypical phenotype of macular and peripapillary retinal atrophy caused by a mutation in the RP2 gene. *Br. J. Ophthalmol.* 88, 528-532.

Dang,C.V., O'Donnell,K.A., Zeller,K.I., Nguyen,T., Osthus,R.C., and Li,F. (2006). The c-Myc target gene network. *Semin. Cancer Biol.* 16, 253-264.

Delous, M, Baala,L., Salomon, R., Laclef,C., Vierkotten, J., Tory,K., Golzio, C., Lacoste, T., Besse, L., Ozilou, C., Moutkine, I., Hellman, N.E., Anselme, I., Silbermann, F., Vesque C., Gerhardt, C., Rattenberry, E., Wolf M.T.F., Gubler M.C., Martinovic, J., Encha-Razavi, F., Boddaert, N., Gonzales, M., Macher, M.A., Nivet, H., Champion, G., Bertheleme, J.P., Niaudet, P., McDonald, F.,

Hildebrandt, F., Johnson, C.A., Vekemans, M., Antignac, C., Ruther, U., Sylvie Schneider-Maunoury, S., Attie´-Bitach, T., and Saunier, S. (2007). The ciliary gene RPGRIP1L is mutated in cerebello-oculo-renal syndrome (Joubert syndrome type B) and Meckel syndrome. *Nat. Gen.* 39, 875-881.

De Luca, A., Torrente, I., Mangino, M., Danesi, R., Dallapiccola, B., and Novelli, G. (2001). Three novel mutations causing a truncated protein within the RP2 gene in Italian families with X-linked retinitis pigmentosa. *Mutat. Res.* 432, 79-82.

Demirci, F.Y., Rigatti, B.W., Wen, G., Radak, A.L., Mah, T.S., Baic, C.L., Traboulsi, E.I., Alitalo, T., Ramser, J., and Gorin, M.B. (2002). X-linked cone-rod dystrophy (locus COD1): identification of mutations in RPGR exon ORF15. *Am. J. Hum. Genet.* 70, 1049-1053.

den Hollander, A.I., Koenekoop, R.K., Mohamed, M.D., Arts, H.H., Boldt, K., Towns, K.V., Sedmak, T., Beer, M., Nagel-Wolfrum, K., McKibbin, M., Dharmaraj, S., Lopez, I., Ivings, L., Williams, G.A., Springell, K., Woods, C.G., Jafri, H., Rashid, Y., Strom, T.M., van der, Z.B., Gosens, I., Kersten, F.F., van Wijk, E., Veltman, J.A., Zonneveld, M.N., van Beersum, S.E., Maumenee, I.H., Wolfrum, U., Cheetham, M.E., Ueffing, M., Cremers, F.P., Inglehearn, C.F., and Roepman, R. (2007). Mutations in LCA5, encoding the ciliary protein lebercilin, cause Leber congenital amaurosis. *Nat. Genet.* 39, 889-895.

den Hollander, A.I., ten Brink, J.B., de Kok, Y.J., van Soest, S., van den Born, L.I., van Driel, M.A., van de Pol, D.J., Payne, A.M., Bhattacharya, S.S., Kellner, U., Hoyng, C.B., Westerveld, A., Brunner, H.G., Bleeker-Wagemakers, E.M., Deutman, A.F., Heckenlively, J.R., Cremers, F.P., and Bergen, A.A. (1999). Mutations in a human homologue of *Drosophila crumbs* cause retinitis pigmentosa (RP12). *Nat. Genet.* 23, 217-221.

Dice, J.F., Terlecky, S.R., Chiang, H.L., Olson, T.S., Isenman, L.D., Short-Russell, S.R., Freundlieb, S., and Terlecky, L.J. (1990). A selective pathway for degradation of cytosolic proteins by lysosomes. *Semin. Cell Biol.* 1, 449-455.

Djamgoz, M.B. and Kolb, H. (1993). Ultrastructural and functional connectivity of intracellularly stained neurones in the vertebrate retina: correlative analyses. *Microsc. Res. Tech.* 24, 43-66.

Dodatko, T., Fedorov, A.A., Grynberg, M., Patskovsky, Y., Rozwarski, D.A., Jaroszewski, L., Aronoff-Spencer, E., Kondraskina, E., Irving, T., Godzik, A., and Almo, S.C. (2004). Crystal structure of the actin binding domain of the cyclase-associated protein. *Biochemistry* 43, 10628-10641.

Dong, Y., Zhu, H., Wang, X., Dalageorgou, C., Carter, N., Spector, T.D., and Snieder, H. (2004). Obesity reveals an association between blood pressure and the G protein beta3-subunit gene: a study of female dizygotic twins. *Pharmacogenetics* 14, 419-427.

Downes, G.B. and Gautam, N. (1999). The G protein subunit gene families. *Genomics* 62, 544-552.

Dryja,T.P., Adams,S.M., Grimsby,J.L., McGee,T.L., Hong,D.H., Li,T., Andreasson,S., and Berson,E.L. (2001). Null RPGRIP1 alleles in patients with Leber congenital amaurosis. *Am. J. Hum. Genet.* 68, 1295-1298.

Dryja,T.P., Adams,S.M., Grimsby,J.L., McGee,T.L., Hong,D.H., Li,T., Andreasson,S., and Berson,E.L. (2001). Null RPGRIP1 alleles in patients with Leber congenital amaurosis. *Am. J. Hum. Genet.* 68, 1295-1298.

Dryja,T.P., McGee,T.L., Hahn,L.B., Cowley,G.S., Olsson,J.E., Reichel,E., Sandberg,M.A., and Berson,E.L. (1990). Mutations within the rhodopsin gene in patients with autosomal dominant retinitis pigmentosa. *N. Engl. J. Med.* 323, 1302-1307.

Dryja,T.P., Rucinski,D.E., Chen,S.H., and Berson,E.L. (1999). Frequency of mutations in the gene encoding the alpha subunit of rod cGMP-phosphodiesterase in autosomal recessive retinitis pigmentosa. *Invest Ophthalmol. Vis. Sci.* 40, 1859-1865.

Elliott,E., Tsvetkov,P., and Ginzburg,I. (2007). BAG-1 associates with Hsc70.Tau complex and regulates the proteasomal degradation of Tau protein. *J. Biol. Chem.* 282, 37276-37284.

Ellis, R.J. (2007). Protein misassembly: macromolecular crowding and molecular chaperones. *Adv. Exp. Med. Biol.* 594, 1-13.

Ellis,R.J. and van der Vies,S.M. (1991). Molecular chaperones. *Annu. Rev. Biochem.* 60, 321-347.

Evans, R. J. Identification and characterisation of RP2 interacting proteins. PhD Thesis/Dissertation, 2007.

Evans,R.J., Chapple,J.P., Grayson,C., Hardcastle,A.J., and Cheetham,M.E. (2005). Assay and functional analysis of the ARL3 effector RP2 involved in X-linked retinitis pigmentosa. *Methods Enzymol.* 404, 468-480.

Ewan,K.B. and Dale,T.C. (2008). The potential for targeting oncogenic WNT/beta-catenin signaling in therapy. *Curr. Drug Targets.* 9, 532-547.

Fan,Y., Esmail,M.A., Ansley,S.J., Blacque,O.E., Boroevich,K., Ross,A.J., Moore,S.J., Badano,J.L., May-Simera,H., Compton,D.S., Green,J.S., Lewis,R.A., van Haelst,M.M., Parfrey,P.S., Baillie,D.L., Beales,P.L., Katsanis,N., Davidson,W.S., and Leroux,M.R. (2004). Mutations in a member of the Ras superfamily of small GTP-binding proteins causes Bardet-Biedl syndrome. *Nat. Genet.* 36, 989-993.

Feng,Y.H. and Karnik,S.S. (1999). Role of transmembrane helix IV in G protein specificity of the angiotensin II type 1 receptor. *J. Biol. Chem.* 274, 35546-35552.

Fenn,J.B., Mann,M., Meng,C.K., Wong,S.F., and Whitehouse,C.M. (1989). Electrospray ionization for mass spectrometry of large biomolecules. *Science* 246, 64-71.

- Fewell,S.W., Pipas,J.M., and Brodsky,J.L. (2002). Mutagenesis of a functional chimeric gene in yeast identifies mutations in the simian virus 40 large T antigen J domain. *Proc. Natl. Acad. Sci. U. S. A* 99 , 2002-2007.
- Fields,S. and Song,O. (1989). A novel genetic system to detect protein-protein interactions. *Nature* 340, 245-246.
- Freeman,B.C., Myers,M.P., Schumacher,R., and Morimoto,R.I. (1995). Identification of a regulatory motif in Hsp70 that affects ATPase activity, substrate binding and interaction with HDJ-1. *EMBO J.* 14, 2281-2292.
- Freund,C.L., Gregory-Evans,C.Y., Furukawa,T., Papaioannou,M., Looser,J., Ploder,L., Bellingham,J., Ng,D., Herbrick,J.A., Duncan,A., Scherer,S.W., Tsui,L.C., Loutradis-Anagnostou,A., Jacobson,S.G., Cepko,C.L., Bhattacharya,S.S., and McInnes,R.R. (1997). Cone-rod dystrophy due to mutations in a novel photoreceptor-specific homeobox gene (CRX) essential for maintenance of the photoreceptor. *Cell* 91, 543-553.
- Frydman,J., Nimmegern,E., Erdjument-Bromage,H., Wall,J.S., Tempst,P., and Hartl,F.U. (1992). Function in protein folding of TRiC, a cytosolic ring complex containing TCP-1 and structurally related subunits. *EMBO J.* 11, 4767-4778.
- Fuchs,S., Nakazawa,M., Maw,M., Tamai,M., Oguchi,Y., and Gal,A. (1995). A homozygous 1-base pair deletion in the arrestin gene is a frequent cause of Oguchi disease in Japanese. *Nat. Genet.* 10, 360-362.
- Fujioka,Y., Taira,T., Maeda,Y., Tanaka,S., Nishihara,H., Iguchi-Ariga,S.M., Nagashima,K., and Ariga,H. (2001). MM-1, a c-Myc-binding protein, is a candidate for a tumor suppressor in leukemia/lymphoma and tongue cancer. *J. Biol. Chem.* 276, 45137-45144.
- Gabriele,T., Tavaría,M., Kola,I., and Anderson,R.L. (1996). Analysis of heat shock protein 70 in human chromosome 21 containing hybrids. *Int. J. Biochem. Cell Biol.* 28, 905-910.
- Gamundi,M.J., Hernan,I., Muntanyola,M., Maseras,M., Lopez-Romero,P., Alvarez,R., Dopazo,A., Borrego,S., and Carballo,M. (2008). Transcriptional expression of cis-acting and trans-acting splicing mutations cause autosomal dominant retinitis pigmentosa. *Hum. Mutat.* 29, 869-878.
- Gao,Y., Thomas,J.O., Chow,R.L., Lee,G.H., and Cowan,N.J. (1992). A cytoplasmic chaperonin that catalyzes beta-actin folding. *Cell* 69, 1043-1050.
- Gaudet,R., Bohm,A., and Sigler,P.B. (1996). Crystal structure at 2.4 angstroms resolution of the complex of transducin betagamma and its regulator, phosducin. *Cell* 87, 577-588.
- Georgopoulos,C. and Welch,W.J. (1993). Role of the major heat shock proteins as molecular chaperones. *Annu. Rev. Cell Biol.* 9, 601-634.

- Gerber,S., Hanein,S., Perrault,I., Delphin,N., Aboussair,N., Leowski,C., Dufier,J.L., Roche,O., Munnich,A., Kaplan,J., and Rozet,J.M. (2007). Mutations in LCA5 are an uncommon cause of Leber congenital amaurosis (LCA) type II. *Hum. Mutat.* 28, 1245.
- Gerber,S., Perrault,I., Hanein,S., Barbet,F., Ducroq,D., Ghazi,I., Martin-Coignard,D., Leowski,C., Homfray,T., Dufier,J.L., Munnich,A., Kaplan,J., and Rozet,J.M. (2001). Complete exon-intron structure of the RPGR-interacting protein (RPGRIP1) gene allows the identification of mutations underlying Leber congenital amaurosis. *Eur. J. Hum. Genet.* 9, 561-571.
- Ghadami,M., Tomita,H.A., Najafi,M.T., Damavandi,E., Farahvash,M.S., Yamada,K., Majidzadeh,A., and Niikawa,N. (2000). Bardet-Biedl syndrome type 3 in an Iranian family: clinical study and confirmation of disease localization. *Am. J. Med. Genet.* 94, 433-437.
- Giessl,A., Trojan,P., Rausch,S., Pulvermuller,A., and Wolfrum,U. (2006). Centrin, gatekeepers for the light-dependent translocation of transducin through the photoreceptor cell connecting cilium. *Vision Res.* 46, 4502-4509.
- Gillespie,P.G. and Beavo,J.A. (1989). cGMP is tightly bound to bovine retinal rod phosphodiesterase. *Proc. Natl. Acad. Sci. U. S. A* 86, 4311-4315.
- Gong,Y., Mo,C., and Fraser,S.E. (2004). Planar cell polarity signalling controls cell division orientation during zebrafish gastrulation. *Nature* 430, 689-693.
- Granzin,J., Wilden,U., Choe,H.W., Labahn,J., Krafft,B., and Buldt,G. (1998). X-ray crystal structure of arrestin from bovine rod outer segments. *Nature* 391, 918-921.
- Grayson,C., Bartolini,F., Chapple,J.P., Willison,K.R., Bhamidipati,A., Lewis,S.A., Luthert,P.J., Hardcastle,A.J., Cowan,N.J., and Cheetham,M.E. (2002a). Localization in the human retina of the X-linked retinitis pigmentosa protein RP2, its homologue cofactor C and the RP2 interacting protein Arl3. *Hum. Mol. Genet.* 11, 3065-3074.
- Grayson,C., Chapple,J.P., Willison,K.R., Webster,A.R., Hardcastle,A.J., and Cheetham,M.E. (2002b). In vitro analysis of aminoglycoside therapy for the Arg120stop nonsense mutation in RP2 patients. *J. Med. Genet.* 39, 62-67.
- Gregory-Evans,K., Kelsell,R.E., Gregory-Evans,C.Y., Downes,S.M., Fitzke,F.W., Holder,G.E., Simunovic,M., Mollon,J.D., Taylor,R., Hunt,D.M., Bird,A.C., and Moore,A.T. (2000). Autosomal dominant cone-rod retinal dystrophy (CORD6) from heterozygous mutation of GUCY2D, which encodes retinal guanylate cyclase. *Ophthalmology* 107, 55-61.
- Gu,S.M., Thompson,D.A., Srikumari,C.R., Lorenz,B., Finckh,U., Nicoletti,A., Murthy,K.R., Rathmann,M., Kumaramanickavel,G., Denton,M.J., and Gal,A. (1997). Mutations in RPE65 cause autosomal recessive childhood-onset severe retinal dystrophy. *Nat. Genet.* 17, 194-197.

- Gurevich,E.V. and Gurevich,V.V. (2006). Arrestins: ubiquitous regulators of cellular signaling pathways. *Genome Biol.* 7, 236.
- Gurevich,V.V. and Benovic,J.L. (1993). Visual arrestin interaction with rhodopsin. Sequential multisite binding ensures strict selectivity toward light-activated phosphorylated rhodopsin. *J. Biol. Chem.* 268, 11628-11638.
- Gurevich,V.V. and Benovic,J.L. (1995). Visual arrestin binding to rhodopsin. Diverse functional roles of positively charged residues within the phosphorylation-recognition region of arrestin. *J. Biol. Chem.* 270, 6010-6016.
- Guzhova,I., Kislyakova,K., Moskaliova,O., Fridlanskaya,I., Tytell,M., Cheetham,M., and Margulis,B. (2001). In vitro studies show that Hsp70 can be released by glia and that exogenous Hsp70 can enhance neuronal stress tolerance. *Brain Res.* 914, 66-73.
- Hagio,Y., Kimura,Y., Taira,T., Fujioka,Y., Iguchi-Arigo,S.M., and Arigo,H. (2006). Distinct localizations and repression activities of MM-1 isoforms toward c-Myc. *J. Cell Biochem.* 97, 145-155.
- Hameed,A., Abid,A., Aziz,A., Ismail,M., Mehdi,S.Q., and Khaliq,S. (2003). Evidence of RPGRIP1 gene mutations associated with recessive cone-rod dystrophy. *J. Med. Genet.* 40, 616-619.
- Hamel,C. (2003). Retinitis pigmentosa. *Orphanet Encyclopedia.*
- Hamel,C. (2007). Cone rod dystrophies. *Orphanet Journal of Rare Diseases* 2:7.
- Hamilton,S.E., Prusti,R.K., Bentley,J.K., Beavo,J.A., and Hurley,J.B. (1993). Affinities of bovine photoreceptor cGMP phosphodiesterases for rod and cone inhibitory subunits. *FEBS Lett.* 318, 157-161.
- Hanson,S.M., Dawson,E.S., Francis,D.J., Van Eps,N., Klug,C.S., Hubbell,W.L., Meiler,J., and Gurevich,V.V. (2008). A model for the solution structure of the rod arrestin tetramer. *Structure.* 16, 924-934.
- Hanson,S.M., Francis,D.J., Vishnivetskiy,S.A., Klug,C.S., and Gurevich,V.V. (2006). Visual arrestin binding to microtubules involves a distinct conformational change. *J. Biol. Chem.* 281, 9765-9772.
- Hanson,S.M., Gurevich,E.V., Vishnivetskiy,S.A., Ahmed,M.R., Song,X., and Gurevich,V.V. (2007). Each rhodopsin molecule binds its own arrestin. *Proc. Natl. Acad. Sci. U. S. A* 104, 3125-3128.
- Hanzal-Bayer,M., Renault,L., Roversi,P., Wittinghofer,A., and Hillig,R.C. (2002). The complex of Arl2-GTP and PDE delta: from structure to function. *EMBO J.* 21, 2095-2106.
- Hardcastle,A.J., Thiselton,D.L., Van Maldergem,L., Saha,B.K., Jay,M., Plant,C., Taylor,R., Bird,A.C., and Bhattacharya,S. (1999). Mutations in the RP2 gene

cause disease in 10% of families with familial X-linked retinitis pigmentosa assessed in this study. *Am. J. Hum. Genet.* *64*, 1210-1215.

He,W., Lu,L., Zhang,X., El Hodiri,H.M., Chen,C.K., Slep,K.C., Simon,M.I., Jamrich,M., and Wensel,T.G. (2000). Modules in the photoreceptor RGS9-1.Gbeta 5L GTPase-accelerating protein complex control effector coupling, GTPase acceleration, protein folding, and stability. *J. Biol. Chem.* *275*, 37093-37100.

Henkel,J., Du,H., Yang,P., Qyang,Y., Kansra,S., Ko,M., Kim,H.W., and Marcus,S. (2001). Bob1, a Gim5/MM-1/Pfd5 homolog, interacts with the MAP kinase kinase Byr1 to regulate sexual differentiation in the fission yeast, *Schizosaccharomyces pombe*. *Differentiation* *67*, 98-106.

Hidalgo-de-Quintana,J., Evans,R.J., Cheetham,M.E., and van der,S.J. (2008). The Leber congenital amaurosis protein AIPL1 functions as part of a chaperone heterocomplex. *Invest Ophthalmol. Vis. Sci.* *49*, 2878-2887.

Higashide,T. and Inana,G. (1999). Characterization of the gene for HRG4 (UNC119), a novel photoreceptor synaptic protein homologous to unc-119. *Genomics* *57*, 446-450.

Higashide,T., McLaren,M.J., and Inana,G. (1998). Localization of HRG4, a photoreceptor protein homologous to Unc-119, in ribbon synapse. *Invest Ophthalmol. Vis. Sci.* *39*, 690-698.

Higashide,T., Murakami,A., McLaren,M.J., and Inana,G. (1996). Cloning of the cDNA for a novel photoreceptor protein. *J. Biol. Chem.* *271*, 1797-1804.

Hillenkamp,F. and Karas,M. (1990). Mass spectrometry of peptides and proteins by matrix-assisted ultraviolet laser desorption/ionization. *Methods Enzymol.* *193*, 280-295.

Hirsch,J.A., Schubert,C., Gurevich,V.V., and Sigler,P.B. (1999). The 2.8 Å crystal structure of visual arrestin: a model for arrestin's regulation. *Cell* *97*, 257-269.

Hong,D.H., Pawlyk,B., Sokolov,M., Strissel,K.J., Yang,J., Tulloch,B., Wright,A.F., Arshavsky,V.Y., and Li,T. (2003). RPGR isoforms in photoreceptor connecting cilia and the transitional zone of motile cilia. *Invest Ophthalmol. Vis. Sci.* *44*, 2413-2421.

Hong,D.H., Pawlyk,B.S., Shang,J., Sandberg,M.A., Berson,E.L., and Li,T. (2000). A retinitis pigmentosa GTPase regulator (RPGR)-deficient mouse model for X-linked retinitis pigmentosa (RP3). *Proc. Natl. Acad. Sci. U. S. A* *97*, 3649-3654.

Hong,J.X., Lee,F.J., Patton,W.A., Lin,C.Y., Moss,J., and Vaughan,M. (1998). Phospholipid- and GTP-dependent activation of cholera toxin and phospholipase D by human ADP-ribosylation factor-like protein 1 (HARL1). *J. Biol. Chem.* *273*, 15872-15876.

- Hong,K., Guerchicoff,A., Pollevick,G.D., Oliva,A., Dumaine,R., de Zutter,M., Burashnikov,E., Wu,Y.S., Brugada,J., Brugada,P., and Brugada,R. (2005). Cryptic 5' splice site activation in SCN5A associated with Brugada syndrome. *J. Mol. Cell Cardiol.* 38, 555-560.
- Horn,D.M., Zubarev,R.A., and McLafferty,F.W. (2000). Automated de novo sequencing of proteins by tandem high-resolution mass spectrometry. *Proc. Natl. Acad. Sci. U. S. A* 97, 10313-10317.
- Hoyt,M.A., Stearns,T., and Botstein,D. (1990). Chromosome instability mutants of *Saccharomyces cerevisiae* that are defective in microtubule-mediated processes. *Mol. Cell Biol.* 10, 223-234.
- Hsu,S.C. and Molday,R.S. (1990). Glyceraldehyde-3-phosphate dehydrogenase is a major protein associated with the plasma membrane of retinal photoreceptor outer segments. *J. Biol. Chem.* 265, 13308-13313.
- Huang,W., Wang,S.L., Lozano,G., and de Crombrugge,B. (2001). cDNA library screening using the SOS recruitment system. *Biotechniques* 30, 94-8, 100.
- Iborra,F., Huet,J., Breant,B., Sentenac,A., and Fromageot,P. (1979). Identification of two different RNase H activities associated with yeast RNA polymerase A. *J. Biol. Chem.* 254, 10920-10924.
- Ishiba,Y., Higashide,T., Mori,N., Kobayashi,A., Kubota,S., McLaren,M.J., Satoh,H., Wong,F., and Inana,G. (2007). Targeted inactivation of synaptic HRG4 (UNC119) causes dysfunction in the distal photoreceptor and slow retinal degeneration, revealing a new function. *Exp. Eye Res.* 84, 473-485.
- Jacobs,S., Schilf,C., Fliegert,F., Kolling,S., Weber,Y., Schurmann,A., and Joost,H.G. (1999). ADP-ribosylation factor (ARF)-like 4, 6, and 7 represent a subgroup of the ARF family characterization by rapid nucleotide exchange and a nuclear localization signal. *FEBS Lett.* 456, 384-388.
- Jones,J., Wu,K., Yang,Y., Guerrero,C., Nillegoda,N., Pan,Z.Q., and Huang,L. (2008). A targeted proteomic analysis of the ubiquitin-like modifier nedd8 and associated proteins. *J. Proteome. Res.* 7, 1274-1287.
- Jones,M.B., Siderovski,D.P., and Hooks,S.B. (2004). The G betagamma dimer as a novel source of selectivity in G protein signaling: GGL-ing at convention. *Mol. Interv.* 4, 200-214.
- Kajiwara,K., Berson,E.L., and Dryja,T.P. (1994). Digenic retinitis pigmentosa due to mutations at the unlinked peripherin/RDS and ROM1 loci. *Science* 264, 1604-1608.
- Kalab,P. and Heald,R. (2008). The RanGTP gradient - a GPS for the mitotic spindle. *J. Cell Sci.* 121, 1577-1586.
- Kalab,P., Pralle,A., Isacoff,E.Y., Heald,R., and Weis,K. (2006). Analysis of a RanGTP-regulated gradient in mitotic somatic cells. *Nature* 440, 697-701.

- Kampinga,H.H., Hageman,J., Vos,M.J., Kubota,H., Tanguay,R.M., Bruford,E.A., Cheatham,M.E., Chen,B., and Hightower,L.E. (2008). Guidelines for the nomenclature of the human heat shock proteins. *Cell Stress. Chaperones*.
- Kaplan,J. (2008). Leber congenital amaurosis: from darkness to spotlight. *Ophthalmic Genet.* 29, 92-98.
- Karim,R., Tse,G., Putti,T., Scolyer,R., and Lee,S. (2004). The significance of the Wnt pathway in the pathology of human cancers. *Pathology* 36, 120-128.
- Keresztes,G., Martemyanov,K.A., Krispel,C.M., Mutai,H., Yoo,P.J., Maison,S.F., Burns,M.E., Arshavsky,V.Y., and Heller,S. (2004). Absence of the RGS9.Gbeta5 GTPase-activating complex in photoreceptors of the R9AP knockout mouse. *J. Biol. Chem.* 279, 1581-1584.
- Kessels,M.M., Engqvist-Goldstein,A.E., Drubin,D.G., and Qualmann,B. (2001). Mammalian Abp1, a signal-responsive F-actin-binding protein, links the actin cytoskeleton to endocytosis via the GTPase dynamin. *J. Cell Biol.* 153, 351-366.
- Kim,J.C., Badano,J.L., Sibold,S., Esmail,M.A., Hill,J., Hoskins,B.E., Leitch,C.C., Venner,K., Ansley,S.J., Ross,A.J., Leroux,M.R., Katsanis,N., and Beales,P.L. (2004). The Bardet-Biedl protein BBS4 targets cargo to the pericentriolar region and is required for microtubule anchoring and cell cycle progression. *Nat. Genet.* 36, 462-470.
- Kim,J.C., Ou,Y.Y., Badano,J.L., Esmail,M.A., Leitch,C.C., Fiedrich,E., Beales,P.L., Archibald,J.M., Katsanis,N., Rattner,J.B., and Leroux,M.R. (2005). MKKS/BBS6, a divergent chaperonin-like protein linked to the obesity disorder Bardet-Biedl syndrome, is a novel centrosomal component required for cytokinesis. *J. Cell Sci.* 118, 1007-1020.
- Kim,J.H., Jung,C.W., Cho,Y.H., Lee,J., Lee,S.H., Kim,H.Y., Park,J., Park,J.O., Kim,K., Kim,W.S., Park,Y.S., Im,Y.H., Kang,W.K., and Park,K. (2005). Somatic VHL alteration and its impact on prognosis in patients with clear cell renal cell carcinoma. *Oncol. Rep.* 13, 859-864.
- Kishimoto,N., Cao,Y., Park,A., and Sun,Z. (2008). Cystic kidney gene seahorse regulates cilia-mediated processes and Wnt pathways. *Dev. Cell* 14, 954-961.
- Klein,W.L., Krafft,G.A., and Finch,C.E. (2001). Targeting small Abeta oligomers: the solution to an Alzheimer's disease conundrum? *Trends Neurosci.* 24, 219-224.
- Kleuss,C., Scherubl,H., Hescheler,J., Schultz,G., and Wittig,B. (1993). Selectivity in signal transduction determined by gamma subunits of heterotrimeric G proteins. *Science* 259, 832-834.
- Klysik,M. (2008). Ciliary syndromes and treatment. *Pathol. Res. Pract.* 204, 77-88.

- Kobayashi,A., Higashide,T., Hamasaki,D., Kubota,S., Sakuma,H., An,W., Fujimaki,T., McLaren,M.J., Weleber,R.G., and Inana,G. (2000). HRG4 (UNC119) mutation found in cone-rod dystrophy causes retinal degeneration in a transgenic model. *Invest Ophthalmol. Vis. Sci.* *41*, 3268-3277.
- Kobayashi,A., Kubota,S., Mori,N., McLaren,M.J., and Inana,G. (2003). Photoreceptor synaptic protein HRG4 (UNC119) interacts with ARL2 via a putative conserved domain. *FEBS Lett.* *534*, 26-32.
- Kornbluth,S., Dasso,M., and Newport,J. (1994). Evidence for a dual role for TC4 protein in regulating nuclear structure and cell cycle progression. *J. Cell Biol.* *125*, 705-719.
- Koutalos,Y. and Ebrey,T.G. (1986). Recent progress in vertebrate photoreception. *Photochem. Photobiol.* *44*, 809-817.
- Kubo,A., Sasaki,H., Yuba-Kubo,A., Tsukita,S., and Shiina,N. (1999). Centriolar satellites: molecular characterization, ATP-dependent movement toward centrioles and possible involvement in ciliogenesis. *J. Cell Biol.* *147*, 969-980.
- Kudryashova,E., Kudryashov,D., Kramerova,I., and Spencer,M.J. (2005). Trim32 is a ubiquitin ligase mutated in limb girdle muscular dystrophy type 2H that binds to skeletal muscle myosin and ubiquitinates actin. *J. Mol. Biol.* *354*, 413-424.
- Kuhn,H. and Wilden,U. (1987). Deactivation of photoactivated rhodopsin by rhodopsin-kinase and arrestin. *J. Recept. Res.* *7*, 283-298.
- Kuhnel,K., Veltel,S., Schlichting,I., and Wittinghofer,A. (2006). Crystal structure of the human retinitis pigmentosa 2 protein and its interaction with Arl3. *Structure.* *14*, 367-378.
- Kuzhandaivelu,N., Cong,Y.S., Inouye,C., Yang,W.M., and Seto,E. (1996). XAP2, a novel hepatitis B virus X-associated protein that inhibits X transactivation. *Nucleic Acids Res.* *24*, 4741-4750.
- Kwitek-Black,A.E., Carmi,R., Duyk,G.M., Buetow,K.H., Elbedour,K., Parvari,R., Yandava,C.N., Stone,E.M., and Sheffield,V.C. (1993). Linkage of Bardet-Biedl syndrome to chromosome 16q and evidence for non-allelic genetic heterogeneity. *Nat. Genet.* *5*, 392-396.
- Lai,M.C., Lin,R.I., and Tarn,W.Y. (2001). Transportin-SR2 mediates nuclear import of phosphorylated SR proteins. *Proc. Natl. Acad. Sci. U. S. A* *98*, 10154-10159.
- Lai,R.K., Perez-Sala,D., Canada,F.J., and Rando,R.R. (1990). The gamma subunit of transducin is farnesylated. *Proc. Natl. Acad. Sci. U. S. A* *87*, 7673-7677.
- Lambright,D.G., Sondek,J., Bohm,A., Skiba,N.P., Hamm,H.E., and Sigler,P.B. (1996). The 2.0 Å crystal structure of a heterotrimeric G protein. *Nature* *379*, 311-319.

- Larbolette,O., Wollscheid,B., Schweikert,J., Nielsen,P.J., and Wienands,J. (1999). SH3P7 is a cytoskeleton adapter protein and is coupled to signal transduction from lymphocyte antigen receptors. *Mol. Cell Biol.* 19, 1539-1546.
- LaVail,M.M. (1980). Circadian nature of rod outer segment disc shedding in the rat. *Invest Ophthalmol. Vis. Sci.* 19, 407-411.
- LaVail,M.M. and Gorrin,G.M. (1987). Protection from light damage by ocular pigmentation: analysis using experimental chimeras and translocation mice. *Exp. Eye Res.* 44, 877-889.
- Lee B.Y., Mahalow A., Smith R.S., Hicks W., Naggert J.K., and Nishina P.M. Prefoldin 5 (pfdn5) is essential for the development of the mouse photoreceptor outer segment. ARVO 15-12-2005.
- Lee,F.J., Huang,C.F., Yu,W.L., Buu,L.M., Lin,C.Y., Huang,M.C., Moss,J., and Vaughan,M. (1997). Characterization of an ADP-ribosylation factor-like 1 protein in *Saccharomyces cerevisiae*. *J. Biol. Chem.* 272 , 30998-31005.
- Lefkowitz,R.J. and Shenoy,S.K. (2005). Transduction of receptor signals by beta-arrestins. *Science* 308, 512-517.
- Leppert,M., Baird,L., Anderson,K.L., Otterud,B., Lupski,J.R., and Lewis,R.A. (1994). Bardet-Biedl syndrome is linked to DNA markers on chromosome 11q and is genetically heterogeneous. *Nat. Genet.* 7, 108-112.
- Leroux,M.R., Fandrich,M., Klunker,D., Siegers,K., Lupas,A.N., Brown,J.R., Schiebel,E., Dobson,C.M., and Hartl,F.U. (1999). MtGimC, a novel archaeal chaperone related to the eukaryotic chaperonin cofactor GimC/prefoldin. *EMBO J.* 18, 6730-6743.
- Lewis,S.A., Tian,G., and Cowan,N.J. (1997). The alpha- and beta-tubulin folding pathways. *Trends Cell Biol.* 7, 479-484.
- Li,J.B., Gerdes,J.M., Haycraft,C.J., Fan,Y., Teslovich,T.M., May-Simera,H., Li,H., Blacque,O.E., Li,L., Leitch,C.C., Lewis,R.A., Green,J.S., Parfrey,P.S., Leroux,M.R., Davidson,W.S., Beales,P.L., Guay-Woodford,L.M., Yoder,B.K., Stormo,G.D., Katsanis,N., and Dutcher,S.K. (2004). Comparative genomics identifies a flagellar and basal body proteome that includes the BBS5 human disease gene. *Cell* 117, 541-552.
- Li,Y.P., Busch,R.K., Valdez,B.C., and Busch,H. (1996). C23 interacts with B23, a putative nucleolar-localization-signal-binding protein. *Eur. J. Biochem.* 237, 153-158.
- Lin,C.Y., Huang,P.H., Liao,W.L., Cheng,H.J., Huang,C.F., Kuo,J.C., Patton,W.A., Massenburg,D., Moss,J., and Lee,F.J. (2000). ARL4, an ARF-like protein that is developmentally regulated and localized to nuclei and nucleoli. *J. Biol. Chem.* 275, 37815-37823.

- Lin,C.Y., Li,C.C., Huang,P.H., and Lee,F.J. (2002). A developmentally regulated ARF-like 5 protein (ARL5), localized to nuclei and nucleoli, interacts with heterochromatin protein 1. *J. Cell Sci.* *115*, 4433-4445.
- Lin,C.Y., Li,C.C., Huang,P.H., and Lee,F.J. (2002). A developmentally regulated ARF-like 5 protein (ARL5), localized to nuclei and nucleoli, interacts with heterochromatin protein 1. *J. Cell Sci.* *115*, 4433-4445.
- Linari,M., Hanzal-Bayer,M., and Becker,J. (1999). The delta subunit of rod specific cyclic GMP phosphodiesterase, PDE delta, interacts with the Arf-like protein Arl3 in a GTP specific manner. *FEBS Lett.* *458*, 55-59.
- Liu,C., Li,Y., Semenov,M., Han,C., Baeg,G.H., Tan,Y., Zhang,Z., Lin,X., and He,X. (2002). Control of beta-catenin phosphorylation/degradation by a dual-kinase mechanism. *Cell* *108*, 837-847.
- Liu,Q., Tan,G., Levenkova,N., Li,T., Pugh,E.N., Jr., Rux,J.J., Speicher,D.W., and Pierce,E.A. (2007a). The proteome of the mouse photoreceptor sensory cilium complex. *Mol. Cell Proteomics.* *6*, 1299-1317.
- Liu,X., Bulgakov,O.V., Darrow,K.N., Pawlyk,B., Adamian,M., Liberman,M.C., and Li,T. (2007b). Usherin is required for maintenance of retinal photoreceptors and normal development of cochlear hair cells. *Proc. Natl. Acad. Sci. U. S. A* *104*, 4413-4418.
- Liu,X., Bulgakov,O.V., Wen,X.H., Woodruff,M.L., Pawlyk,B., Yang,J., Fain,G.L., Sandberg,M.A., Makino,C.L., and Li,T. (2004). AIPL1, the protein that is defective in Leber congenital amaurosis, is essential for the biosynthesis of retinal rod cGMP phosphodiesterase. *Proc. Natl. Acad. Sci. U. S. A* *101*, 13903-13908.
- Llorca,O., McCormack,E.A., Hynes,G., Grantham,J., Cordell,J., Carrascosa,J.L., Willison,K.R., Fernandez,J.J., and Valpuesta,J.M. (1999). Eukaryotic type II chaperonin CCT interacts with actin through specific subunits. *Nature* *402*, 693-696.
- Llorca,O., Smyth,M.G., Marco,S., Carrascosa,J.L., Willison,K.R., and Valpuesta,J.M. (1998). ATP binding induces large conformational changes in the apical and equatorial domains of the eukaryotic chaperonin containing TCP-1 complex. *J. Biol. Chem.* *273*, 10091-10094.
- Loew,A., Ho,Y.K., Blundell,T., and Bax,B. (1998). Phosducin induces a structural change in transducin beta gamma. *Structure.* *6*, 1007-1019.
- Lolkema,M.P., Mans,D.A., Ulfman,L.H., Volpi,S., Voest,E.E., and Giles,R.H. (2008). Allele-specific regulation of primary cilia function by the von Hippel-Lindau tumor suppressor. *Eur. J. Hum. Genet.* *16*, 73-78.
- Macara,I.G. (2001). Transport into and out of the nucleus. *Microbiol. Mol. Biol. Rev.* *65*, 570-94, table.

- Macario,A.J. and Conway,D.M. (2001). The molecular chaperone system and other anti-stress mechanisms in archaea. *Front Biosci.* 6, D262-D283.
- Maita,H., Kitaura,H., Ariga,H., and Iguchi-Ariga,S.M. (2005). Association of PAP-1 and Prp3p, the products of causative genes of dominant retinitis pigmentosa, in the tri-snRNP complex. *Exp. Cell Res.* 302 , 61-68.
- Makino,E.R., Handy,J.W., Li,T., and Arshavsky,V.Y. (1999). The GTPase activating factor for transducin in rod photoreceptors is the complex between RGS9 and type 5 G protein beta subunit. *Proc. Natl. Acad. Sci. U. S. A* 96, 1947-1952.
- Mans,D.A., Voest,E.E., and Giles,R.H. (2008). All along the watchtower: Is the cilium a tumor suppressor organelle? *Biochim. Biophys. Acta.*
- Marszalek,J.R., Liu,X., Roberts,E.A., Chui,D., Marth,J.D., Williams,D.S., and Goldstein,L.S. (2000). Genetic evidence for selective transport of opsin and arrestin by kinesin-II in mammalian photoreceptors. *Cell* 102, 175-187.
- Martin-Benito,J., Boskovic,J., Gomez-Puertas,P., Carrascosa,J.L., Simons,C.T., Lewis,S.A., Bartolini,F., Cowan,N.J., and Valpuesta,J.M. (2002). Structure of eukaryotic prefoldin and of its complexes with unfolded actin and the cytosolic chaperonin CCT. *EMBO J.* 21, 6377-6386.
- Mashima,Y., Saga,M., Hiida,Y., Imamura,Y., Kudoh,J., and Shimizu,N. (2000). Novel mutation in RP2 gene in two brothers with X-linked retinitis pigmentosa and mtDNA mutation of leber hereditary optic neuropathy who showed marked differences in clinical severity. *Am. J. Ophthalmol.* 130 , 357-359.
- Maw,M., Kumaramanickavel,G., Kar,B., John,S., Bridges,R., and Denton,M. (1998). Two Indian siblings with Oguchi disease are homozygous for an arrestin mutation encoding premature termination. *Hum. Mutat. Suppl 1*, S317-S319.
- McClellan,A.J., Xia,Y., Deutschbauer,A.M., Davis,R.W., Gerstein,M., and Frydman,J. (2007). Diverse cellular functions of the Hsp90 molecular chaperone uncovered using systems approaches. *Cell* 131, 121-135.
- McCudden,C.R., Hains,M.D., Kimple,R.J., Siderovski,D.P., and Willard,F.S. (2005). G protein signaling: back to the future. *Cell Mol. Life Sci.* 62, 551-577.
- McGinnis,J.F., Matsumoto,B., Whelan,J.P., and Cao,W. (2002). Cytoskeleton participation in subcellular trafficking of signal transduction proteins in rod photoreceptor cells. *J. Neurosci. Res.* 67, 290-297.
- McKie,A.B., McHale,J.C., Keen,T.J., Tarttelin,E.E., Goliath,R., Lith-Verhoeven,J.J., Greenberg,J., Ramesar,R.S., Hoyng,C.B., Cremers,F.P., Mackey,D.A., Bhattacharya,S.S., Bird,A.C., Markham,A.F., and Inglehearn,C.F. (2001). Mutations in the pre-mRNA splicing factor gene PRPC8 in autosomal dominant retinitis pigmentosa (RP13). *Hum. Mol. Genet.* 10, 1555-1562.

- Mears,A.J., Gieser,L., Yan,D., Chen,C., Fahrner,S., Hiriyanna,S., Fujita,R., Jacobson,S.G., Sieving,P.A., and Swaroop,A. (1999). Protein-truncation mutations in the RP2 gene in a North American cohort of families with X-linked retinitis pigmentosa. *Am. J. Hum. Genet.* *64*, 897-900.
- Meindl,A., Carvalho,M.R., Herrmann,K., Lorenz,B., Achatz,H., Lorenz,B., Apfelstedt-Sylla,E., Wittwer,B., Ross,M., and Meitinger,T. (1995). A gene (SRPX) encoding a sushi-repeat-containing protein is deleted in patients with X-linked retinitis pigmentosa. *Hum. Mol. Genet.* *4*, 2339-2346.
- Mendelsohn,A.R. and Brent,R. (1999). Protein interaction methods--toward an endgame. *Science* *284*, 1948-1950.
- Mendes,H.F., van der,S.J., Chapple,J.P., and Cheetham,M.E. (2005). Mechanisms of cell death in rhodopsin retinitis pigmentosa: implications for therapy. *Trends Mol. Med.* *11*, 177-185.
- Mendez,A., Lem,J., Simon,M., and Chen,J. (2003). Light-dependent translocation of arrestin in the absence of rhodopsin phosphorylation and transducin signaling. *J. Neurosci.* *23*, 3124-3129.
- Miano,M.G., Testa,F., Filippini,F., Trujillo,M., Conte,I., Lanzara,C., Millan,J.M., De Bernardo,C., Grammatico,B., Mangino,M., Torrente,I., Carrozzo,R., Simonelli,F., Rinaldi,E., Ventruto,V., D'Urso,M., Ayuso,C., and Ciccodicola,A. (2001). Identification of novel RP2 mutations in a subset of X-linked retinitis pigmentosa families and prediction of new domains. *Hum. Mutat.* *18*, 109-119.
- Minami,Y., Hohfeld,J., Ohtsuka,K., and Hartl,F.U. (1996). Regulation of the heat-shock protein 70 reaction cycle by the mammalian DnaJ homolog, Hsp40. *J. Biol. Chem.* *271*, 19617-19624.
- Miyaguchi,K. and Hashimoto,P.H. (1992). Evidence for the transport of opsin in the connecting cilium and basal rod outer segment in rat retina: rapid-freeze, deep-etch and horseradish peroxidase labelling studies. *J. Neurocytol.* *21*, 449-457.
- Molday,R.S. and Molday,L.L. (1998). Molecular properties of the cGMP-gated channel of rod photoreceptors. *Vision Res.* *38*, 1315-1323.
- Morano,K.A. (2007). New tricks for an old dog: the evolving world of Hsp70. *Ann. N. Y. Acad. Sci.* *1113*, 1-14.
- Morera,S., Lascu,I., Dumas,C., LeBras,G., Briozzo,P., Veron,M., and Janin,J. (1994a). Adenosine 5'-diphosphate binding and the active site of nucleoside diphosphate kinase. *Biochemistry* *33*, 459-467.
- Moréra, S., LeBras, G., Lascu, I., Lacombe, M.L., Véron M., Janin J. (1994b). Refined X-ray structure of *Dictyostelium discoideum* nucleoside diphosphate kinase at 1.8 Å resolution. *J Mol Biol.* *11*, 243(5):873-90.

- Mori,K., Maeda,Y., Kitaura,H., Taira,T., Iguchi-Arigo,S.M., and Arigo,H. (1998). MM-1, a novel c-Myc-associating protein that represses transcriptional activity of c-Myc. *J. Biol. Chem.* 273, 29794-29800.
- Morimoto,R.I. (2008). Proteotoxic stress and inducible chaperone networks in neurodegenerative disease and aging. *Genes Dev.* 22, 1427-1438.
- Morimura,H., Fishman,G.A., Grover,S.A., Fulton,A.B., Berson,E.L., and Dryja,T.P. (1998). Mutations in the RPE65 gene in patients with autosomal recessive retinitis pigmentosa or leber congenital amaurosis. *Proc. Natl. Acad. Sci. U. S. A* 95, 3088-3093.
- Morshauer,R.C., Hu,W., Wang,H., Pang,Y., Flynn,G.C., and Zuiderweg,E.R. (1999). High-resolution solution structure of the 18 kDa substrate-binding domain of the mammalian chaperone protein Hsc70. *J. Mol. Biol.* 289, 1387-1403.
- Muller,S., Straub,A., Schroder,S., Bauer,P.H., and Lohse,M.J. (1996). Interactions of phosphatidylinositol-3-OH kinase with defined G protein beta gamma-subunits. *J. Biol. Chem.* 271, 11781-11786.
- Muzio,M., Chinnaiyan,A.M., Kischkel,F.C., O'Rourke,K., Shevchenko,A., Ni,J., Scaffidi,C., Bretz,J.D., Zhang,M., Gentz,R., Mann,M., Krammer,P.H., Peter,M.E., and Dixit,V.M. (1996). FLICE, a novel FADD-homologous ICE/CED-3-like protease, is recruited to the CD95 (Fas/APO-1) death-inducing signaling complex. *Cell* 85, 817-827.
- Nair,K.S., Balasubramanian,N., and Slepak,V.Z. (2002). Signal-dependent translocation of transducin, RGS9-1-Gbeta5L complex, and arrestin to detergent-resistant membrane rafts in photoreceptors. *Curr. Biol.* 12, 421-425.
- Nair,K.S., Hanson,S.M., Kennedy,M.J., Hurley,J.B., Gurevich,V.V., and Slepak,V.Z. (2004). Direct binding of visual arrestin to microtubules determines the differential subcellular localization of its splice variants in rod photoreceptors. *J. Biol. Chem.* 279, 41240-41248.
- Nair,K.S., Hanson,S.M., Mendez,A., Gurevich,E.V., Kennedy,M.J., Shestopalov,V.I., Vishnivetskiy,S.A., Chen,J., Hurley,J.B., Gurevich,V.V., and Slepak,V.Z. (2005). Light-dependent redistribution of arrestin in vertebrate rods is an energy-independent process governed by protein-protein interactions. *Neuron* 46, 555-567.
- Nakazawa,M., Wada,Y., and Tamai,M. (1998). Arrestin gene mutations in autosomal recessive retinitis pigmentosa. *Arch. Ophthalmol.* 116, 498-501.
- Neer,E.J. and Clapham,D.E. (1988). Roles of G protein subunits in transmembrane signalling. *Nature* 333, 129-134.
- Neer,E.J., Schmidt,C.J., Nambudripad,R., and Smith,T.F. (1994). The ancient regulatory-protein family of WD-repeat proteins. *Nature* 371, 297-300.

- Nekrasova,E.R., Berman,D.M., Rustandi,R.R., Hamm,H.E., Gilman,A.G., and Arshavsky,V.Y. (1997). Activation of transducin guanosine triphosphatase by two proteins of the RGS family. *Biochemistry* 36, 7638-7643.
- Neubert,T.A., Johnson,R.S., Hurley,J.B., and Walsh,K.A. (1992). The rod transducin alpha subunit amino terminus is heterogeneously fatty acylated. *J. Biol. Chem.* 267, 18274-18277.
- Nichols,W.C., Uniacke,S.K., Pankratz,N., Reed,T., Simon,D.K., Halter,C., Rudolph,A., Shults,C.W., Conneally,P.M., and Foroud,T. (2004). Evaluation of the role of Nurr1 in a large sample of familial Parkinson's disease. *Mov Disord.* 19, 649-655.
- Nishimura,D.Y., Fath,M., Mullins,R.F., Searby,C., Andrews,M., Davis,R., Andorf,J.L., Mykytyn,K., Swiderski,R.E., Yang,B., Carmi,R., Stone,E.M., and Sheffield,V.C. (2004). Bbs2-null mice have neurosensory deficits, a defect in social dominance, and retinopathy associated with mislocalization of rhodopsin. *Proc. Natl. Acad. Sci. U. S. A* 101, 16588-16593.
- Nishimura,D.Y., Swiderski,R.E., Searby,C.C., Berg,E.M., Ferguson,A.L., Hennekam,R., Merin,S., Weleber,R.G., Biesecker,L.G., Stone,E.M., and Sheffield,V.C. (2005). Comparative genomics and gene expression analysis identifies BBS9, a new Bardet-Biedl syndrome gene. *Am. J. Hum. Genet.* 77, 1021-1033.
- Novoselova,T.V., Margulis,B.A., Novoselov,S.S., Sapozhnikov,A.M., van der,S.J., Cheetham,M.E., and Guzhova,I.V. (2005). Treatment with extracellular HSP70/HSC70 protein can reduce polyglutamine toxicity and aggregation. *J. Neurochem.* 94, 597-606.
- Nurnberg,B., Gudermann,T., and Schultz,G. (1995). Receptors and G proteins as primary components of transmembrane signal transduction. Part 2. G proteins: structure and function. *J. Mol. Med.* 73, 123-132.
- Ostrowski,L.E., Blackburn,K., Radde,K.M., Moyer,M.B., Schlatzer,D.M., Moseley,A., and Boucher,R.C. (2002). A proteomic analysis of human cilia: identification of novel components. *Mol. Cell Proteomics.* 1, 451-465.
- Palczewski,K., Buczylo,J., Ohguro,H., Annan,R.S., Carr,S.A., Crabb,J.W., Kaplan,M.W., Johnson,R.S., and Walsh,K.A. (1994). Characterization of a truncated form of arrestin isolated from bovine rod outer segments. *Protein Sci.* 3, 314-324.
- Palczewski,K., Kumasaka,T., Hori,T., Behnke,C.A., Motoshima,H., Fox,B.A., Le,T., I, Teller,D.C., Okada,T., Stenkamp,R.E., Yamamoto,M., and Miyano,M. (2000). Crystal structure of rhodopsin: A G protein-coupled receptor. *Science* 289, 739-745.
- Pan,X., Eathiraj,S., Munson,M., and Lambright,D.G. (2006). TBC-domain GAPs for Rab GTPases accelerate GTP hydrolysis by a dual-finger mechanism. *Nature* 442, 303-306.

- Pawlyk,B.S., Smith,A.J., Buch,P.K., Adamian,M., Hong,D.H., Sandberg,M.A., Ali,R.R., and Li,T. (2005). Gene replacement therapy rescues photoreceptor degeneration in a murine model of Leber congenital amaurosis lacking RPGRIP. *Invest Ophthalmol. Vis. Sci.* *46*, 3039-3045.
- Pazour,G.J., Agrin,N., Leszyk,J., and Witman,G.B. (2005). Proteomic analysis of a eukaryotic cilium. *J. Cell Biol.* *170*, 103-113.
- Pazour,G.J., Wilkerson,C.G., and Witman,G.B. (1998). A dynein light chain is essential for the retrograde particle movement of intraflagellar transport (IFT). *J. Cell Biol.* *141*, 979-992.
- Pelletier,V., Jambou,M., Delphin,N., Zinovieva,E., Stum,M., Gigarel,N., Dollfus,H., Hamel,C., Toutain,A., Dufier,J.L., Roche,O., Munnich,A., Bonnefont,J.P., Kaplan,J., and Rozet,J.M. (2007). Comprehensive survey of mutations in RP2 and RPGR in patients affected with distinct retinal dystrophies: genotype-phenotype correlations and impact on genetic counseling. *Hum. Mutat.* *28*, 81-91.
- Perrault,I., Hanein,S., Gerber,S., Barbet,F., Ducroq,D., Dollfus,H., Hamel,C., Dufier,J.L., Munnich,A., Kaplan,J., and Rozet,J.M. (2004). Retinal dehydrogenase 12 (RDH12) mutations in leber congenital amaurosis. *Am. J. Hum. Genet.* *75*, 639-646.
- Peterson,J.J., Orisme,W., Fellows,J., McDowell,J.H., Shelamer,C.L., Dugger,D.R., and Smith,W.C. (2005). A role for cytoskeletal elements in the light-driven translocation of proteins in rod photoreceptors. *Invest Ophthalmol. Vis. Sci.* *46*, 3988-3998.
- Pinto,M.R., Gorin,P.A., Wait,R., Mulloy,B., and Barreto-Bergter,E. (2005). Structures of the O-linked oligosaccharides of a complex glycoconjugate from *Pseudallescheria boydii*. *Glycobiology* *15*, 895-904.
- Pipe D.M. and Rapley L.J. (1984). Ocular anatomy and histology. The Association of Dispensing Opticians).
- Ponting,C.P., Mott,R., Bork,P., and Copley,R.R. (2001). Novel protein domains and repeats in *Drosophila melanogaster*: insights into structure, function, and evolution. *Genome Res.* *11*, 1996-2008.
- Ramprasad,V.L., Soumitra,N., Nancarrow,D., Sen,P., McKibbin,M., Williams,G.A., Arokiasamy,T., Lakshmiathy,P., Inglehearn,C.F., and Kumaramanickavel,G. (2008). Identification of a novel splice-site mutation in the Lebercilin (LCA5) gene causing Leber congenital amaurosis. *Mol. Vis.* *14*, 481-486.
- Randazzo,P.A. and Kahn,R.A. (1995). Myristoylation and ADP-ribosylation factor function. *Methods Enzymol.* *250*, 394-405.
- Ranson,N.A., White,H.E., and Saibil,H.R. (1998). Chaperonins. *Biochem. J.* *333 (Pt 2)*, 233-242.

- Reddy,V.S., Day,I.S., Thomas,T., and Reddy,A.S. (2004). KIC, a novel Ca²⁺-binding protein with one EF-hand motif, interacts with a microtubule motor protein and regulates trichome morphogenesis. *Plant Cell* 16, 185-200.
- Reidel,B., Goldmann,T., Giessl,A., and Wolfrum,U. (2008). The translocation of signaling molecules in dark adapting mammalian rod photoreceptor cells is dependent on the cytoskeleton. *Cell Motil. Cytoskeleton*.
- Ribbeck,K., Lipowsky,G., Kent,H.M., Stewart,M., and Gorlich,D. (1998). NTF2 mediates nuclear import of Ran. *EMBO J.* 17, 6587-6598.
- Ritco-Vonsovici,M. and Willison,K.R. (2000). Defining the eukaryotic cytosolic chaperonin-binding sites in human tubulins. *J. Mol. Biol.* 304, 81-98.
- Rittinger,K., Walker,P.A., Eccleston,J.F., Smerdon,S.J., and Gamblin,S.J. (1997). Structure at 1.65 Å of RhoA and its GTPase-activating protein in complex with a transition-state analogue. *Nature* 389, 758-762.
- Rivolta,C., Sharon,D., DeAngelis,M.M., and Dryja,T.P. (2002). Retinitis pigmentosa and allied diseases: numerous diseases, genes, and inheritance patterns. *Hum. Mol. Genet.* 11, 1219-1227.
- Rivolta,C., Sweklo,E.A., Berson,E.L., and Dryja,T.P. (2000). Missense mutation in the USH2A gene: association with recessive retinitis pigmentosa without hearing loss. *Am. J. Hum. Genet.* 66, 1975-1978.
- Rock,C.O., Cronan,J.E., Jr., and Armitage,I.M. (1981). Molecular properties of acyl carrier protein derivatives. *J. Biol. Chem.* 256, 2669-2674.
- Roepman,R. and Wolfrum,U. (2007). Protein networks and complexes in photoreceptor cilia. *Subcell. Biochem.* 43, 209-235.
- Roepman,R., Bauer,D., Rosenberg,T., van Duijnhoven,G., van,d., V, Platzer,M., Rosenthal,A., Ropers,H.H., Cremers,F.P., and Berger,W. (1996). Identification of a gene disrupted by a microdeletion in a patient with X-linked retinitis pigmentosa (XLRP). *Hum. Mol. Genet.* 5, 827-833.
- Roepman,R., Bernoud-Hubac,N., Schick,D.E., Mauerer,A., Berger,W., Ropers,H.H., Cremers,F.P., and Ferreira,P.A. (2000). The retinitis pigmentosa GTPase regulator (RPGR) interacts with novel transport-like proteins in the outer segments of rod photoreceptors. *Hum. Mol. Genet.* 9, 2095-2105.
- Rohlich,P. (1975). The sensory cilium of retinal rods is analogous to the transitional zone of motile cilia. *Cell Tissue Res.* 161, 421-430.
- Rosenzweig,D.H., Nair,K.S., Wei,J., Wang,Q., Garwin,G., Saari,J.C., Chen,C.K., Smrcka,A.V., Swaroop,A., Lem,J., Hurley,J.B., and Slepak,V.Z. (2007). Subunit dissociation and diffusion determine the subcellular localization of rod and cone transducins. *J. Neurosci.* 27, 5484-5494.
- Ross,A.J., May-Simera,H., Eichers,E.R., Kai,M., Hill,J., Jagger,D.J., Leitch,C.C., Chapple,J.P., Munro,P.M., Fisher,S., Tan,P.L., Phillips,H.M.,

- Leroux, M.R., Henderson, D.J., Murdoch, J.N., Copp, A.J., Eliot, M.M., Lupski, J.R., Kemp, D.T., Dollfus, H., Tada, M., Katsanis, N., Forge, A., and Beales, P.L. (2005). Disruption of Bardet-Biedl syndrome ciliary proteins perturbs planar cell polarity in vertebrates. *Nat. Genet.* 37, 1135-1140.
- Ross, E.M. and Wilkie, T.M. (2000). GTPase-activating proteins for heterotrimeric G proteins: regulators of G protein signaling (RGS) and RGS-like proteins. *Annu. Rev. Biochem.* 69, 795-827.
- Saini, D.K., Kalyanaraman, V., Chisari, M., and Gautam, N. (2007). A family of G protein betagamma subunits translocate reversibly from the plasma membrane to endomembranes on receptor activation. *J. Biol. Chem.* 282, 24099-24108.
- Sakanaka, C., Sun, T.Q., and Williams, L.T. (2000). New steps in the Wnt/beta-catenin signal transduction pathway. *Recent Prog. Horm. Res.* 55, 225-236.
- Sakono, M., Zako, T., Ueda, H., Yohda, M., and Maeda, M. (2008). Formation of highly toxic soluble amyloid beta oligomers by the molecular chaperone prefoldin. *FEBS J.* 275, 5982-5993.
- Satou, A., Hagio, Y., Taira, T., Iguchi-Arigo, S.M., and Ariga, H. (2004). Repression of the c-fms gene in fibroblast cells by c-Myc-MM-1-TIF1beta complex. *FEBS Lett.* 572, 211-215.
- Schmidt, C.J., Thomas, T.C., Levine, M.A., and Neer, E.J. (1992). Specificity of G protein beta and gamma subunit interactions. *J. Biol. Chem.* 267, 13807-13810.
- Schrick, J.J., Vogel, P., Abuin, A., Hampton, B., and Rice, D.S. (2006). ADP-ribosylation factor-like 3 is involved in kidney and photoreceptor development. *Am. J. Pathol.* 168, 1288-1298.
- Schurmann, A., Kolling, S., Jacobs, S., Saftig, P., Krauss, S., Wennemuth, G., Kluge, R., and Joost, H.G. (2002). Reduced sperm count and normal fertility in male mice with targeted disruption of the ADP-ribosylation factor-like 4 (Arl4) gene. *Mol. Cell Biol.* 22, 2761-2768.
- Schwahn, U., Lenzner, S., Dong, J., Feil, S., Hinzmann, B., van Duijnhoven, G., Kirschner, R., Hemberger, M., Bergen, A.A., Rosenberg, T., Pinckers, A.J., Fundele, R., Rosenthal, A., Cremers, F.P., Ropers, H.H., and Berger, W. (1998). Positional cloning of the gene for X-linked retinitis pigmentosa 2. *Nat. Genet.* 19, 327-332.
- Sharon, D., Bruns, G.A., McGee, T.L., Sandberg, M.A., Berson, E.L., and Dryja, T.P. (2000). X-linked retinitis pigmentosa: mutation spectrum of the RPGR and RP2 genes and correlation with visual function. *Invest Ophthalmol. Vis. Sci.* 41, 2712-2721.
- Sharon, D., Sandberg, M.A., Rabe, V.W., Stillberger, M., Dryja, T.P., and Berson, E.L. (2003). RP2 and RPGR mutations and clinical correlations in patients with X-linked retinitis pigmentosa. *Am. J. Hum. Genet.* 73, 1131-1146.

Sheffield,V.C., Carmi,R., Kwitek-Black,A., Rokhlina,T., Nishimura,D., Duyk,G.M., Elbedour,K., Sunden,S.L., and Stone,E.M. (1994). Identification of a Bardet-Biedl syndrome locus on chromosome 3 and evaluation of an efficient approach to homozygosity mapping. *Hum. Mol. Genet.* 3, 1331-1335.

Shehata,B.M., Stockwell,C.A., Castellano-Sanchez,A.A., Setzer,S., Schmotzer,C.L., and Robinson,H. (2008). Von Hippel-Lindau (VHL) disease: an update on the clinico-pathologic and genetic aspects. *Adv. Anat. Pathol.* 15, 165-171.

Shevchenko,A., Wilm,M., Vorm,O., and Mann,M. (1996). Mass spectrometric sequencing of proteins silver-stained polyacrylamide gels. *Anal. Chem.* 68, 850-858.

Shu,X., Fry,A.M., Tulloch,B., Manson,F.D., Crabb,J.W., Khanna,H., Faragher,A.J., Lennon,A., He,S., Trojan,P., Giessl,A., Wolfrum,U., Vervoort,R., Swaroop,A., and Wright,A.F. (2005). RPGR ORF15 isoform co-localizes with RPGRIP1 at centrioles and basal bodies and interacts with nucleophosmin. *Hum. Mol. Genet.* 14, 1183-1197.

Siebert,R., Leroux,M.R., Scheufler,C., Hartl,F.U., and Moarefi,I. (2000). Structure of the molecular chaperone prefoldin: unique interaction of multiple coiled coil tentacles with unfolded proteins. *Cell* 103, 621-632.

Simons,C.T., Staes,A., Rommelaere,H., Ampe,C., Lewis,S.A., and Cowan,N.J. (2004). Selective contribution of eukaryotic prefoldin subunits to actin and tubulin binding. *J. Biol. Chem.* 279, 4196-4203.

Simons,M., Gloy,J., Ganner,A., Bullerkotte,A., Bashkurov,M., Kronig,C., Schermer,B., Benzing,T., Cabello,O.A., Jenny,A., Mlodzik,M., Polok,B., Driever,W., Obara,T., and Walz,G. (2005). Inversin, the gene product mutated in nephronophthisis type II, functions as a molecular switch between Wnt signaling pathways. *Nat. Genet.* 37, 537-543.

Slavotinek,A.M., Stone,E.M., Mykytyn,K., Heckenlively,J.R., Green,J.S., Heon,E., Musarella,M.A., Parfrey,P.S., Sheffield,V.C., and Biesecker,L.G. (2000). Mutations in MKKS cause Bardet-Biedl syndrome. *Nat. Genet.* 26, 15-16.

Slepak,V.Z. and Hurley,J.B. (2008). Mechanism of light-induced translocation of arrestin and transducin in photoreceptors: interaction-restricted diffusion. *IUBMB. Life* 60, 2-9.

Sohocki,M.M., Bowne,S.J., Sullivan,L.S., Blackshaw,S., Cepko,C.L., Payne,A.M., Bhattacharya,S.S., Khaliq,S., Qasim,M.S., Birch,D.G., Harrison,W.R., Elder,F.F., Heckenlively,J.R., and Daiger,S.P. (2000). Mutations in a new photoreceptor-pineal gene on 17p cause Leber congenital amaurosis. *Nat. Genet.* 24, 79-83.

Sokolov,M., Lyubarsky,A.L., Strissel,K.J., Savchenko,A.B., Govardovskii,V.I., Pugh,E.N., Jr., and Arshavsky,V.Y. (2002). Massive light-driven translocation of

transducin between the two major compartments of rod cells: a novel mechanism of light adaptation. *Neuron* **34**, 95-106.

Sokolov,M., Strissel,K.J., Leskov,I.B., Michaud,N.A., Govardovskii,V.I., and Arshavsky,V.Y. (2004). Phosducin facilitates light-driven transducin translocation in rod photoreceptors. Evidence from the phosducin knockout mouse. *J. Biol. Chem.* **279**, 19149-19156.

Sondek,J., Bohm,A., Lambright,D.G., Hamm,H.E., and Sigler,P.B. (1996). Crystal structure of a G protein beta gamma dimer at 2.1A resolution. *Nature* **379**, 369-374.

Song,X., Raman,D., Gurevich,E.V., Vishnivetskiy,S.A., and Gurevich,V.V. (2006). Visual and both non-visual arrestins in their "inactive" conformation bind JNK3 and Mdm2 and relocalize them from the nucleus to the cytoplasm. *J. Biol. Chem.* **281**, 21491-21499.

Song,X.Q., Meng,F., Ramsey,D.J., Ripps,H., and Qian,H. (2005). The GABA rho1 subunit interacts with a cellular retinoic acid binding protein in mammalian retina. *Neuroscience* **136**, 467-475.

Spek,C.A., Greengard,J.S., Griffin,J.H., Bertina,R.M., and Reitsma,P.H. (1995). Two mutations in the promoter region of the human protein C gene both cause type I protein C deficiency by disruption of two HNF-3 binding sites. *J. Biol. Chem.* **270**, 24216-24221.

Sprang,S.R. (1997). G protein mechanisms: insights from structural analysis. *Annu. Rev. Biochem.* **66**, 639-678.

Stearns,T. (1990). The yeast microtubule cytoskeleton: genetic approaches to structure and function. *Cell Motil. Cytoskeleton* **15**, 1-6.

Steinberg,R.H., Wood,I., and Hogan,M.J. (1977). Pigment epithelial ensheathment and phagocytosis of extrafoveal cones in human retina. *Philos. Trans. R. Soc. Lond B Biol. Sci.* **277**, 459-474.

Steinborn,K., Maulbetsch,C., Priester,B., Trautmann,S., Pacher,T., Geiges,B., Kuttner,F., Lepiniec,L., Stierhof,Y.D., Schwarz,H., Jurgens,G., and Mayer,U. (2002). The Arabidopsis PILZ group genes encode tubulin-folding cofactor orthologs required for cell division but not cell growth. *Genes Dev.* **16**, 959-971.

Stephan,A., Vaughan,S., Shaw,M.K., Gull,K., and McKean,P.G. (2007). An essential quality control mechanism at the eukaryotic basal body prior to intraflagellar transport. *Traffic*. **8**, 1323-1330.

Sterne-Marr,R., Gurevich,V.V., Goldsmith,P., Bodine,R.C., Sanders,C., Donoso,L.A., and Benovic,J.L. (1993). Polypeptide variants of beta-arrestin and arrestin3. *J. Biol. Chem.* **268**, 15640-15648.

Stevenson,V.A. and Theurkauf,W.E. (2000). Actin cytoskeleton: putting a CAP on actin polymerization. *Curr. Biol.* **10**, R695-R697.

Stirling,P.C., Bakhoun,S.F., Feigl,A.B., and Leroux,M.R. (2006). Convergent evolution of clamp-like binding sites in diverse chaperones. *Nat. Struct. Mol. Biol.* 13, 865-870.

Stirling,P.C., Cuellar,J., Alfaro,G.A., El Khadali,F., Beh,C.T., Valpuesta,J.M., Melki,R., and Leroux,M.R. (2006). PhLP3 modulates CCT-mediated actin and tubulin folding via ternary complexes with substrates. *J. Biol. Chem.* 281, 7012-7021.

Stoetzel,C., Laurier,V., Davis,E.E., Muller,J., Rix,S., Badano,J.L., Leitch,C.C., Salem,N., Chouery,E., Corbani,S., Jalk,N., Vicaire,S., Sarda,P., Hamel,C., Lacombe,D., Holder,M., Odent,S., Holder,S., Brooks,A.S., Elcioglu,N.H., Silva,E.D., Rossillion,B., Sigaudy,S., de Ravel,T.J., Lewis,R.A., Leheup,B., Verloes,A., Amati-Bonneau,P., Megarbane,A., Poch,O., Bonneau,D., Beales,P.L., Mandel,J.L., Katsanis,N., and Dollfus,H. (2006). BBS10 encodes a vertebrate-specific chaperonin-like protein and is a major BBS locus. *Nat. Genet.* 38, 521-524.

Stoetzel,C., Muller,J., Laurier,V., Davis,E.E., Zaghloul,N.A., Vicaire,S., Jacquelin,C., Plewniak,F., Leitch,C.C., Sarda,P., Hamel,C., de Ravel,T.J., Lewis,R.A., Friederich,E., Thibault,C., Danse,J.M., Verloes,A., Bonneau,D., Katsanis,N., Poch,O., Mandel,J.L., and Dollfus,H. (2007). Identification of a novel BBS gene (BBS12) highlights the major role of a vertebrate-specific branch of chaperonin-related proteins in Bardet-Biedl syndrome. *Am. J. Hum. Genet.* 80, 1-11.

Strissel,K.J. and Arshavsky,V.Y. (2004). Myosin III illuminates the mechanism of arrestin translocation. *Neuron* 43, 2-4.

Strissel,K.J., Lishko,P.V., Trieu,L.H., Kennedy,M.J., Hurley,J.B., and Arshavsky,V.Y. (2005). Recoverin undergoes light-dependent intracellular translocation in rod photoreceptors. *J. Biol. Chem.* 280, 29250-29255.

Strissel,K.J., Sokolov,M., Trieu,L.H., and Arshavsky,V.Y. (2006). Arrestin translocation is induced at a critical threshold of visual signaling and is superstoichiometric to bleached rhodopsin. *J. Neurosci.* 26, 1146-1153.

Swan,D.G., Hale,R.S., Dhillon,N., and Leadlay,P.F. (1987). A bacterial calcium-binding protein homologous to calmodulin. *Nature* 329, 84-85.

Tamkun,J.W., Kahn,R.A., Kissinger,M., Brizuela,B.J., Rulka,C., Scott,M.P., and Kennison,J.A. (1991). The arflike gene encodes an essential GTP-binding protein in *Drosophila*. *Proc. Natl. Acad. Sci. U. S. A* 88, 3120-3124.

Tanaka,T., Ames,J.B., Harvey,T.S., Stryer,L., and Ikura,M. (1995). Sequestration of the membrane-targeting myristoyl group of recoverin in the calcium-free state. *Nature* 376, 444-447.

Tang,Y.C., Chang,H.C., Hayer-Hartl,M., and Hartl,F.U. (2007). SnapShot: molecular chaperones, Part II. *Cell* 128, 412.

- Thiselton,D.L., Zito,I., Plant,C., Jay,M., Hodgson,S.V., Bird,A.C., Bhattacharya,S.S., and Hardcastle,A.J. (2000). Novel frameshift mutations in the RP2 gene and polymorphic variants. *Hum. Mutat.* 15, 580.
- Thoma,C.R., Frew,I.J., Hoerner,C.R., Montani,M., Moch,H., and Krek,W. (2007). pVHL and GSK3beta are components of a primary cilium-maintenance signalling network. *Nat. Cell Biol.* 9, 588-595.
- Thompson,D.A., Li,Y., McHenry,C.L., Carlson,T.J., Ding,X., Sieving,P.A., Apfelstedt-Sylla,E., and Gal,A. (2001). Mutations in the gene encoding lecithin retinol acyltransferase are associated with early-onset severe retinal dystrophy. *Nat. Genet.* 28, 123-124.
- Tian,G., Vainberg,I.E., Tap,W.D., Lewis,S.A., and Cowan,N.J. (1995). Specificity in chaperonin-mediated protein folding. *Nature* 375, 250-253.
- Tissieres,A., Mitchell,H.K., and Tracy,U.M. (1974). Protein synthesis in salivary glands of *Drosophila melanogaster*: Relation to chromosome puffs. *J. Mol. Biol.* 85, 389-398.
- Troutt,L.L. and Burnside,B. (1988). Microtubule polarity and distribution in teleost photoreceptors. *J. Neurosci.* 8, 2371-2380.
- Trumpp-Kallmeyer,S., Hoflack,J., Bruinvels,A., and Hibert,M. (1992). Modeling of G protein-coupled receptors: application to dopamine, adrenaline, serotonin, acetylcholine, and mammalian opsin receptors. *J. Med. Chem.* 35, 3448-3462.
- Tsuchiya,H., Iseda,T., and Hino,O. (1996). Identification of a novel protein (VBP-1) binding to the von Hippel-Lindau (VHL) tumor suppressor gene product. *Cancer Res.* 56, 2881-2885.
- Ugrinova,I., Monier,K., Ivaldi,C., Thiry,M., Storck,S., Mongelard,F., and Bouvet,P. (2007). Inactivation of nucleolin leads to nucleolar disruption, cell cycle arrest and defects in centrosome duplication. *BMC. Mol. Biol.* 8, 66.
- Usui,T., Tanimoto,N., Ueki,S., Takagi,M., Hasegawa,S., Abe,H., Sekiya,K., and Nakazawa,M. (2004). ERG rod a-wave in Oguchi disease. *Vision Res.* 44, 535-540.
- Vainberg,I.E., Lewis,S.A., Rommelaere,H., Ampe,C., Vandekerckhove,J., Klein,H.L., and Cowan,N.J. (1998). Prefoldin, a chaperone that delivers unfolded proteins to cytosolic chaperonin. *Cell* 93, 863-873.
- van der Spuy, J., Chapple,J.P., Clark,B.J., Luthert,P.J., Sethi,C.S., and Cheetham,M.E. (2002). The Leber congenital amaurosis gene product AIPL1 is localized exclusively in rod photoreceptors of the adult human retina. *Hum. Mol. Genet.* 11, 823-831.
- Van Valkenburgh,H., Shern,J.F., Sharer,J.D., Zhu,X., and Kahn,R.A. (2001). ADP-ribosylation factors (ARFs) and ARF-like 1 (ARL1) have both specific and

- shared effectors: characterizing ARL1-binding proteins. *J. Biol. Chem.* 276, 22826-22837.
- Vaney,D.I., Nelson,J.C., and Pow,D.V. (1998). Neurotransmitter coupling through gap junctions in the retina. *J. Neurosci.* 18 , 10594-10602.
- Veltel,S., Gasper,R., Eisenacher,E., and Wittinghofer,A. (2008a). The retinitis pigmentosa 2 gene product is a GTPase-activating protein for Arf-like 3. *Nat. Struct. Mol. Biol.* 15, 373-380.
- Veltel,S., Kravchenko,A., Ismail,S., and Wittinghofer,A. (2008b). Specificity of Arl2/Arl3 signaling is mediated by a ternary Arl3-effector-GAP complex. *FEBS Lett.* 582, 2501-2507.
- Vervoort,R., Lennon,A., Bird,A.C., Tulloch,B., Axton,R., Miano,M.G., Meindl,A., Meitinger,T., Ciccodicola,A., and Wright,A.F. (2000). Mutational hot spot within a new RPGR exon in X-linked retinitis pigmentosa. *Nat. Genet.* 25, 462-466.
- Vetter,I.R. and Wittinghofer,A. (2001). The guanine nucleotide-binding switch in three dimensions. *Science* 294, 1299-1304.
- Vinson,C.R., Conover,S., and Adler,P.N. (1989). A *Drosophila* tissue polarity locus encodes a protein containing seven potential transmembrane domains. *Nature* 338, 263-264.
- Vishnivetskiy,S.A., Raman,D., Wei,J., Kennedy,M.J., Hurley,J.B., and Gurevich,V.V. (2007). Regulation of arrestin binding by rhodopsin phosphorylation level. *J. Biol. Chem.* 282, 32075-32083.
- Vithana,E.N., Abu-Safieh,L., Allen,M.J., Carey,A., Papaioannou,M., Chakarova,C., Al Maghtheh,M., Ebenezer,N.D., Willis,C., Moore,A.T., Bird,A.C., Hunt,D.M., and Bhattacharya,S.S. (2001). A human homolog of yeast pre-mRNA splicing gene, PRP31, underlies autosomal dominant retinitis pigmentosa on chromosome 19q13.4 (RP11). *Mol. Cell* 8, 375-381.
- Vogel,M., Mayer,M.P., and Bukau,B. (2006). Allosteric regulation of Hsp70 chaperones involves a conserved interdomain linker. *J. Biol. Chem.* 281, 38705-38711.
- Vorster,A.A., Rebello,M.T., Coutts,N., Ehrenreich,L., Gama,A.D., Roberts,L.J., Goliath,R., Ramesar,R., and Greenberg,L.J. (2004). Arg120stop nonsense mutation in the RP2 gene: mutational hotspot and germ line mosaicism? *Clin. Genet.* 65, 7-10.
- Vuong,T.M., Chabre,M., and Stryer,L. (1984). Millisecond activation of transducin in the cyclic nucleotide cascade of vision. *Nature* 311, 659-661.
- Wacker,W.B. (1987). Retinal autoimmunity: two decades of research. *Jpn. J. Ophthalmol.* 31, 188-196.

Wait,R., Gianazza,E., Eberini,I., Sironi,L., Dunn,M.J., Gemeiner,M., and Miller,I. (2001). Proteins of rat serum, urine, and cerebrospinal fluid: VI. Further protein identifications and interstrain comparison. *Electrophoresis* 22, 3043-3052.

Wall,M.A., Coleman,D.E., Lee,E., Iniguez-Lluhi,J.A., Posner,B.A., Gilman,A.G., and Sprang,S.R. (1995). The structure of the G protein heterotrimer Gi alpha 1 beta 1 gamma 2. *Cell* 83, 1047-1058.

Wang,D.Y., Chan,W.M., Tam,P.O., Baum,L., Lam,D.S., Chong,K.K., Fan,B.J., and Pang,C.P. (2005a). Gene mutations in retinitis pigmentosa and their clinical implications. *Clin. Chim. Acta* 351, 5-16.

Wang,W., Ding,J., Allen,E., Zhu,P., Zhang,L., Vogel,H., and Yang,Y. (2005b). Gigaxonin interacts with tubulin folding cofactor B and controls its degradation through the ubiquitin-proteasome pathway. *Curr. Biol.* 15, 2050-2055.

Watanabe,K., Ozaki,T., Nakagawa,T., Miyazaki,K., Takahashi,M., Hosoda,M., Hayashi,S., Todo,S., and Nakagawara,A. (2002). Physical interaction of p73 with c-Myc and MM1, a c-Myc-binding protein, and modulation of the p73 function. *J. Biol. Chem.* 277, 15113-15123.

Watanabe,N., Miyake,Y., Wakabayashi,T., and Usukura,J. (1999). Periciliary structure of developing rat photoreceptor cells. A deep etch replica and freeze substitution study. *J. Electron Microsc.* (Tokyo) 48, 929-935.

Wess,J. (1997). G protein-coupled receptors: molecular mechanisms involved in receptor activation and selectivity of G protein recognition. *FASEB J.* 11, 346-354.

Wieland,T. (2007). Interaction of nucleoside diphosphate kinase B with heterotrimeric G protein betagamma dimers: consequences on G protein activation and stability. *Naunyn Schmiedebergs Arch. Pharmacol.* 374, 373-383.

Willardson,B.M. and Howlett,A.C. (2007). Function of phosphducin-like proteins in G protein signaling and chaperone-assisted protein folding. *Cell Signal.* 19, 2417-2427.

Wilm,M., Shevchenko,A., Houthaeve,T., Breit,S., Schweigerer,L., Fotsis,T., and Mann,M. (1996). Femtomole sequencing of proteins from polyacrylamide gels by nano-electrospray mass spectrometry. *Nature* 379, 466-469.

Wolfe,J.T., Wang,H., Howard,J., Garrison,J.C., and Barrett,P.Q. (2003). T-type calcium channel regulation by specific G protein betagamma subunits. *Nature* 424, 209-213.

Wolfrum,U., Giessl,A., and Pulvermuller,A. (2002). Centrins, a novel group of Ca²⁺-binding proteins in vertebrate photoreceptor cells. *Adv. Exp. Med. Biol.* 514, 155-178.

Xi,Q., Pauer,G.J., Marmorstein,A.D., Crabb,J.W., and Hagstrom,S.A. (2005). Tubby-like protein 1 (TULP1) interacts with F-actin in photoreceptor cells. *Invest Ophthalmol. Vis. Sci.* 46, 4754-4761.

- Yamaki,K., Tsuda,M., Kikuchi,T., Chen,K.H., Huang,K.P., and Shinohara,T. (1990). Structural organization of the human S-antigen gene. cDNA, amino acid, intron, exon, promoter, in vitro transcription, retina, and pineal gland. *J. Biol. Chem.* *265*, 20757-20762.
- Yamamoto,S., Sippel,K.C., Berson,E.L., and Dryja,T.P. (1997). Defects in the rhodopsin kinase gene in the Oguchi form of stationary night blindness. *Nat. Genet.* *15*, 175-178.
- Yang,J., Liu,X., Yue,G., Adamian,M., Bulgakov,O., and Li,T. (2002). Rootletin, a novel coiled-coil protein, is a structural component of the ciliary rootlet. *J. Cell Biol.* *159*, 431-440.
- Yang,Z., Peachey,N.S., Moshfeghi,D.M., Thirumalaichary,S., Chorich,L., Shugart,Y.Y., Fan,K., and Zhang,K. (2002). Mutations in the RPGR gene cause X-linked cone dystrophy. *Hum. Mol. Genet.* *11*, 605-611.
- Yoneda,Y., Hieda,M., Nagoshi,E., and Miyamoto,Y. (1999). Nucleocytoplasmic protein transport and recycling of Ran. *Cell Struct. Funct.* *24*, 425-433.
- Yoon,J.H., Qiu,J., Cai,S., Chen,Y., Cheetham,M.E., Shen,B., and Pfeifer,G.P. (2006). The retinitis pigmentosa-mutated RP2 protein exhibits exonuclease activity and translocates to the nucleus in response to DNA damage. *Exp. Cell Res.* *312*, 1323-1334.
- Yoshida,T., Kitaura,H., Hagio,Y., Sato,T., Iguchi-Arigo,S.M., and Arigo,H. (2008). Negative regulation of the Wnt signal by MM-1 through inhibiting expression of the wnt4 gene. *Exp. Cell Res.* *314*, 1217-1228.
- Yoshii,M., Murakami,A., Akeo,K., Nakamura,A., Shimoyama,M., Ikeda,Y., Kikuchi,Y., Okisaka,S., Yanashima,K., and Oguchi,Y. (1998). Visual function and gene analysis in a family with Oguchi's disease. *Ophthalmic Res.* *30*, 394-401.
- Young,R.W. (1978). The daily rhythm of shedding and degradation of rod and cone outer segment membranes in the chick retina. *Invest Ophthalmol. Vis. Sci.* *17*, 105-116.
- Young,T.L., Woods,M.O., Parfrey,P.S., Green,J.S., Hefferton,D., and Davidson,W.S. (1999). A founder effect in the newfoundland population reduces the Bardet-Biedl syndrome I (BBS1) interval to 1 cM. *Am. J. Hum. Genet.* *65*, 1680-1687.
- Zhang,H., Liu,X.H., Zhang,K., Chen,C.K., Frederick,J.M., Prestwich,G.D., and Baehr,W. (2004). Photoreceptor cGMP phosphodiesterase delta subunit (PDEdelta) functions as a prenyl-binding protein. *J. Biol. Chem.* *279*, 407-413.
- Zhou,C., Cunningham,L., Marcus,A.I., Li,Y., and Kahn,R.A. (2006). Arl2 and Arl3 regulate different microtubule-dependent processes. *Mol. Biol. Cell* *17*, 2476-2487.

Zhou,H., Li,S.H., and Li,X.J. (2001). Chaperone suppression of cellular toxicity of huntingtin is independent of polyglutamine aggregation. *J. Biol. Chem.* 276, 48417-48424.

Zito,I., Downes,S.M., Patel,R.J., Cheetham,M.E., Ebenezer,N.D., Jenkins,S.A., Bhattacharya,S.S., Webster,A.R., Holder,G.E., Bird,A.C., Bamiou,D.E., and Hardcastle,A.J. (2003). RPGR mutation associated with retinitis pigmentosa, impaired hearing, and sinorespiratory infections. *J. Med. Genet.* 40, 609-615.

Appendix

General Reagents

PCR Master Mix (ABgene, AB-0575/DC) 2 X

1.3 units ThermoPrime DNA *taq* polymerase
 150 mM Tris-HCL pH 8.8
 40 mM (NH₄)₂SO₄
 3 mM MgCl₂
 0.02 % (v/v) Tween20®
 0.4 mM each dATP, dCTP, dGTP, dTTP

siRNA buffer 5 X

300 mM KCl,
 30 mM HEPES-pH 7.5
 1.0 mM MgCl₂

Resolving Gel for SDS-PAGE (10 %)

1.5 M Tris-HCl pH 8.8	2.5 ml
30 % Acrylamide:Bis	3.3 ml
ddH ₂ O	4.0 ml
10 % (w/v) SDS	0.1 ml
10 % (w/v) APS	0.1 ml
Tetramethylethylenediamine (TEMED)	0.005 ml

Stacking Gel for SDS-PAGE (3 %)

0.5M Tris-HCl pH6.8	1.25 ml
30 % Acrylamide:Bis	0.65 ml
ddH ₂ O	3.00 ml
10 % (w/v) SDS	0.05 ml
10 % (w/v) APS	0.05 ml
TEMED	0.01 ml

SDS-PAGE Running Buffer x1 in H₂O

Tris-HCl	25 mM
Glycine	190 mM
SDS	3.5 mM

Laemmli SDS-PAGE Sample Buffer x2 in H₂O

Tris-HCl (pH6.8)	125 mM
Glycerol	20 % (v/v)
SDS	4 % (v/v)
2-β Mercaptoethanol	10 % (v/v)
Bromophenol Blue	0.2 % (w/v)

Western Blotting Transfer Buffer x1 in H₂O

Tris-HCl	25 mM
Glycine	190 mM
Methanol	20 % (v/v)

Coomassie Gel Stain

Methanol	25 % (v/v)
Acetic acid	25 % (v/v)
Coomassie brilliant blue (R-250)* in H ₂ O	0.25 % (w/v)

Coomassie De-Stain

Methanol	25 %
Acetic acid in H ₂ O	10 %

Ponceau S Stain

Trichloroacetic acid (TCA)	3 % (w/v)
Ponceau S in H ₂ O	0.2 % (w/v)

Western Blotting Blocking Buffer

"Marvel" milk powder	5 % (w/v)
Tween-20®	0.05 % (v/v)
In Phosphate buffered saline (PBS)	

LB Media

Bacto®-tryptone	1 % (w/v)
Bacto®-yeast extract	0.5 % (w/v)
NaCl	1 % (w/v)
up to 1 litre with H ₂ O and autoclave	

LB Agar

Bacto®-tryptone	1 % (w/v)
Bacto®-yeast extract	0.5 % (w/v)
NaCl	1 % (w/v)
Bacto®-agar	1.5 % (w/v)
up to 1 litre with H ₂ O and autoclave, cool to 55°C before adding antibiotic	

Chloramphenicol Stock

340mg in 10 ml ethanol

Add 1 ml to 1 litre LB

Ampicillin Stock

1g in 20 ml water

Add 1 ml to 1 litre LB before use

TE Buffer in H₂O

Tris-HCl (pH 7.5)

10 mM

EDTA

1 mM

Phosphate-buffered Saline (PBS)

NaCl

145 mM

NaH₂PO₄

3.6 mM

Na₂HPO₄

10.5 mM

in H₂O

Autoclave before use

TAE Buffer

Tris-HCl

40 mM

Acetic Acid

40 mM

EDTA

1 mM

in H₂O

RIPA buffer

Tris-cl pH 7.4

50mM

NaCl

150mM

NP40

1 % (v/v)

Na-deoxycholate

0.25 % (w/v)

Yeast Specific Reagents

LiOAc/TE Solution

LiOAc

100 mM

TE in H₂O

Filter sterilise

40 % PEG LiOAc/TE Solution

LiOAc

10 mM

PEG₄₀₀₀

40 % (w/v)

TE in H₂O

Filter sterilise

SU Buffer

SDS	5 % (w/v)
Tris-HCl (pH 6.8) in H ₂ O	125 mM
EDTA	0.1 mM
Bromophenol blue	0.005 % (w/v)
Urea	8 M

Store at -20°C. Add DTT 15 mg/ ml prior to use.

YPAD Broth

Yeast extract	1 % (w/v)
Bacto®-peptone	2 % (w/v)
Dextrose	2 % (w/v)
Adenine Sulfate	0.004 % (w/v)

up to 1 litre with water and autoclave

YPAD Agar

Yeast extract	1 % (w/v)
Bacto-peptone	2 % (w/v)
Dextrose	2 % (w/v)
Adenine Sulfate	0.004 % (w/v)
Agar	15 % (w/v)

Up to 1 litre with water and autoclave

SD/Glucose Minimal Media

Yeast nitrogen base without amino acids	0.17 % (w/v)
Ammonium sulphate	0.5 % (w/v)
Dextrose	2 % (w/v)
Add Agar for plates, omit for media	15 % (w/v)

Make upto 900 ml with water and autoclave

Add 100 ml appropriate 10x dropout solution after cooling to 55°C

SD/Galactose Minimal Media

Yeast nitrogen base without amino acids	0.17 % (w/v)
Ammonium sulphate	0.5 % (w/v)
Galactose	2 % (w/v)
Raffinose	1 % (w/v)
Add Agar for plates, omit for media	15 % (w/v)

Make upto 900 ml with water and autoclave

Add 100 ml appropriate 10x dropout solution after cooling to 55°C

<u>10x Dropout Solution in H₂O</u>	Weight (mg/litre)
L-Isoleucine	300
L-Valine	1500
L-Adenine hemisulphate salt	200
L-Arginine HCl	500
L-Histidine HCl monohydrate	200
L-Leucine	1000
L-Lysine HCl	500
L-Methionine	200
L-Phenylalanine	500
L-Threonine*	2000
L-Tryptophan	500
L-Tyrosine	500
L-Uracil	200
L-Glutamic Acid	1000
L-Aspartic Acid*	1000
L-Serine	400

Reagents for general subcellular fractionation.

Buffer C.

HEPES pH 7.9	20 mM
MgCl ₂	2 mM
KCl	100 mM
EDTA	5 mM
Sucrose	250 mM
Glycerol	10 % (v/v)

Buffer N.

HEPES pH 7.9	20 mM
MgCl ₂	2 mM
NaCl	50 mM
EDTA	5 mM
Glycerol	5 % (v/v)

Buffer M.

HEPES pH 7.9	20 mM
MgCl ₂	2 mM
KCl	100 mM
EDTA	5 mM
Sucrose	250 mM
Glycerol	5 % (v/v)
sodium deoxycholate	0,5 % (w/v)
NP-40	1 % (v/v)

Buffer CS.

PIPES pH 6.8

10 mM

MgCl₂

2 mM

NaCl

150 mM

EDTA

5 mM

Sucrose

250 mM

SDS

1 % (w/v)